Morphology control in metallocene-catalyzed polyolefin synthesis

Dissertation
zur Erlangung des Grades
„Doktor der Naturwissenschaften“

am Fachbereich Chemie, Pharmazie und Geowissenschaften
der Johannes Gutenberg-Universität Mainz
Vorgelegt von

Daejune Joe
geboren in Seoul, Süd-Korea

Mainz 2013

"An expert is a person who has made all the mistakes which can be made in a very narrow field."

Niels Bohr (1885-1962) Physicist

Dekan: [redacted]

1. Berichterstatter: [redacted]

2. Berichterstatter: [redacted]

Tag der mündlichen Prüfung: 17.09.2013

Die vorliegende Arbeit wurde in der [redacted] am Max-Planck-Institut für Polymerforschung in Mainz unter Anleitung von [redacted] ausgeführt.

Herrn Professor [redacted] danke ich für seine wissenschaftliche und persönliche Unterstützung sowie für zahlreiche motivierende Diskussionsbereitschaft.

Dedicated to my family members for their support

Table of contents

List of Figures

List of Tables

Abbreviations

ACP	Advanced cascade process
ADMET	Acyclic diene metathesis
AFM	Atomic force microscopy
ansa-Metallocene	Bridged ethylene bis(indenyl)complexes
ATR	Attenuated total reflection
aPP	Atatic polypropylene
Ar	Argon gas
-b-	Block copolymer
BDMAEE	Bis(2-dimethylaminoethyl)ether
BET	Burnauer, Emmett and Teller
BHC	1,4-Bis(hydroxymethyl)cyclohexane
BODIPY	boron-dipyrromethene
C_4	Butene
C_6	Hexene
-co-	Copolymer
Cat.	Catalytic system
COC	Cyclic olefin copolymer
Cp	Cyclopentadienyl
CGC	Constrained geometry catalyst
CSTR	Continuous stirred tank reactor
CTC	Concurrent tandem catalysis
DABCO	1,4-diazabicyclo[2.2.2]octane
DCM	Dichloromethane
DLS	Dynamic light scattering
DMA	*N*,*N*`-Dimethylanilinium
DMAO	Dried methylaluminoxane
DMF	*N, N*`-Dimethylformamide
DP	Degree of polymerization
DSC	Differential scanning calorimetry
EDX	Energy dispersive X-ray
EPDM	Ethylene-propylene-diene terpolymer
ESI	Electron spectroscopic imaging
FI	(Phenoxy-imine) complexes
FTIR	Fourier transform infrared spectroscopy

GPC	Gel permeation chromatography
HDPE	High density polyethylene
HSP	Hollow silica particle
ICI	Imperial chemical industries
ICP-OES	Inductively coupled plasma-optical emission spectrometry
Ind	Indenyl
iPP	Isotatic polypropylene
ITC	Isothermal titration calorimetry
LCB	Long chain branches
LDPE	Low density polyethylene
LLDPE	Linear low density polyethylene
LN_2	Liquid nitrogen
LSCFM	Laser scanning confocal fluorescence microscopy
MAO	Methylaluminoxane
MCP	Bis(methylcyclopentadienyl)zirconium(IV) dichloride
MDI	4,4'-Methylenebis(phenyl isocyanate)
Molwt%	Molecular weight percent
M_n	Number average molecular weight, kg/mol
M_w	Weight average molecular weight, kg/mol
MWD	Molecular weight distribution
$NaAlEt_4$	Sodium tetraethylaluminium
NB	Norbornene
NMP	N-methyl-2-pyrrolidone
NMR	Nuclear magnetic resonance
PDI	Polydispersity
PE	Polyethylene
$P_{Ethylene}$	Ethylene pressure
PEO	Poly(ethyleneoxide)
PI	Poly(isoprene)
PMMA	Poly(methylmetaacrylate)
PP	Polypropylene
PPO	Poly(propyleneoxide)
PS	Polystyrene
PU	Polyurethane
PVA	Polyvinyl alcohol

PVDF	Poly(vinylidene fluoride)
rac-	Racemic
RhoB	Rhodamine B
ROMP	Ring opening metathesis polymerization
RT	Room temperature
SCB	Short chain branches
SEM	Scanning electron microscopy
STED	Stimulated emission depletion microscopy
STEM	Scanning transition emission microscopy
sPP	Syndiotatic polypropylene
sPS	Syndiotatic polystyrene
TBS	*tert*-Butyl dimethyl silyl
TCB	1,2,4-Trichlorobenzene
TEA	Triethylaluminium
TEM	Transmission electron microscopy
T_g	Glass transition temperature
TGA	Thermogravimetric analysis
THF	Tetrahydrofuran
TIBA	Triisobutylaluminium
TIPS	Triisobutyl silyl
T_m	Melting point
TMA	Trimethylaluminium
Tol	Toluene
TPC	Triphenyl carbenium
UHMWPE	Ultra high molecular weight polyethylene
WCA	Weakly coordinating anion
wt%	Weight percent
Z/N	Ziegler-Natta

CHAPTER 1

General Introduction

1 General Introduction

1.1 Polyolefins

As polyolefins comprise the largest portion of organic thermoplastic polymers (*Figure 1-1*),[1] a general overview is described in terms of their definition, application fields and market share. Since polyolefins can be found almost everywhere in our daily life, they are also called "commodity thermoplastics". The term polyolefin means "oil-like" and refers to the oily or waxy texture of this class of plastic resins. This class of polymers is also commonly referred to as "polyalkene", although "polyolefin" is still typically found in organic chemistry and the petrochemical industry. At the molecular level, polyolefins are created by the polymerization of simple olefin molecules, also known as "alkenes", with the general formula, C_nH_{2n}. For instance, polyethene is a polyolefin produced by polymerization of ethene. The other types of polyolefins include polypropene (from propene), polybutene (from butene) and so on. Commonly, polyethene and polypropene are called polyethylene (PE) and polypropylene (PP), respectively. Among them, PE (HDPE, LLDPE and LDPE; they will be briefly explained in **Section 1.3**) is the most produced polymer which had a market share of approximately 38 % in 2010 (*Figure 1-1*). General detail in the differences and structures of these polymers is given in **Section 1.2** (Classification of polyethylenes).

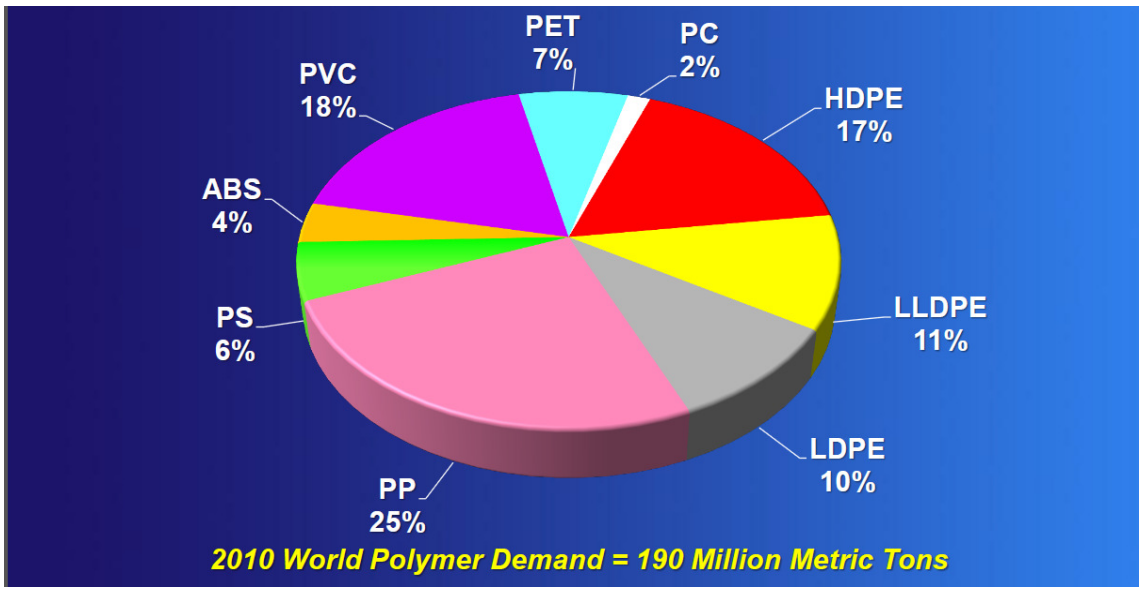

Figure 1-1. Global plastics consumption in 2010[1]

Polyolefins are non-polar, odorless and nonporous materials that are used in consumer goods, structural plastics, food packaging, textiles and industrial products. As polyolefins are capable of keeping goods safe from moisture, dust, and static, they also can be applied in higher-end consumer goods like compact disks (CDs) and electronics, and in a diverse range of fields over the world.

Due to the broad application of polyolefins, the global consumption of polyethylene reached 129 million metric tons (m.t.) in 2012 and is forecasted to grow 4 % annually for the next 5 years according to an iHS report[2] (*Figure 1-2*). This represents nearly 6 million m.t. per year of demand growth, which would result in total consumption near 158 million m.t. by 2017. To give a better understanding of the volume of the annually produced polyethylene in 2012, it was calculated that it corresponds to 59 times of the great pyramid of Giza in Egypt.[3]

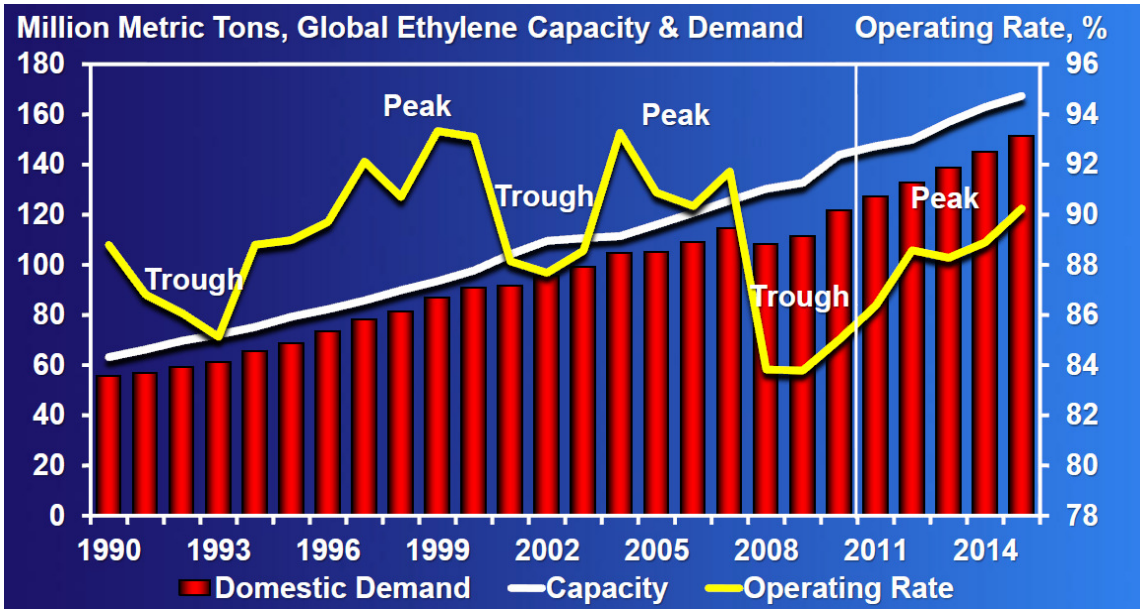

Figure 1-2. Global capacity & demand of polyethylene[1]

1.2 General history of polyolefins

The history of polyolefins started with "serendipity" by a German scientist, Hans von Pechmann. He discovered a white waxy resin accidentally at the end of the 19th century while working with a form of methane in ether. In 1900, his colleagues, Eugene Bamberger and Friedrich Tschirner identified the white waxy resin contained long methylene chains, and it was "polymethylene" that is very close to "polyethylene". However the resin, Mr. Pechmann had discovered, was difficult to process and had no practical value. After 34

years from the first accidental discovery of polymethylene, two British organic chemists at Imperial Chemical Industries (ICI) in Northwich, England, Eric W. Fawcett and Reginald O. Gibson had found a part of an autoclave covered with a waxy substance during working with ethylene gas at high pressures. Upon applying several hundred atmospheres to a mixture of ethylene and benzaldehyde in the autoclave, the white and waxy resin was produced. However, it was difficult to reproduce the reaction since the reaction was initiated by trace amounts of oxygen contaminated in their glassware. Thus it was not easy to control the amount of oxygen corresponding to the ethylene gas until 1935. Another scientist at ICI, Michael Perrin had developed a reproducible process for polyethylene synthesis which was performed under high pressures up to 1500 bar and at temperatures up to 250 degrees Celsius. It became the foundation for industrial production of low density polyethylene (LDPE). Its first commercial application came during World War II (WW II). The British used it as electrical insulation for vital military applications in radar because the polymer was an ideal material for coating telecommunication systems to be laid on the ocean floor. It met the requirements due to its high dielectric constant, low dielectric loss at high frequencies, high moisture resistance and excellent flexibility. Thus the substance, LDPE contributed to the Allied victory in WW II and was highly classified during WW II. After the war, research was continued on the ICI process. DuPont started LDPE production with commercial scale under licensing from ICI in 1942.[4]

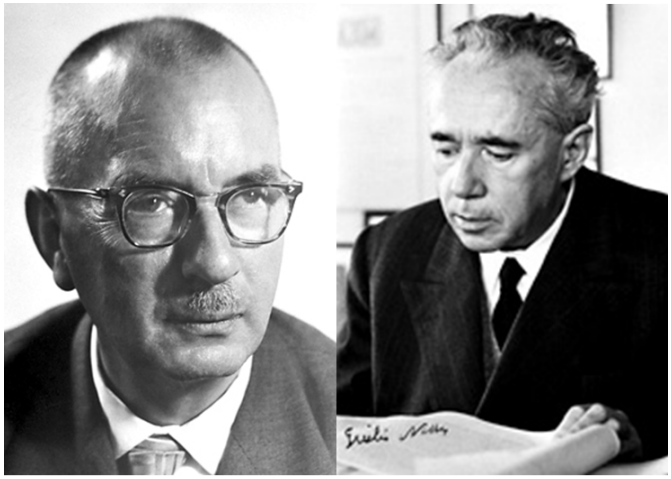

Figure 1-3. Photo of the Ziegler-Natter process discovers, Karl Ziegler[5] (left) and Giulio Natta[6] (right)

Thereafter, in the early 1950s, chromium oxide-based catalysts for ethylene polymerization had been discovered by workers at Phillips Petroleum.[7] The catalysts, generally known as Phillips catalysts, were highly effective for the ethylene polymerization at lower

temperatures as compared to the ICI process.[8] Later, in 1953 a German scientist, Karl Ziegler (*Figure 1-3*) at the Kaiser Wilhelm Institute (renamed to Max-Planck-Institute für Kohlenforschung), Mülheim an der Ruhr and Erhard Holzkamp developed a new process for the synthesis of high density polyethylene (HDPE).[9, 10] The process (commonly known as Ziegler process) employed a catalytic system consisting of a mixture of titanium trichloride (α-$TiCl_3$) and an alkylaluminum derivative (*e.g.* Et_2AlCl). The catalytic system helped to decrease the operating pressures dramatically (~ 100 bar). As early as 1955, further development was made by an Italian scientist, Giulio Natta (*Figure 1-3*) who extended the method to other olefins and developed further variations of the Ziegler process.[11-13] He reported propylene polymerization by the combination of crystalline α-$TiCl_3$ and triethylaluminium ($AlEt_3$) as a cocatalyst.[11, 12] The discovery of in a stereo-regulated isotactic polypropylene (iPP) by Natta was the first example that nature can be mimicked to create stereo-specific structures like that of natural polymers. These two historical discoveries are together called the Ziegler-Natta process (Z/N process). Due to their contribution to the development of polyolefins, they were awarded the Nobel Prize for Chemistry in 1963. Furthermore, remarkable development in a vast range of polyolefin materials and global production followed. In 1958, the Japanese chemical company, Sumitomo Chemicals, started to produce polyolefins at a commercial scale. Hanhwa Petrochemical in South Korea built up a plant for polyolefin production in 1973. Such a successful commercialization of polyolefins led to the greater research in the Z/N process to understand the mechanism.

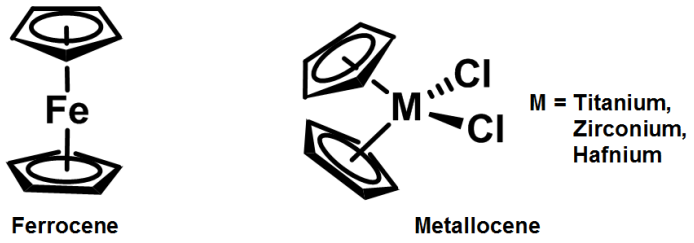

Figure 1-4. Chemical structure of ferrocene and metallocene

To elucidate the Z/N process, development of single site catalysts is considered. Thus complexes of titanium, such as Cp_2TiCl_2, are synthesized with η^5-coordinated cyclopentadienyl (Cp) units, which results in a similar structure to ferrocene (*Figure 1-4*). Activated titanium complexes with trialkylaluminum as a cocatalyst for the Z/N process have low activity towards ethylene and show no activity for propylene. Thus, its industrial application is limited. In 1974, however, Sinn and Kaminsky observed the enhanced

activity in weakly active catalytic system ($Cp_2ZrMe_2/AlMe_3$) by addition of water, although water is ironically known as a poison to the Z/N process. In 1980s, they reported very high activities of single-center catalysts with a combination of methylaluminoxane (MAO), which is formed by partial hydrolysis of $AlMe_3$. The revolutionary discovery of MAO as a cocatalyst for metallocenes ignited an intensive research in the area of metallocene catalyst development and immobilization. As a result, ExxonMobil commercialized metallocene-based polyolefin production in 1991. Another turning point in the polyolefin industry was the synthesis of isotatic polypropylene (iPP) using C_2-symmetric metallocenes, discovered by Brintzinger.[14] By further modifying the ligand structure of C_2-symmetric metallocenes, stetreoseletvity and thermal stabilities were enhanced. During the 1990s, a considerable amount of research has been carried out on non-metallocene catalysts (known as "post-metallocenes") involving late-transition metals.[15-18] The latest development in the catalytic polymerization of olefins has emerged with the discovery of post-metallocenes based on dimine complexes of nickel and palladium and of phenoxy-imine complexes of zirconium and nickel. Discovery of highly active α-diimine nickel catalysts, which can produce branched polyethylene with only ethylene (without using comonomers) by a "chain-walking" mechanism, triggered further research in post-metallocenes.[19-21] Interestingly, post-metallocene complexes with late transition metals (Ni, Pd) are capable of synthesizing functionalized polyolefins due to their higher resistance against polar groups, as compared to that of early transition metals (Ti, Zr, Hf).[18, 22] Later, development of group 4 transition metal complexes having bis(phenoxy-imine) ligands, known as FI catalysts, were reported.[23] Theses catalysts yield ultra high molecularweight polyethylenes (UHMWPE) with an extremely high molecular weight (>2 million $g \cdot mol^{-1}$) and a narrow molecular weight distribution.[24, 25] More recently, developments in synthesis of polycarbonates and polyketones with post-metallocene catalysts are of great interest in industry and academia.[26, 27] More details in these catalytic systems such as Z/N, Phillips, metallocene and post-metallocene complexes are further described in **Section 1.4**.

1.3 Classification of polyethylenes

As polyethylenes (PEs) represent a major demand in the global polymer market (*Figure 1-1*), better insight in the classification of PEs is necessary. Depending on the density and branching, PEs can be generally classified as low density polyethylene (LDPE), high density polyethylene (HDPE) and linear low density polyethylene (LLDPE). There is one more polyethylene named ultra-high molecular polyethylene (UHMWPE) which is a HDPE with a molecular weight between 2 and 10 million g/mol. A general structure of the PEs is

featured in *Figure 1-5*. A specific description of the each PEs is followed by the order of development.

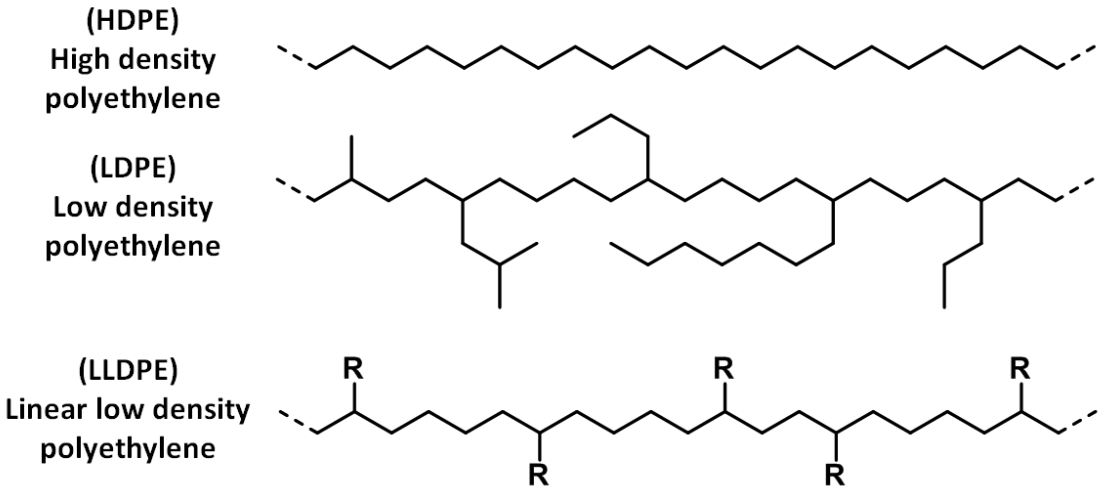

Figure 1-5. General structures for the various classifications of polyethylenes

1.3.1 Low density polyethylene (LDPE)

Low density polyethylene (LDPE) is exclusively synthesized by a radical polymerization whereas other types of polyethylene are produced by metal-catalyzed polymerization. As aforementioned, LDPE was discovered at ICI in 1930s and is the first practically produced polyethylene in the early 1940s. This polymer is made by a radical polymerization using initiators under critical conditions and thus branches are created due to intramolecular and intermolecular chain transfer during polymerization. It is made using supercritical ethylene (T: 282.4 K, P: 50.4 bar) under severe polymerization conditions in (i) autoclaves (1500 – 2000 atm, 180 – 290 ºC) or (ii) tubular reactors (1500 – 3500 atm, 140 – 180 ºC). Due to the harsh conditions, LDPE has uncontrolled lengths of branches induced by side reactions, such as a "back-biting" mechanism[28, 29] and chain transfer to polymer backbones of short chain branches (SCB) and long chain branches (LCB), respectively (*Figure 1-6*). The total number of side chains can range from 15 − 30 per 500 monomer units (1000 C atoms) depending on the polymerization conditions.[30]

During the propagation step, the active center (radical) is transferred from the end of the growing chain to a position on one of the ethylene carbons and the process continues forming longer and longer polyethylene chains. For introducing SCBs, the radical is transferred from the end of the growing chain to a position along the back of the chain and chain growth proceeds from this position. For LCB introduction to the polymer backbone,

the radical is transferred from the end of the growing chain to a position on a dead chain that allows that chain to begin forming a long chain branch.

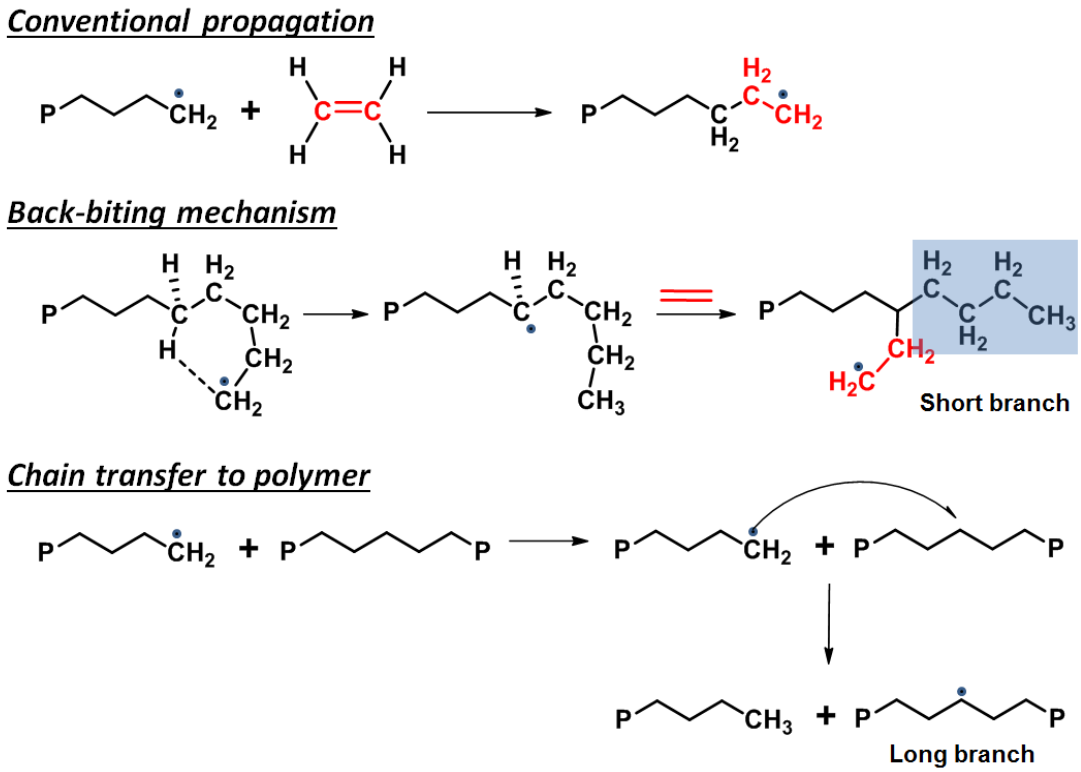

Figure 1-6. A typical propagation mechanism for free radical polymerization of LDPE

1.3.2 High density polyethylene (HDPE)

Until the 1950s, only type of polyethylene produced was low density polyethylene (LDPE). Since Karl Ziegler was trying to perform the polymerization under mild conditions, a great contribution to producing high density polyethylene (HDPE) is made. Generally, HDPE is made with Ziegler-Natta (Z/N) catalysts or Phillips catalysts in a conventional slurry process (See **Section 1.5** for processes). This class of polyethylenes has a totally different structure from LDPE. HDPEs have a much lower degree of branching (0.5 − 3 side chains per 1000 C atoms) when compared with LDPE (15 − 30 side chains per 1000 C atoms). Due to the fact that chain transfer to polymer is not possible in coordination polymerization, long chain branches are limited. Thus HDPEs are referred to as linear polyethylenes. Difference between LDPE and HDPE is the degree of branching which determines its mechanical properties. For instance, low degree of branching in HDPE is more crystalline (70 − 90 %) compared to the case of LDPE (40 − 60 %). This increases polymer density (0.94 − 0.96 g/mL *vs.* 0.91 − 0.93 g/mL) and crystalline melting temperature (133 − 138 ºC *vs.* 105 − 115 ºC).

1.3.3 Linear low density polyethylene (LLDPE)

Linear low density polyethylene (LLDPE) is similar to low density polyethylene (LDPE) but the topology of long chain branches (LCB) is distinct from that of LDPEs. LLDPE can be only produced by coordination catalysts of Phillips type, Z/N and metallocenes. Among them, Z/N systems are still the predominant type for LLDPE production. LLDPE is a copolymer of ethylene with α-olefins (generally small amounts of 1-butene, 1-hexene, or 1-octene) which determine the precise length of branches with much better control. This method of polymerization incorporates short side-chains or branches on the ethylene backbone and the resulting polymers, linear low-density polyethylenes, were first developed commercially in the late 1970s. The properties of LLDPE are very similar to that of LDPE which is now being supplanted by LLDPE. However, many of the desirable properties of LDPE can not be achieved by LLDPE due to the absence of LCBs. By the development of LLDPE, the economics of the low pressure, solvent-free process eliminate the need to build new high-pressure plants. Note that PE products with even lower densities, 0.88 g/cm^3, are sometimes called "very low-density polyethylene" (VLDPE) but are chemically identical to LLDPE. More recently, development of LLDPE synthesis without using α-olefins, known as "tandem catalysis", is reported by employing two metallocene catalysts: one for ethylene oligomerization and the other for copolymerization of ethylene with the oligomers. This is further discussed in **Chapter 5**.

1.3.4 Ultra high molecular weight polyethylene (UHMWPE)

Ultra high molecular weight polyethylene (UHMWPE) is a HDPE which has extremely high molecular weight (over 2 million g/mol) with a narrow molecular weight distribution. As a result, UHMWPE is a very tough material and has the highest impact strength among all thermoplastics. Although the polymer has no branches, the density is determined as only 940 kg/m^3, because the extremely high viscosity hinders the crystallization process. As it is difficult to process, studies in encapsulating UHMWPE with LLDPE to increase elasticity is described in **Chapter 6**.

1.4 Catalytic systems

The nature of the titanium complexes in a Ziegler-Natta-catalyst or the chrominum complexes in a Phillips catalyst or (post-) metallocenes is decisive for the properties of the

polyolefin such as molecular weight, molecular weight distribution and degree of branching. As catalytic systems are important, a better understanding of the systems is required. Aside from radical polymerization of olefins, there are basically four main types of coordination catalytic system for polyolefin synthesis: 1) Phillips system, 2) Ziegler-Natta system, 3) metallocene catalysts and 4) post-metallocene catalysts. A general introduction of these systems is descried in this section.

1.4.1 Phillips systems

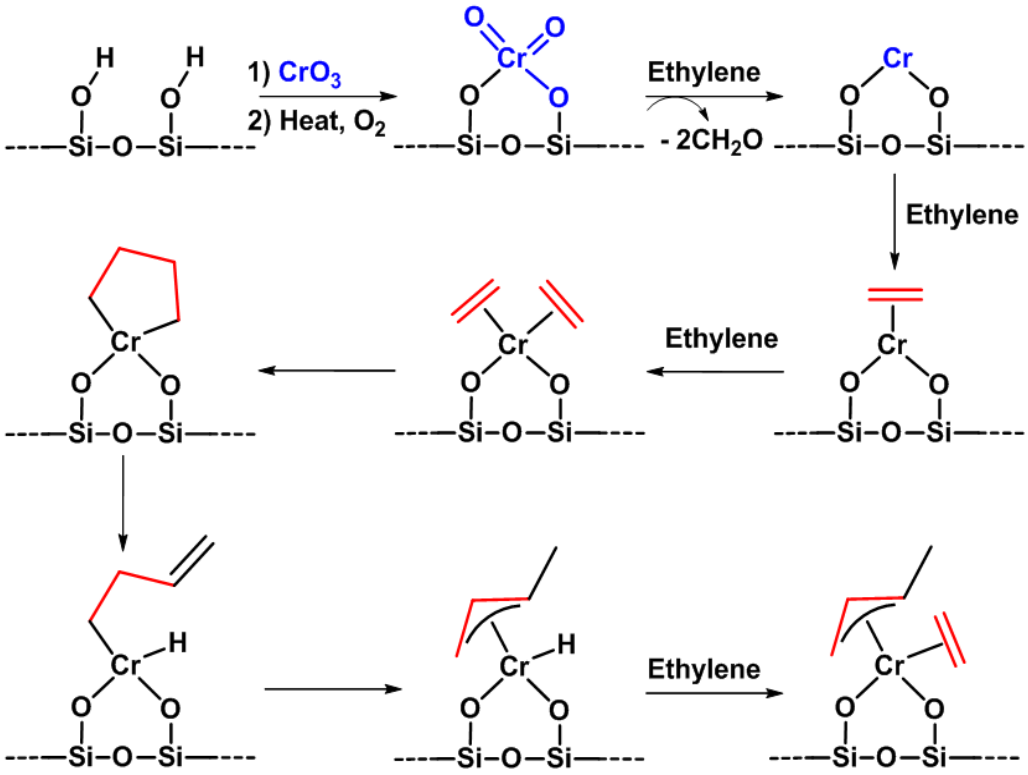

Figure 1-7. Phillips catalyst and its polymerization with ethylene

Phillips catalysts are chromium oxide-based complexes supported on silica or alumina for ethylene polymerization, which was discovered by Paul Hogan and Robert Banks at Phillips Petroleum in the early 1950s (*Figure 1-7*). The catalyst is prepared by adsorption of a chromium compound, mostly chromium trioxide, onto an amorphous silica support and subsequent reduction by exposure to ethylene. The catalyst does not require addition of chemical activators before the polymerization, since the active site is produced prior to the polymerization by thermal activation at high temperatures (*e.g.* 600 °C). However, performance of some chromium catalysts developed in the 1970s − 1980s is improved by metal alkyls.[31, 32] Due to the relatively simple preparation procedure and no-need for an

activator (cocatalyst), they are still used to produce more than 30 % of polyethylene worldwide. The Phillips systems produce various types of high density polyethylene (HDPE) with particularly high molar mass but are incapable of polymerizing propylene.

1.4.2 Ziegler-Natta systems

Table 1-1. Generations of Ziegler-Natta catalysts for propylene polymerization[33, 34]

generation (year)	**catalyst composition**	**productivity**[a] kg_{PP}/g_{Cat}	**isotactic index** %	**mmmm** %	M_w/M_n
First (1954)	α-$TiCl_3 \cdot 0.33AlCl_3$ + $AlEt_2Cl$	2 – 4	90 – 94		
Second (1968)	α-$TiCl_3 \cdot AlEt_2Cl$	10 – 15	94 – 97		
(1970)	$MgCl_2/TiCl_4$ + AlR_3	15	40	50 – 60	
Third (1971)	$MgCl_2/TiCl_4$/benzoate + AlR_3/benzoate	15 – 30	95 – 97	90 – 94	8 – 10
Fourth (1980)	$MgCl_2/TiCl_4$/phthalate + AlR_3/silane	40 – 70	95 – 99	94 – 99	6.5 – 8
Fifth (1988)	$MgCl_2/TiCl_4$/diether + AlR_3	100 – 130	95 – 98	95 – 97	5 – 5.5
	$MgCl_2/TiCl_4$/diether + AlR_3/silane	70 – 100	98 – 99	97 – 99	4.5 – 5
"Next" (1999)	$MgCl_2/TiCl_4$/succinate + AlR_3/silane	40 – 70	95 – 99	95 – 99	10 – 15

a) Polymerization conditions: liquid propylene, 70 °C, H_2

Since the first discovery of the Ziegler-Natta (Z/N) system in 1953 by Karl Ziegler and further development by Giulio Natta to the stereospecific polymerization of propylene (isotactic polypropylene) in industrial production, various modifications of the system allow for its continuing dominance in the polyolefin market (*Table 1-1*). For instance, introducing $MgCl_2$ as a support to $TiCl_4$-based catalyst (2nd generation) exhibited improved productivities over the first generation of the Z/N system (*Table 1-1*). Please note that this heterogenization of the Z/N system innovated production process in terms of morphology control, improved processablitiy and handling of the final product.

Although productivity of the Z/N system was enhanced to 15 kg of polypropylene per gram of catalyst (kg_{PP}/g_{Cat}) by heterogenization with $MgCl_2$ as a support, this benefit did not outweigh the need for an additional process such as either de-ashing step or extraction of final polymer. As a result, removal of the catalytic compounds which acted as impurities in the final product was necessary. The major objective was thus to develop high activity catalysts, which resulted in low catalyst residues in the final polymer. Throughout the developments over the few decades (*Table 1-1*), Z/N catalysts have been modified by combination with different additives (internal and external donors) which have resulted in high productivities (> 100 kg_{PP}/g_{Cat}) that an additional removal procedure of catalyst compounds from the obtained polymer has been eliminated economically impractical. Furthermore, by introduction of the donors to Z/N system, stereoselectivity has been dramatically improved (~ 99 %).

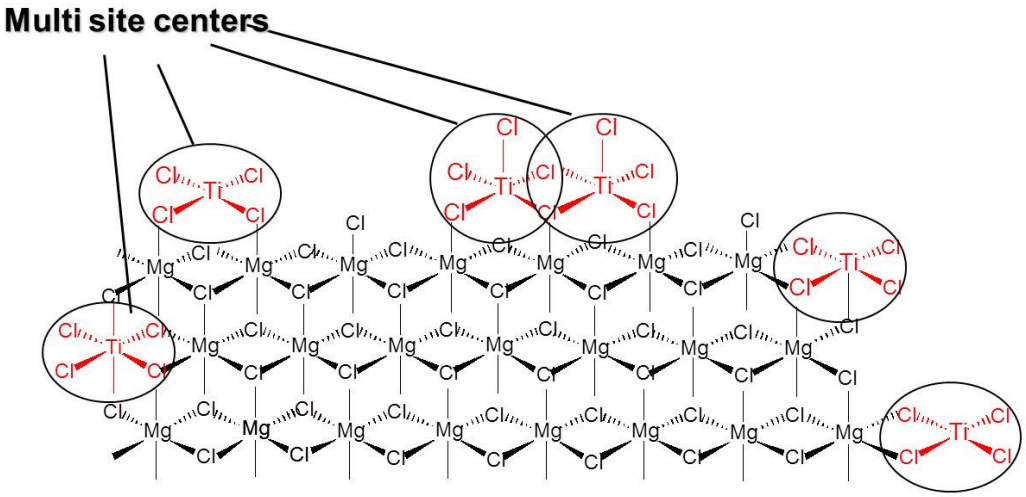

Figure 1-8. Multi-site active centers in Ziegler-Natta catalyst[35]

As Z/N systems are achieved by adsorption of $TiCl_4$ on a crystal surface of $MgCl_2$, $TiCl_4$ can be bound in a different way which results in a multi-site catalyst (*Figure 1-8*). Due to the different activities of multi-active site, relatively broad molecular weight distributions of polyolefins are obtained. Despite this drawback, however, Z/N catalysts are still the dominant catalyst systems in commercial polyolefin production.

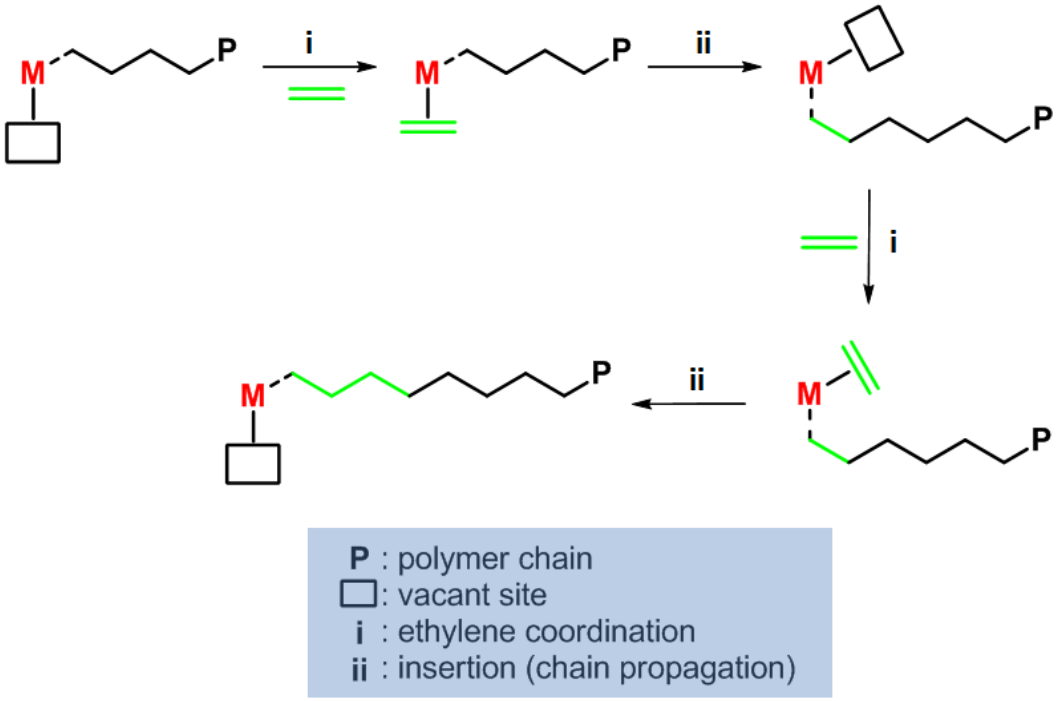

Figure 1-9. Cossee-Arlman mechanism for olefin polymerization

For better understanding of olefin polymerization with Z/N systems, Cossee and Arlman proposed a monometallic mechanism for olefin polymerization using Z/N process, wherein the active center contains a transition metal-carbon bond (*Figure 1-9*).[36-38] This mechanism is also applied to the olefin polymerization with metallocene complexes.

1.4.3 Metallocene and post-metallocene complexes

Metallocene has a similar structure with ferrocene and is a generic term for a transition metal complex bearing one or two η^5-coordinated cyclopentadienyl (Cp) groups to the central metal (*Figure 1-4*). As a result, metallocene has a single active site in contrast to the Z/N system. The unique nature of "single-center" catalysts leads to uniformity in the metallocene-catalyzed polyolefin synthesis in terms of narrow molecular weight distributions. In addition, metallocene is typically soluble and therefore can be used as either a homogeneous catalyst or supported on inert carriers such as silica, alumina, and magnesium chloride (more detail about immobilization is described in **Section 1.6**).

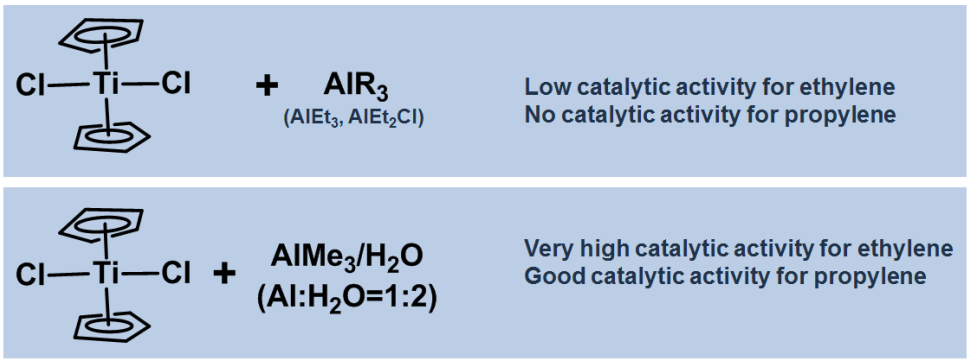

Figure 1-10. Metallocene activation with alkylaluminum without and with water presence

In 1957, the progress in metallocenes was initiated by the observation of Natta and Breslow that the homogeneous Cp_2TiCl_2/AlR_3 (*e.g.* $AlEt_2Cl$, $AlEt_3$) system could produce polyethylene (*Figure 1-10*).[39] Although it showed low activity, this system is more suitable for basic research on the chemical nature of the heterogeneous Z/N catalysts, since Ziegler catalysts for ethylene polymerization are generally insoluble in the reaction medium.[3, 39] Due to this low activity, however, metallocene complexes have gained less commercial interest. Lately, the recognition of the importance of water presence in the Cp_2TiCl_2/AlR_3 system[40] led to the great discovery of a powerful cocatalyst, methylaluminoxane (MAO).[41] (see also **Chapter 8** about cocatalysts) Active species of the metallocene/MAO system have featured high activities in polymerization of both ethylene and propylene. This discovery has ignited intensive research in metallocene complexes for olefin polymerization.

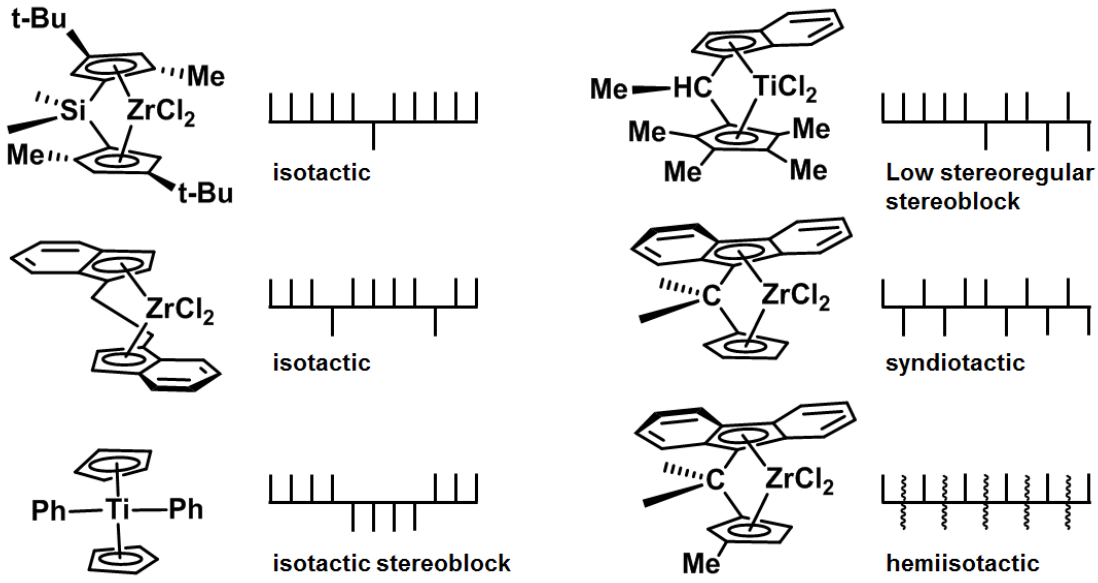

Figure 1-11. Correlation of polypropylene microstructures with metallocene structures

The most attractive point of metallocene catalysts is the easy tailoring of the microstructure of obtained polyolefins (in particular, polypropylene) by convenient substitution of the cyclopentadienyl group(s) with larger aromatic one(s) such as fluorenyl or benzindeneyl and by bridging them with silylene or alkylene moieties (*Figure 1-11*). For instance, bridged ethylene bis(indenyl)complexes (commonly known as *ansa*-metallocenes) were first prepared by Brintzinger and co-workers in 1982. By applying these metallocenes to propylene polymerization, different tacticities of polypropylene (atactic, isotactic, syndiotactic or hemitactic) are obtained depending on the ligand structure of the catalysts (*Figure 1-11*). Such properties of metallocene systems, high catalytic activity, narrow range of molecular masses of the obtained polyolefins and the possibility of controlling the catalytic properties by variation of ligand structure have further stimulated their broad industrial production.

As briefly outlined in *Figure 1-12*, revolutionary developments in synthesizing new types of metallocene complexes have been made since the discovery in 1957 that biscyclopentadienyltitanocene dichloride (Cp_2TiCl_2) when activated with alkylaluminum chlorides (AlR_3) was a competent ethylene polymerization catalyst. In 1986, mono-cyclopendienyltitanium chloride ("half-metallocene") affords the synthesis of syndiotactic polystyrene (sPS) firstly with metallocene complex.[42] In 1992, Dow reported a totally new type of metallocene complex named "constrained geometry catalyst" (CGC) as versatile catalyst in polyolefin synthesis. In particular, the CGC can produce high density polyethylenes with high activity and linear low density polyethylene with high α-olefin incorporations.[43] In 1995, Waymouth reported the synthesis of isotactic–atactic block polypropylene using the bis(3-phenyl)indenyl zirconium dichloride/MAO system.[44]

After the successful development in metallocene catalysts, the exploration of other transition metal complexes bearing non-cyclopentadienyl (Cp) ligands has led to further research in the catalytic polymerization of olefins.[45] It has come up with the discovery of "non-metallocene" single site catalysts (known as "post-metallocenes") based on dimine complexes of nickel and palladium and of phenoxy-imino complexes of zirconium and nickel.[15-17] Highly active nickel complex with a ligand of α-diimine discovered by Brookhart has initiated intensive research in post-metallocenes.[19-21] The most outstanding property of the nickel complexes is that they are capable of producing branched polyethylene by a "chain-walking" mechanism[46] leading to polyolefins having short chain branches (SCB) in the absence of α-olefin comonomers (*Figure 1-13*).

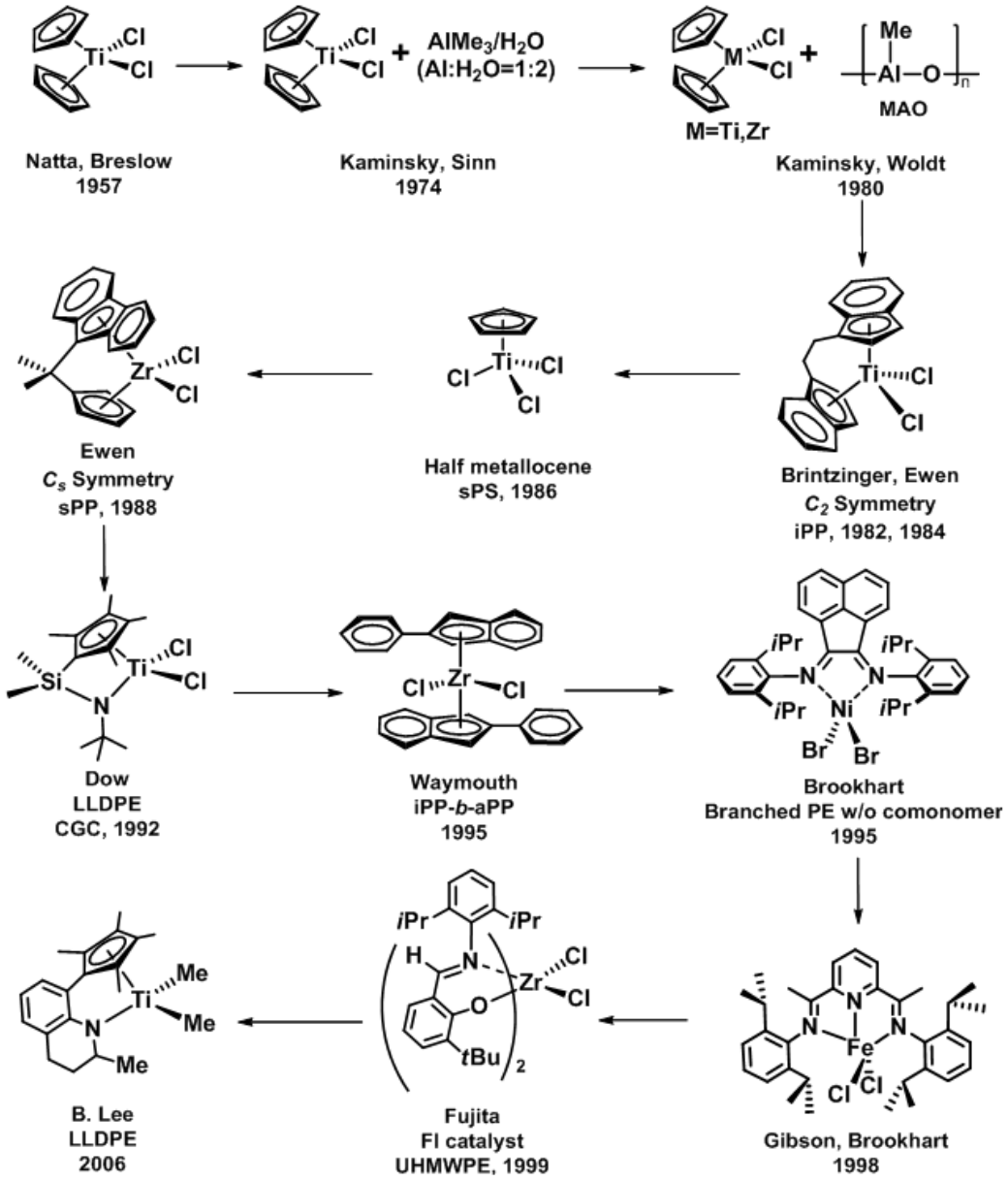

Figure 1-12. Revolutionary development of homogeneous metallocene catalysts for olefin polymerization[47]

In the last two decades, post-metallocene catalysts for olefin polymerization have been developed based on bis(imino), bis(imino)pyridyl, bis(phenoxy-imino), bis(pyrrolylimino) and other complexes of transition metals.[22, 48-51] Furthermore, post-metallocenes with late transition metals (Ni, Pd, Co) can produce polar polyolefins due to the lower oxophilicity of late transition metals, compared to that of metallocenes (Ti, Zr, Hf).[22, 52-54] In parallel, early transition metals bearing non-Cp ligands have been studied. In 1999, Fujita reported phenoxy-imine zirconium catalysts (FI catalysts, originated from Japanese pronunciation of phenoxy-imine) for the production of polyethylene with extremely high molecular weights (Over 2 million $g \cdot mol^{-1}$) and narrow molecular weight distribution.[23, 48, 55] Later, intensive research in the group of Lee led to the development of *ortho*-phenylene-bridged titanium

complexes.[56, 57] For the synthesis of LLDPE, they display a higher comonomer incorporation, activity and molecular weight, as compared to the one from the Dow's CGC.[56, 57]

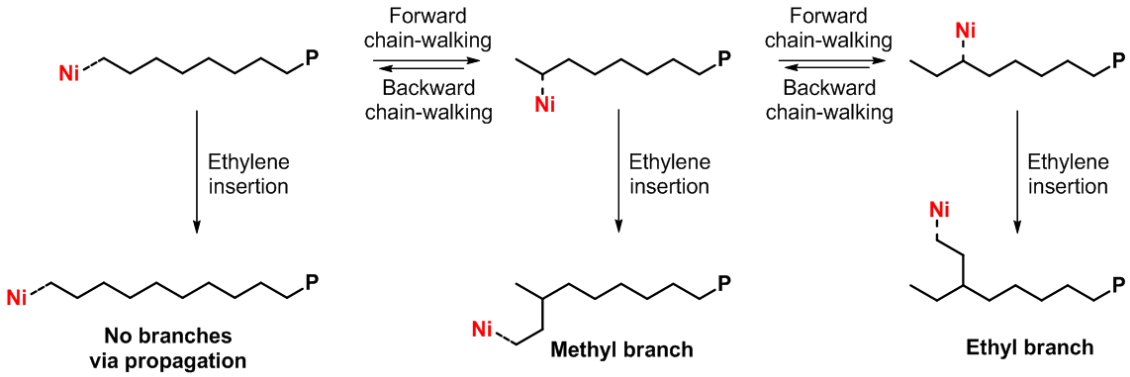

Figure 1-13. Chain walking mechanism with a nickel complex for introducing short chain branches (SCB) to polymer chain

More recently, post-metallocene catalysts have led to new synthetic methods to produce various polymers such as polycarbonate. In view of atom efficiency, polycarbonate can be synthesized using epoxides and carbon dioxide (CO_2). In 1969, Inoue reported the copolymerization of epoxides and CO_2 in the presence of $ZnEt_2$ and water.[58] Thereafter, this discovery led to intensive research based on synthesis of diiminato-zinc, salen-chromium and salen-cobalt complexes.[59, 60] However, their catalytic activities were unsuitable for commercialization. Recently, B. Lee and coworkers reported the synthesis of polycarbonate catalyzed by superactive salen-cobalt complexes (*Figure 1-14*).[61-63] The complexes have proven to be the most active catalyst for the copolymerization of CO_2 with epoxides towards the synthesis of polycarbonates hitherto.[27] As a result, it is transferred to a commercial production of SK Chemicals in South Korea.

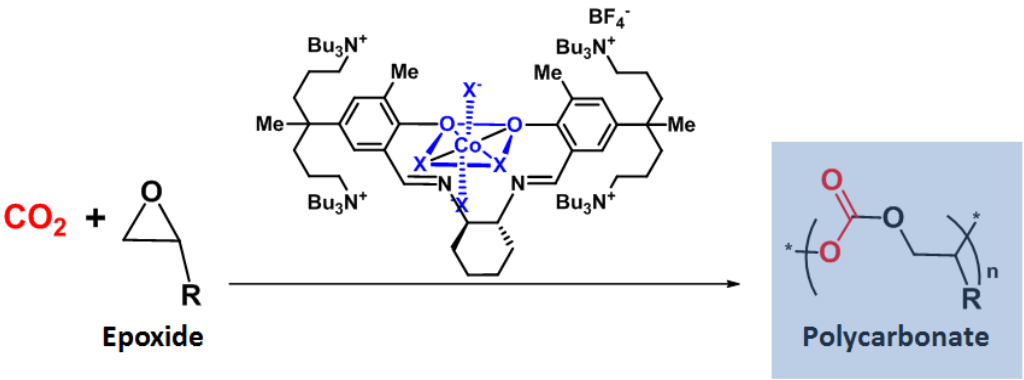

Figure 1-14. Chemical structure of salen-cobalt complex and copolymerization of epoxides and CO_2 towards polycarbonate

1.5 Processes

A brief overview of general processes in industrial polyolefin production is provided in this section. Commercial production of polyolefins utilizes four major types of processes such as radical (high pressure), solution-phase, gas-phase, and slurry-phase (*Table 1-2*). The first two processes (radical and solution-phase) are performed for homogeneous olefin polymerization under high pressure. By further developments in catalytic systems (*e.g.* hetereogenization Z/N system), slurry and gas-phase reactors have been utilized in order to perform olefin polymerization in heterogeneous media under milder reactor conditions. Each process is capable of producing particular polyolefins with versatile advantages in performance.

Table 1-2. Polymerization processes and reactor operating conditions[64]

reactor type	**radical process**	**solution-phase process**	**slurry process**	**gas-phase process**
	tubular or autoclave	CSTR	loop or CSTR	fluidized or stirred bed
reactor pressure [bar]	1200 – 3000	~ 100	2 – 25	20 – 30
reactor temp. [°C]	130 – 350	130 – 250	85 – 100	70 – 115
polymerization mechanism	Free radical	Coordination	Coordination	Coordination
location of polymerization	Monomer phase	Solvent	Solid	Solid

1.5.1 Radical process

As described in **Section 1.3.1.**, radical processes have the longest history among polymerization methods. This polymerization process is a free radical reaction which is initiated by oxygen or peroxides and affords production of low density polyethylene (LDPE) with short and long chain branches. Polyethylene with higher molecular weight can be obtained by increasing the polymerization pressure up to very high pressure (~ 3,000 bar). When the conversion of this process reaches to 20 %, it should be terminated due to the high viscosity in the reactor. The major advantage of the radical process is

allowing for the production of polyolefin films with high clarity, since there is no need to use a diluent (organic solvent) and an inert carrier.

1.5.2 Solution process

The solution process for polyolefin synthesis was first operated with the conventional Ziegler-Natta (Z/N) catalysts in the 1950s. It operates in a continuously stirred tank reactor (CSTR) with a solvent (generally, aliphatic hydrocarbon) under relatively high temperatures from 130 to 250 °C. This temperature range helps to keep the process in solution since polyolefins (PEs and PPs) stay in a melt. As a result, no additional procedure for removing the solvent is required, as the solvent can be vaporized and recycled due to the high temperature. In addition, it can shorten the reaction time (1 − 10 min) which increases productivity. However, by increasing the reaction time, solution viscosity linearly increases which is limiting high molecular weight polymers. Nowadays, solution-based technologies are mostly replaced by slurry and gas phase reactors. However, it still operates for synthesis of copolymers with a low softening point and/or high solubility. Especially, commercial production of ethylene copolymers with octene is exclusively limited to the solution process. Furthermore, it is capable of being utilized for production of emerging synthetic rubbers in the market such as ethylene-propylene-diene terpolymers (EPDM).

1.5.3 Slurry process

In contrast to radical and solution processes, the slurry process allows heterogeneous olefin polymerization under mild reaction conditions (> 100 °C and 2 − 25 bar). As olefin polymerization is an extremely exothermic reaction, removal of the generated heat effectively is a key-issue for the slurry process. The typical slurry CSTR process (*Figure 1-15*) is equipped with a cooling jacket to remove the heat generated during olefin polymerization. As the cooling jacket is insufficient for removal of heat from the diluent, additional cooling equipment is provided by supplying a heat exchanger and pre-cooled diluent. The slurry process is relatively expensive to build and operate due to the requirement of extra procedures such as centrifuging to remove the "heavy" diluent, recovery of the diluent and steam dryer. However, it is still used due to the robustness of the process.

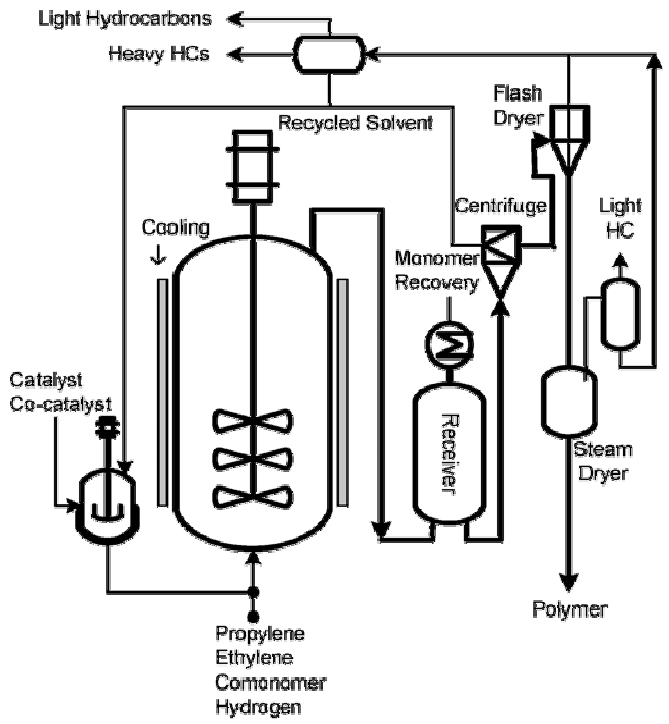

Figure 1-15. Schematic representation of the CSTR process[3]

In order to overcome the drawbacks in CSTR slurry, a loop slurry system was developed by Phillips Petroleum and has been exploited commercially since 1970. As shown in *Figure 1-16*, reactors are pipes equipped with multiple cooling jackets for improving heat removal. By increasing the ratio of surface area to volume, effective maintenance of the temperature during the reaction is achieved. To shorten the procedure, usage of "light" diluent (isobutane) is considered in this case. Although liquidized isobutane as a diluent creates the problem of poor solubility and solvent-induced swelling of the polymer particles, extra procedures can be eliminated by vaporizing the isobutane after polymerization.

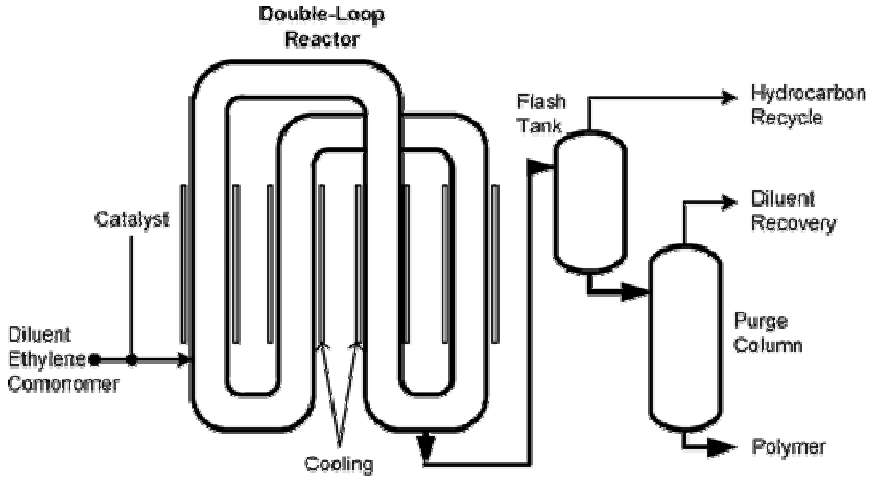

Figure 1-16. Schematic representation of the double slurry loop (Phillips) process[3]

1.5.4 Gas-phase process

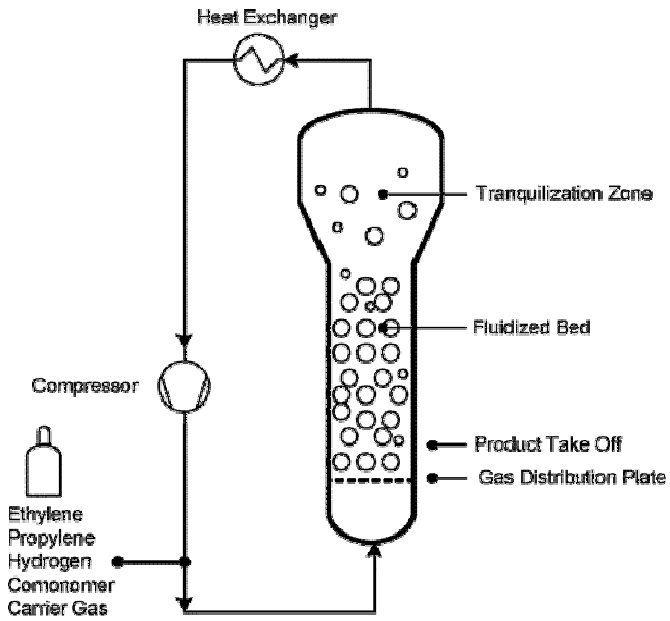

Figure 1-17. Schematic representation of a gas-phase polymerization process[3]

The gas-phase process was first developed by Union Carbide. A schematic representation of a gas-phase polymerization process is shown in *Figure 1-17*. In contrast to the highly pressurized ethylene polymerization, the gas-phase process needs just a few tenth pressure of ethylene without diluents. As a result, total energy consumption and cost of building up a plant are reduced to ¼ and ½, respectively. Furthermore, nearly the full range of polyethylene grades can be produced by the gas-phase processes. For these reasons, the gas-phase process has become the most dominant and widespread process in polyethylene production. For gas-phase ethylene polymerizations, immobilization of catalyst on support materials is mandatory. The catalysts-immobilized on particles are dispersed in a fluidized bed reactor which is a large cylinder reactor. In the reactor, the particles are fluidized by a gas flow with a carefully tuned strength to suspend the particles but not too fast to avoid blowing the particles out. However, gas phase processes have some disadvantages. In particular, heat removal from the reactor is critical because if the reactor is not properly cooled, agglomeration of the particles or chunk formation can result.

1.6 Support materials

Since most of the modern commercial polyolefin catalysts are heterogeneous Ziegler-Natta (Z/N) or Phillips systems, industrial mass polymerization is generally carried out either with a slurry process or as a gas-phase process. In order to achieve compatibility with current industrial facilities for polyolefin production, new catalytic systems, such as

metallocenes and post-metallocenes, must be supported. Although supporting a catalyst is leading to a heterogenization and generally reduces the catalytic activity, it provides advantages in terms of the morphology control of the polyolefins and preventing intermolecular catalyst deactivation (dimer formation).[65] To optimize the performance of the catalyst in this way, it has been shown that the amount of cocatalsyts (particularly MAO) is dramatically reduced as compared to homogeneous conditions. Controlling particle growth produces polymer particles with controlled shapes that replicate those of the starting catalyst particles and eliminate reactor fouling (sheeting of the reactor walls forms an isolating layer between the reaction medium and the cooled wall). As the selection of a support is profoundly crucial for improving final properties of polyolefin products, a brief overview of various supports and the requirements for support is described as follow.

1.6.1 Requirements for supports

The carriers (support materials) must have the following characteristics:[3, 66-70]

1. Spherical shape
2. Micrometer-ranged diameter
3. Narrow particle size distribution
4. Porosity
5. Mechanical properties : fragmentablity

These are practical reasons for these particular requirements. Spherical particles facilitate handling of the product after olefin polymerization since the final polyolefin products replicate the original morphology of the supports. Additionally, micrometer-ranged diameters and narrow size distributions of supports are required to prevent agglomeration of supports and to achieve regular size of the final products, respectively. High porosity of supports affords increased surface area which leads to more places for immobilized catalysts. Pores should also be interconnected (open-pore structure) so that the supports can be broken into small fragments during olefin polymerization. The catalyst carrier must be mechanically stable to avoid the formation of polymer fines (dust). On the other hand, it must be sufficiently fragile to undergo fragmentation into particles of sub-micrometer size by the hydraulic forces exerted by the growing polymer. Extensive fragmentation and uniform particle growth are key features in the replication process to achieve good morphology control.

1.6.2 Inorganic supports

There has been intensive research in inorganic supports such as silica,[71-74] alumina,[75] and magnesium chloride.[76, 77] Among them, amorphous and porous SiO_2 gels are most commonly applied as supports for MAO-activated metallocene catalysts, as they possess high surface area and porosity, good mechanical properties, and are stable and inert under reaction and processing conditions. To understand the silica particles, a general synthetic procedure is given in in *Figure 1-18*, commercially applied porous silica particles are agglomerates (*secondary particles*) composed of nanometer-sized non-porous granulates (*primary particles*).[78] These primary particles are commonly prepared by neutralization of aqueous alkali metal silicates with an acid.[79] The average sizes of the secondary particles, which should be in the micrometer-range, are mainly altered by the nozzle pressure of a spray drying process with the primary particles. This process is suitable for large-scale production.

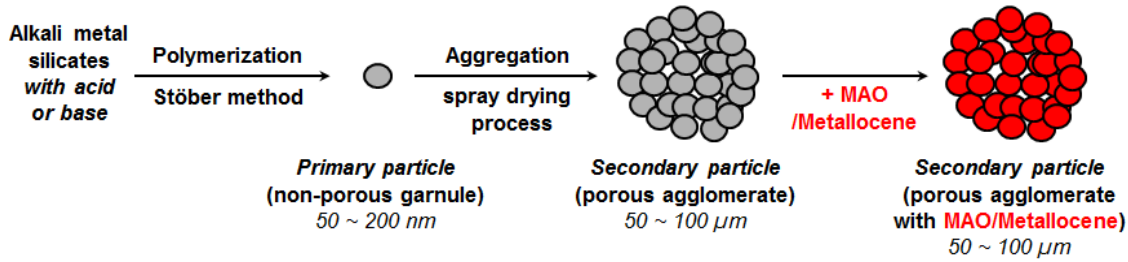

Figure 1-18. Schematic drawing for silica particle preparation

Immobilization of the catalysts can generally be categorized by these three different supporting methods:

1. Absorption on the support without pretreatment.[80] [81]
2. Chemical modification of silica with MAO[82], alkylaluminum[83], organosilanes.[84, 85]
3. In-situ synthesis of metallocenes on silica.[72]

1.6.3 Organic supports

Compared to inorganic supports, organic supports are relatively less studied. Since the middle of 1990s, usage of organic-based support materials has been considered for metallocene-supported polyolefin synthesis. Polystyrene (PS) is the most applied carrier and the methods of catalylst immobilization can be classified in four categories:[86]

1. Swelling process.

2. Post modification of a preformed PS support.
3. Copolymerization of styrene with a functionalized ligand.
4. Via non-covalent bonding.

1.6.3.1 Swelling process

One of the simplest ways of supporting metallocenes on organic particles is encapsulation of the metallocenes into polystyrene (PS) beads. The metallocene can be introduced in the gel-type particles by a simple swelling-shrinking process carried out in the presence of a solvent. By controlling the amount of divinylbezene as crosslinker, some properties such as swellabllity and mechanical strength of the PS can be altered. For instance, very low levels of crosslinker (< 1%) yield mechanically weak swollen resin networks, easily damaged by shear. On the other hand, highly crosslinked gel-type resin networks, although mechanically stronger, may swell too little even in a very 'good' solvent and not allow all networks to be penetrated and exploited.

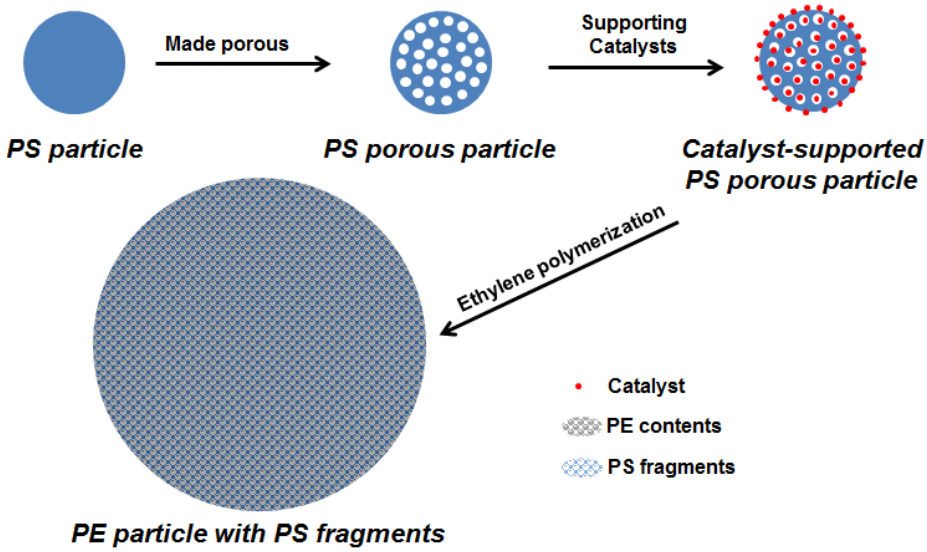

Figure 1-19. Schematic diagram for the preparation of a PE-PS blend

Collman et al.[87] reported that styrene copolymers crosslinked with 2 % of divinylbenzene are mobile enough to allow ligands attached to the polymer beads to act as chelates. Consequently, this copolymer is not rigid (solvent swelled) enough to prevent dimerization of attached unstable species (to bring nonadjustment sites together). Hong et al.[88] demonstrated a simple encapsulation technique to immobilize metallocene catalysts inside the gel type-PS particles by the swelling-shrinking characteristic of the PS support, because no complex chemical reactions are necessary. However, it is a potential problem of this

method that the enclosed catalyst easily falls off during polymerization. By controlling the amount of cross-linker (divinylbenzene), the influence of the swelling response of the poly(styrene-*co*-methyl methacrylate-*co*-divinylbenzene) particles/Cp_2ZrCl_2 was studied.[89] In addition, porous PS support particles were tested for metallocene catalyzed ethylene polymerization.[90]

1.6.3.2 Post-modification of a preformed PS support

By a post-modification of a preformed polystyrene (PS), metallocenes have been chemically linked to the PS. In particular, Grubbs and coworkers reported attachment of metallocene (Cp_2TiCl_2) on polystyrene (PS) bead via a step-wise chemical construction (*Figure 1-20*).[65] They observed the polymer-attached metallocene avoids dimerization of the reduced metallocene complexes. Soga et al. also demonstrated the preparation of polymer-supported metallocene catalysts (*ansa*-metallocene complexes) using lithiated polystyrene/2 % divinylbenzene copolymer beads.[91] Lately, Klapper et al. have introduced cyclopentadiene (Cp) unit(s) to PS resins for the irreversible attachment of metallocene which achieved by Diels-Alder reaction.[92, 93]

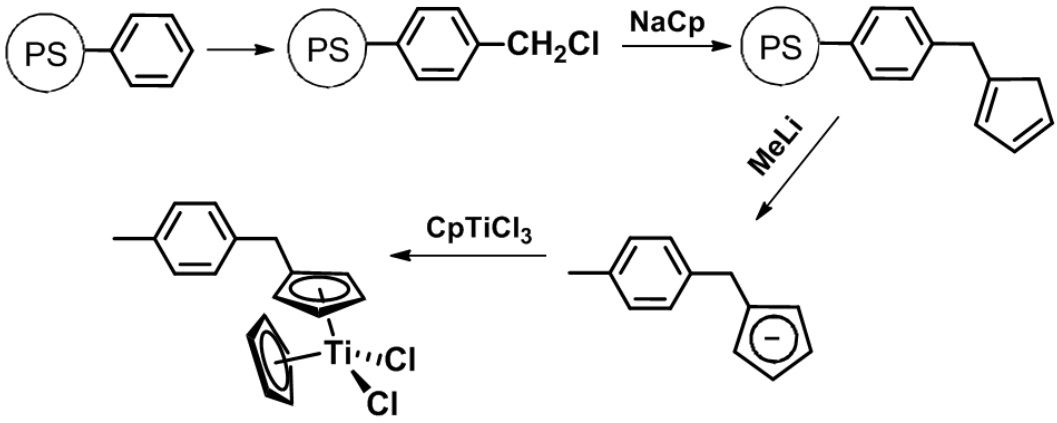

Figure 1-20. The attachment of homogeneous catalysts to polystyrene-divinylbenzene copolymer[65]

1.6.3.3 Copolymerization of styrene with a functionalized ligand

By a copolymerization of styrene with vinyl-functionalized metallocenes, polystyrene (PS) resin-bound metallocenes have also been produced. In particular, Hu et. al. prepared metallocene-bound PS resin by the copolymerization of styrene with *ansa*-zirconocene complex bearing an allyl substituted silane bridge in the presence of radical initiator (*Figure*

1-21).[94] Jin and coworkers also demonstrated metallocene complexes with an allyl group copolymerized with styrene.[95] Furthermore, copolymerization of styrene with a post-metallocene (iron-based catalyst) bearing one or two allyl groups is performed.[96]

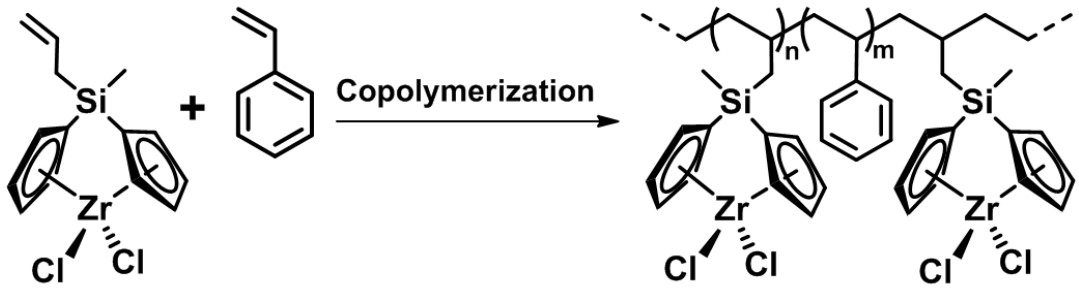

Figure 1-21. Allyl substituted silane bridged metallocene and resulting copolymer

1.6.3.4 Via non-covalent bonding

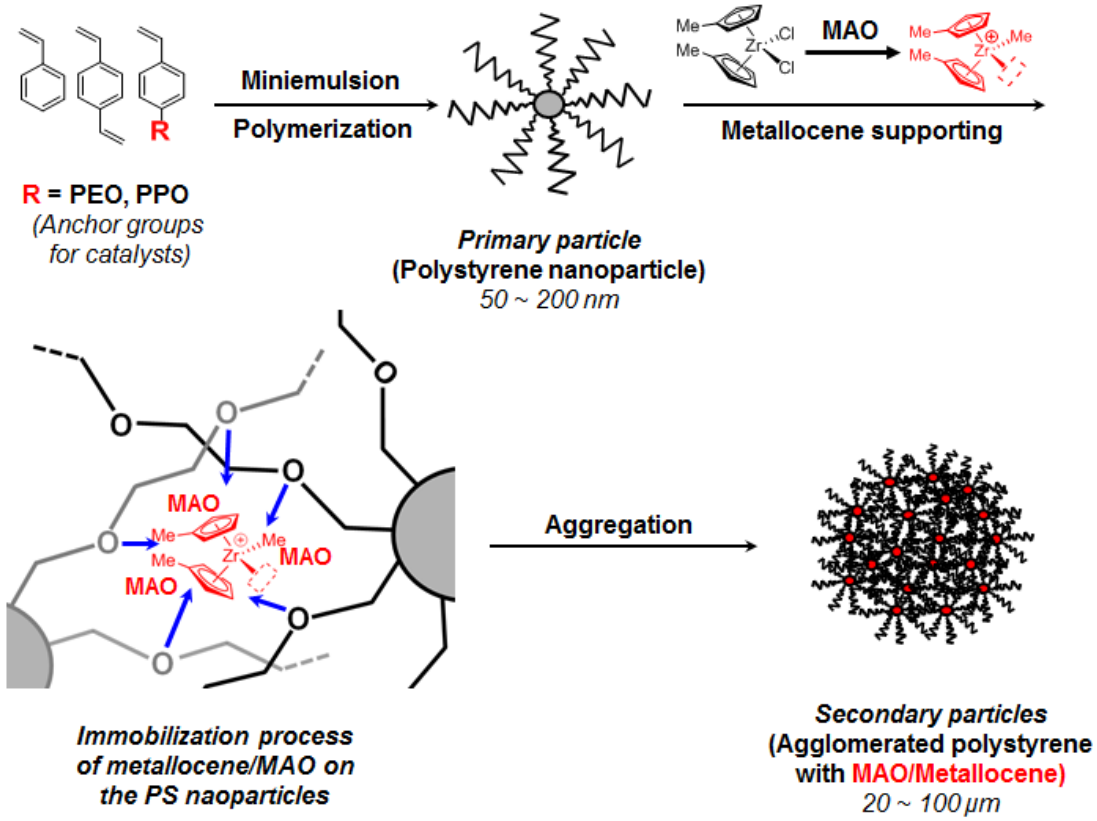

Figure 1-22. Immobilization procedure of a metallocene catalyst on PEO-functionalized PS nanoparticles

Supporting a metallocene via non-covalent bonding is a relatively new approach. As activated metallocene species have a cationic character, they can be immobilized via

nucleophilic interaction. Particularly, Roscoe et al. reported non-interacting polystyrene (PS) support from chlorobenzyl-PS resin towards weakly coordinating cocatalyst.[97, 98] Klapper et al. demonstrated olefin polymerization with the metallocene/PS particles covered by methoxy groups[99], poly(ethylene oxide) (PEO)[68, 100] or poly(propylene oxide) (PPO) chains.[101, 102] The nucleophilic groups enhance the affinity towards immobilization of the MAO/metallocene complexes through nucleophilic aluminum–oxygen interactions. Furthermore, pyridine groups were introduced to remove trace amounts of trimethylamine (TMA) that originate from MAO and also hamper activation of post-metallocenes.[103]

1.7 References

[1] *http://www.polyacs.net/Workshops/11Polyolefins/images/Presentations/Rappaport.pdf*.

[2] R. Westervelt, *http://www.chemweek.com/* **March 21, 2013**, *IHS WPC: Ethylene profit outlook muted by weaker demand, supply surge: Eramo.*

[3] J. R. Severn, J. C. Chadwick, R. Duchateau, N. Friederichs, *Chemical Reviews* **2005**, *105*, 4073.

[4] *"Poly – The All Star Plastic". Popular Mechanics (Popular Mechanics Company): P. 126* **July 1949**.

[5] *https://en.wikipedia.org/wiki/Karl_Ziegler.*

[6] *https://en.wikipedia.org/wiki/Giulio_Natta.*

[7] R. L. B. J. P. Hogan, *U.S. Patent 2,825,721* **1958**.

[8] M. P. McDaniel, "Supported Chromium Catalysts for Ethylene Polymerization", in *Advances in Catalysis*, H.P. D.D. Eley and B.W. Paul, Eds., Academic Press, 1985, p. 47.

[9] K. Ziegler, E. Holzkamp, H. Breil, H. Martin, *Angewandte Chemie* **1955**, *67*, 541.

[10] K. Ziegler, *Belgian Patent 533,362*.

[11] G. Natta, *Journal of Polymer Science* **1955**, *16*, 143.

[12] G. Natta, P. Pino, P. Corradini, F. Danusso, E. Mantica, G. Mazzanti, G. Moraglio, *Journal of the American Chemical Society* **1955**, *77*, 1708.

[13] G. Natta, M. Farina, M. Ragazzini, *Italian Patent Application 39004/56,* **1956**.

[14] H. H. Brintzinger, D. Fischer, R. Mulhaupt, B. Rieger, R. M. Waymouth, *Angewandte Chemie-International Edition in English* **1995**, *34*, 1143.

[15] W. Keim, F. H. Kowaldt, R. Goddard, C. Krüger, *Angewandte Chemie International Edition in English* **1978**, *17*, 466.

[16] W. Keim, R. Appel, A. Storeck, C. Krüger, R. Goddard, *Angewandte Chemie International Edition in English* **1981**, *20*, 116.

[17] U. Klabunde, R. Mulhaupt, T. Herskovitz, A. H. Janowicz, J. Calabrese, S. D. Ittel, *Journal of Polymer Science Part A: Polymer Chemistry* **1987**, *25*, 1989.

[18] T. R. Younkin, E. F. Conner, J. I. Henderson, S. K. Friedrich, R. H. Grubbs, D. A. Bansleben, *Science* **2000**, *287*, 460.

[19] L. K. Johnson, C. M. Killian, M. Brookhart, *Journal of the American Chemical Society* **1995**, *117*, 6414.

[20] S. D. Ittel, L. K. Johnson, M. Brookhart, *Chemical Reviews* **2000**, *100*, 1169.

[21] V. M. Möhring, G. Fink, *Angewandte Chemie International Edition in English* **1985**, *24*, 1001.

[22] S. J. Na, D. J. Joe, S. S, W.-S. Han, S. O. Kang, B. Y. Lee, *Journal of Organometallic Chemistry* **2006**, *691*, 611.

[23] H. Makio, N. Kashiwa, T. Fujita, *Advanced Synthesis & Catalysis* **2002**, *344*, 477.

[24] J. D. Scollard, D. H. McConville, *Journal of the American Chemical Society* **1996**, *118*, 10008.

[25] C. M. Killian, D. J. Tempel, L. K. Johnson, M. Brookhart, *Journal of the American Chemical Society* **1996**, *118*, 11664.

[26] J. H. Park, J. Y. Jeon, J. J. Lee, Y. Jang, J. K. Varghese, B. Y. Lee, *Macromolecules* **2013**, *46*, 3301.

[27] D. J. Darensbourg, S. J. Wilson, *Green Chemistry* **2012**, *14*, 2665.

[28] M. J. Roedel, *Journal of the American Chemical Society* **1953**, *75*, 6110.

[29] D. Stoiljkovich, S. Jovanovich, *Die Makromolekulare Chemie* **1981**, *182*, 2811.

[30] "*Principles of Polymerization, Fourth Edition.*", John Wiley & Sons, Inc.

[31] M. M. B. Beaulieu, and P. DesLauriers, *International Conference on Polyolefins, Society of Plastics Engineers, Houston, TX* **February 27, 2005**.

[32] F.J.Karol, *Encyclopedia of Polymer Science and Technology* **1976**, *Suppl. Vol. 1*, p. 120.

[33] Y. V. Kissin, "*Isospecific Polymerization of Olefins with Heterogeneous Ziegler-Natta Catalysts*", Springer-Verlag, New York, 1985.

[34] M. E.P., "*Polypropylene Handbook*", Jr. Hanser Publishers, München, 1996.

[35] V. Virkkunen, *Academic disseratation at University of Helsinki, Finland* **2005**.

[36] E. J. Arlman, *Journal of Catalysis* **1964**, *3*, 89.

[37] E. J. Arlman, P. Cossee, *Journal of Catalysis* **1964**, *3*, 99.

[38] P. Cossee, *Journal of Catalysis* **1964**, *3*, 80.

[39] G. Natta, P. Pino, G. Mazzanti, U. Giannini, E. Mantica, M. Peraldo, *Journal of Polymer Science* **1957**, *26*, 120.

[40] W. Kaminsky, H.-J. Vollmer, E. Heins, H. Sinn, *Die Makromolekulare Chemie* **1974**, *175*, 443.

[41] H. Sinn, W. Kaminsky, H.-J. Vollmer, R. Woldt, *Angewandte Chemie* **1980**, *92*, 396.

[42] N. Ishihara, T. Seimiya, M. Kuramoto, M. Uoi, *Macromolecules* **1986**, *19*, 2464.

[43] J. A. M. Canich, *U.S. Patent 5,0626,798* **1991**.

[44] G. W. Coates, R. M. Waymouth, *Science* **1995**, *267*, 217.

[45] G. J. Domski, J. M. Rose, G. W. Coates, A. D. Bolig, M. Brookhart, *Progress in Polymer Science* **2007**, *32*, 30.

[46] Z. Guan, P. M. Cotts, E. F. McCord, S. J. McLain, *Science* **1999**, *283*, 2059.

[47] S. Park, Y. Han, S. K. Kim, J. Lee, H. K. Kim, Y. Do, *Journal of Organometallic Chemistry* **2004**, *689*, 4263.

[48] Y. T. T. Fujita, M. Mitani, S. Matsui, J. Saito, M. Nitabaru, K. Sugi, H. Makio, T. Tsutsui, *EP 0 874 005, 1998*.

[49] B. L. Small, M. Brookhart, A. M. A. Bennett, *Journal of the American Chemical Society* **1998**, *120*, 4049.

[50] G. J. P. Britovsek, V. C. Gibson, S. J. McTavish, G. A. Solan, A. J. P. White, D. J. Williams, B. S. Kimberley, P. J. Maddox, *Chemical Communications* **1998**, *0*, 849.

[51] B. Y. Lee, H. Y. Kwon, S. Y. Lee, S. J. Na, S.-i. Han, H. Yun, H. Lee, Y.-W. Park, *Journal of the American Chemical Society* **2005**, *127*, 3031.

[52] V. C. Gibson, S. K. Spitzmesser, *Chemical Reviews* **2002**, *103*, 283.

[53] S. Mecking, L. K. Johnson, L. Wang, M. Brookhart, *Journal of the American Chemical Society* **1998**, *120*, 888.

[54] W. Liu, J. M. Malinoski, M. Brookhart, *Organometallics* **2002**, *21*, 2836.

[55] S. Matsui, T. Fujita, *Catalysis Today* **2001**, *66*, 63.

[56] D. J. Cho, C. J. Wu, S. S, W.-S. Han, S. O. Kang, B. Y. Lee, *Organometallics* **2006**, *25*, 2133.

[57] C. Ji Wu, S. Hoon Lee, H. Yun, B. Yeoul Lee, *Journal of Organometallic Chemistry* **2006**, *691*, 5626.

[58] S. Inoue, H. Koinuma, T. Tsuruta, *Journal of Polymer Science Part B: Polymer Letters* **1969**, *7*, 287.

[59] Z. Qin, C. M. Thomas, S. Lee, G. W. Coates, *Angewandte Chemie International Edition* **2003**, *42*, 5484.

[60] M. R. Kember, A. Buchard, C. K. Williams, *Chemical Communications* **2011**, *47*, 141.

[61] S. S, J. K. Min, J. E. Seong, S. J. Na, B. Y. Lee, *Angewandte Chemie International Edition* **2008**, *47*, 7306.

[62] E. K. Noh, S. J. Na, S. S, S.-W. Kim, B. Y. Lee, *Journal of the American Chemical Society* **2007**, *129*, 8082.

[63] S. J. Na, S. S, A. Cyriac, B. E. Kim, J. Yoo, Y. K. Kang, S. J. Han, C. Lee, B. Y. Lee, *Inorganic Chemistry* **2009**, *48*, 10455.

[64] *http://www.klmtechgroup.com/PDF/Articles/Fluidized-Bed-Reactor.pdf*.

[65] R. H. Grubbs, C. Gibbons, L. C. Kroll, W. D. Bonds, C. H. Brubaker, *Journal of the American Chemical Society* **1973**, *95*, 2373.

[66] B. Heurtefeu, C. Bouilhac, É. Cloutet, D. Taton, A. Deffieux, H. Cramail, *Progress in Polymer Science* **2011**, *36*, 89.

[67] G. Fink, B. Steinmetz, J. Zechlin, C. Przybyla, B. Tesche, *Chemical Reviews* **2000**, *100*, 1377.

[68] M. Koch, A. Falcou, N. Nenov, M. Klapper, K. Müllen, *Macromolecular Rapid Communications* **2001**, *22*, 1455.

[69] V. F. Tisse, F. Prades, R. Briquel, C. Boisson, T. F. L. McKenna, *Macromolecular Chemistry and Physics* **2010**, *211*, 91.

[70] R. Quijada, R. Rojas, L. Alzamora, J. Retuert, F. M. Rabagliati, *Catalysis Letters* **1997**, *46*, 107.

[71] T. Uozumi, T. Toneri, K. Soga, T. Shiono, *Macromolecular Rapid Communications* **1997**, *18*, 9.

[72] K. Soga, H. J. Kim, T. Shiono, *Macromolecular Chemistry and Physics* **1994**, *195*, 3347.

[73] J.-H. Yim, K.-J. Chu, K.-W. Choi, S.-K. Ihm, *European Polymer Journal* **1996**, *32*, 1381.

[74] J. C. W. Chien, D. He, *Journal of Polymer Science Part A: Polymer Chemistry* **1991**, *29*, 1603.

[75] K. Soga, T. Uozumi, M. Saito, T. Shiono, *Macromolecular Chemistry and Physics* **1994**, *195*, 1503.

[76] S. S. Sarma, S. Sivaram, *Macromolecular Chemistry and Physics* **1997**, *198*, 495.

[77] G. G. Hlatky, *Chemical Reviews* **2000**, *100*, 1347.

[78] Y. J. Jang, K. Bieber, C. Naundorf, N. Nenov, M. Kapper, K. Mullen, D. Ferrari, S. Knoke, G. Fink, *E-Polymers* **2005**.

[79] Y. Yamauchi, P. Gupta, K. Sato, N. Fukata, S.-i. Todoroki, S. Inoue, S. Kishimoto, *Journal of the Ceramic Society of Japan* **2009**, *117*, 198.

[80] J. H. Z. dos Santos, S. Dorneles, F. C. Stedile, J. Dupont, M. M. de Camargo Forte, I. J. R. Baumvol, *Macromolecular Chemistry and Physics* **1997**, *198*, 3529.

[81] J. D. Kim, J. B. P. Soares, *Macromolecular Rapid Communications* **1999**, *20*, 347.

[82] J. D. Kim, J. B. P. Soares, G. L. Rempel, *Macromolecular Rapid Communications* **1998**, *19*, 197.

[83] D.-H. Lee, S.-Y. Shin, D.-H. Lee, *Macromolecular Symposia* **1995**, *97*, 195.

[84] D.-h. Lee, K.-b. Yoon, S.-k. Noh, *Macromolecular Rapid Communications* **1997**, *18*, 427.

[85] B. L. Moroz, N. V. Semikolenova, A. V. Nosov, V. A. Zakharov, S. Nagy, N. J. O'Reilly, *Journal of Molecular Catalysis A: Chemical* **1998**, *130*, 121.

[86] S. C. Hong, H. T. Ban, N. Kishi, J. Jin, T. Uozumi, K. Soga, *Macromolecular Chemistry and Physics* **1998**, *199*, 1393.

[87] J. P. Collman, L. S. Hegedus, M. P. Cooke, J. R. Norton, G. Dolcetti, D. N. Marquardt, *Journal of the American Chemical Society* **1972**, *94*, 1789.

[88] S. C. Hong, U. Rief, M. O. Kristen, *Macromolecular Rapid Communications* **2001**, *22*, 1447.

[89] L. Shi, Y. Qin, W. Cheng, H. Chen, T. Tang, *Polymer* **2007**, *48*, 2481.

[90] Y. Qin, T. Tang, Z. Zhao, *Chemical Communications* **2004**, *0*, 222.

[91] H. Nishida, T. Uozumi, T. Arai, K. Soga, *Macromolecular Rapid Communications* **1995**, *16*, 821.

[92] M. Stork, M. Koch, M. Klapper, K. Müllen, H. Gregorius, U. Rief, *Macromolecular Rapid Communications* **1999**, *20*, 210.

[93] W. Wang, L. Wang, J. Wang, Z. Ma, J. Wang, *Journal of Applied Polymer Science* **2005**, *97*, 1632.

[94] H. Zhu, G.-X. Jin, N. Hu, *Journal of Organometallic Chemistry* **2002**, *655*, 167.

[95] J. Zhang, G.-X. Jin, *Inorganic Chemistry Communications* **2006**, *9*, 683.

[96] C. Liu, G. Jin, *New Journal of Chemistry* **2002**, *26*, 1485.

[97] S. B. Roscoe, J. M. J. Fréchet, J. F. Walzer, A. J. Dias, *Science* **1998**, *280*, 270.

[98] S. B. Roscoe, C. Gong, J. M. J. Fréchet, J. F. Walzer, *Journal of Polymer Science Part A: Polymer Chemistry* **2000**, *38*, 2979.

[99] M. Koch, M. Stork, M. Klapper, K. Müllen, H. Gregorius, *Macromolecules* **2000**, *33*, 7713.

[100] N. Nenov, M. Koch, M. Klapper, K. Mullen, *Polymer Bulletin* **2002**, *47*, 391.

[101] Y.-J. Jang, N. Nenov, M. Klapper, K. Müllen, *Polymer Bulletin* **2003**, *50*, 343.

[102] Y.-J. Jang, N. Nenov, M. Klapper, K. Müllen, *Polymer Bulletin* **2003**, *50*, 351.

[103] C. Naundorf, S. Matsui, J. Saito, T. Fujita, M. Klapper, K. Müllen, *Journal of Polymer Science Part A: Polymer Chemistry* **2006**, *44*, 3103.

CHAPTER 2

Motivation and Objectives

2 Motivation and Objectives

The work presented in this dissertation includes two distinct aspects of the metallocene catalyst field. First, immobilization technique of metallocenes on a fiber, spherical particle and core-shell structured support are studied towards morphology control in polyolefin synthesis. Second, modulating metallocene activity by controlling a size of borates based on dendrimer-chemistry is studied.

Chapter 3 presents the usage of polyurethane particles as supports for metallocene-catalyzed polyolefin synthesis. Since supporting metallocene is profoundly crucial for industrial processes, finding a suitable support material is necessary. To date, inorganic particles, particularly silica gel, have been studied and are dominantly used. Alternatively, organic-based supports have also been studied due to their convenient modification. However, introducing porosity to an organic support had not been conducted previously. To fulfill the fundamental requirements of supports, such as micrometer-diameter, narrow size distribution, controlled porosity and mechanical strength, polyurethane (PU) is considered with various porosities, via control of the employed water in the emulsion polymerization. Within this study, the effect of PU porosity on the catalytic activity will be investigated.

The objective of the **Chapter 4** is the direct synthesis of polyethylene fibers using supported metallocene. Industrially, fibrous polyolefins are of interest as they can be used in various fields. However, direct processing of polyolefins into fibers via electrospinning has encountered limitations such as electrospinning in a melt state, usage of inorganic salts to overcome low conductivity, removal of the salt, poor morphology control and changes in microstructure. Therefore, usage of anisotropic supports would be an alternative method to synthesize polyolefin fibers without further processing after olefin polymerization. Here, spherical supports replicate the final morphology of the products. Electrospun fibers based on polyvinyl alcohol (PVA) were used as supports for metallocene-catalyzed polyethylene synthesis. In this case, however, the morphology of the final product was not controlled due to the lack of interaction between metallocene and supports. To circumvent the problem, introducing anchoring units such as nucleophilic groups to anisotropic supports are considered. For instance, Jang and Naundorf in our group reported that polystyrene (PS) nanoparticles containing poly(ethylene oxide) (PEO) groups are capable of interacting

with pre-activated metallocene species (cationic character) strongly. Therefore, transformation of PEO-functionalized PS nanoparticles into fibers is considered by colloid electrospinning. Thus, these nucleophilic groups can be used for immobilizing pre-activated metallocene complexes. The effect of this non-covalent interaction between catalysts and supports in morphology control of final product will be investigated.

Chapter 5 is an extension of the work presented in **Chapter 4**. The objective of the Chapter is demonstration of "concurrent tandem catalysis" towards the synthesis of linear low density polyethylene (LLDPE) using ethylene as a single monomer feed. Since PEO-functionalized PS nanoparticles embedded on electrospun fibers show a strong interaction with metallocene catalysts and afford HDPE-coated fibers with well-controlled morphology in **Chapter 4**, synthesis of LLDPE is subsequently considered to show the typical applications of anisotropic supports. In order to perform tandem catalysis for LLDPE synthesis using ethylene as a single monomer feed, the employed catalyst must be adapted and work under the same conditions. As most metallocene catalysts for ethylene oligomerization work under harsh conditions (over 30 bar of ethylene and above 100 °C), finding a suitable oligomerization catalyst, which works under mild conditions (range of 1 to 5 bar of ethylene and below 70 °C), is the primary challenge. Another consideration is the selective conversion of ethylene to oligomers (mainly C_4-C_8 fraction). Thus, a catalyst (**A**) for ethylene oligomerization will be immobilized in silica particles and another catalyst (**B**) for ethylene copoplymerization with the oligomers (*in-situ* generated by **A**) will be immobilized on the electrospun fibers. The gas-phase tandem catalysis will be performed using ethylene as a single monomer feed. Its tandem activity in LLDPE synthesis by varying the ratio of [**A**]/[**B**] will be studied as well as the effect on the number of branches and melting points Furthermore, the ability to recycle **A** will be tested since it is supported on silica particles.

The objective of **Chapter 6** is synthesis of UHMWPE having a layer of LLDPE to enhance the processablity. It demonstrates the synthesis of spatially resolved polyolefins in the same particle via selective catalyst loading of metallocene catalysts. Two metallocene catalysts (**A** and **B**) are supported in the core and shell, respectively, via step-wise construction. Since the synthesis of hard core-soft shell polyolefins in single particles using ethylene as a single monomer feed is considered, three different catalysts are required as followed: one catalyst (**A**) supported in the core is responsible to synthesize UHMWPE whereas another catalyst (**B**) supported in the shell copolymerizes ethylene with α-olefins

that are generated *in-situ* by an oligomerization catalyst (**C**) supported on silica particles, separately. Individual systems for LLDPE and UHMWPE synthesis will be initially tested to qualitatively and quantitatively determine the roles of the catalysts. Thereafter, synthesis of LLDPE-UHMWPE core-shell particles via a combination of tandem catalysis and selective catalyst loading of metallocene catalysts will be conducted. Since these two polyolefins coexist in a particle, GPC and DSC will show no evidence of the spatially resolved core-shell particles containing two different polyolefins. Therefore, in order to elucidate the inner-morphology of the spatially resolved polyolefin core-shell particles, various microscopic techniques will be employed such as cryo-TEM, SEM, STEM with EDX and hyper-mapping, AFM and LSCFM.

Chapter 7 presents the usage of hollow silica particles (HSP) as a support in metallocene-catalyzed polyolefin synthesis. The objective of the chapter is to suppress the amount of supports by using HSPs as supports. Supports for metallocene catalysts are required for industrial processes. Ironically, residual supports often become impurities after olefin polymerization. Furthermore, the supports hamper the clarity of the polyolefin product. Therefore, minimizing the amount of supports is considered by using hollow supports. HSPs are synthesized by a sol-gel method on polystyrene-*co*-acrylate microspheres as scarifying templates. By controlling the immobilizing procedure of metallocene catalysts with the HSPs, the catalyst can be immobilized either inside or around the HSPs. After olefin polymerization, the locations of fragmented HSPs will give an evidence to identify the immobilization place.

Chapter 8 investigates modulating the catalytic activity of metallocene catalysts by controlling the size of borates as cocatalysts. Methylaluminoxane (MAO) (aforementioned in **Chapter 1**) is a strong and mostly applied cocatalyst for metallocene complexes. However, MAO has drawbacks such as undefined structure, required usage of excess amounts, expensive raw material (trimethyl aluminum) and storage issue. As an alternative cocatalyst, boron-based cocatalysts have been studied. Unlike MAO, boron-based cocatalysts have a chemically well-defined structure and require only a stoichiometric ratio to metallocenes. However, studies on boron-based cocatalysts have been relatively less reported due to their sensitivity towards impurities and difficulties to control reaction conditions. It is speculated that the catalytic activity of metallocene species can be controlled by electron density of the central metal. To control the electron density, lowering the ionic interaction between cationic metallocene species (activated form with a

vacant site) and cocatalyst (counter anion, *e.g.* borates) can be considered. Indeed, Marks and Eugene reported that catalytic activity of metallocene towards ethylene polymerization is enhanced by modulating the diameter of borates with bulky groups on *para*-position of commercially available borate, $B(C_6F_5)_4$. As one of the specialties in the Müllen group is dendrimer chemistry, introducing tetraphenyl dendrons groups on *para*-position of $B(C_6F_5)_4$ is considered to increase the size of the borate. By increasing the generations of dendrimer, the size of the borates can be chemically tailored, and thus the anionic character of borates on the outer surface of dendritic borates can be suppressed. Using these bulky and rigid dendritic borates with different generations, the influence of the various borates on the catalytic activity of *rac*-$C_2H_4(Ind)_2ZrMe_2$ will be studied in a homogeneous condition.

Chapter 9 provides a summay of **Chapters 3 – 8** and an outlook to the future of the polyolefin field with a few suggestions based on experimental knowledge. In particular, via copolymerization of ethylene and poly(ethylene oxide) (PEO)-functionalized norbornene using metallocene, the obtained copolymer can be applied as a binder for membrane in batteries. Since the copolymer possesses PEO groups as a strong anchoring unit, inorganic particles such as alumina or silica can be bound to the copolymers. A membrane in batteries is generally polyethylene (PE), polypropylene (PP) or PE/PP composites. As a result, the membrane has low thermal stability. In order to enhance the thermal stability of the membrane, coating with a thermally stable material is an option if the coating material has no inference on the membrane. Thus, ethylene/PEO-norbornene copolymer can be applied as binding polymer for a membrane in batteries.

Chapter 10 describes the experimental set-ups including implementation of reactors for olefin polymerization and general immobilization method of metallocene catalysts on supports. Furthermore, purification method of liquids and gases is described as metallocene-catalyzed polyolefin synthesis is highly required these fundamental maintenance.

CHAPTER 3

Porous Polyurethane Particles

Abstract: Porous polyurethane particles (PU) are presented as uniform fragmentable supports for metallocene catalysts. The micrometer-sized particles which have a narrow size distribution and a controlled porosity are prepared by a non-aqueous emulsion polymerization in a single step. The porosity of the PU particles is controlled by introducing a defined amount of water into the emulsion polymerization. A complex of metallocene/methylaluminoxane is immobilized on the PU supports and used for the ethylene polymerization in a gas phase reactor. The surface and morphology of the polyethylene/polyurethane particles are characterized by using scanning electron microscopy. Homogeneous fragmentation of the support material is observed during the polymerization and affords product particles with a spherical shape and narrow size distribution. The fragmentation behavior of the polyurethane microspheres throughout the ethylene polymerization is monitored by laser scanning confocal fluorescence microscopy (LSCFM) which is a non-destructive method in contrast to other techniques. A homogeneous distribution of PU in the polyethylene particles is proven by the optical sectioning of LSCFM.

3 Porous Polyurethane Particles

3.1 Introduction

The polymers produced from homogeneous olefin polymerization via metallocenes are obtained only in dust or lump form which is not suitable for industrial applications. For processability a flowable powder is required which can only be produced by supporting metallocenes on solid carriers rather than in homogeneous processes.[1] Such a heterogeneous approach (metallocene on supports) provides better morphology control and higher bulk densities of the obtained particles, prevents reactor-fouling and finally results in a product that is much easier to process. Additionally, the use of a supporting material is the only way to run metallocene polymerizations without a solvent in a gas-phase reactor.

As fragmentation behavior of supports for metallocene-catalyzed polyolefin synthesis is of interest due to its impact on the properties of the final product, the mechanism of polyolefin particle growth is well discussed in several literatures.[2-4] Generally, olefin polymerization is initiated when metallocene-immobilized supports come into contact with monomer under inert conditions. As a consequence, the monomer diffuses into the supports and reaches active centers where olefin polymerization takes place. The olefin polymerization rate is commonly dependent on the type of applied catalyst and support, reaction conditions, purity of monomers, set-up of the reactor and other variables. In this section, fragmentation behaviors of most commonly studied supports, silica and polystyrene particles, are briefly described.

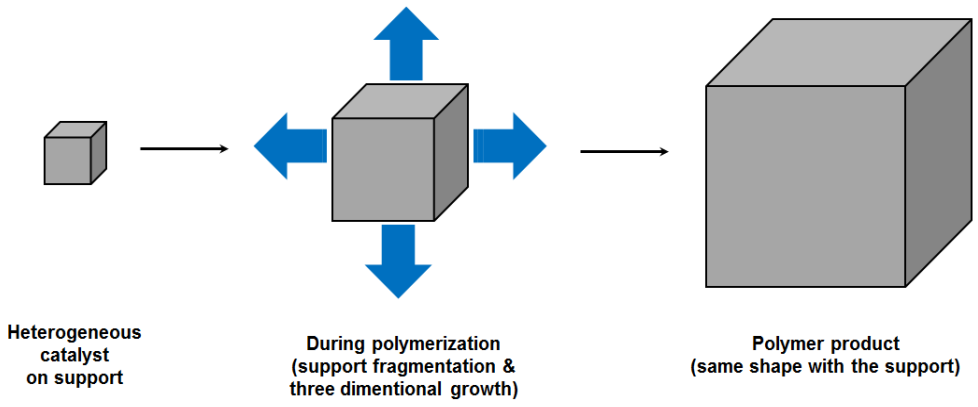

Figure 3-1. Replication effect of catalyst support to final product

During the polymerization with heterogeneous catalysts, the support acts as a template for the product particle formation. The obtained products (polyolefin) thus mirror the corresponding shapes of the support applied (*Figure 3-1*). It is generally called as "replication effect".

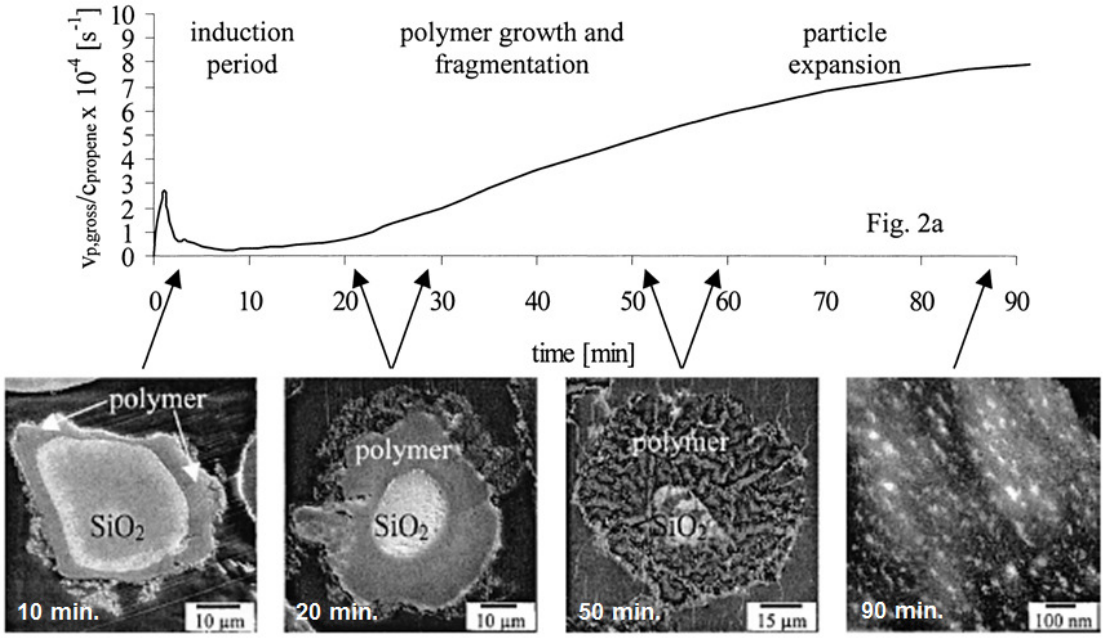

Figure 3-2. Fragmentation behavior of silica support at various polymerization times

Using silica particles as supports for metallocene, Fink et al. studied fragmentation behavior as a function of olefin polymerization time (*Figure 3-2*).[4] At the early stage of olefin polymerization, only the outer layer of the silica particles is exposed to the monomer and fragments (generally known as the "induction period"). By further increasing the polymerization time, monomer diffuses into the core of the silica and reacts with catalyst which leads to the formation of polyolefin in the core. Further polyolefin growth causes fragmentation of the silica supports. At the end of the polymerization, small nanometer-scale fragments from silica particles remain while particle expansion continues with polyolefin growth. As polyolefin formation started from the outer of the silica supports and moving into the core of the silica subsequently, this fragmentation mode is called "layer-by-layer" fragmentation.[5]

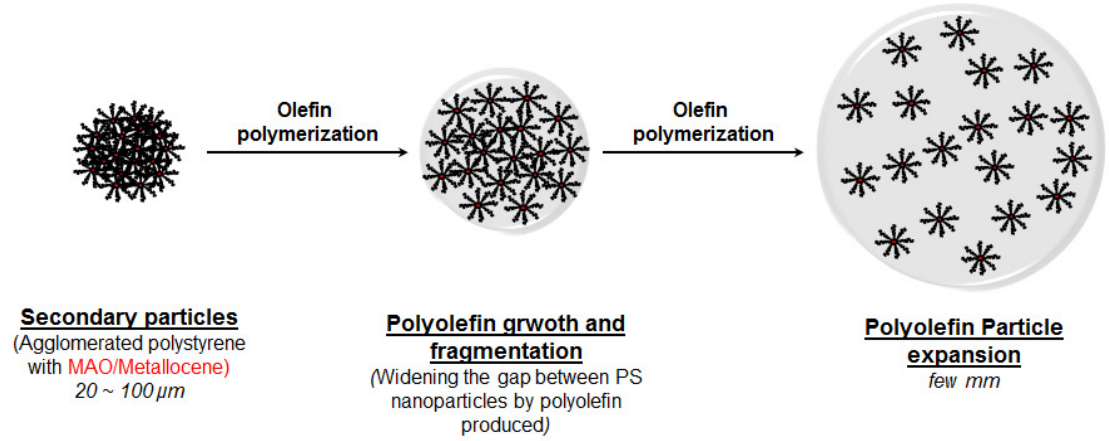

Figure 3-3. Fragmentation behavior of PS supports through olefin polymerization

In organic supports, polystyrene (PS) particles are relatively less studied compared to silica particles. In the case of micrometer-sized PS particles, Jang et al. reported that metallocene supported on the PS beads exhibited almost no fragmentation and thus can not be considered a reasonable alternative to inorganic supports.[6] This is due to the irreversible cross-linking. However, a different fragmentation behavior during olefin polymerization was reported upon decreasing the particle size between 20 and 200 nm (*Figure 3-3*).[6] Unlike silica particles, the PS nanoparticles form secondary particles with a size of 20 to 100 μm.[6-8] The aggregates of nanometer-sized PS particles fragmented into the whole nanoparticles already at the beginning of the polymerization.[6, 9] The fragmentation behavior of the secondary particles (aggregates) thus is called "multi-grain" mode.[6]

3.2 Objective

Herein, finding an ideal support for metallocene-catalyzed polyolefin synthesis is demonstrated using a polyurethane (PU) particle. As described in **Section 1.6.1** (Requirements for support), such a support must have a spherical shape with a micrometer-ranged diameter and a narrow particle size distribution, and furthermore a porosity and proper mechanical properties. Since PU has excellent mechanical properties, the introduction of the other requirements is demonstrated (*Figure 3-4*). To fulfill the requirements (spherical shape, micrometer-ranged diameter, and a narrow particle size distribution), the preferred method for the synthesis of suitable PU microspheres is via nonaqueous emulsion polymerization. The porosity of the PU microspheres can be generated by adding small amounts of water which controls the formation of pores, since its reaction with the isocyanate generates CO_2. The porous PU particles are advantageous as they possess uniform shape, a controlled size with a narrow size distribution and a well-defined morphology. In this chapter, therefore, the applicability of porous PU microspheres as porous organic supporting materials is demonstrated in a heterogeneous catalytic system with immobilized metallocenes.

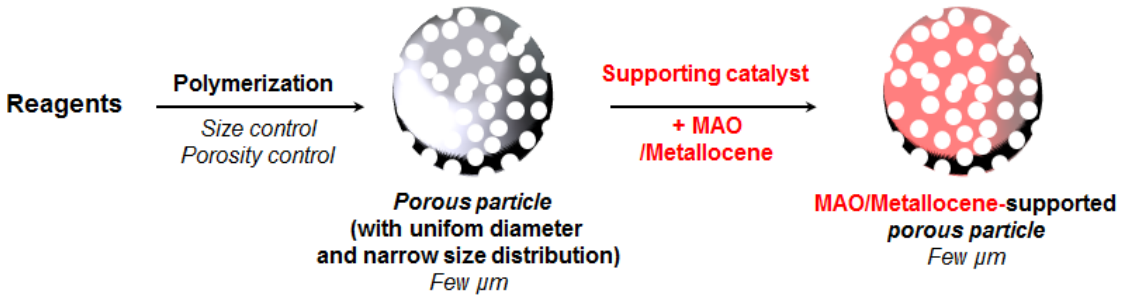

Figure 3-4. Schematic drawing for an ideal support for metallocene-catalyzed polyolefin synthesis

3.3 Results and discussion

3.3.1 Synthesis of porous polyurethane particles

In order to apply PU as a support material for metallocene-catalyzed polyolefin synthesis, as mentioned in **Section 1.6.1**, several requirements, such as spherical shape, micrometer ranged diameter, narrow particle size distribution and porosity, are mandatory. By performing an emulsion polymerization, the first three requirements are satisfied via a uniform shaping procedure. For introducing porosity, water was added during the polymerization (*Figure 3-5*).[24] The presence of water in a diisocyanate-containing emulsion leads to the release of CO_2 and the generation of polyurea. The amount of water controls the quantity of released CO_2 which is responsible for the resulting porosity and pore size.[10, 11] In an aqueous emulsion, this process is difficult to control due to the continuous phase. Thus, a nonaqueous system was introduced to generate PU particles with a defined porosity due to the exact amount of water. This system has previously proven its applicability towards the formation of PU nanoparticles.[12]

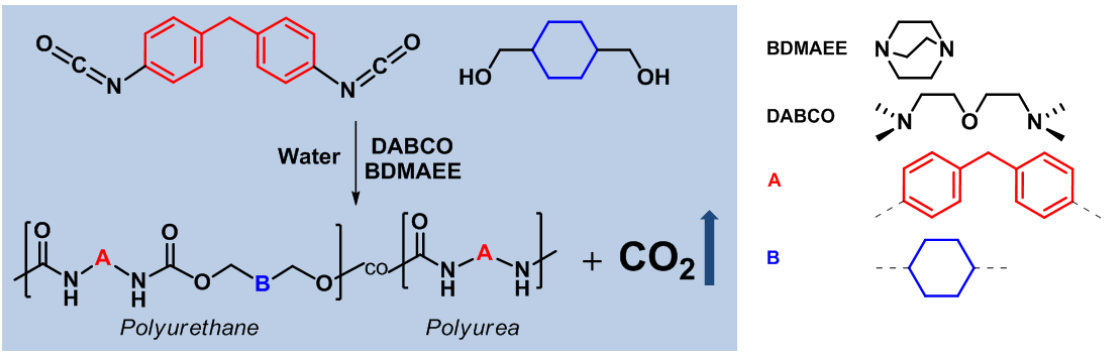

Figure 3-5. Reaction scheme for the formation of polyurethane in the presence of water

A typical nonaqueous emulsion system consists of two immiscible organic solvents that are stabilized by an amphiphilic block copolymer.[12, 13] In particular, a mixture of DMF and cyclohexane is well-stabilized by a polyisoprene-*block*-polymethylmethacrylate (PI-*b*-PMMA) copolymer and leads to the generation of "microreactors", wherein the polymerization can occur. The applied PI-*b*-PMMA copolymer had a number average molecular weight of 60 kg·mol^{-1} with a polydispersity of 1.03. Due to the low interfacial tension between the two organic solvents, a high molecular weight of the emulsifier is necessary. The molar block composition of this polymer was 69 % PI and 31 % PMMA with degrees of polymerization for PI and PMMA being 677 and 142, respectively. This

composition leads to both a good steric repulsion between the dispersed droplets and to an anchoring effect inside the droplets.[14, 15]

In the presence of the PI-*b*-PMMA copolymer, the polymerization of PU microspheres was performed using two different catalysts: 1,4-diazobicyclo[2.2.2]octane (DABCO) and bis(2-dimethylaminoethyl) ether (BDMAEE). In general, higher intermolecular forces between water and catalyst result in a greater ability to decompose the isocyanate to CO_2 and amine.[16] Whereas BDMAEE effectively promotes the reaction of water and isocyanate leading to urea formation, DABCO coordinates larger isocyanates and alcohol and favors the urethane formation.[16] Due to this selectivity of the catalysts, a polymerization in the presence of only one catalyst does not lead to porous PU particles, since either non-porous PU particles (catalyst: DABCO) or no particles at all (catalyst: BDMAEE) are obtained. Hence, a combination of both catalysts is necessary for the formation of both PU and polyurea and to produce porous particles, depending on the amount of water in the emulsion. The polymerization of PU particle is performed in emulsion using various amount of water, and the experimental conditions and polymerization results are summarized in *Table 3-1*.

Table 3-1. Experimental conditions and results of the preparation of PU microspheres in non-aqueous emulsion polymerization[a)]

sample	amount of water	surface area[b)]	D_h[c)] (DLS)	D[d)] (SEM)	M_n[e)]	MWD[e)]	molar ratio of urethane /urea[f)]
	mmol	$m^2 \cdot g^{-1}$	μm	μm	$kg \cdot mol^{-1}$		%
1	0	2.8	2.03 ± 0.39	2.07 ± 0.31	5.3	1.65	79
2	0.78	3.7	2.02 ± 0.23	1.74 ± 0.40	8.7[g)]	1.52[g)]	24
3	1.67	15.1	2.36 ± 0.30	1.93 ± 0.26	6.6[g)]	1.37[g)]	18
4	3.27	6.8	2.27 ± 0.19	1.86 ± 0.42	6.5[g)]	1.36[g)]	14

a) Emulsion: DMF (26.0 mmol) dispersed in cyclohexane (185 mmol) stabilized by PI-*b*-PMMA (0.21 g); Polymerization: BHC (1.5 mmol) + MDI (1.6 mmol) + DABCO (0.10 mmol) + BDMAEE (0.31 mmol) + water (0 – 3.27 mmol) at ambient temperature for 15 min;

b) hydrodynamic diameter determined via DLS;

c) average diameter of 100 randomly chosen particles from various SEM micrographs;
d) degree of polymerization determined via GPC *vs.* PMMA standards;
e) molecular-weight distribution determined via GPC *vs.* PMMA standards;
f) derived from FTIR-spectroscopy measurements;
g) *N*-methylated polymer, since the polymer was insoluble before methylation.

The molecular weight of sample 1 (*Table 3-1*) was 5.3 kg·mol^{-1}, as derived from gel permeation chromatography (GPC, PMMA standard) measurements. This implies, according to the Carothers equation,[17] a conversion of 0.99 for this step-growth reaction. The molecular weight distribution (MWD) was 1.65. The molecular weights of the polymers, derived from the polymerizations in the presence of water, could not be obtained at first due to the insolubility of this polymer resulting from the "hard" urea-segments in the polymer chain, which form hydrogen bonds.[18, 19] To distinguish the molecular weights of these polymers, *N*-methylation of the urea-segments was conducted in order to eliminate the hydrogen bonds.[20] The *N*-methylated polymers are well-soluble in DMF and possess molecular weights up to 8.7 kg·mol^{-1} with MWD as low as 1.36.

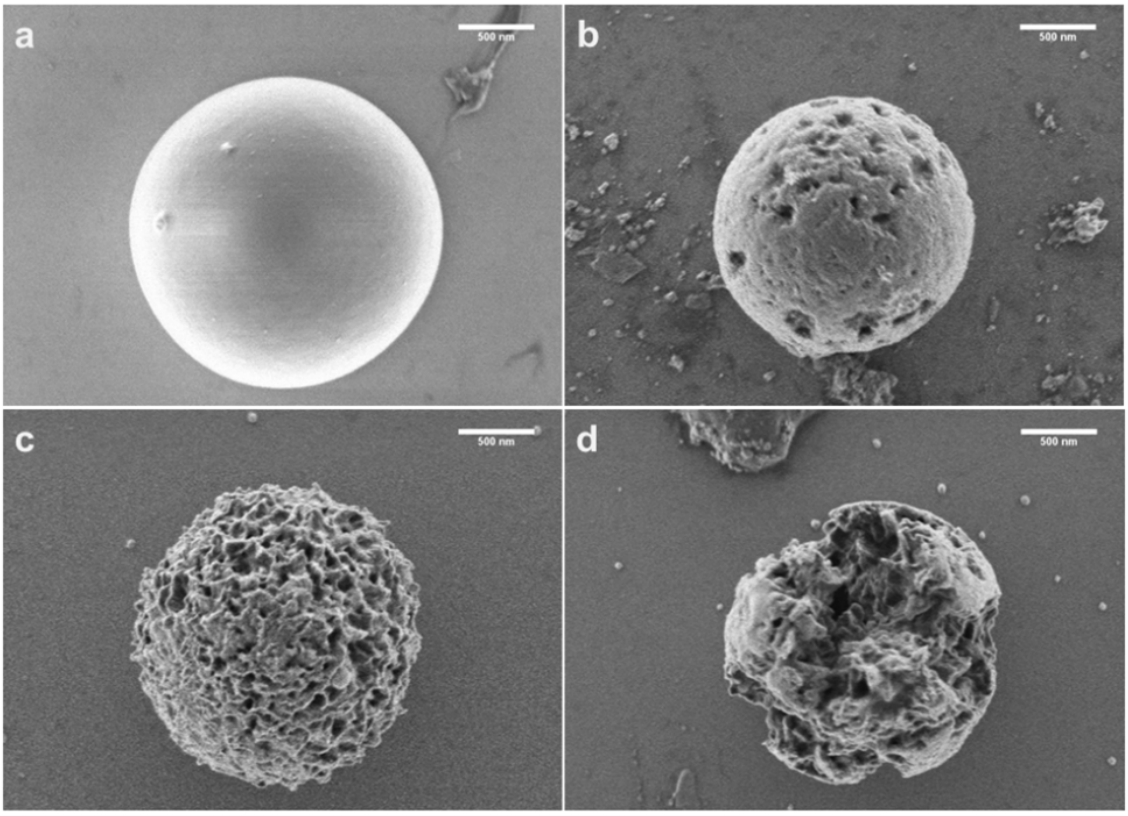

Figure 3-6. SEM micrographs of (a) non-porous and (b-d) porous PU particles by varying the the amount of water (a-d: 0, 0.78, 1.67 and 3.27 mmol of water.)

Non-aqueous emulsions afford PU particles having approximate diameters of 2 μm and uniform spherical shape. The spherical shape of the particles originates from the exclusive

solubility of all reaction components in the dispersed phase. As can be derived from SEM micrographs (*Figure 3-6*), the particle morphology is determined by the amount of released CO_2, which is again connected to the amount of added water in the emulsion. Thus, the surface morphology ranges from smooth to highly-porous (sample 1-3). In the case of sample 4 (*Figure 3-6d*), the amount of released CO_2 appears to be sufficient to rupture the resulting particles. The mean pore diameters of the spherical porous particles ranged from 58 ± 27 nm (sample 2; *Figure 3-6b*) to 89 ± 27 nm (sample 3; *Figure 3-6c*). This indicates a growth in pore diameter due to the blowing effect caused by the higher amount of released CO_2.

Depending on the employed amount of water (from 0 to 3.27 mmol), the surface areas of these particles are varied in the range of approximately 3 to 15 $m^2 \cdot g^{-1}$ (*Table 3-1*). From the low surface areas of these particles, it is assumed that very small nanopores are not formed. This is desirable since MAO activated complexes can only be adsorbed into larger pores due to the cage-like structure of MAO. Sample 4 dispays an even lower surface area, due to the rupture of the particle. These features show that porosity can be well adjusted by the addition of defined range of water without losing shape control. Comparing these results with silica, which delivers broad particle size distribution and irregular shape of secondary particles,[4] the porous PU particles are advantageous: they possess uniform shape, a controlled size with a narrow size distribution and a well-defined morphology. However, the surface area of PU particles is relatively lower than that of conventional silica. Further increase in porosity of PU particles was not achieved in this study due to the rupture of PU particles by the sufficient amount of released CO_2.

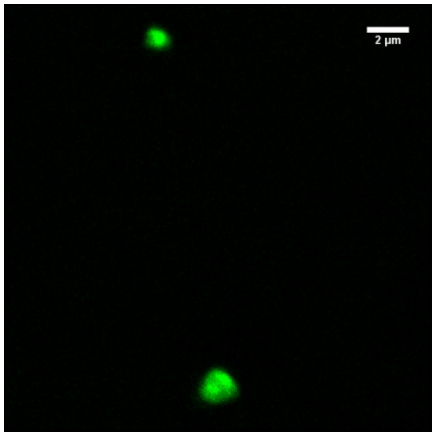

Figure 3-7. LSCFM image of the porous particles stained with Rhodamine B

To homogeneously immobilize metallocene catalyst/MAO complexes onto supporting materials, the pores in the supports should be interconnected with one another. In order to demonstrate the presence of an open pore architecture, the porous particles (sample 3; *Figure 3-6c*) were stained with a fluorescent dye and visualized via laser-scanning confocal fluorescence microscope (LSCFM). Rhodamine B (RhoB) was chosen as the staining dye due to its high solubility in methanol and suitable emission wavelength for LSCFM studies.[21] In *Figure 3-7*, RhoB-stained porous PU particles show the accessibility of the inner particle-pores, since the dye is well distributed over the whole PU microspheres and not only on the surface. This demonstrates that two main requirements, a very homogeneous particle size and an open porous structure, for good metallocene-catalyzed polymerization supports have already been fulfilled.

3.3.2 Ethylene polymerization on polyurethane particles

To investigate the feasibility of polyurethane (PU) microspheres for heterogeneous polyolefin (PO) synthesis, bis(methylcylcopentadienly)zirconium(IV) dichloride (MCP) was chosen as a model catalyst. For immobilization on the organic supports, the catalyst was dissolved in toluene and pre-activated with methylaluminoxane (MAO) which is the most common cocatalyst for metallocenes. The PU microspheres obtained via non-aqueous emulsion polymerization were dried under vacuum at elevated temperature and the MAO/MCP mixtures were added. These MAO/MCP complex-containing PU particles were obtained after filtration through a glass frit and were used after drying under vacuum. The correlation between catalytic activity towards ethylene polymerization and surface areas of PU microparticles was studied in a gas phase reactor. Typically, the polymerizations were performed at 3 bar of ethylene and 40 °C. To facilitate a comparison, all samples were prepared under the same conditions with respect to the amount of PU particles, concentration of metallocene catalyst, ratio of MAO/MCP, temperature and drying time under vacuum. The results of the ethylene polymerization in the gas phase reactor are summarized in *Table 3-2*.

Table 3-2. Ethylene polymerization results of the PU particles in a gas phase reactor[a)]

sample[b)]	amount of catalyst	MAO	[Al]/[Zr]	activity	T_m[c)]	M_w[d)]	MWD[d)]
	μmol	μmol		kgPE·(mol Zr·h·bar)$^{-1}$	°C	kg·mol^{-1}	
1	3.1	310	100	6	n/d	n/d	n/d
2	3.1	310	100	39	137.5	1077	5.8
3	3.1	310	100	202	139.0	657	15.8
4	3.1	310	100	177	139.6	627	17.1

a) Polymerization conditions: 3 bar of ethylene at 40 °C for 30 min ;
b) corresponding sample numbers in *Table 3-1*;
c) determined by DSC;
d) analyzed by GPC (PS-standard).

Typical activities of MAO/MCP supported on PU particles toward ethylene polymerization are displayed in the range of 6 to 202 kg of polymer (mol of Zr·h·bar)$^{-1}$ at 40 °C. Sample 3 exhibits the highest catalytic activity for the gas-phase homopolymerization of ethylene, followed by samples 4, 2 and 1 in decreasing order (*Table 3-2*). These results of catalytic activity demonstrate a correlation with surface area. It is expected that a sample with higher surface area can immobilize more active species and thus results in enhanced activity. In addition, this is in good agreement with literature as it is known that the higher surface area of the support, especially for silica in heterogeneous polyolefin synthesis, provides more anchoring sites for activated catalysts.[22] Based on this and the determined activities, it is inferred that sample 3 contains more immobilized catalyst than samples 4, 2, and 1 in that order.

To characterize the melting behavior of the products, DSC measurements were performed. The samples possess melting points (T_m) in the range of 137 – 140 °C (*Table 3-2*) which are slightly higher than typical values for high density polyethylene (HDPE) and it attributed to the presence of PU fragments. The weight-averaged molecular weights (M_w) were measured by GPC after extracting the soluble part in 1,2,4-trichlorobenzene (TCB) at 140 °C. In this way, polyolefins can be selectively extracted as PU is insoluble in TCB. The M_w of the

soluble polymer is determined to be in the range of 627 to 1,077 kg·mol^{-1} which are typical values for metallocene catalysts. However, the molecular weight distributions (MWD) of 6 to 17 are unusually broad for metallocene-immobilized ethylene polymerization. The direct reason for these broad MWDs is uncertain, however, a number of possible explanation can be suggested.

The broad MWDs might be explained by the formation of a multi-site catalyst from urea and urethane segments. As M_w increases with the urea content of the different PU supports (*Table 3-1*), it is assumed that the urea reacts with the cationic metallocene species (after MAO activation), leading to a catalytic site with a different activity than the non-bonded complex. Another explanation might be the fragmentation behavior of the mechanically strong PU particles. In the case of heterogeneous catalysts on conventional silica, ethylene mostly reacts with catalyst immobilized on the surface of the silica, and by fragmentation of polyethylene/silica layer, monomer diffuses further into the core of the silica and reacts with catalyst (commonly known as "layer by layer" mechanism, see also **Section 3.1**). If the fragmentation at the early stage is hindered by the mechanically strong support, catalyst immobilized on the surface could produce polyethylene with higher M_w, prior to fragmentation and exposure of fresh catalytic sites. Furthermore, a highly packed surface with HDPE would limit the diffusion of ethylene into the core of PU, and thus the production of polymer with lower M_w. occurs. This may lead to the broad MWD of the polyethylene. Although each of these explanations is possible, the exact reason was not further pursed. However, this broader MWD may be more beneficial for future processing applications.

The growth of particles over the olefin polymerization time is typically related to the surface area and particle size of the supports. Therefore, the influence of the surface area on the activity toward ethylene polymerization was investigated using a gas phase reactor equipped with an optical video microscope comparing non-porous PU particles (sample 1, *Table 3-1*) and highly porous PU particles (sample 3, *Table 3-1*).

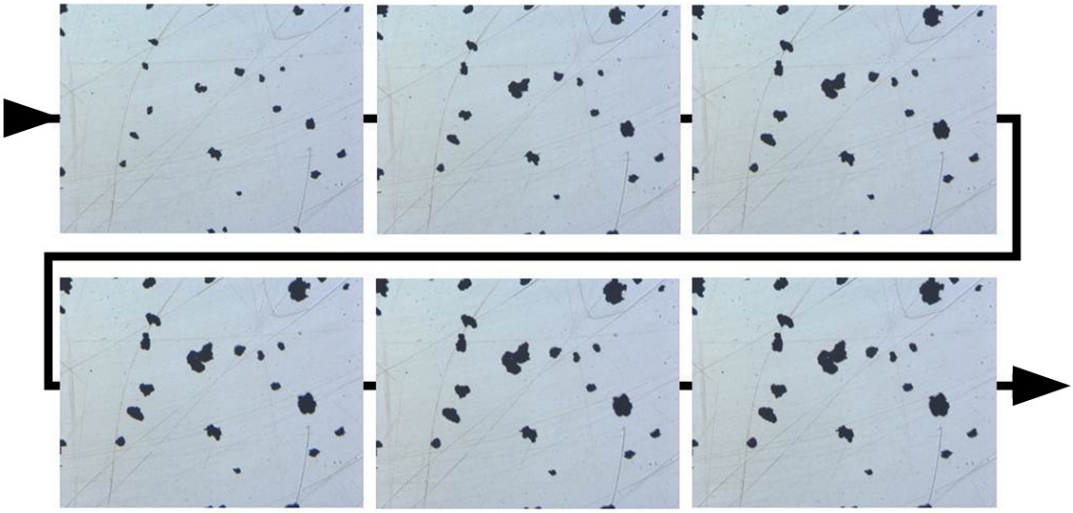

Figure 3-8. Images of particles growth from the gas phase reactor equipped with videomicroscopy

Ethylene polymerizations were performed for 20 min at 40 °C and 3 bar of ethylene. During the ethylene polymerization, MCP/MAO supported PU particles were photographed every 10 s using the optical video microscope. Images of the particles growths of MCP/MAO supported porous PU during ethylene polymerization are shown in *Figure 3-8*. The volume of the PU particles was calculated from the photographs based on the assumption that all particles have isotropic shape. The values of volume were normalized and plotted as a function of polymerization time (*Figure 3-9*).

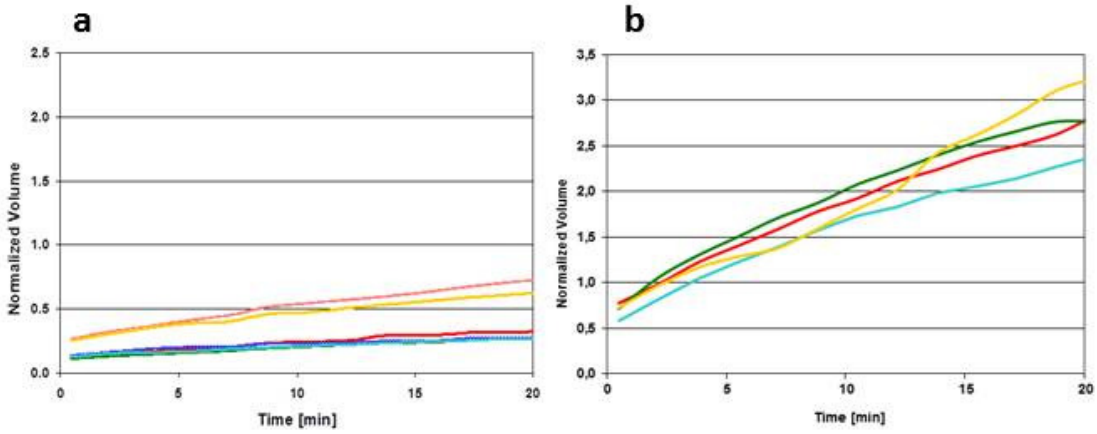

Figure 3-9. Graphs of normalized volume of (a) non-porous PU microspheres and (b) highly porous PU microspheres as a function of ethylene polymerization time from a gas phase reactor equipped with an optical microscope

The highly porous PU particles show significant volume changes during ethylene polymerization, when compared to the non-porous particles. Similar behavior is observed in the literature when studying aggregates of nanoparticles *vs.* Merryfield resins[23] of similar

size corresponding to the studied porous and nonporous supports.[6] In the case of the resins, the catalysts are localized only at the surface of the particle. This results in a highly active catalyst layer where the diffusion is too limited to deliver sufficient monomer. As a result the activity drops. Additionally, overheating may occur in this highly active zone forming a very dense molten layer which further limits the diffusion. In the case of a fragmentable and porous support, the catalyst is homogeneously distributed within the whole particle. Diffusion problems and overheating effects become negligible, and the activity remains high. Furthermore, due to fragmentation, large cracks are formed facilitating the monomer transport into the interior of the supported catalyst system.[4]

3.3.3 Morphology of the obtained polyolefin/polyurethane particles

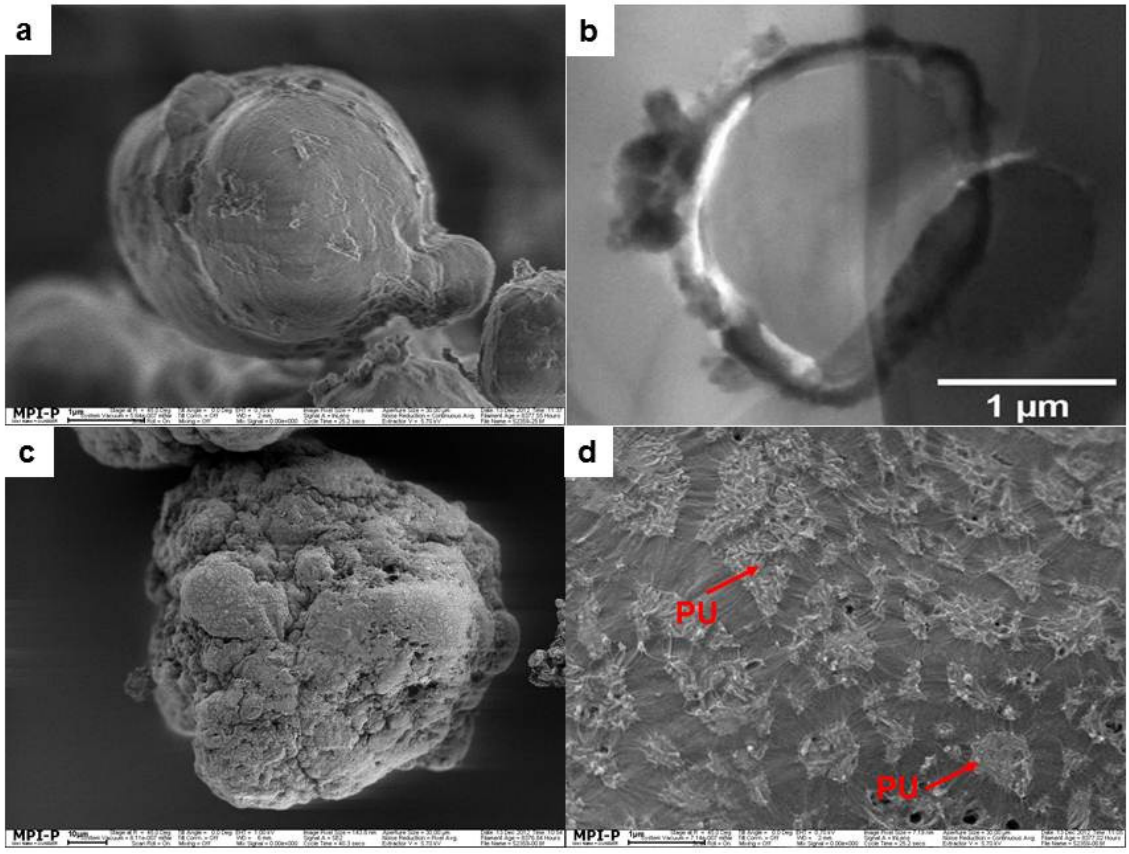

Figure 3-10. (a,b) SEM and cryo-TEM micrographs of non-porous PU particle, (c,d) SEM micrographs of most porous PU particle after ethylene polymerization

Morphology of the final products, especially the spherical shape, is important for the processing of polyolefins. Morphology studies on the PE particles obtained from a gas phase reactor were conducted via SEM and cryo-TEM (*Figure 3-10*). For non-porous PU particles (sample 1, *Table 3-2*), the smooth surface vanished after 5 min of ethylene

polymerization as shown in *Figure 3-10a*. For elucidating the internal structure of the PE particle, they were studied via cryo-TEM. By this method, two phases with different contrasts were detected in the particles (*Figure 3-10b*). For the non-porous particles, a brighter spherical part in the core originates from the PU. The darker rim corresponds to the PE formed by the MCP/MAO complexes. This core-shell structure indicates that the MCP/MAO complexes were immobilized only on the outer surface of the non-porous PU particles, which led to ethylene polymerization spatially around the PU particles.

For the highly porous PU particles, a significant growth of the diameter of the supporting particle was observed during the ethylene polymerization (sample 3, *Table 3-2*). According to the SEM micrograph shown in *Figure 3-10c*, the obtained products are ~100 μm diameter particles with a spherical shape. At higher resolution, it is observed that the outer layer of the obtained products was composed of PE and fragmented PU as shown in *Figure 3-10d*. Before ethylene polymerization, the mean pore diameter of the highly porous PU particles was 89 ± 27 nm, as derived from the SEM micrograph of *Figure 3-6c*. Remarkably, the distance between the PU fragments becomes much wider after ethylene polymerization (*Figure 3-10d*). It indicates a fragmentation induced by the mechanical stresses of the growing PE chains in the pores. Cryo-TEM shows no distinguishable boundary between PU and PE which also indicates a homogeneous distribution of PU in PE. In order to further investigate the fragmentation behavior of PU in the PE particles, laser scanning confocal fluorescence microscopy (LSCFM) was applied. This technique allows the optical sectioning of an object containing a suitable dye without any physical destruction of the sample itself. [6, 8]

After staining the highly porous PU particles with a fluorescence dye, Rhodamine B (RhoB), ethylene polymerization was performed under the same conditions as previously mentioned for non-stained PU particles. A comparison between the catalytic activities of stained and non-stained particles shows negligible differences, indicating that RhoB has no influence on the polymerization. To compare the morphologies of stained and non-stained particle, SEM was performed. As shown in *Figure 3-11a*, the outer layer of the ethylene polymerized particle is composed of PE and the fragmented PU, revealing similar fragmentation behavior as the non-stained case. Information on the internal structure of the PE particles was obtained by LSCFM.

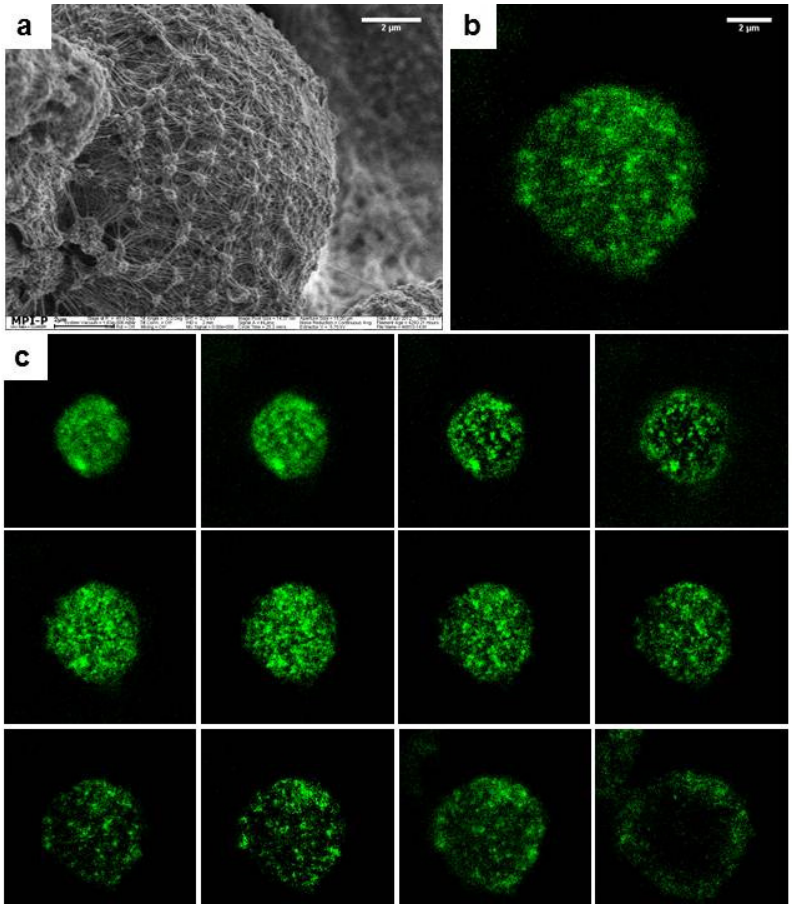

Figure 3-11. (a) SEM micrograph of the ethylene polymerized particles obtained from metallocene supported on the dye stained porous PU particle. LSCFM micrographs of (b) a single PE particle and (c) its 16 slices of PE particle by optical sectioning from top to middle

Figure 3-11b displays the fluorescence images of a PE particle produced with a gas phase reactor after a 30 min polymerization. The PE particles having a diameter of around 10 μm, maintain their spherical shape and display multiple fluorescent spots (green colored) that are considered to be PU fragments. The spherical shape of PE particles indicates that the replicated fragmentation of PU particles occurs during ethylene polymerization, and the monomer can continuously diffuse to the active sites within the PU particles. By optical sectioning of LSCFM, the PE particles are further investigated from bottom to middle. *Figure 3-11c* shows the homogeneous distribution of the dye throughout the PE particle, indicating the porous PU particle is well fragmented and dispersed during the ethylene polymerization. The fragmentation behavior of the PU particles implies that metallocene catalysts have been evenly immobilized over the support materials since otherwise the LSCFM would contain larger inhomogenities.

3.4 Conclusion

Metallocene-catalyzed ethylene polymerization has been performed using organic supports based on polyurethanes (PU) which possess micrometer-sized diameters with a controlled morphology, size distribution and porosity. While up to now, supports for metallocenes, in particular silica and polystyrene nanoparticles, have always needed a two-step procedure. In this study, PU particles as supports were prepared in a simple one-pot reaction. The PU microspheres can be easily adjusted in size and porosity in a non-aqueous emulsion polymerization by adding small amounts of water to form CO_2 as blowing agent. The advantage of such supports is obvious. A process based on the agglomeration of nanoparticles, as it is the case for silica supports or organic nanoparticles, always results in secondary particles with a non-spherical shape and a broad size distribution. As replication of the shape and size normally occurs when using them as supports, the products are not very uniform. Industry overcomes this by sieving of the supports. The PU system here avoids the agglomeration step as the porosity of the supports is obtained by combining particle formation with a blowing process. Further separation of the particles is not required, and they can be directly used as uniform carriers in the olefin polymerization. Other essential requirements for metallocene supports are also fulfilled by these particles. They are fragmentable and the catalyst can be loaded within the whole particle due to the open pore structure. In this way, the microporous PU particles possess all necessary properties to consider them as an excellent alternative to commonly used inorganic or organic supports.

3.5 Experimental part

3.5.1 General procedures and materials

All air and water sensitive reactions were performed using standard Schlenk techniques or a glovebox system under inert atmosphere. 4,4´-Methylenebis(phenyl isocyanate) (MDI) (98% purity), 1,4-diazabicyclo[2.2.2]octane (DABCO), 1,4-bis(hydroxymethyl)cyclohexane (BHC) and bis(2-dimethylaminoethyl)ether (BDMAEE) were purchased from Sigma-Aldrich and used as received. *N,N´*-Dimethylformamide (DMF) and cyclohexane were obtained from Acros organics, dried over CaH_2 and stored over molecular sieves (4 Å) after distillation under inert conditions. Polyisoprene-*block*-polymethylmethacrylate (PI-*b*-PMMA) copolymer was prepared using a sequential anionic polymerization technique.[23] Bis(methylcyclopentadienyl)zirconium(IV) dichloride (97 % purity) was purchased from Aldrich and used as received. The cocatalyst, methylaluminoxane (MAO), was purchased from Aldrich as a 10 wt% solution in toluene. Dried toluene (Acros, stored with activated 4 Å molecular sieves) for the supporting procedure was purchased and used after further purification via distillation over Na/K alloy and benzophenone. Ethylene was purified by passing through columns of activated 4 Å molecular sieves and BASF R3-15 deoxygenation catalyst. The ethylene gas was additionally purified over a $NaAlEt_4$ column followed by an activated 4 Å molecular sieve column for ethylene polymerizations in a gas phase reactor.

3.5.2 Preparation of the porous polyurethane particles

The synthesis of PU particles were performed [redacted] and donated for this experiment. The porous PU particles were synthesized by self-expansion in non-aqueous emulsion. PI-*b*-PMMA copolymer (0.210 g) was magnetically stirred in cyclohexane (15.60 g, 185 mmol) at room temperature. BHC (0.216 g, 1.50 mmol), DABCO (0.012 g, 0.10 mmol) and BDMAEE (0.050 g, 0.31 mmol) were dissolved in DMF (1.430 g, 19.5 mmol) and then added dropwise to the cyclohexane/PI-*b*-PMMA dispersion. The emulsion was treated by sonication for 15 min using a Bandelin Sonorex RK255H ultrasonic bath operating at 640 W. During sonication a defined amount of water was added. MDI (0.400 g, 1.60 mmol) was dissolved in DMF (0.480 g, 6.50 mmol) and added dropwise to the emulsion under inert atmosphere. The emulsion was stirred for 15 min at room temperature in order to generate polyurethane particles with a water-dependent

porosity. A sample was taken out of the emulsion in order to analyze the particle size and morphology via dynamic light scattering (DLS) and scanning electron microscopy (SEM). The particles of the remaining emulsion were precipitated in methanol and separated by centrifugation to form 0.60 g of a white solid. The degree of polymerization (DP) and the molecular weight distribution (MWD) were determined via GPC after drying the solid under vacuum.

3.5.3 Structural characterization of porous polyurethane particles

To determine the molecular weight and the MWD of the polyurethane, gel permeation chromatography (GPC) was carried out at 30 °C using MZ-Gel SDplus 10E6, 10E4 and 500 columns in tetrahydrofuran (THF) as the eluent *vs.* PMMA standards. The detector was an ERC RI-101 differential refractometer. The composition of the block copolymers was determined by ^{1}H-NMR spectroscopy (Bruker Avance spectrometer, 300 MHz) in dichloromethane (DCM) *via* peak analysis. SEM (Zeiss Gemini 912) was performed on samples prepared via drop-casting of the particle dispersion on a silica wafer. DLS was used to determine the size of generated polyurethane particles. The measurements were performed on a Malvern Zetasizer 3000 with a fixed scattering angle of 90° and on an ALV/LSE-5004-correlator using a He/Ne-laser operating at 632.8 nm. Fourier transform infrared (FTIR) measurements were performed on a Nicolet 730 FTIR spectrometer using a thermo electron endurance attenuated total reflection (ATR) single-reflection ATR crystal. The specific BET surface area of the porous PU particles was examined by nitrogen adsorption and desorption isotherms at 77 K with a Micromeritcs Tristar II 3020 analyzer (USA).

3.5.4 Staining the polyurethane particles with Rhodamine B

The PU particles (100 mg) were placed in a 50 mL round-bottomed flask with 10 mL of methanol. The solution of Rhodamine B (4.7 mg, 0.01 mmol) in methanol (10 mL) was separately prepared and added to the flask. The flask was mounted on a shaker at 100 rpm at ambient temperature overnight. The solution was removed by a syringe and 20 mL of fresh methanol was added again to wash the particles. This procedure was repeated several times until there was no leaching of the dye from the particles. The Rhodamine B-stained PU particles were filtered and dried under reduced pressure.

3.5.5 Immobilization of the metallocene catalyst on the polyurethane particles

The immobilization of the catalyst on the PU particles was carried out under inert atmosphere. The PU particles were dried overnight at elevated temperature under reduced pressure and delivered into a glovebox. The particles (0.5 g) were placed in a 50 mL Schlenk flask with 20 mL of dry toluene. In order to remove the trace amount of water in the particles, the flask was mounted on a shaker at 100 rpm. After 3 h, the toluene was removed by a syringe and 20 mL of fresh toluene was added. This procedure was repeated 3 times. After removal of toluene from the flask, a mixture of 4.0 mL toluene and 1.0 mL of a 1.0 M MAO solution was added into the flask and shaken for additional 3 h to make sure there was no residual water in the particles. The particles were washed with toluene (3 × 5 mL) prior to addition of the catalytic solution. Separately, bis(methylcyclopentadienyl)zirconium(IV) dichloride (MCP) (10 mg, 0.03 mmol) was dissolved in toluene (5 mL) and stirred for 5 min to preactivate with the addition of MAO solution. The solution of MCP/MAO complex was added to the flask containing the particles at room temperature, and the flask was shaken at 100 rpm overnight. The resulting particles were washed with toluene (3 × 5 mL) and dried under reduced pressure. The calculated support loading was estimated to be 33 μmol of Zr·(g of PU particles)$^{-1}$. The aluminum to zirconium ratio was estimated as 100:1.

3.5.6 Polymerization procedure in a gas phase reactor

All polymerizations were performed in a customized autoclave (gas phase reactor) equipped with an external heating controller and a connection line to ethylene supply. The reactor has a 50 mL volume and is mounted with a silver-coated plate in the middle of the reactor. Prior to polymerizations, to remove moisture and oxygen in a gas-phase reactor, the reactor was dried under vacuum with 5.0×10^{-4} mbar at 80 °C overnight and then delivered into a glovebox. The MCP supported PU particles were mounted on a silver coated plate in a gas-phase reactor. The DMAO solid and a metallocene supported on the particles were placed at the bottom of the reactor. The role of the DAMO is to further purify the ethylene gas, as the gas-phase reactor is extremely sensitive to moisture. A small portion of the particle-supported metallocene was applied as an internal standard. After removal from the glove box, the reactor was connected with a vacuum line which has an internal ethylene supply valve. The line was heated overnight at 150 °C under reduced

pressure to remove residual moisture. To start the polymerization, the reactor was heated to the desired temperature by an external heating controller. After stabilizing the temperature, the reactor was charged with 3 bar of ethylene. The polymerization was stopped by releasing the pressure after the desired polymerization time, and subsequently, the PU particles were exposed to air to quench the active catalysts. The DMAO solids were placed in a beaker containing n-hexane and were quenched by sequential addition of isobutanol, ethanol, methanol and water under extreme care.

3.5.7 Characterization of polyethylene/polyurethane composites

Melting points (T_m) of products were determined by differential scanning calorimeter (DSC) using a heating rate of 10 °C/min in the temperature range of 20 – 200 °C. The obtained polymer was dissolved in 1,2,4-trichlorobenzene (2.0 g/L concentration) for GPC measurements. After filtration by a glass syringe equipped with a membrane (Milipore, Miltex^{TM} membrane, 5.0 μm LS), GPC was performed on a Waters 150-C gel permeation chromatograph at 145 °C using three TSKgel columns (two sets of TSKgelGMH$_{HR}$-H(S)HT and TSKgelGMH$_6$-HTL) with refractive index detection and calibration *vs.* narrow polystyrene standards. The polymers dissolved in 1,2,4-trichlorobenze/d^2-1,1´,2,2´-tetrachloroethane (2/1, *v*/*v*) were characterized by ^{13}C NMR at 393 K. For morphological observations, SEM was carried out at low-voltage using a LEO 1530 Gemini, Zeiss. Laser scanning confocal fluorescence microscopy (LSCFM) was performed using a Zeiss Axiovert 200M equipped with a LSM 510 ConfoCor 2. For cryo-sectioning with a Leica ultracut UCT, the particles were embedded in a mold using an epoxy resin and embedded samples were prepared with a deisred thickness. The 60 nm thick samples were placed on a 300 mesh carbon-coated copper grid for cryo-transmission electron micrographs (TEM). Cryo-TEM was carried out with a Zeiss EM912 operating at 80 kV. The analysis of the particle diameters from SEM and TEM micrographs was done using the ImageJ program.

3.6 References

[1] F. Langhauser, J. Kerth, M. Kersting, P. Kölle, D. Lilge, P. Müller, *Die Angewandte Makromolekulare Chemie* **1994**, *223*, 155.

[2] T. F. McKenna, J. B. P. Soares, *Chemical Engineering Science* **2001**, *56*, 3931.

[3] J. R. Severn, J. C. Chadwick, R. Duchateau, N. Friederichs, *Chemical Reviews* **2005**, *105*, 4073.

[4] G. Fink, B. Steinmetz, J. Zechlin, C. Przybyla, B. Tesche, *Chemical Reviews* **2000**, *100*, 1377.

[5] X. Zheng, J. Loos, *Macromolecular Symposia* **2006**, *236*, 249.

[6] Y. J. Jang, C. Naundorf, M. Klapper, K. Mullen, *Macromolecular Chemistry and Physics* **2005**, *206*, 2027.

[7] M. Koch, A. Falcou, N. Nenov, M. Klapper, K. Müllen, *Macromolecular Rapid Communications* **2001**, *22*, 1455.

[8] Y. J. Jang, K. Bieber, C. Naundorf, N. Nenov, M. Kapper, K. Mullen, D. Ferrari, S. Knoke, G. Fink, *E-Polymers* **2005**.

[9] C. Naundorf, D. Ferrari, G. Rojas, G. Fink, M. Klapper, K. Müllen, *Macromol React Eng* **2009**, *3*, 456.

[10] V. R. H. Haugen, M. Brunner, J. Will, E. Wintermantel, *Journal of Materials Science: Materials in Medicine* **2004**, *15*, 343.

[11] A. S. S. Guelcher, A. Hafeman, K. Gallagher, J. Doctor, S. Khetan, S. McBride, J. Hollinger, *Tissue engineering* **2007**, *13*, 2321.

[12] K. Müller, M. Klapper, K. Müllen, *Colloid and Polymer Science* **2007**, *285*, 1157.

[13] K. Müller, M. Klapper, K. Müllen, *Journal of Polymer Science Part A: Polymer Chemistry* **2007**, *45*, 1101.

[14] K. Müller, M. Klapper, K. Müllen, *Macromolecular Rapid Communications* **2006**, *27*, 586.

[15] M. Antonietti, K. Landfester, *Progress in Polymer Science* **2002**, *27*, 689.

[16] T. E. L. M. E. Rogers, J. Wiley, *"Frontmatter", in Synthetic Methods in Step-Growth Polymers, John Wiley & Sons, Inc* **2003**, p. 197.

[17] P. J. Flory, *"Principles of polymer chemistry", Cornell University Press, Ithaca* **1953**.

[18] H. K. G. Rossmy, W. Lidy, H. Schator, M. Wiemann, *Journal of Cellular Plastics* **1981**, *17*, 319.

[19] G. L. W. J. P. Armistead, R. B. Turner, *Journal of applied polymer science* **1988**, *35*, 601.

[20] R. A. G. T. H. Mourey, T. G. Bryan, R. F. Thornbury, R. Blevins, R. J. Perry, S. R. Turner, *Journal of Applied Polymer Science* **1992**, *45*, 1983.

[21] A. Chow, W. Branagh, J. Chance, *Talanta* **1990**, *37*, 407.

[22] F. Silveira, G. P. Pires, C. F. Petry, D. Pozebon, F. C. Stedile, J. H. Z. d. Santos, A. Rigacci, *Journal of Molecular Catalysis A: Chemical* **2007**, *265*, 167.

[23] S. B. Roscoe, J. M. J. Fréchet, J. F. Walzer, A. J. Dias, *Science* **1998**, *280*, 270.

CHAPTER 4

High Density Polyethylene (HDPE) Fibers

Polyethylene fibers by metallocenes supported on electrospun nanoparticles

Abstract: The formation of polyethylene fibers via metallocene-catalyzed polymerization using anisotropic organic supports is presented. In contrast to other inorganic or organic supports, this process allows the formation of shape-anisotropic polyolefin fibers without further processing. Herein, shape anisotropic supports are obtained by electrospinning of a mixture of polyvinyl alcohol and polystyrene nanoparticles and used as templates for the formation of polyolefin fibers. After immobilization of the metallocene catalyst, the polymerization of ethylene generates fibers with diameters in the range of 0.3 to 2 micrometers, depending on polymerization time. A variety of characterization techniques such as cryo-TEM, SEM and laser scanning confocal fluorescence microscopy (LSCFM) are used to verify the templating effect of the electrospun fibers. Indeed, the polyethylene layer homogenously surrounds the shape-anisotropic support, and a core-sheath structure is obtained.

4 High Density Polyethylene Fibers

4.1 Polyolefin fibers

The synthesis of fibers based on polyolefins is of great interest in textile industries due to their low cost when compared to other polymers. The fibrous polyolefins are made into ropes, carpets, automotive fabrics, disposable diapers, protective clothing and medical care materials.[1, 2] The production of polyolefin fibers has high cost, however, since they are mostly converted from bulk polyolefin beads to fibers via indirect method such as melt spinning and solvent spinning. In this chapter, the direct synthesis of polyolefin fibers is addressed via metallocene immobilization techniques using a replication effect.

To transform polymers into fibers with various diameters in the range of few nm to μm, electrospinning is a simple and versatile technique (*Figure 4-1*).[3, 4] For electrospinning, a polymer must be soluble in a polar solvent to provide conductivity. Although various polymers have been electrospun,[5] there are few examples of electrospinning using polyolefins.[6-9] This is due to the difficulty of electrospinning these polyolefins.

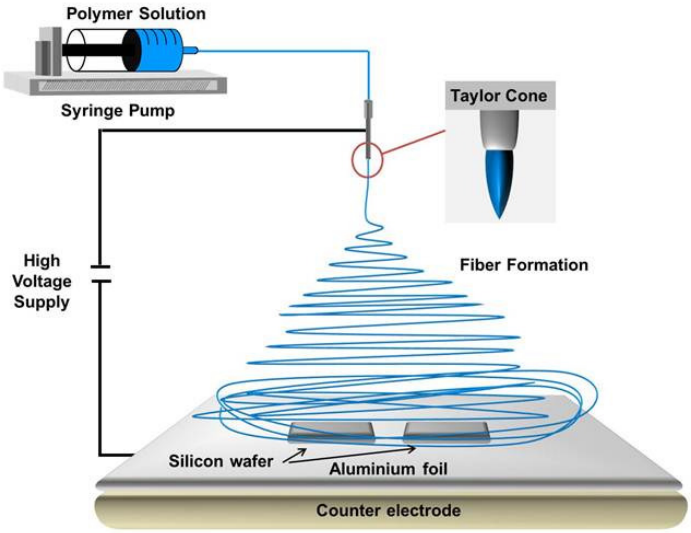

Figure 4-1. Schematic drawing of electrospinning set-up

Many important polyolefins, for example polyethylene, are crystalline at room temperature and therefore insoluble. Due to this insolubility, high temperatures above the melting point (T_m), are required for electrospinning polyolefins.[7-9] For instance, Larrondo and Manley performed electrospinning of polyethylene both from the melt at 200 – 220 °C and by diluting in paraffin at 100 °C.[6, 10, 11] After electrospinning, however, washing procedure is

required to remove the paraffin. This is not a trivial procedure and risk modifying the structure of the fiber. Givens et al. demonstrated electrospinning of linear low density polyethylene (LLDPE) dissolved in *p*-xylene containing 0.2 % *tert.*-butylammonium bromide.[7] Due to the low conductivity of the diluent, the addition of the salt was required to increase the dielectric constant of the polymer solution. Furthermore, to avoid the use of solvents, the melt electrospinning of polymers is attractive from the perspective of productivity and environmental considerations. However, the method is limited by the fact that nanofibers with diameters of less than 400 nm and with a narrow diameter distribution cannot be fabricated.

In order to synthesize polyolefin fibers directly from the supports, introducing anisotropic supports for metallocene-catalyzed polyolefin synthesis is considered. Indeed, Müller et. al. reported a direct formation of polyolefin fibers using anisotropic supports.[12, 13] Via electrospinning of polyvinyl alcohol (PVA), anisotropic supports are prepared and used for immobilizing a metallocene catalyst (*Figure 4-2*).

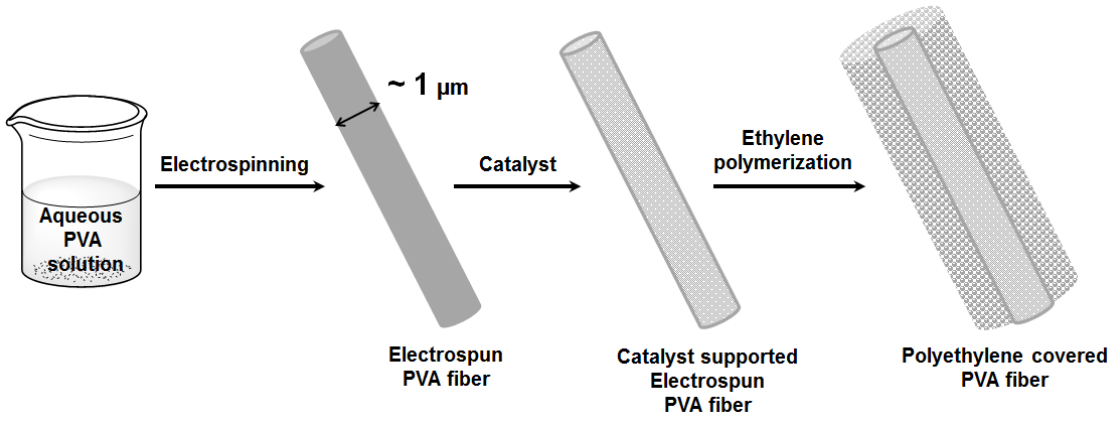

Figure 4-2. Schematic drawing of ethylene polymerization on electrospun PVA fibers

By ethylene polymerization using the metallocene-supported PVA fibers, polyethylene-surrounded PVA fibers are achieved (*Figure 4-3*). Under extremely low pressure of ethylene (0.5 bar), the replication effect of the anisotropic PVA supports can be observed (*Figure 4-3a,b*) whereas a poor morphology of the final products is detected upon increasing the ethylene pressure above 1.0 bar (*Figure 4-3c,d*). It is assumed that the poor morphology control is associated with negligible interactions between PVA fibers and the complex of metallocene/MAO.

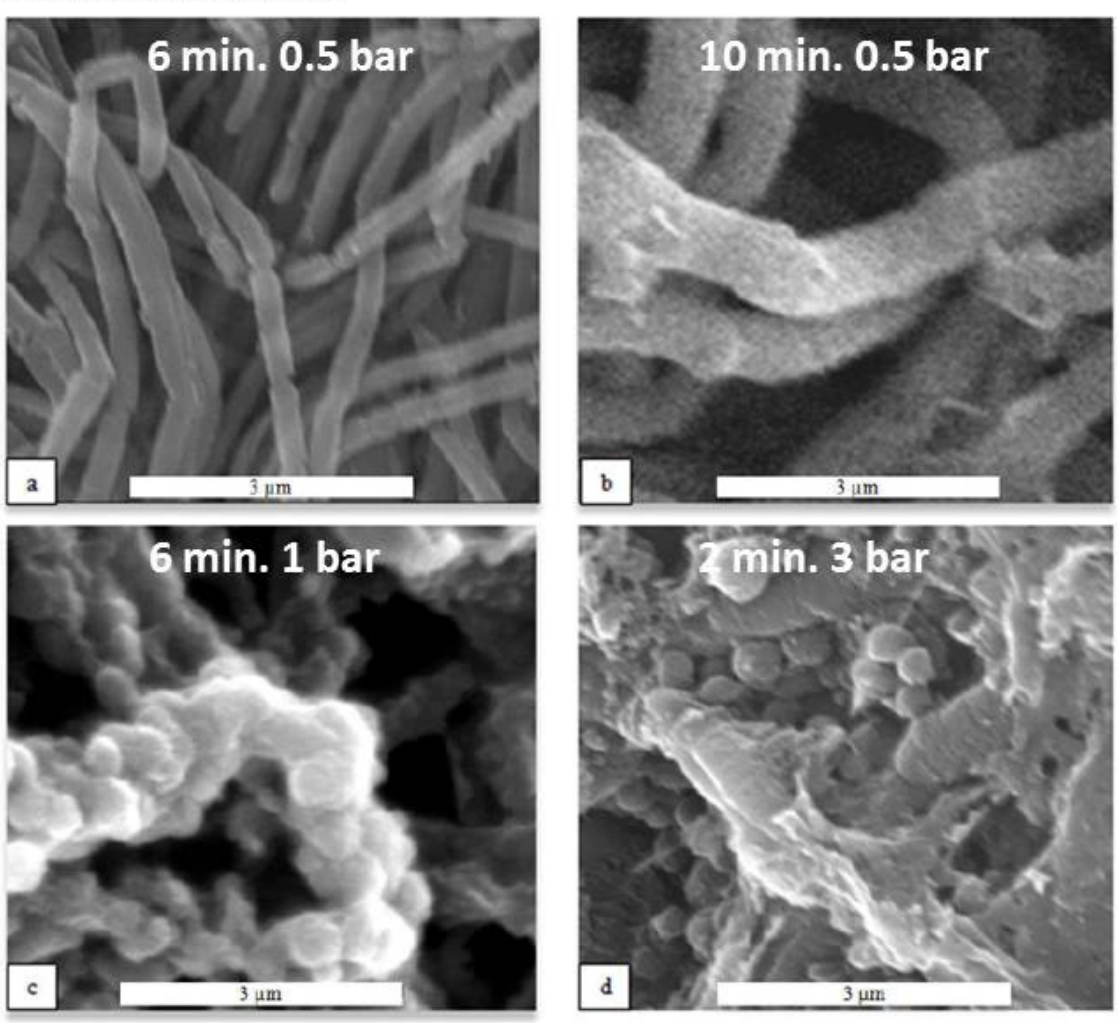

Figure 4-3. SEM micrographs of ethylene polymerized electrospun PVA fibers with various reaction conditions

To date, spherical particles have mostly been applied as supports, and therefore only spherical polyolefin particles have been obtained due to the replication effect (**Section 3.1**). For many applications, however, polyolefin fibers are desired, *e.g.* for membranes or for reinforcement in composite materials. These fibers are usually generated by an additional processing step. Therefore, a facile method for production of fibers directly out of the reactor is highly suitable.

4.2 Objectives

In this chapter, introducing anisotropic fibers as supports is addressed instead of isotropic spherical particles. Based on previous results of Müller et. al.(*Figure 4-2*),[12, 13] it is expected that polyolefin fibers should be obtained in the polymerization process, according to the replication effect. However, unlike these previous attempts, supports which interact more strongly with the catalysts will be used to better control the fiber morphology and prevent the uncontrolled fragmentation of the support at an early stage of the polymerization.[14] Stronger interactions will be promoted by introducing nucleophilic chains, *e.g.* poly(ethylene oxide) (PEO), on the surface of PS nanoparticles instead of polymer chains aggregates. Due to the nucleophilic PEO groups, the interaction between support and metallocene becomes enhanced and the fragmentation slows down.[14-17]

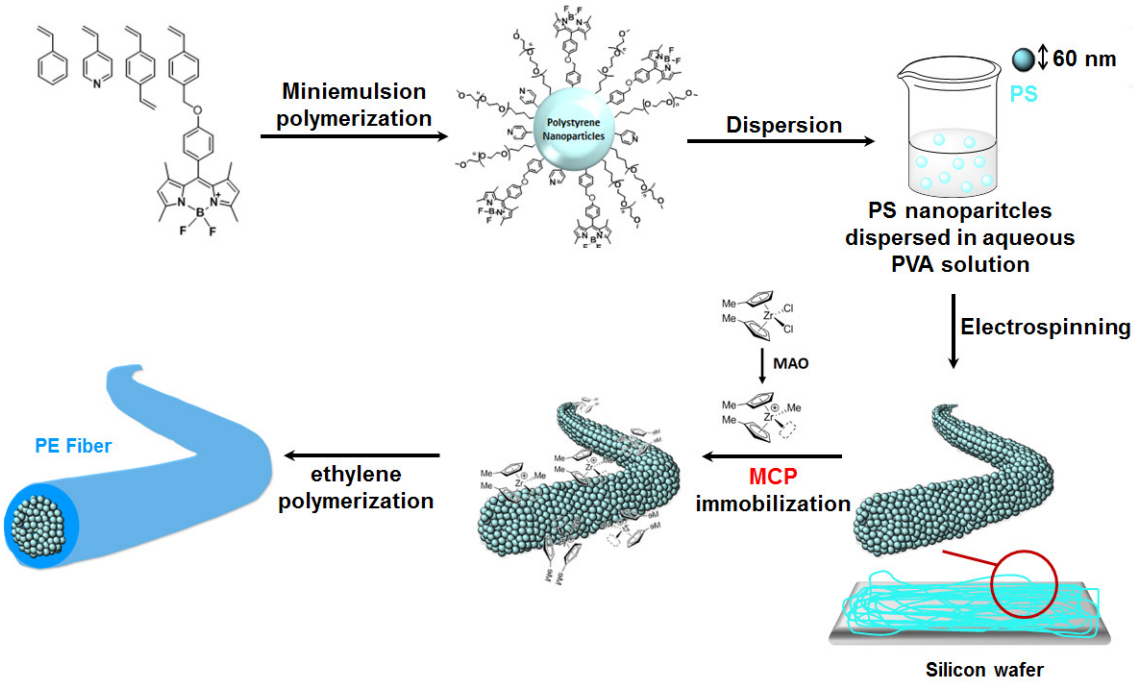

Figure 4-4. Schematic drawing for the preparation of PE fibers by supported metallocene catalysts on electrospun fibers

Therefore, as shown in *Figure 4-4*, this new strategy consists of using the aforementioned PS nanoparticles (isotropic building blocks) to produce fibers (anisotropic supports). The transformation is conveniently carried out by the well-established colloid-electrospinning process,[18] as generally demonstrated for polymer[4, 19-21] or inorganic nanoparticles.[22, 23] As PEO-functionalized PS nanoparticles are introduced into the anisotropic fibers, the methylaluminoxane (MAO) activated metallocene, bis(methylcyclopentadienyl)zirconium(IV) dichloride (MCP), can non-covalently interact

with the PEG-chains on the fibers. The anisotropic supports play a role as a template for the formation of uniform polyolefin fibers because the shape is perfectly replicated during the olefin polymerization. These supports offer the possibility to synthesize polyolefin fibers with a controlled diameter determined by the polymerization time as well as the electrospinning parameters. Furthermore, since fragmentation studies are required in heterogeneous metallocene polymerizations (**Chapter 3**), laser scanning fluorescence miscroscopy (LSCFM) will be applied by simply copolymerizing a fluorescence dye to the PS nanoparticles (*Figure 4-4*).

4.3 Results and discussion

4.3.1 Synthesis of the anisotropic supports with polystyrene nanoparticles

To prepare anisotropic supports via colloid electrospinning, isotropic polystyrene (PS) nanoparticles were initially synthesized via copolymerization of styrene, 4-vinylpyridine, divinylbenzene and a styryl boron-dipyrromethene (BODIPY) dye in a miniemulsion as shown in *Figure 4-5*. Lutensol AT 50 (PEO-ethoxy fattyalcohol) was used as an emulsifier to stabilize the miniemulsion and to provide the anchoring groups for the immobilization of metallocene complexes. As PS nanoparticles are chemically linked with a BODIPY dye, they show maximum emission at 510 nm which is in good agreement with non-linked BODIPY, and there was no negative influence by the chemical linkage.[20] By the addition of 0.05 mol% of the styryl BODIPY dye during the copolymerization of the PS nanoparticles, fragmentation studies of supports after ethylene polymerization can conveniently be carried out with laser scanning confocal fluorescence microscopy (LSCFM). The mean diameter of the PS nanoparticles was measured by dynamic light scattering (DLS) and scanning electron microscopy (SEM) (*Figure 4-7a*).

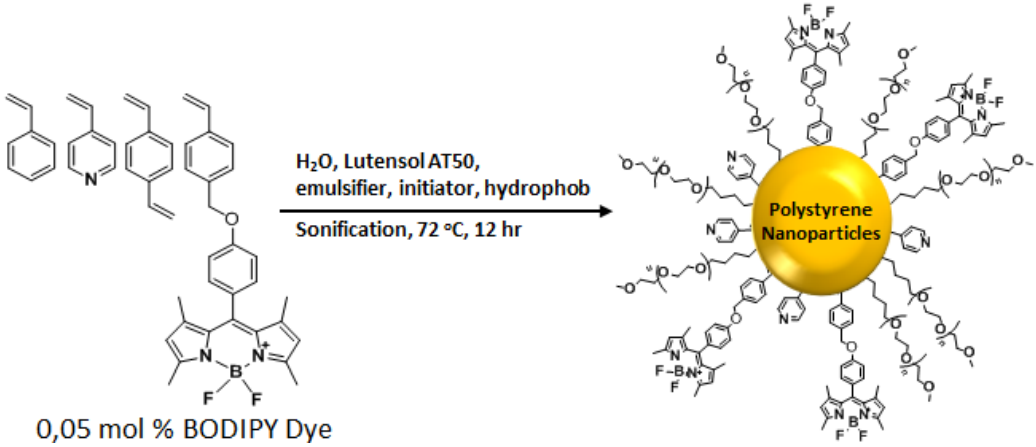

Figure 4-5. Synthetic scheme for the preparation of PS nanoparticles chemically linked with BODIPY dye

Via colloid electrospinning of the PS nanoparticles in the presence of polyvinyl alcohol (PVA), transformation of PS nanoparticles into anisotropic fibers is achieved (*Figure 4-6*). The roles of PVA are important by acting as an adhesive for the spherical building blocks and delivering a viscosity to the mixture for electrospinning. The obtained fibers show an

average diameter of ~ 200 nm (*Figure 4-7b-d*). The assembled PS nanoparticles are still visible in the electrospun fibers and keep their initial diameter and spherical shape (*Figure 4-7d*). Therefore, transformation of isotropic objects (spherical PS nanoparticles) to anisotropic supports (electrospun fibers) is successfully conducted via colloid electrospinning.

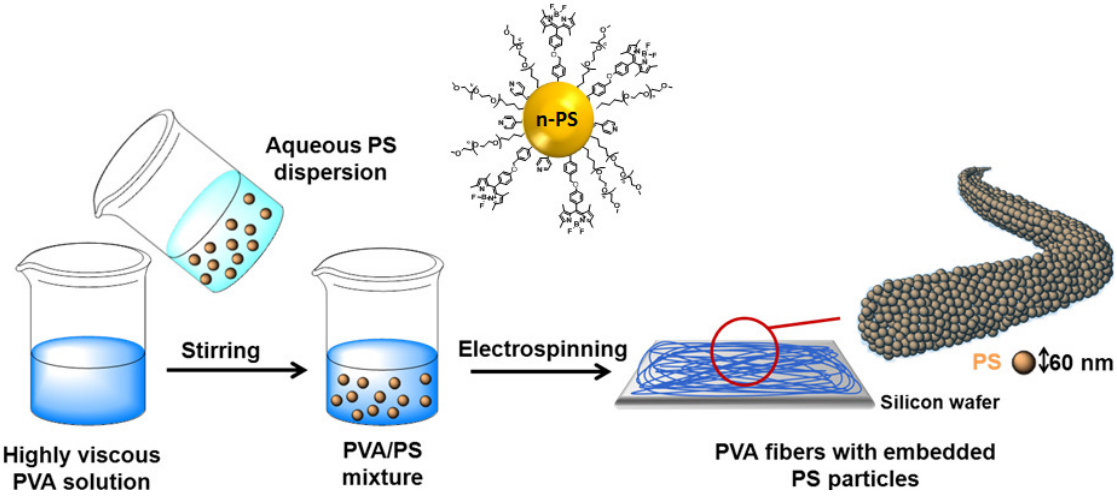

Figure 4-6. Synthetic scheme of electrospun fibers with the PS nanoparticles

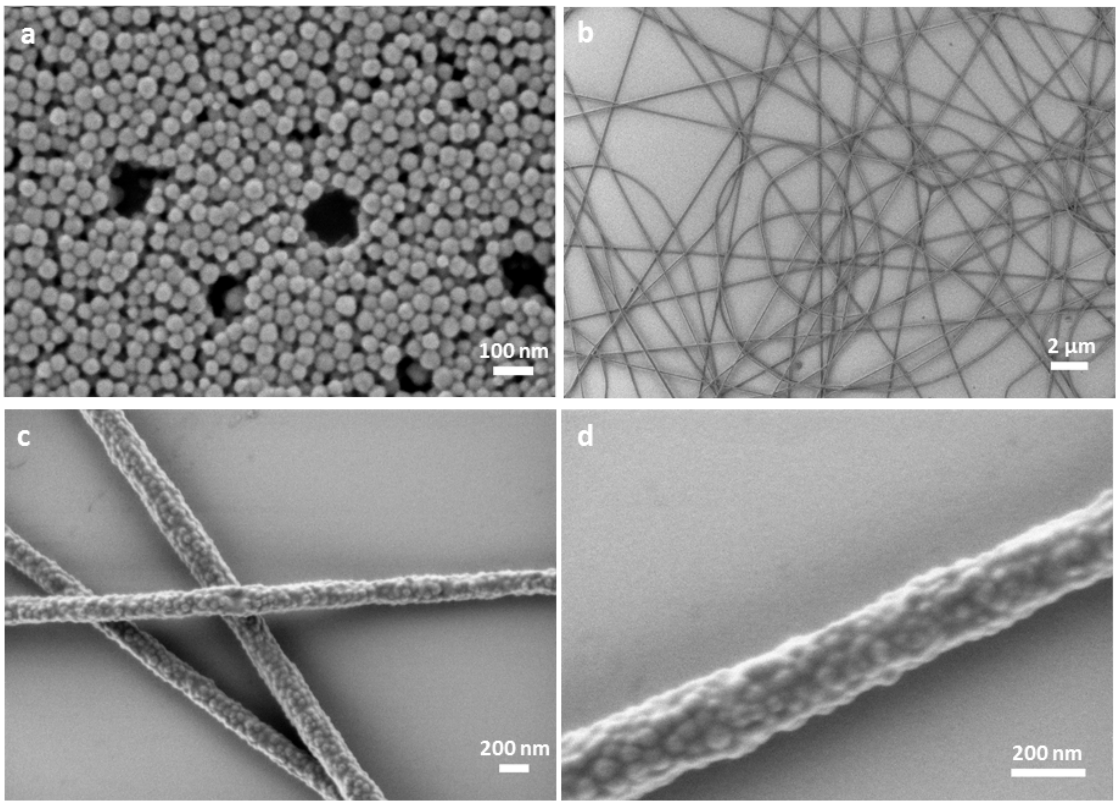

Figure 4-7. (a) SEM micrograph of functionalized PS nanoparticles synthesized by miniemulsion polymerization, and (b-d) SEM micrograph of electrospun fibers with embedded PS nanoparticles

4.3.2 Immobilizing metallocene on the electrospun fibers

In order to perform the olefin polymerization with the anisotropic supports, immobilization of a metallocene complex is conducted. Since the electrospun fibers possess PEO groups as nucleophilic anchoring units on the surface, the cationic character of MAO-activated metallocene catalysts can non-covalently interact with the fibers, as previously shown in *Figure 1-21* (**Chapter 1**). Before supporting MAO-activated metallocene catalyst (MCP), the electrospun fibers were also treated with MAO which acts as a scavenger to remove the residual moisture in the support. Finally, the solution of the MCP/MAO was added to the fibers and gently shaken to immobilize the complex of MCP/MAO. Thereafter, the fiber was washed and dried. To elucidate the structure of the fiber after the immobilization procedure, the fibers were measured by SEM and no change in the fibers was observed, *i.e.* this was a non-destructive technique.

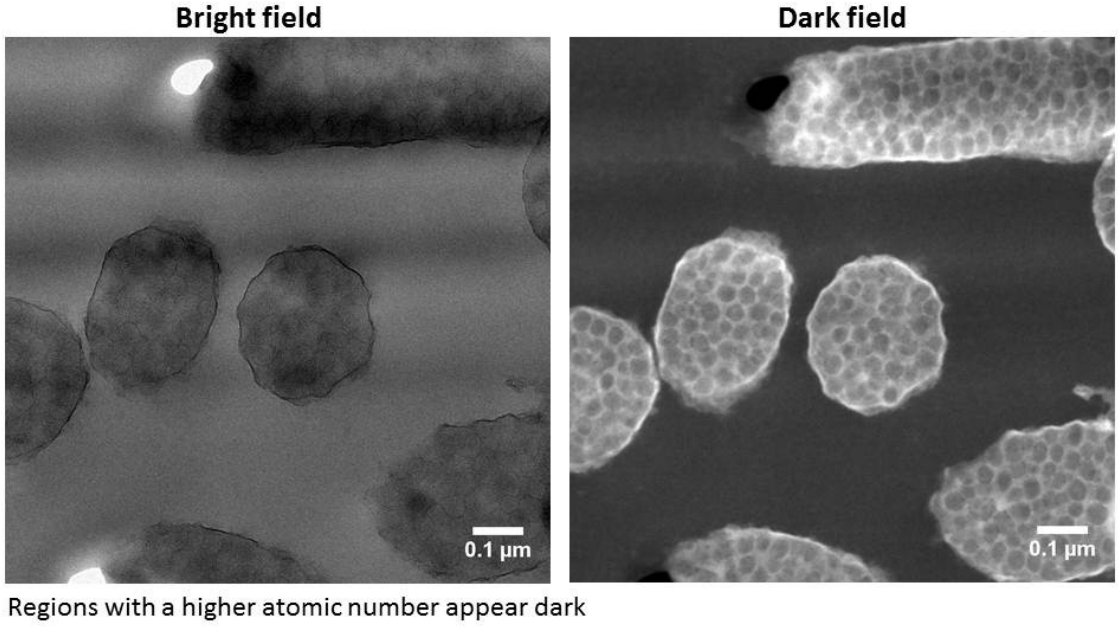

Figure 4-8. TEM micrographs of cryo-sectioned electrospun fibers after immobilizing MCP/MAO

To check the successful immobilization of the MCP/MAO complex, the fibers were cryo-sectioned and measured by TEM under dark and bright field. As shown in *Figure 4-8*, the TEM micrograph in bright field displays slightly darker regions around the outer line of the fibers which comes from an element with a higher atomic number. As zirconium from MCP has the highest atomic number, it might indicate the existence of MCP around the fibers. The bright and white areas originate from air bubbles formed during molding for

cryo-sectioning (bright field, *Figure 4-8*). Interestingly, the TEM micrograph in dark field (*Figure 4-8*) exhibits assembled PS nanoparticles in the fiber which maintain their spherical shape and are specifically separated due to the presence of PVA.

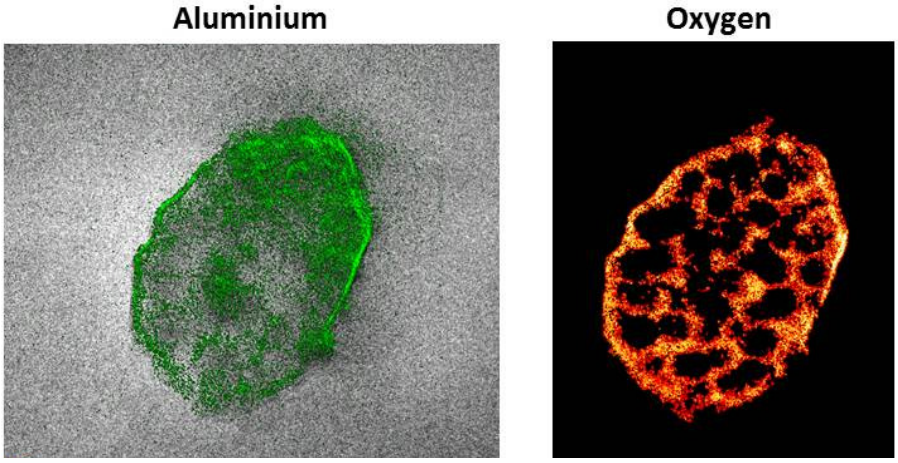

Figure 4-9. Electron mapping of (left) aluminum and (right) oxygen on the TEM micrograph

For checking the specific element distribution over the cryo-sectioned fibers, TEM-ESI (electron spectroscopic imaging) was conducted. The distribution of "aluminum" (originated from only MAO/MCP complex) and "oxygen" (from PVA and MAO/MCP complex) are detected whereas no "zirconium" (from MCP) was detected due to the low content. *Figure 4-9* shows that aluminum is almost exclusively observed at the outer surface of the fibers, and oxygen is distributed selectively over the fibers except in the regions of the PS particles. It implies that PVA is holding the PS nanoparticles, and MAO is coated around the electrospun fibers.

4.3.3 Ethylene polymerization of the electrospun fibers in a gas phase reactor

For the ethylene homopolymerization in a gas phase reactor, the fibers, immobilized with MCP/MAO, were placed on the upper stage (a silver coated plate) of the reactor (*Figure 4-10*). In the bottom of the reactor, DMAO solids and internal standard particles were placed. As DMAO reacts with moisture, ethylene can be additionally purified. For the internal standard particles, silica particles treated with an activated metallocene catalyst were applied. The growth of these silica particles acts as an indicator to validate that the

polymerization was successfully performed since they have catalytic activity under the same conditions.

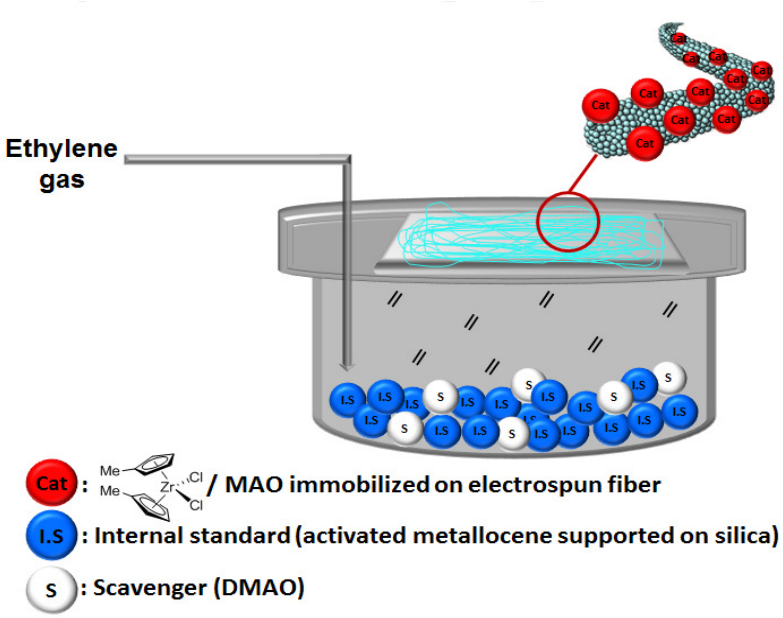

Figure 4-10. Schematic drawing of the ethylene homopolymerization in a gas phase reactor

Ethylene polymerization was performed in a gas phase reactor under 3.0 bar of ethylene at 40 °C. An extremely low [Al]/[Zr] ratio (170/1) was applied when compared to a homogeneous system which requires almost 10 fold higher ratios. Such a low ratio is typical for olefin polymerizations with supporting metallocenes.[24-26] After a desired reaction time, the polymerization was terminated by releasing the monomer and quenched by exposure to air. The activity was determined by gravimetric analysis. The obtained polyethylene was extracted from the fibers for characterization. The results of the ethylene polymerization in the gas phase reactor are summarized in *Table 4-1*.

Table 4-1. Characteristics for the ethylene polymerization from the nanofibers in a gas phase reactor[a)]

entry	maximum loaded catalyst	amount of catalyst	MAO	[Al]/[Zr]	activity	T_m[b)]	M_w[c)]
	µmol Zr /(g fiber)	µmol	µmol		kgPE/(mol Zr h bar)	°C	kg·mol^{-1}
1	25	2.17	370	170	121	135.6	659
2	25	2.43	410	170	96	135.8	790

a) Polymerization under 3 bar of ethylene at 40 °C for 30 min;
b) determined by DSC;
c) analyzed by GPC (PS-standard).

To indicate the formation of polyethylene, the extracted polymers are characterized by ^{13}C NMR spectroscopy and show one single peak at 29.98 ppm.[27] This singlet indicates that the polyethylene produced by MCP/MAO is high density polyethylene (HDPE) with no branches. A typical melting temperature of the HDPE is also detected as approximately 136 °C by DSC. The molecular weight (M_w) measured by GPC was determined to be in the range of 659 and 790 kg·mol^{-1}. These results are very similar to values for non-supported polymerizations,[28] indicating that the fibrous support has no negative influence on the polymerization behavior of the catalyst. The activity being in the range of 90 – 130 kgPE·(mol Zr·h·bar)$^{-1}$ corresponds to the typical values for supported MCP/MAO. From these results, it can be concluded that the nucleophilic groups, especially the hydroxy groups of PVA, do not negatively influence the activity of the catalysts. TGA thermograms (under nitrogen atmosphere) of the PE fibers show that the decomposition starts at 280-290 °C, which is attributed to the decomposition of PVA since PE typically degrades above 400 °C.[28]

4.3.4 Morphology of the polyolefin fibers

In order to deliver additional information about the polymerization process, the morphology of the PE fibers (*e.g.* surface morphology and diameter) was studied by various optical techniques (SEM, TEM and LSCFM). After 10 min of ethylene polymerization (*Figure 4-11b*), the structure of the spherical particle on the surface of the fibers vanishes as the fibers are covered by the PE. In addition, the mean diameter of the fibers increases from 250 nm to 350 nm (*Figure 4-11a*). By further increasing the ethylene polymerization times, an increased mean diameter of the fibers to the micrometer range with well-defined structures is observed (*Figure 4-11c-d).* After longer reaction times, the fibrous structure disappears as the PE grows in three dimensions and fills the gaps between the fibers. The homogeneous growth of the fibers demonstrates that the diameters of the PE fibers can be easily controlled by the polymerization times.

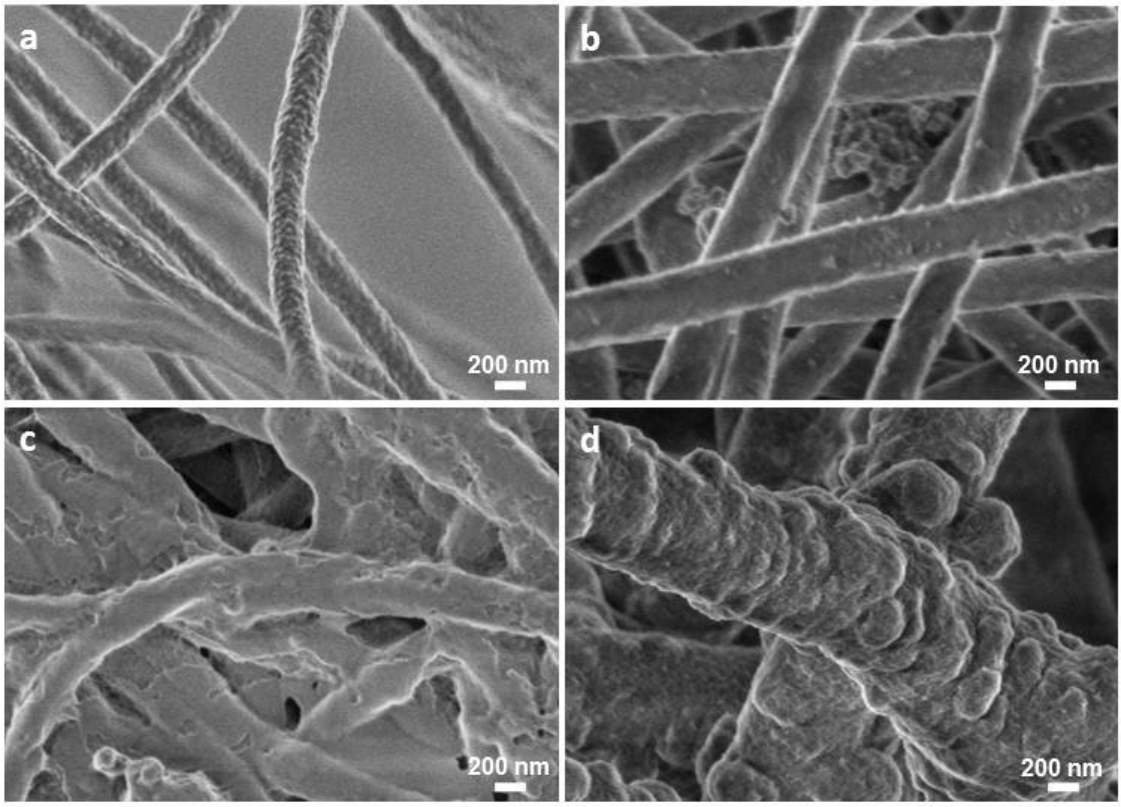

Figure 4-11. SEM micrographs of electrospun nanofibers with ethylene polymerized in a gas phase reactor for (a) 0 min, (b) 10 min, (c) 30 min and (d) 60 min at 40 °C and 3.0 bar of ethylene

To understand the fragmentation behavior of the electrospun fibers during ethylene polymerization, further studies were required since homogeneous growth of the fibers was observed. The inner morphology of the ethylene polymerized fibers is therefore studied by means of SEM and cryo-TEM. For SEM microscopy (*Figure 4-12*), the PE fibers were processed by two different methods either by stretching at room temperature or fractured at a low temperature by liquid nitrogen. From the stretched PE fibers, SEM micrographs show sectioned PE fiber with extended core materials, induced by stretching (*Figure 4-12a,b*). Extended electrospun fibers (core) can be associated with the presence of PVA in the electrospun fiber. As the PE fibers were stretched out at room temperature, PVA can be selectively extended whereas PE layers fracture upon extention. From the PE fibers fractured using liquid nitrogen, SEM micrographs (*Figure 4-12c,d*) show more clearly a core-sheath structure consisting of spherical PS nanoparticles located in the core and a surrounding PE layer. The boundary between the assembled PS nanoparticles and PE layer is clearly visualized. Cryo-TEM experiments (*Figure 4-13*) also indicate the formation of core-sheath fibers. The domains with a darker spherical core were identified as PS nanoparticles in the electrospun fibers and the brighter surrounding layers as PE.

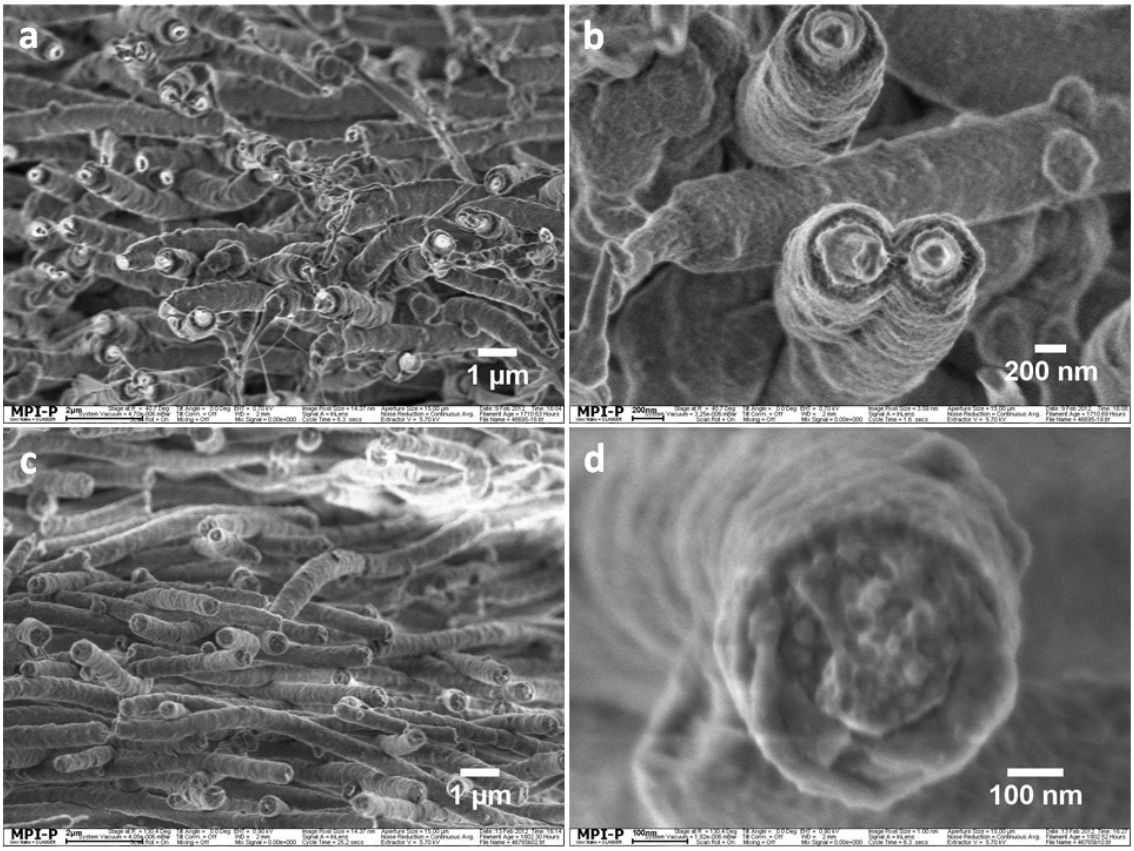

Figure 4-12. SEM micrographs of PE fibers prepared by (a,b) stretching at room temperature and (c,d) fractured at low temperature using liquid nitrogen

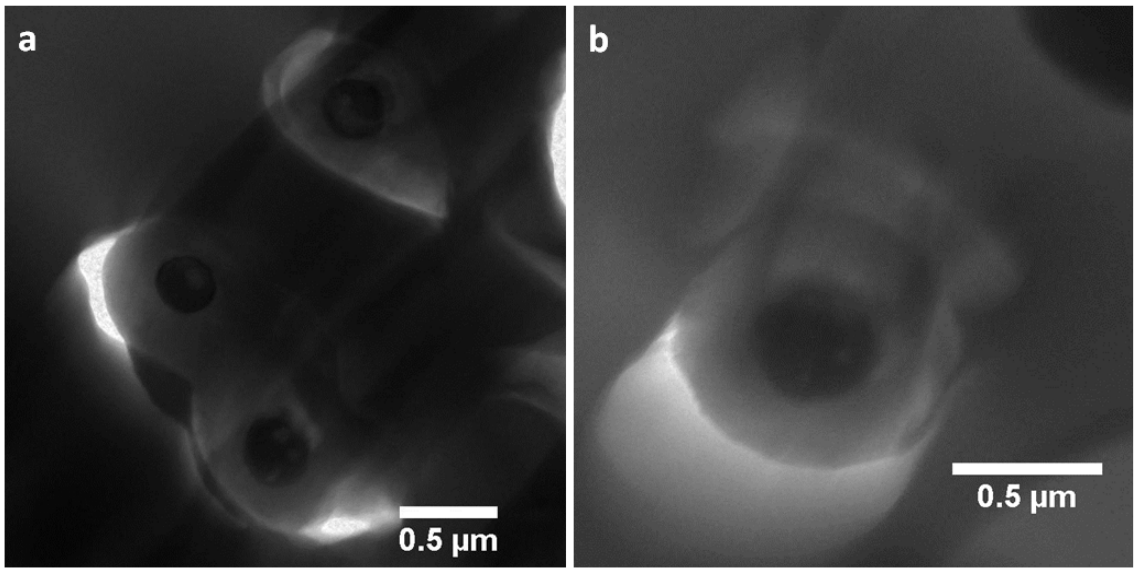

Figure 4-13. TEM micrograph of cryo-sectioned PE fibers

To further investigate the distribution of the electrospun fibers in the product, laser scanning confocal fluorescence microscopy (LSCFM) was employed by applying a fluorescence dye to the carrier. No additional staining procedure is followed as the PS nanoparticles were already tagged with the styryl-boron-dipyrromethene (BODIPY).

LSCFM had previously proven successful in studying the fragmentation of spherical supports[17, 29] including porous polyurethane particles (**Chapter 3**). PE fibers obtained after a polymerization time of 30 min show a fluorescent continuous inner core with a diameter of 250 nm (*Figure 4-14*).

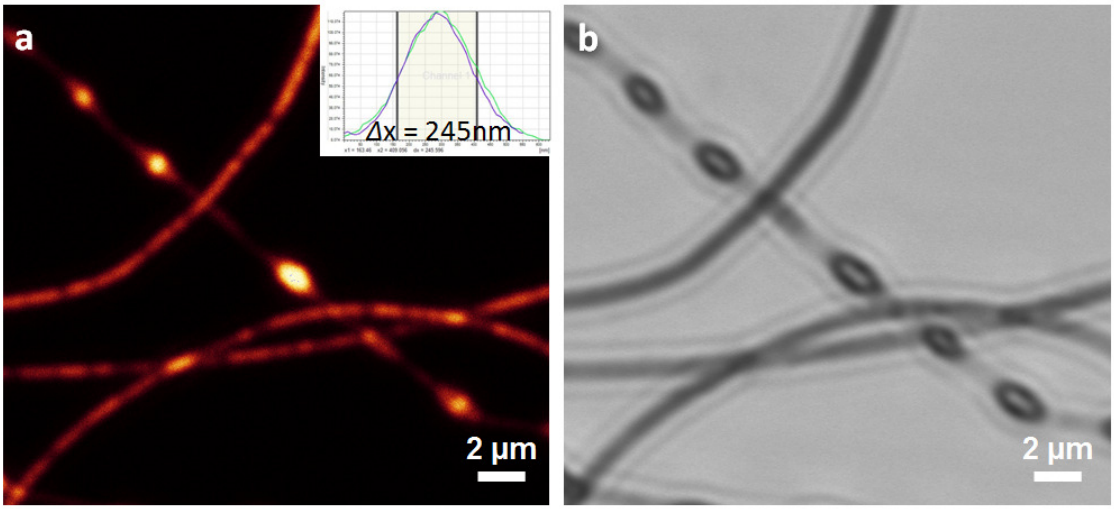

Figure 4-14. (a) LSCFM and (b) transmission image of the PE fibers obtained after 30 min of polymerization under 3.0 bar ethylene at 40 °C in a gas phase reactor

As no fluorescence was detected in the surrounding PE layer, it is assumed that the PS nanoparticles probably do not fragment during the polymerization process and remain in the core of the product fiber. This observation is in contrast to the previously studied spherical organic supports based on aggregates of nanoparticles where after polymerization the fragments are homogenously distributed in the products.[26, 30] It is also an indication that the metallocenes were only supported on the surface of the fibers and not between the nanoparticles. Therefore, the ethylene polymerizations proceed only at the surface of the fibers and not within the PS nanoparticles which would be required for a fragmentation of the support.

4.4 Outlook

Herein the synthesis of core-sheath structured fibers made by ethylene polymerization of the selectively loaded MAO/MCP complex on electorspun fibers is presented. Such morphology is associated by the presence of PVA as adhesive in the electrospun fibers. By using the properties of unfragmented electrospun fibers, production of an electrical cable can be suggested by adding a conductive polymer to the core as polyolefins are good insulators.

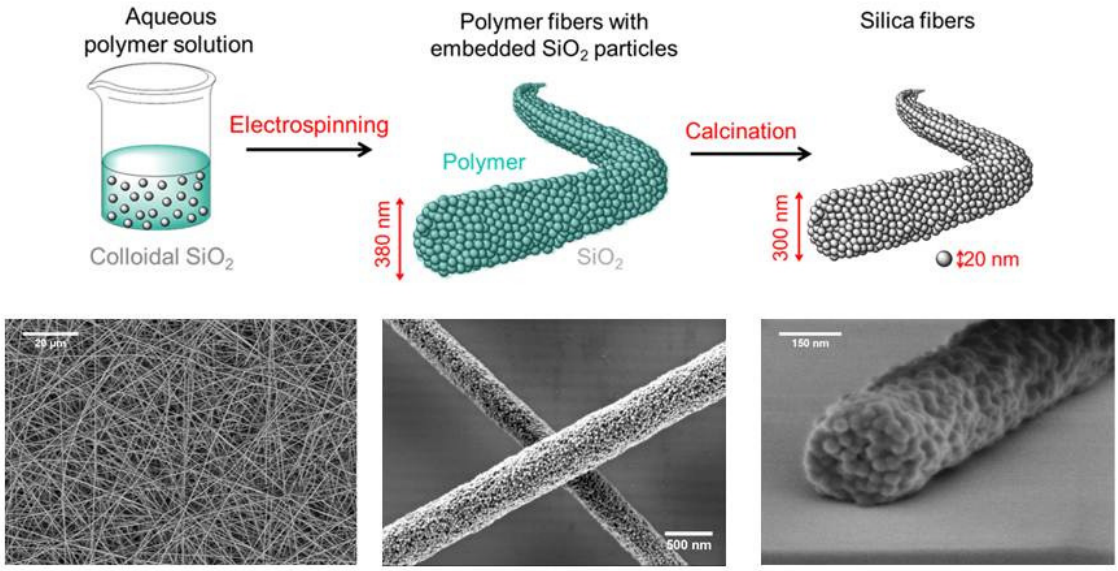

Figure 4-15. Silica-electrospun fibers obtained via colloid electrospinning

Another point to suggest is a synthetic method for producing pure polyolefin fibers. By substituting the electrospun PS fibers into a fiber material which is fragmentable during the olefin polymerization, pure polyolefin fiber can be also achieved. As previously explained, silica gels are commonly applied supports for metallocene-catalyzed polyolefin synthesis since they can be broken down into small fragments during the olefin polymerization. Friedemann et al. reported "silica fibers", prepared by colloid electrospinning of silica nanoparticles in the presence of PVA and subsequently calcinating the PVA as shown in *Figure 4-15*. By this procedure, silica-electrospun fibers were obtained with 380 nm diameter, comprised of silica particles with a mean diameter of 20 nm. One could consider that applying silica-based electrospun fibers as a support for metallocene to afford polyolefin fibers.

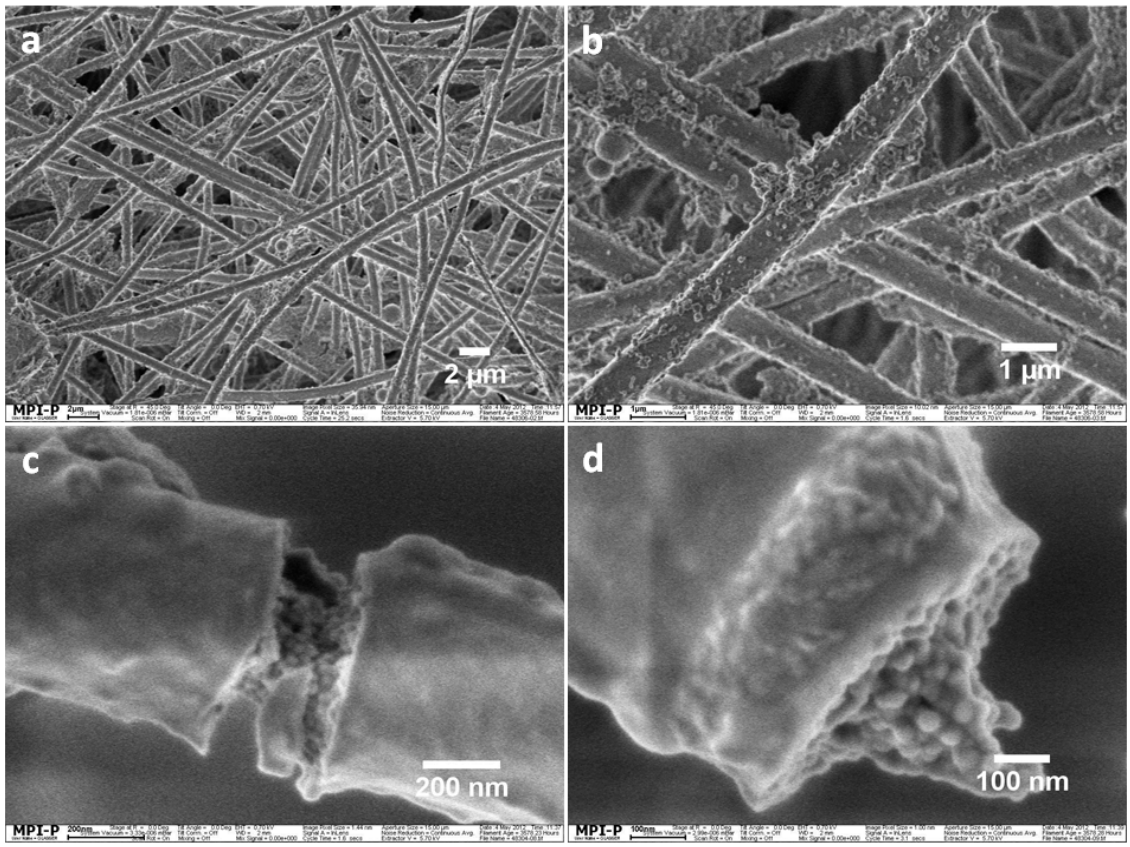

Figure 4-16. Ethylene polymerized fiber based on silica-electrospun fibers

For instance, by immobilizing bis(phenoxy-imino)titanium complexes on the silica-based electrospun fibers, mechanically robust polyethylene, ultra high molecular weight polyethylene (UHMWPE) fibers can be also prepared directly from ethylene polymerization. The product fibers are determined with an approximate diameter of 800 nm, comprised of unfragmented silica particles in the core of the fiber (*Figure 4-16*). By modulating the conditions of ethylene polymerization, the silica particles can be fully fragmented and results almost pure polymer fiber. Furthermore, UHMWPE is relatively difficult to process into fibers due to extremely high molecular weight (over 2 million g/mol). Although this project was not further studied, it would be a potential method to produce polyolefin-based fiber without processing after polymerization.

4.5 Conclusion

The production of polyolefin fibers and mats in a one-pot procedure has been shown by using the replication effect of the support´s shape. Previously, only spherical particles have been obtained in olefin polymerization with supported metallocene catalysts. Shape anisotropic supports for catalysts were fabricated by electrospinning PEO-functionalized PS nanoparticles in the presence of PVA. After immobilization of a metallocene on the electrospun fibers, polymerizations of ethylene in a gas phase reactor were performed. Mats of uniform polyethylene fibers were obtained. Remarkably, the diameter of the fiber products was determined by the polymerization time. SEM, cryo-TEM and LSCFM investigations on the mats show that the produced fibers display a core-sheath structure consisting of PS nanoparticles and PVA in the core and PE in the sheath.

This represents an easy method to directly fabricate well-defined polyolefin fibers in the reactor without any further processing. Because a non-covalent supporting method is used, various other catalysts can also be applied as a template. Thus, polymers of different tacticity, crystallinity and molecular weight can be conveniently tailored according to the properties of the catalysts and olefins. By using the unfragmented behavior of the electrospun fibers, furthermore, an electrical cable can be produced by simply employing to the core since polyolefins (sheath) are good insulators. By using three-dimensional supports such as mats, this synthetic pathway for core-sheath fiber allows for an alternative methodology to fabricate a membrane with porosity controlled by varying the polymerization time. Furthermore, new types of reinforced composite materials could be also produced by blending fibers of UHMWPE with a more flexible LDPE.

4.6 Experimental part

4.6.1 General procedure and materials

Styrene (Aldrich), divinylbenzene (Fluka), and 4-vinyl pyridine (Aldrich) were dried over CaH_2 and distilled under reduced pressure. Lutensol AT50 (PEO-ethoxy fatty alcohol) was donated by BASF AG and used without further purification. Cetyltrimethylammonium bromide (Sigma), hexadecane (Merck-Schuchardt), α,α´-azodiiso-butyramidine dihydrochloride (Fluka) poly(vinyl alcohol) (PVA) (M_w ~ 125,000 g·mol^{-1}, Polysciences Inc., 88 mol% hydrolyzed) were used as received.

4.6.2 Synthesis of styryl-boron-dipyrromethene (BODIPY) dye

The 4-[(4-vinylbenzyl)oxy]benzaldehyde (**1**) was prepared according to a literature procedure.[31] Suspension of 4-vinylbenzyl chloride (5.0 g, 320 mmol), 4-hydroxybenzaldehyde (4.0 g, 1 eq) and potassium carbonate (8.0 g, 60 mmol) in acetone were refluxed overnight. After removal of the inorganic salts, a brown oil was obtained via evaporation. By addition of n-hexane, a yellow solid was precipitated and collected by filtration. After drying in a vacuum, 4-[(4-vinylbenzyl)oxy]benzaldehyde (**1**) was yielded with 60 % (4.0 g).

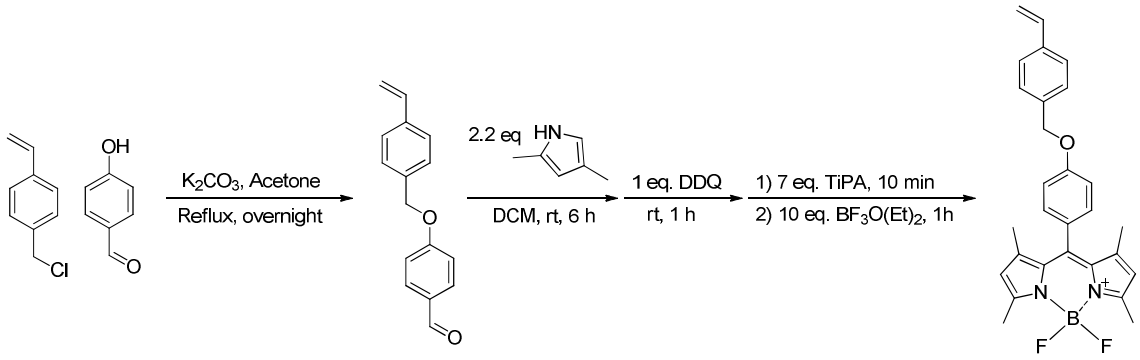

1 **2**

For the synthesis of styryl boron-dipyrromethene dye (BODIPY) (**2**), 2,4-dimethyl-1*H*-pyrrole (1.44 g, 15.11 mmol) was added to the solution of **1** in 10 mL dry dichloromethane in the presence of 3 drops of trifluoroacetic acid. The mixture was stirred at room temperature for 6 h. Subsequently, 2,3-dichloro-5,6-dicyanobenzoquinone (1.71 g, 7.55 mmol) was added and stirred for an additional 1 h. Triisopropylamine (7.58 g, 52.88 mmol) was then added. After 10 minutes, boron trifluoride etherate (10.64 g, 75.54 mmol) was

added and stirred for 1 h. The reaction was quenched by the addition of water (50 mL), and the mixture was extracted with pentane (3 × 50 mL). The combined organic fractions were dried over $MgSO_4$ and evaporated under reduced pressure. Styryl BODIPY (**2**) was obtained as a red crystalline solid with an overall yield of 12 % (0.37 g).
^{1}H NMR (300 MHz $CDCl_3$ [ppm]): δ = 7.47-7.40 (q, 4H, 4 × *H*-Ar), 7.19-7.06 (q, 4H, 4 × *H*-Ar), 6.74 (dd, *J* = 14, 10 Hz, 1H, *H*C=CH_2), 5.98 (s, 2H, *H*-pyrrole), 5.79 (d, *J* = 14 Hz, 1H, H=CH-*H*), 5.28 (d, *J* = 10 Hz, 1H, H=CH-*H*), 5.11 (s, 2H, CH_2-Ar), 2.55 (s, 6H, 2 × CH_3-pyrrole), 1.43 (s, 6H, 2 × CH_3-pyrrole) ^{13}C NMR (75 MHz, $CDCl_3$ [ppm]): δ = 159.28, 155.30, 143.15, 141.76, 137.54, 136.38, 135.98, 131.83, 129.25, 127.80, 127.42, 126.44, 121.10, 115.62, 114.26, 69.97, 14.56.

4.6.3 Preparation of the PEO-functionalized PS nanoparticles with styryl BODIPY

Cetyltrimethylammonium bromide (0.48 g, 1.31 mmol) and Lutensol AT50 (0.40 g, 0.16 mmol, 0.15 mol%, 3.5 wt%) were dissolved in deionized water (100 mL) and stirred for 30 min at 40 °C. Styrene (5.0 g, 48.0 mmol, 47 mol%), 4-vinylpyridine (5.0 g, 47.3 mmol, 46 mol%), divinylbenzene (0.91 g, 7.0 mmol, 6 mol%) as a crosslinker, styryl BODIPY (**2**) (25 mg, 54.8 μmol) as a fluorescence dye and hexadecane (0.42 g, 1.86 mmol) as a hydrophobe were mixed and added to the water/emulsifier mixture at room temperature. The solution was stirred for 30 min and then ultrasonicated with a Branson Sonifier 450W with 70 % power under ice cooling for 7 min to form a miniemulsion. The miniemulsion was degassed with argon for 20 min and then heated to 72 °C. α,α´-Azodiiso-butyramidinedihydrochloride (0.21 g, 0.77 mmol) was dissolved in 10 mL deionized water, degassed for 20 min and added to the miniemulsion. After 12 h, the polymerization was terminated and cooled to room temperature. The dispersion of BODIPY-linked polystyrene (PS) nanoparticles was stored in a brown glass bottle to avoid bleaching of the dye.

4.6.4 Electrospinning of the PS nanoparticles

The electrospinning of the PS nanoparticles was performed [redacted] with an electrospin cabin dual voltage (IME Technologies), applying a positive voltage of 10 kV and a tip-to-collector distance of 9.7 cm. To a 9.0 wt% aqueous solution of PVA prepared

at 85 °C, the dispersed PS nanoparticles were added to reach a weight ratio PVA:PS of 1:1. The mixture was stirred with a vortex at 2400 rpm for 5 min to ensure that the nanoparticles were completely dispersed. The final concentrations of PS and PVA in the electrospinning solution were 45 $mg \cdot mL^{-1}$.During the experiments the flow of the dispersions was held constant at 2.0 $\mu L \cdot min^{-1}$ using a syringe pump (PHD 22/2000, Harvard Apparatus). The grounded counter electrode was covered with aluminum foil, and the fibers were directly spun on either silicon wafers or glass slides with dimensions of 2.5 × 5 cm placed in the center of the deposition area. The obtained composite fiber mats were then dried at room temperature for 12 h under reduced pressure to evaporate the water.

4.6.5 Immobilizing procedure for metallocene/MAO on the electrospun fibers

Prior to immobilization of the metallocene catalysts, the fibers were submerged in 5 mL of dry toluene in a customized flask under an inert atmosphere. In order to extract the residual water from the fibers, the flask was mounted on a shaker at 100 rpm. After 3 h the toluene was removed and fresh toluene was added for additional extraction of water. This procedure was repeated 3 times. After removal of toluene from the flask, a mixture of 4.0 mL toluene and 1.0 mL of a 1.0 M MAO solution (prepared from DMAO) was added in the flask and shaken for an additional 3 h to ensure the complete removal of the residual water from the fibers by the action of the MAO as scavenger. Subsequently, the fibers were washed with fresh toluene (3 × 5 mL). Bis(methylcyclopentadienyl)zirconium(IV) dichloride (MCP) (10 mg, 0.03 mmol) was dissolved in toluene (5 mL) and stirred for 5 min to preactivate by the addition of 1 mL of 1.0 M MAO solution. The MAO-preactivated catalyst solution was added to the flask containing the fibers at room temperature, and the flask was shaken at 100 rpm overnight. The resulting fibers were washed with fresh toluene (3 × 5 mL) and dried under reduced pressure. The maximum loaded MCP on the fiber was calculated to be 25 $\mu mol\ Zr \cdot (g\ of\ fiber)^{-1}$. The aluminum to zirconium ratio was estimated to be 170:1.

4.6.6 Polymerization procedure in a gas-phase reactor

All polymerizations were performed according to the procedure described in **Section 3.5.6**. The MCP supported fibers were mounted on a silver coated plate in a gas-phase reactor.

4.6.7 Characterization of materials

All polymers were characterized with DSC, GPC, NMR, SEM and LSCFM according to the procedure described in **Section 3.5.7**. For cryo-sectioning, the fibers were embedded in an epoxy resin. The embedded fibers were sectioned with a desired thickness with Leica ultracut UCT under LN_2 flow. The cryo-sectioned samples with 60 nm thickness were placed on a 300 mesh carbon-coated copper grid for cryo-transmission electron micrographs (TEM). Cryo-TEM was carried out with a Zeiss EM912 operating at 80 kV. For SEM with cryo-sectioned samples, the 200 nm thick samples were applied.

4.7 References

[1] http://en.wikipedia.org/wiki/Olefin_fiber.

[2] http://www.kpolymers.com/polymers-use.asp.

[3] D. Li, Y. Xia, *Advanced Materials* **2004**, *16*, 1151.

[4] A. Greiner, J. H. Wendorff, *Angewandte Chemie International Edition* **2007**, *46*, 5670.

[5] Z.-M. Huang, Y. Z. Zhang, M. Kotaki, S. Ramakrishna, *Composites Science and Technology* **2003**, *63*, 2223.

[6] L. Larrondo, R. St. John Manley, *Journal of Polymer Science: Polymer Physics Edition* **1981**, *19*, 909.

[7] S. R. Givens, K. H. Gardner, J. F. Rabolt, D. B. Chase, *Macromolecules* **2007**, *40*, 608.

[8] D. M. Rein, L. Shavit-Hadar, R. L. Khalfin, Y. Cohen, K. Shuster, E. Zussman, *Journal of Polymer Science Part B: Polymer Physics* **2007**, *45*, 766.

[9] A. J. van Reenen, L. Keulder, *Macromolecular Materials and Engineering* **2010**, *295*, 666.

[10] L. Larrondo, R. St. John Manley, *Journal of Polymer Science: Polymer Physics Edition* **1981**, *19*, 933.

[11] L. Larrondo, R. St. John Manley, *Journal of Polymer Science: Polymer Physics Edition* **1981**, *19*, 921.

[12] O. M. Kristen, R. Muellhaupt, G. Mueller, *WO 2009/015804 A1* **2009**.

[13] G. F. J. Mueller, *Doctorate dissertation at Albert-Ludwigs-Universität Freiburg* **2010**.

[14] Y.-J. Jang, N. Nenov, M. Klapper, K. Müllen, *Polymer Bulletin* **2003**, *50*, 351.

[15] Y.-J. Jang, N. Nenov, M. Klapper, K. Müllen, *Polymer Bulletin* **2003**, *50*, 343.

[16] M. Klapper, Y.-J. Jang, K. Bieber, T. Nemnich, N. Nenov, K. Müllen, *Macromolecular Symposia* **2004**, *213*, 131.

[17] Y. J. Jang, K. Bieber, C. Naundorf, N. Nenov, M. Kapper, K. Mullen, D. Ferrari, S. Knoke, G. Fink, *E-Polymers* **2005**.

[18] D. Crespy, K. Friedemann, A.-M. Popa, *Macromolecular Rapid Communications* **2012**, *33*, 1978.

[19] A. Stoiljkovic, M. Ishaque, U. Justus, L. Hamel, E. Klimov, W. Heckmann, B. Eckhardt, J. H. Wendorff, A. Greiner, *Polymer* **2007**, *48*, 3974.

[20] K. Friedemann, A. Turshatov, K. Landfester, D. Crespy, *Langmuir : the ACS journal of surfaces and colloids* **2011**, *27*, 7132.

[21] S. Agarwal, A. Greiner, *Polymers for Advanced Technologies* **2011**, *22*, 372.

[22] K. Friedemann, T. Corrales, M. Kappl, K. Landfester, D. Crespy, *Small* **2012**, *8*, 144.

[23] N. Horzum, R. Muñoz-Espí, G. Glasser, M. M. Demir, K. Landfester, D. Crespy, *ACS Applied Materials & Interfaces* **2012**, *4*, 6338.

[24] M. Koch, A. Falcou, N. Nenov, M. Klapper, K. Müllen, *Macromolecular Rapid Communications* **2001**, *22*, 1455.

[25] C. Naundorf, S. Matsui, J. Saito, T. Fujita, M. Klapper, K. Müllen, *Journal of Polymer Science Part A: Polymer Chemistry* **2006**, *44*, 3103.

[26] M. Klapper, S. Nenov, T. Diesing, K. Müllen, *Macromolecular Symposia* **2007**, *260*, 90.

[27] M. R. Ribeiro, A. Deffieux, M. F. Portela, *Industrial & Engineering Chemistry Research* **1997**, *36*, 1224.

[28] M. Kaminaka, K. Soga, *Polymer* **1992**, *33*, 1105.

[29] Y. J. Jang, C. Naundorf, M. Klapper, K. Mullen, *Macromolecular Chemistry and Physics* **2005**, *206*, 2027.

[30] N. Nenov, M. Koch, M. Klapper, K. Müllen, *Polymer Bulletin* **2002**, *47*, 391.

[31] M. Heinenberg, B. Menges, S. Mittler, H. Ritter, *Macromolecules* **2002**, *35*, 3448.

CHAPTER 5

Linear Low Density Polyethylene (LLDPE) Fibers

Abstract: The fiber formation from linear low density polyethylene (LLDPE), using ethylene as a single feed, has been achieved by a combination of concurrent tandem catalysis and the use of anisotropic supports obtained by the colloid electrospinning technique. The tandem catalysis for the synthesis of LLDPE, containing 8 to 15 branches per 1000 carbon atoms, is embedded on electrospun fibers as anisotropic templates. In this approach, α-olefins (mainly C_4–C_6 fractions) are generated *in situ* from the ethylene feed by $CoCl_2N_2^{2Th}$/methylaluminoxane (MAO) (**1**) supported on silica particles and used for ethylene copolymerization by $(MeCp)_2ZrCl_2$/MAO (**2**) supported on fibers acting as morphological templates. This approach produces LLDPE nearly exclusively comprised of ethyl branches, greater than 99 % among the total branches, in the form of micrometer-sized fibers with a well-defined morphology. A decrease in the melting point of the produced LLDPE to 122 °C, indicating a greater number of branches in the polymer backbone, is achieved by increasing the amount of oligomerization catalyst **1**. Furthermore, the silica-supported catalyst **1** can be recovered and used again without a significant loss in catalytic activity.

5 Linear Low Density Polyethylene Fibers

5.1 Linear low density polyethylene synthesis

Linear low density polyethylene (LLDPE) is one of the most mechanically flexible materials among polyolefins. LLDPE has penetrated nearly all traditional markets of polyethylene. It is used for applications in plastic bags, sheets and insulating jackets of electric cables due to the improved mechanical properties, induced by the incorporating comonomers.[1] As breifely mentioned in **Section 1.3.3**, LLDPE comprises a polymer backbone with short branched side chains. Copolymerization of ethylene and a comonomer, such as butene, hexene, octene or other α-olefin, is conventionally used. Physical properties such as density and melting point can be tuned by the type and concentration of the comonomers and by the polymerization conditions such as temperature and pressure. LLDPE is typically produced by the Ziegler-Natta (Z/N) polymerization, unlike the synthesis of low density polyethylene (LDPE) using radical polymerization.[2, 3] Besides the Z/N process, LLDPE can also be produced by several other methods using coordination catalysts. These methods are briefly described in this chapter. Using a coordination catalytic system towards the synthesis of LLDPE, studies on anisotropic supports are summarized.

Ziegler-Natta (Z/N) polymerization of LLDPE was commercialized in the late 1970's and is still in use although with numerous modifications and improvements.[4] In Z/N polymerizations, transition metal halides like $TiCl_4$ are traditionally used as catalysts. The "heterogeneous identity" of the catalyst active sites in the Z/N system typically results in relatively broad molecular weight distributions (MWD $\sim 4-12$) of the polyolefin produced. In contrast to the more traditional Z/N heterogeneous catalysts, a relatively high number of homogeneous single-site transition metal complexes such as metallocenes[5-8] have emerged in the last several years as effective and easily tunable catalysts for the tailored production of LLDPE materials. Besides the Z/N system, LLDPEs can be produced from metallocene-catalyzed copolymerizations (commonly abbreviated "mLLDPE"). The resulting copolymers present lower MWDs compared to those prepared from the Z/N systems. In addition, metallocene catalysts present a higher efficiency for the comonomer incorporation, and therefore, a lower feeding ratio of the comonomer is needed.[4, 6] However, for both mLLDPE and Z/N LLDPE processes, the presence of comonomers in the feed is mandatory for introducing branched side chains into the polymer backbone. As the production costs are dominated by the price of the purified α-

olefins, a method for the production of LLDPE with ethylene as a single feed would represent a more profitable alternative.[9] In contrast to conventional LLDPE synthesis, the following examples do not require the addition of α-olefin for introducing branches. By the help of an α-diimino nickel complex via a "chain walking mechanism", Brookhart developed the synthesis of branched polyethylene using only ethylene as a single feed.[10]

A relatively new approach for LLDPE synthesis is the combination of multiple catalysts for one synthetic operation.[11-13] Such a combination of two or more catalysts is called "tandem catalysis" (*Figure 5-1*). D. Beach and Y. V. Kissin first demonstrated LLDPE synthesis by using a catalytic system capable of simultaneous ethylene dimerization and copolymerization of 1-butene formed *in situ* with ethylene.[12] *Figure 5-1* shows a schematic for the formation of LLDPE from the tandem oligomerization (**I**) and its further ethylene copolymerization (**II**). Ethylene, a single feed monomer, reacts with **I** to generate α-olefins *in situ*.[14] The role of **II** is to polymerize ethylene and incorporate the α-olefins into the growing chain.

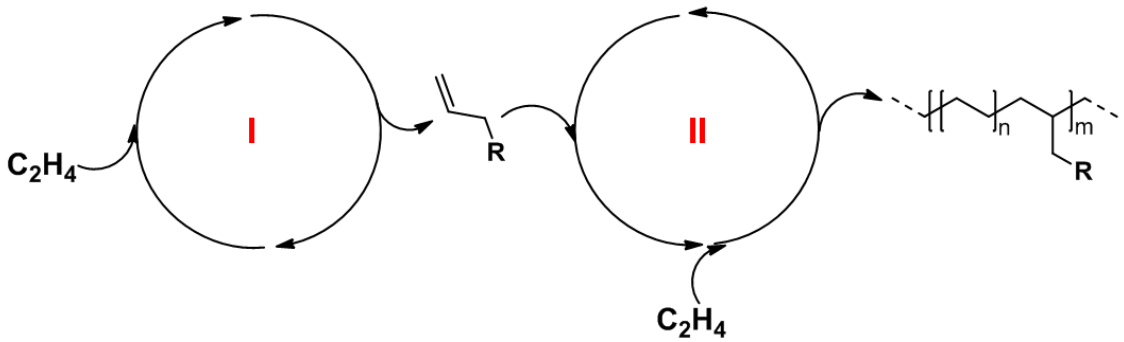

Figure 5-1. General schematic of tandem catalysis for LLDPE synthesis

For the successful collaboration of **I** and **II**, the reactivity of the two metal complexes towards ethylene must be matched.[9, 15-21] Importantly, they must not interfere chemically and also function under the same conditions such as temperature, monomer pressure and etc.[12] Although tandem catalysis has been a field of interest in the polyolefin community for the last decade, the process is not cost effective, and the differences in reactivity usually yield either a high content of oligomers or polyethylene with only a minimal fraction of branches. The need for other alternatives is still present. The main idea is to use one single reactor where two processes can occur simultaneously and cheaply under the same reaction conditions. Such a process will ultimately lead to the formation of α-olefins *in-situ* and copolymerization with ethylene, thus forming linear low density polyethylene (LLDPE).

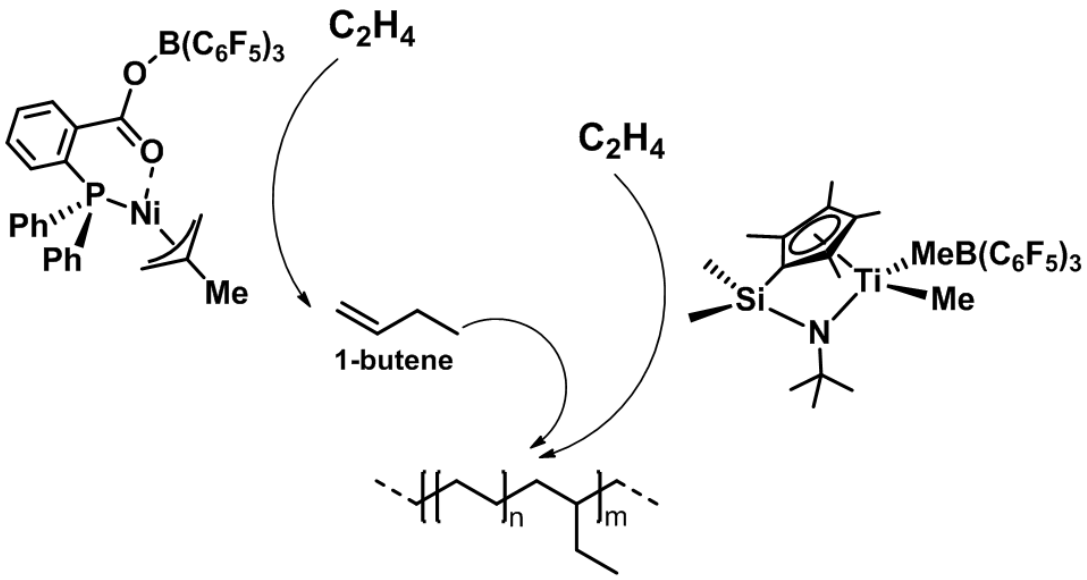

Figure 5-2. An example of LLDPE synthesis via tandem catalysis using ethylene as a single monomer feed

One example for the synthesis of LLDPE via tandem catalysis is shown in *Figure 5-2*.[22] A nickel complex generates 1-butene from ethylene and subsequently the titanium complex copolymerizes ethylene with the 1-butene. It affords ethyl-branched LLDPE using ethylene as a single monomer feed.

5.2 Objective

LLDPE is relatively easy to process when compared to high density polyethylene (HDPE) due to its lower melting temperature. Owing to the high viscosity of LLDPE in the melt state, however, its processing into fibers encounters difficulties.[23, 24] LLDPE fibers have been prepared by solution electrospinning in the presence of a salt, *e.g. t*-butylammonium bromide.[24] The addition of the salt is vital to overcome the issue of the low conductivity of the solution, driven by the low dielectric constant of the solvent *p*-xylene.[24] However, the removal of the salt may affect the surface morphology although the salt is not present on the fiber surface. In addition, elevated temperatures above the melting points of LLDPE are still necessary during electrospinning procedures. To cope with these issues, the development of alternative synthetic methods for the formation of LLDPE fibers is required.

Herein, a new method for preparing LLDPE fibers is described based on a combination of "concurrent tandem catalysis" (CTC) and the use of an anisotropic support for metallocene catalysts. It was demonstrated in **Chapter 4** that selective immobilization of $(MeCp)_2ZrCl_2$/MAO on electrospun fibers consisting of poly(ethylene glycol) (PEG)-modified polystyrene (PS) nanoparticles results in HDPE fibrous material with a well-defined core-sheath structure. The synthesis of LLDPE via CTC is demonstrated on the electrospun fibers, which can be employed as a platform for various polyolefins.

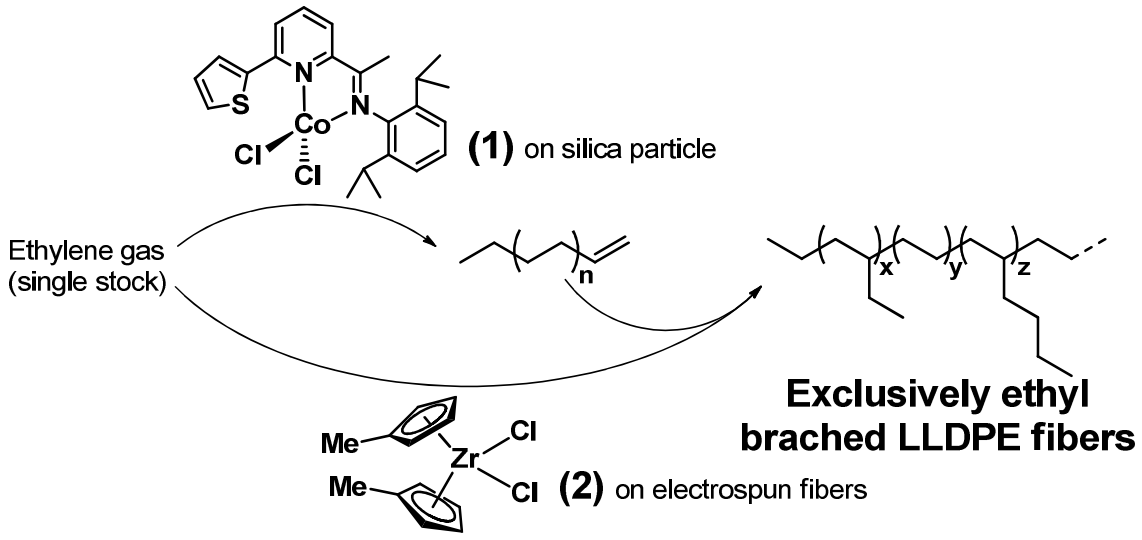

Figure 5-3. Concurrent tandem catalysis of $CoCl_2N^{2Th}$ (**1**) and $(MeCp)_2ZrCl_2$ (**2**) for the synthesis of LLDPE fibers

For a successful tandem catalysis, the applied metallocenes must be adjusted to each other under same reaction conditions. As the copolymerization catalyst, the $(MeCp)_2ZrCl_2$ (**2**)/MAO system is chosen as a model catalytic species and is immobilized on the electrospun fibers. In order to perform tandem catalysis for LLDPE synthesis in a gas phase reactor, the first prerequisite for oligomerization catalysts is suitable activity with the copolymerization catalyst. The catalyst for oligomerization should work under the temperature range of 30 − 100 °C and ethylene pressure range of 1 − 5 bar. Therefore, the catalytic system, $CoCl_2N_2^{2Th}$ (**1**)/MAO, is selected for the oligomerization of ethylene. The catalyst **1**/MAO is known to produce α-olefins with a Schulz-Flory α-value of about 0.08 (butenes 92.0 %, hexenes 7.4 %) under mild condition.[15] Indeed, tandem copolymerization of the catalyst **1** with various types of metallocene catalysts was studied to generate LLDPE as isotropic particles but not as fibers.[25-27] In this study, electrospun fibers as anisotropic templates for synthesizing LLDPE by heterogeneous tandem catalysis are applied, based on the activation by MAO of **1** for oligomerization and **2** for copolymerization of ethylene and the α-olefins (*Figure 5-3*). The anisotropic supports are formed by colloid electrospinning. LLDPE in the form of micrometer diameter fibers is obtained by the cooperative combination of the electrospun fibers as supports for metallocenes and the tandem system using ethylene as a single feed.

5.3 Results and discussion

It has been demonstrated that $(MeCp)_2ZrCl_2$/methylaluminoxane (MAO) can selectively be immobilized around the electrospun fibers consisting of poly(ethylene glycol) (PEG)-modified polystyrene (PS) nanoparticles and affords a high density polyethylene (HDPE) fibrous material with a well-defined core-sheath structure (**Chapter 4**). Based on this precedent, a combination of the immobilized $(MeCp)_2ZrCl_2$/MAO system on electrospun fibers with a properly selected oligomerization catalyst ($CoCl_2N^{2Th}$/MAO) is considered for the set-up of a gas-phase *tandem* copolymerization protocol aimed at preparing linear low density polyethylene (LLDPE) fibrous materials.

To achieve the concurrent tandem catalytic (CTC) system, the most important factor is that the applied catalysts must be compatible to avoid interference between catalytic species.[28] In addition, it would be necessary that the reactivity of the applied catalysts is well-harmonized under the same polymerization conditions.[28] For the successful application of CTC, the determination of the individual reactivity of the catalysts is thus crucial. The catalytic activity of the $CoCl_2N_2^{2Th}$ (**1**)/MAO towards the ethylene oligomerization has been previously reported.[15] Since the same class of zirconocene (Cp_2ZrCl_2) was applied to the CTC before,[21] its derivative $(MeCp)_2ZrCl_2$ (**2**) is chosen as a model catalyst for ethylene/α-olefins copolymerization. In addition, **2**/MAO system was previously applied to the electrospun fibers for HDPE synthesis (**Chapter 4**) so that the activity of concurrent tandem system can be compared with the ethylene homopolymeriztion.

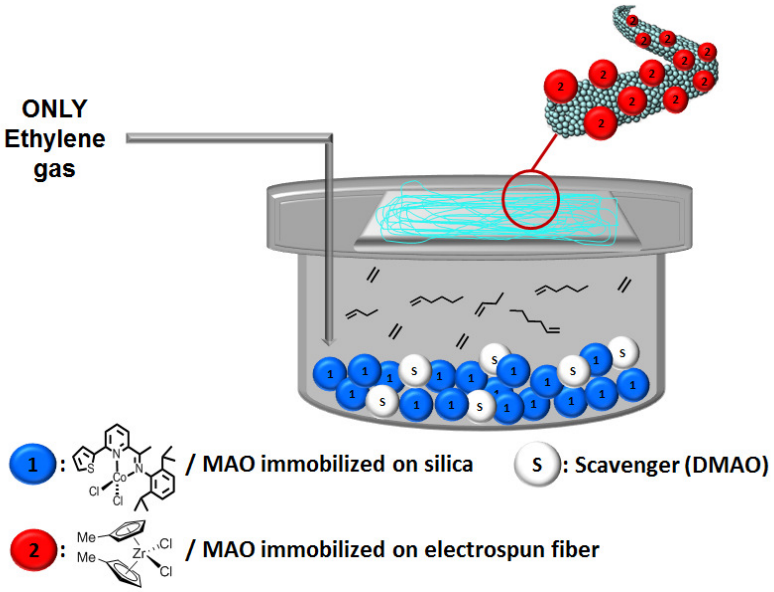

Figure 5-4. Schematic drawing of the CTC procedure in a gas phase reactor

In order to perform the CTC for LLDPE synthesis by the combination of catalysts **1** and **2** with solely ethylene in a gas phase reactor, the oligomerization catalyst **1** was supported on silica particles and placed in the bottom of the reactor with scavenger particles (*Figure 5-4*). The ethylene/α-olefin copolymerization catalyst **2** was immobilized on the electrospun fibers, and the fiber was placed on the upper stage (a silver coated plate) of the reactor. Since ethylene is firstly fed to the bottom of the reactor, it can be purified once again with scavenger particles and reacts with catalyst **1**, converting ethylene to α-olefins. As a consequence, a mixture of ethylene and α-olefins concurrently exists in the gas phase reactor and leads to a copolymerization by catalyst **2** immobilized on the fibers. The *tandem* copolymerization for the synthesis of LLDPE was tested, and the results are summarized in *Table 5-1*.

Table 5-1. Tandem copolymerization results of catalyst **1** [$(MeCp)_2ZrCl_2$] immobilized electrospun fibers with combination of catalyst **2** [$CoCl_2N_2^{2Th}$] supported on silica particles in a gas phase reactor[a)]

entry	Cat. 1 Co[b)]	Cat. 2 Zr[c)]	χ_{Co}[d)]	A[e)]	total branch[f)]	C_2 br	C_4 br	M_w[g)]	M_w/M_n[g)]	T_m[h)]
	μmol	μmol			‰	%	%	kg.mol^{-1}		°C
1	-	0.67	0.00	121	-	-	-	659	9.3	135
2	1.35	0.67	0.67	30	8	>99	<1	360	6.8	126
3[i)]	1.35	0.67	0.67	35	7	>99	<1	405	7.8	128
4	2.70	0.67	0.80	23	13	>99	<1	308	5.7	123
5	4.05	0.67	0.86	21	15	>99	<1	265	5.2	122

a) Ethylene pressure 3 bar, temperature 40 °C, polymerization time 30 min;
b) 0, 40, 40, 80, and 120 mg of $CoCl_2N_2^{2Th}$ immobilized silica particles (33.8 μmol of $CoCl_2N_2^{2Th}$·(g silica)$^{-1}$) are applied, respectively;
c) 20 mg of $(MeCp)_2ZrCl_2$ immobilized fibers (33.3 μmol of $(MeCp)_2ZrCl_2$·(g fiber)$^{-1}$) are applied;
d) [Co]/([Co]+[Zr]);
e) activity expressed as kg of polyolefin (mol of Zr·h·bar)$^{-1}$;
f) number of branches per 1000 carbon atoms calculated from ^{13}C NMR at 130 °C;
g) analyzed by GPC (PS-standard);
h) determined by DSC;
i) $CoCl_2N_2^{2Th}$ supported on silica particles are recovered from entry 2.

While increasing the ratio of $[CoCl_2N_2^{2Th}]/[(MeCp)_2ZrCl_2]$ (χ_{Co}), the activity of the tandem system in a gas phase reactor has slightly decreased from 30 to 21 kg of polyolefin (mol of Zr·h·bar)$^{-1}$. Comparing the homopolymerization catalyzed by **2** (entry 1), a negative "comonomer effect"[29] is observed in all tandem systems at 0.67 to 0.86 values of χ_{Co} (entries 2 – 5). A decrease in the catalytic activity for copolymerization above certain concentrations of comonomers can be attributed to an increase of the comonomer fraction in the growing polymer chain, which may hamper the diffusion rates of the ethylene to the active sites.[30] It can also be associated with rapid consumption of ethylene feed due to the high reactivity of the catalyst **2**.[15] The influence of χ_{Co} on the copolymer properties has also been studied by DSC analysis. The melting points (T_m) for the copolymers produced by the *tandem* system, decrease from 135 °C (for the HDPE produced by catalyst **2** only – entry 1) down to 122 °C (for the LLDPE produced by the tandem system at higher χ_{Co}). By increasing the values of χ_{Co} from 0.67 to 0.86, a slight decrease in T_m from 126 to 122 °C is observed due to the reduced polymer crystallinity as a consequence of α-olefins incorporation. The decreased value of T_m indicates the formation of branches which restrict close packing in the main polymer backbone.

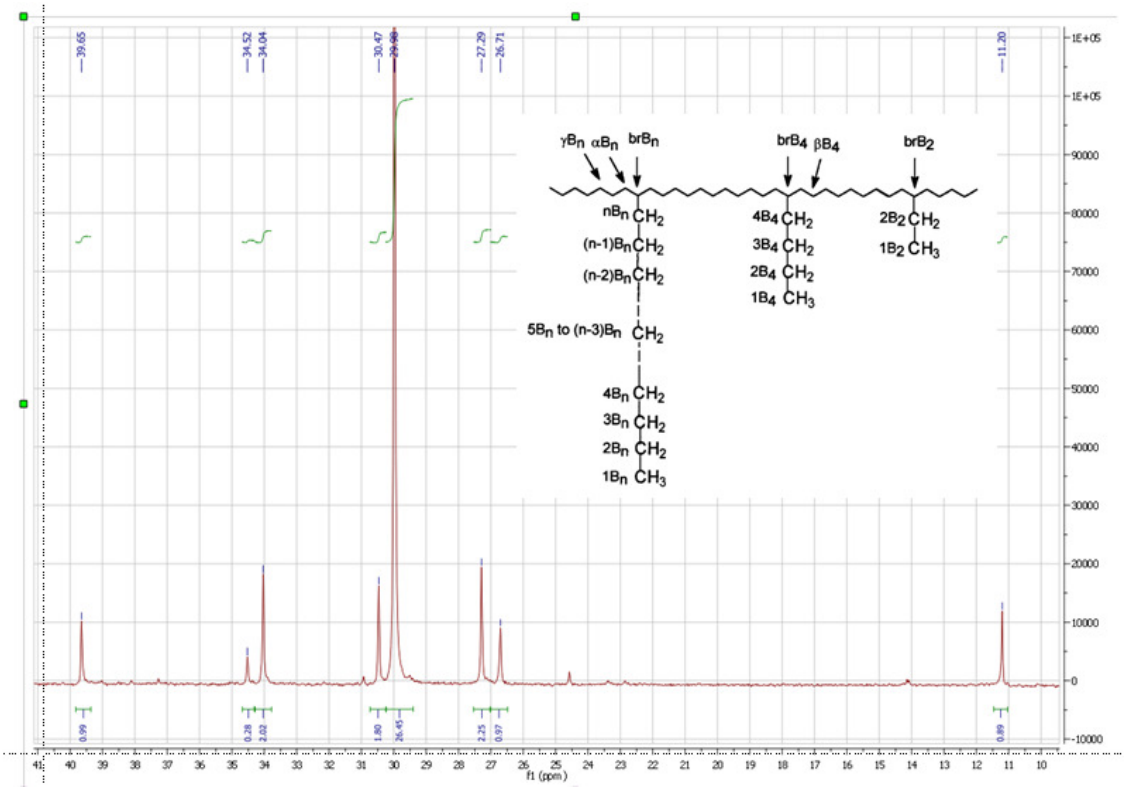

Figure 5-5. ^{13}C NMR spectrum of extracted polymers from the ethylene polymerized fibers

Accordingly, GPC analyses on all the copolymers show the influence of χ_{Co} on the copolymer properties. Lower molecular weights (M_n) for copolymers produced by tandem

systems are measured by GPC comparing to the HDPE produced in the absence of oligomerization catalyst **1** (entry 1). By varying the values of χ_{Co} from 0 to 0.86, a significant decrease in MWD is observed. α-Olefins have been reported to act as chain termination reagents when too concentrated, consequently resulting in a decrease in M_w and a narrower MWD.[29]

The presence of branches in the copolymers is demonstrated by the ^{13}C NMR spectra. The copolymers, produced by the tandem system on the electrospun fibers, are extracted by 1,2,4-trichlorobenzene at 135 °C and mixed with d^4-1,1,2,2-tetrachloroethane. The NMR spectra of the extracted copolymers suggest the formation of LLDPE with exclusively ethyl branches varying from 8 to 15 per 1000 carbon atoms. In all cases, less than 1 % of butyl branches among the total branches are detected (a representative spectrum is shown in *Figure 5-5*). It is commonly recognized that a higher content of comonomers leads to a reduction in T_m of the material, driven by the loss of crystallinity. Since the tandem catalyzed LLDPE have almost exclusively ethyl branches with different contents in the range of 8 to 15, a correlation between T_m and ethyl branching contents of the obtained copolymers is studied. It is reported that melting points decrease linearly with increasing contents of ethyl branching in copolymers.[31] The number of ethyl branching in the obtained LLDPE is confirmed by observing a similar trend of their T_m in these studies.

Since oligomerization catalyst **1** is supported on silica particles, it can be recovered under inert conditions and re-used in a subsequent tandem copolymerization (entry 3, *Table 5-1*). According to the experimental outcome, it can be inferred that the recovered oligomerization catalyst maintains its activity almost unchanged. Indeed, repeated *tandem* copolymerization (entry 2 *vs.* 3) shows only a slight decrease in the number of branches in the LLDPE produced (from 8 to 7 every 1000 C atoms) together with an increase in the final polymer crystallinity (T_m from 126 to 128 °C) and polymer molecular weight (from 360 to around 405 $kg \cdot mol^{-1}$). This slightly reduced catalytic activity of **1** is reasonably ascribed to a partial catalyst deactivation due to contamination by non-volatile α-olefins produced by **1** itself. Indeed, the silica-supported **1** is indefinitely stable if stored under inert atmosphere. However, the production of higher olefins (even in traces) during the *tandem* copolymerization tests is expected to slowly "poison" the catalytic active sites of **1**. A lower concentration of α-olefins is expected to increase the activity of the catalyst **2** (*i.e.* the homopolymerization has a higher activity). As a result, a slight increase in the *tandem*

copolymerization activity (from 30 to 35 kg of polyolefin (mol of Zr·h·bar)$^{-1}$ produced) is observed from entry 2 to entry 3.

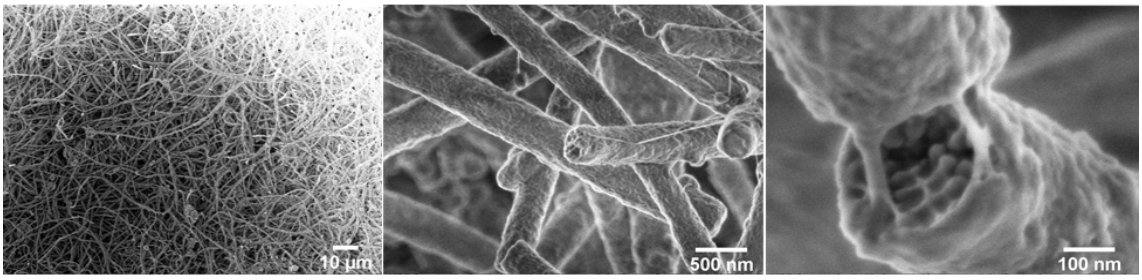

Figure 5-6. SEM micrographs of the LLDPE fibers with different magnitudes

In order to characterize the morphology, the produced materials were studied by scanning electron microscopy (SEM) as shown in *Figure 5-6*. In all cases, SEM micrographs reveal the formation of electrospun fibers coated with LLDPE. The fibers have a homogeneous length (corresponding to the electrospun fibers) and diameter (from approximately 250 nm to larger diameters depending on the copolymerization time) indicating a highly homogeneous polyolefin coating around the tubes. Spherical polystyrene nanoparticles are clearly observed in the core of the fibers. Unlike solution-phase *tandem* copolymerization processes for the production of composites,[15] the morphology of the LLDPEs produced by the gas-phase *tandem* approach does not change upon varying the value of the χ_{Co}. In addition to that, polyethylene is found to grow exclusively on the anisotropic fibers with no excess of flakes or wires throughout the whole scanned area. Although this approach is basically limited to light (volatile) monomers, this gas-phase protocol avoids any possible leaching of the catalytic systems used. As a matter of fact the oligomerization system can be conveniently recovered and reused for subsequent *tandem* copolymerization steps whereas the copolymerization process takes place homogeneously and exclusively at the surface of electrospun fiber.

5.4 Conclusion

The synthesis of LLDPE in the form of fibers with a well-defined morphology and exclusively ethyl short chain branches is presented by using a combination of anisotropic supports as fibers and a tandem catalyst system of two heterogeneous metallocene catalysts using ethylene as a sole feed. The tandem catalysis system is performed by a cooperative action of $CoCl_2N_2^{2Th}$ (**1**) for producing α-olefins and $(MeCp)_2ZrCl_2$ (**2**) for ethylene copolymerization with the concurrently produced α-olefins. The anisotropic supports are prepared via colloid electrospinning of polystyrene (PS) nanoparticles that have poly(ethylene glycol) (PEG) chains. The non-covalent interaction between cationic MAO-activated **2** and the PEG chains from the PS nanoparticles leads to a well-defined formation of LLDPE coating around the electrospun fibers. The respective role of **1**/MAO immobilized on silica particles and **2**/MAO immobilized on the electrospun fibers promotes the formation of LLDPE coated fibers, containing from 8 to 15 branches per 1000 carbon atoms. ^{13}C NMR analysis proves the almost exclusive existence of ethyl branches (higher than 99 %). A negative comonomer effect is observed by varying the value of χ_{Co} due to the high concentration of comonomers, driven by high reactivity of catalyst **2** supported on silica particles. A decrease in T_m of the LLDPE results when increasing the value of χ_{Co}. The recovered catalyst species **1**/MAO supported on silica particles are used without a significant loss in catalytic activity. All these features demonstrate the synthesis of various polyolefins using the electrospun fibers as anisotropic templates for the immobilization of single-site catalysts. This combination would be an alternative approach to synthesize LLDPE in a form of fibers directly from metallocene immobilization technique.

5.5 Experimental part

5.5.1 General procedures and materials

Silica particles (Evonik, S-50) were received and used after calcination for 48 h at 300 °C at 1.0×10^{-3} mbar. The imino(pyridine) cobalt complex, $CoCl_2N_2^{2Th}$, was synthesized [redacted] according to the published procedure[25] and used as received.

5.5.2 Immobilization procedure for $(MeCp)_2ZrCl_2$ (MCP) on the electrospun fibers

According to the procedures described in **Section 4.6**, the preparation of polystyrene nanoparticles and electrotrospun fibers, and immobilization of $(MeCp)_2ZrCl_2$ (MCP) on the electrospun fibers were performed.

5.5.3 Immobilization procedure for $CoCl_2N^{2Th}$ on silica particles

Under inert conditions, the dried silica gel (0.3 g) was dispersed in dried toluene and mixed with a 1.0 M MAO in toluene before stirring overnight. After removal of the solution, the silica/MAO mixture was prepared. The oligomerization catalyst, a cobalt(II) iminopyridyl complex ($CoCl_2N_2^{2Th}$), (10 mg, 0.02 mmol) was dissolved in toluene and was activated by the addition of 1.0 mL of 1.0 M MAO solution. After stirring for 30 min, 3 mL of $CoCl_2N_2^{2Th}$/MAO solution was added to the silica/MAO mixture. After shaking for additional 2 h, the supernatant toluene solution was removed by filtration. The $CoCl_2N_2^{2Th}$/MAO immobilized on silica particles were washed 3 times with 20 mL of toluene and dried under vacuum. After this, the $CoCl_2N_2^{2Th}$/MAO immobilized silica particles were ready to use in a gas phase reactor for oligomerization of ethylene. The maximum loaded $CoCl_2N_2^{2Th}$ on silica was calculated to be 33.8 μmol cobalt/g of silica particle.

5.5.4 Tandem copolymerization process in a gas phase reactor

All tandem copolymerizations were performed according to the procedure described in **Section 3.5.6**. The silica particle-immobilized $CoCl_2N_2^{2Th}$/MAO was placed in the bottom of the reactor together with DMAO as a scavenger to purify ethylene once again. The MCP/MAO supported electrospun fibers were mounted on the silver-coated plate in the gas phase reactor. Note that ethylene is fed to the bottom of the reactor first so that ethylene can be once again purified with scavenger and also reacts with the $CoCl_2N_2^{2Th}$/MAO immobilized silica particles preferentially to produce α-olefins.

5.5.5 Materials characterization

All polymers were characterized with DSC, GPC, and SEM according to the procedure described in **Section 3.5.7**. To check the comonomer incorporation, the polymers dissolved in 1,2,4-trichlorobenze/d^2-1,1´,2,2´-tetrachloroethane (2/1, *v*/*v*) were characterized by ^{13}C NMR at 393 K. From the ^{13}C NMR spectra, the number of branches was calculated by Dr. Giuliano Giambastiani.

5.6 References

[1] H. F. B. Mark, N. M.; Overberger, C. G.; Menges, G., *Eds.; Wiley-Interscience: New York* **1985**, *6*, 429.

[2] D. Stoiljkovich, S. Jovanovich, *Die Makromolekulare Chemie* **1981**, *182*, 2811.

[3] M. J. Roedel, *Journal of the American Chemical Society* **1953**, *75*, 6110.

[4] A. Razavi, *Comptes Rendus de l'Académie des Sciences - Series IIC - Chemistry* **2000**, *3*, 615.

[5] S. J. Na, D. J. Joe, S. S, W.-S. Han, S. O. Kang, B. Y. Lee, *Journal of Organometallic Chemistry* **2006**, *691*, 611.

[6] G. G. Hlatky, *Coordination Chemistry Reviews* **1999**, *181*, 243.

[7] S. D. Ittel, L. K. Johnson, M. Brookhart, *Chemical Reviews* **2000**, *100*, 1169.

[8] M. Atiqullah, M. Tinkl, R. Pfaendner, M. N. Akhtar, I. Hussain, *Polymer Reviews* **2010**, *50*, 178.

[9] F. Alobaidi, Z. Ye, S. Zhu, *Journal of Polymer Science Part A: Polymer Chemistry* **2004**, *42*, 4327.

[10] Z. Guan, P. M. Cotts, E. F. McCord, S. J. McLain, *Science* **1999**, *283*, 2059.

[11] R. W. Barnhart, G. C. Bazan, T. Mourey, *Journal of the American Chemical Society* **1998**, *120*, 1082.

[12] D. L. Beach, Y. V. Kissin, *Journal of Polymer Science: Polymer Chemistry Edition* **1984**, *22*, 3027.

[13] J.-C. Wasilke, S. J. Obrey, R. T. Baker, G. C. Bazan, *Chemical Reviews* **2005**, *105*, 1001.

[14] L. G. Furlan, *Doctorate dissertation at Universite de Rennes 1* **2005**.

[15] A. Toti, G. Giambastiani, C. Bianchini, A. Meli, S. Bredeau, P. Dubois, D. Bonduel, M. Claes, *Chemistry of Materials* **2008**, *20*, 3092.

[16] F.-W. Yan, H. Xu, C.-Y. Guo, M.-G. Zhang, X.-H. Zhang, H.-J. Yang, G.-Q. Yuan, *Journal of Applied Polymer Science* **2009**, *112*, 2298.

[17] Z. Zhang, C. Guo, N. Cui, Y. Ke, Y. Hu, *Journal of Applied Polymer Science* **2004**, *94*, 1690.

[18] J. Zhang, B.-G. Li, H. Fan, S. Zhu, *Journal of Polymer Science Part A: Polymer Chemistry* **2007**, *45*, 3562.

[19] M. Yang, W. Yan, X. Hao, B. Liu, L. Wen, P. Liu, *Macromolecules* **2009**, *42*, 905.

[20] E. D. Schwerdtfeger, C. J. Price, J. Chai, S. A. Miller, *Macromolecules* **2010**, *43*, 4838.

[21] C. Bianchini, G. Giambastiani, A. Meli, I. Rios, A. Toti, E. Passaglia, M. Frediani, *Topics in Catalysis* **2008**, *48*, 107.

[22] K. Musikabhumma, T. P. Spaniol, J. Okuda, *Journal of Polymer Science Part A: Polymer Chemistry* **2003**, *41*, 528.

[23] N. Platzer, *Industrial & Engineering Chemistry Product Research and Development* **1983**, *22*, 158.

[24] S. R. Givens, K. H. Gardner, J. F. Rabolt, D. B. Chase, *Macromolecules* **2007**, *40*, 608.

[25] C. Bianchini, G. Giambastiani, G. Mantovani, A. Meli, D. Mimeau, *Journal of Organometallic Chemistry* **2004**, *689*, 1356.

[26] C. Bianchini, D. Gatteschi, G. Giambastiani, I. Guerrero Rios, A. Ienco, F. Laschi, C. Mealli, A. Meli, L. Sorace, A. Toti, F. Vizza, *Organometallics* **2007**, *26*, 726.

[27] C. Bianchini, G. Mantovani, A. Meli, F. Migliacci, F. Laschi, *Organometallics* **2003**, *22*, 2545.

[28] Z. J. A. Komon, G. C. Bazan, *Macromolecular Rapid Communications* **2001**, *22*, 467.

[29] C. Przybyla, B. Tesche, G. Fink, *Macromolecular Rapid Communications* **1999**, *20*, 328.

[30] J. H. Z. dos Santos, T. Uozumi, T. Teranishi, T. Sano, K. Soga, *Polymer* **2001**, *42*, 4517.

[31] R. van Grieken, C. Martin, J. Moreno, O. Prieto, J. M. Bravo, *Macromolecular Symposia* **2007**, *259*, 174.

CHAPTER 6

Core-Shell Particles

Abstract: Spatially resolved two different polyolefins in a single particle, using ethylene as a single feed, is demonstrated via a combination of concurrent tandem catalysis and the use of core-shell particles as supporting materials obtained by a stepwise construction method. The combination promotes the formation of a hard core-soft shell polyolefin particle via a one-pot synthesis. The synthesis of the core-shell particles containing two polyolefins, ultra high molecular weight polyethylene (UHMWPE) and linear low density polyethylene (LLDPE) in the core and shell, respectively, is performed by a cooperative action of three different metallocene catalysts: catalyst **A** supported in the core is for the synthesis of UHMWPE. For the synthesis of LLDPE on the shell using only ethylene, "concurrent tandem catalysis" has been adopted. Catalyst **B** supported on the shell copolymerizes ethylene with α-olefins that are in situ generated by catalyst **C** supported on silica separately. By varying the amount of the oligomerization catalyst **C**, a slight increase in total activity of catalyst **A** and **B** is observed due to the positive "comonomer effect". A lower crystallinity of the LLDPE formed on the shell, induced by incorporated comonomers, contributes the higher diffusion of ethylene to the active sites of catalyst **A** supported in the core. To visualize the formation of spatially resolved UHMWPE core-LLDPE shell, the inner-morphology of the polyolefin particles is studied along with various microscopic techniques such as cryo-TEM, SEM, STEM, AFM and LSCFM.

6 Core-Shell Particles

6.1 Blending polyolefins

Blending of two or many polymers has become one of the perspective and convenient way to develop new materials with good performance.[1, 2] The blending of different types of polyethylenes (PEs) has attracted growing interest due to its potential for achieving improved physical properties and better processabilities, compared to those of the pure PEs.[3-5] Among PEs, ultra high molecular weight polyethylene (UHMWPE) is distinguished by outstanding mechanical properties,[6] leading it applicable in bullet proof jackets, protection helmets, implants for joints and fishing nets.[7-10] It is a special class of high density polyethylene (HDPE) with the weight average molecular weight (M_w) generally over 1.0 million g·mol^{-1} whereas HDPE typically has $0.5 - 3.0 \times 10^2$ kg·mol^{-1}. Due to high melt viscosity given by the high M_w,[3] conventional processes, such as tubular extrusion blowing and screw extrusion techniques, can not be applied exception for compression molding and random extrusion.[7, 11, 12] Thus the enhanced mechanical properties imply a high cost of processing UHMWPE.[13] Despite the process applied, in addition, all products of UHMWPE possess fusion defects or grain-boundaries and UHMWPE eventually fails in many applications.[14] To overcome the limitations, introducing elasticity to UHMWPE can be considered by simple blending with other polyolefins (*e.g.* branched polyethylenes).[13] As an alternative method, preparation of UHMWPE particles having spatially resolved LLDPE layer is demonstrated in this chapter. Furthermore, some other examples are described with the developments of process technologies.

In the case of UHMWPE, blending other polyolefins is often aimed at improving the processability.[13, 15] For instance, blending UHMWPE with a conventional linear low-density polyethylene (LLDPE) was performed.[3, 16] The processability can be thus enhanced, since the viscosity is expected to be significantly lower.[3, 17] In addition, this exerts improvements of the impact strength and also the environmental stress-cracking resistance. As a minor blend component, the addition of up to 10 wt% of UHMWPE to low density polyethylene (LDPE) can improve the elongation flow and birefringence of LDPE/UHMWPE blends.[18] Melt miscibility can occur between blends of UHMWPE and linear low density polyethylene (LLDPE) providing that the blends are prepared by sequential loading.[3] Blending UHMWPE with LLDPE can increase the crystallization rate of LLDPE and such blends show high interfacial adhesion between the blend

components.[19] UHMWPE is also inherently difficult to process due to its high melt viscosity. Blending UHMWPE and conventional linear PE can result in superior mechanical properties, improved processability and enhanced crystallinity.[20]
However, simple blending of two different polymers leads to ill-defined mixtures.[21] To overcome these drawbacks, addition of block, graft, or other copolymers as compatibilizers is generally applied.[22-24] Since this approach is unsuitable for the synthesis of polyolefins, the development of a versatile method is considered such as Novolen process, advanced cascade technology and supporting techniques. A brief introduction of the development is described in following sections.

6.1.1 Process technologies

6.1.1.1 Novolen process

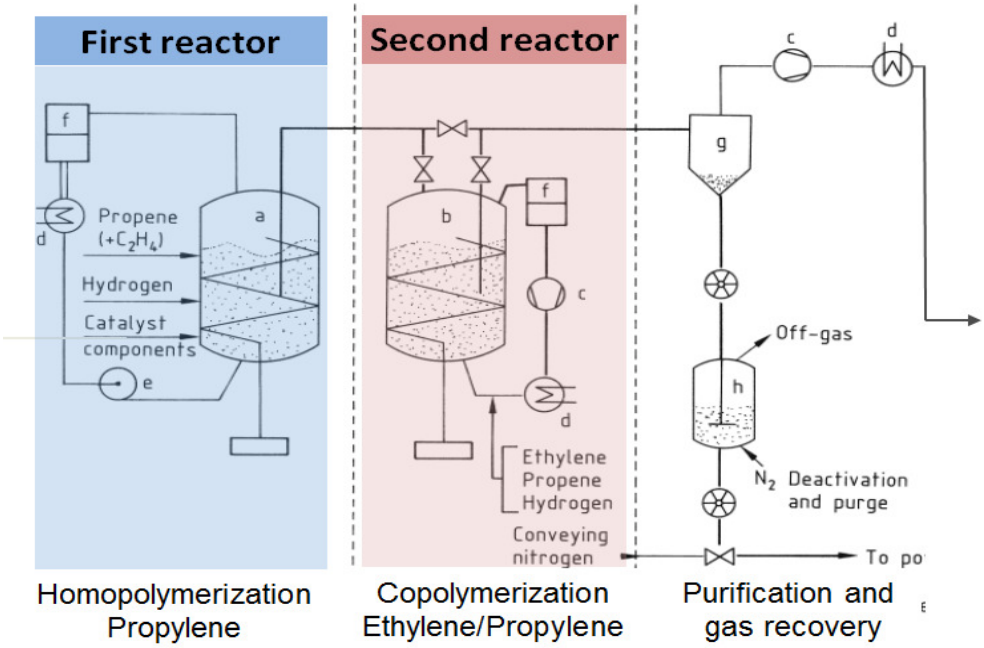

Figure 6-1. Schematic drawing of Novolen process

The Novolen technology is a flexible process to produce diverse polypropylenes (PP) with various consistencies.[25, 26] Impact PP homopolymers and copolymers are produced in two vertical stirred gas-phase reactors in series. As shown in *Figure 6-1*, in the first, which operates at 80 °C and 20 – 35 bar monomer pressure and produces PP, liquid propylene is injected to cool the exothermic polymerization by evaporating. The product is continuously transferred to cyclone and either deactivated with steam or transferred to the second reactor, which operates at 60 °C and 10 – 25 bar. Ethylene and propylene are

copolymerized to cover the tough, but brittle particles of isotactic PP with a softer copolymer.

6.1.1.2 Advanced cascade process

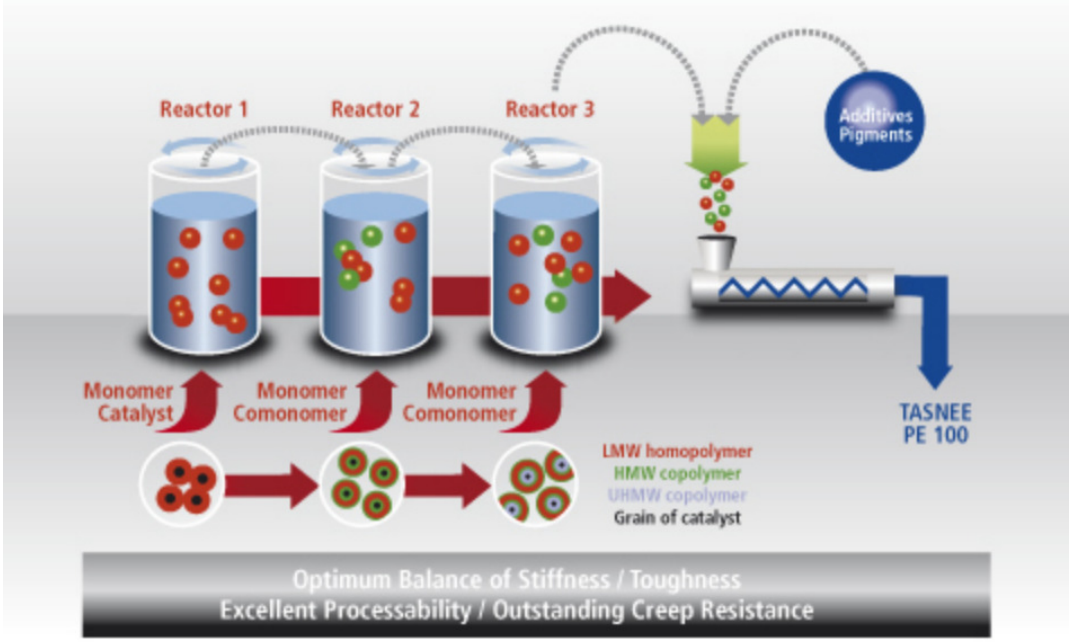

Figure 6-2. Schematic drawing of the advanced cascade process

The advanced cascade process (ACP) is the most advanced technology that makes multimodal high density polyethylene (HDPE).[27] The ACP process has generally three slurry reactors connected in cascades, enabling the production of HDPE with a various properties (*Figure 6-2*). By utilizing the ACP, the produced HDPE posseses balanced stiffness/toughness, impact resistance, a high stress cracking resistance and processing advantages used in film, blow molding and pipe applications.

6.1.2 Core-shell particles

A major drawback of the cascade processes using two or three reactors is the difficulty to avoid a partial decomposition of the active centers due to moisture and oxygen during the transfer of the intermediate to the final reactor. Additionally, the cascade processes are limited to synthesize two totally different polymers with a spatial resolution. Therefore, it would be preferable to form core-shell polyolefin particles in a one-pot reaction and in a more defined way. Indeed, as an alternative method for synthesizing impact copolymers, core-shell polyolefin particles have been reported based on spatially resolved loading

technique of two different catalysts. In contrast to the process technologies (Novolen and ACP process), only one single reactor can be employed by using core-shell particles to achieve impact polymers. As shown in *Figure 6-3*, the core-shell particles can be prepared by sequential immobilization of different catalysts on silica (core) and polystyrene nanoparticles (shell).[28] Since two catalysts are respectively loaded on the core and shell, the particles afford spatially resolved polyolefin particles. By a step-wise construction, organic-inorganic hybrid supports can be prepared and play a role as templates for the final product morphology. Using these hybrid supports, spatially resolved polypropylenes (atatic and isotactic polypropylene) in a particle were produced via a one-pot synthesis.

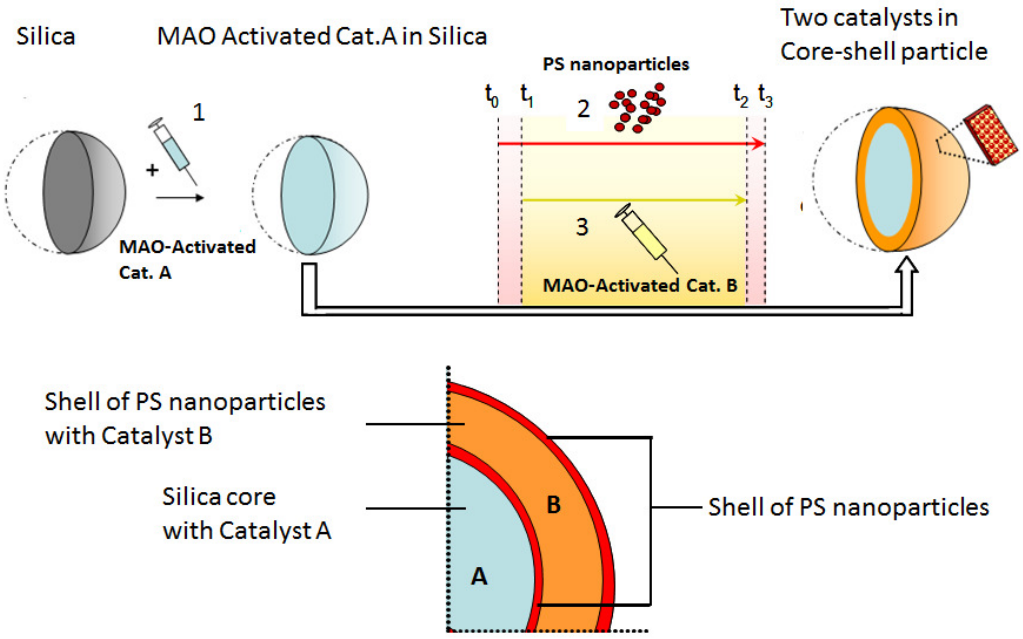

Figure 6-3. Schematic drawing of preparing spatially loaded organic-inorganic hybrid supports

6.2 Objective

A synthetic approach to produce UHMWPE having a layer of LLDPE is addressed in this chapter based on the selective loading of catalysts on the organic-inorganic hybrid supports. To synthesize the spatially resolved polyolefin particles with UHMWPE and LLDPE in the core and shell, respectively, a proper combination of catalysts is crucial. For the synthesis of UHMWPE, group IV transition metal complexes bearing two phenoxy-imine ligands, which display excellent catalytic performance, are considered. The metal complexes are often called "FI catalysts".[29] In order to perform the polymerization in a gas phase reactor and avoid the extra addition of α-olefins, an alternative method in synthesizing LLDPE is considered. Indeed, several examples have been reported that LLDPE can be synthesized using ethylene as a single monomer feed by "concurrent tandem catalysis" (CTC, see also **Section 5.1**), employing two or more different single-site catalysts in the same reactor.[30-39]

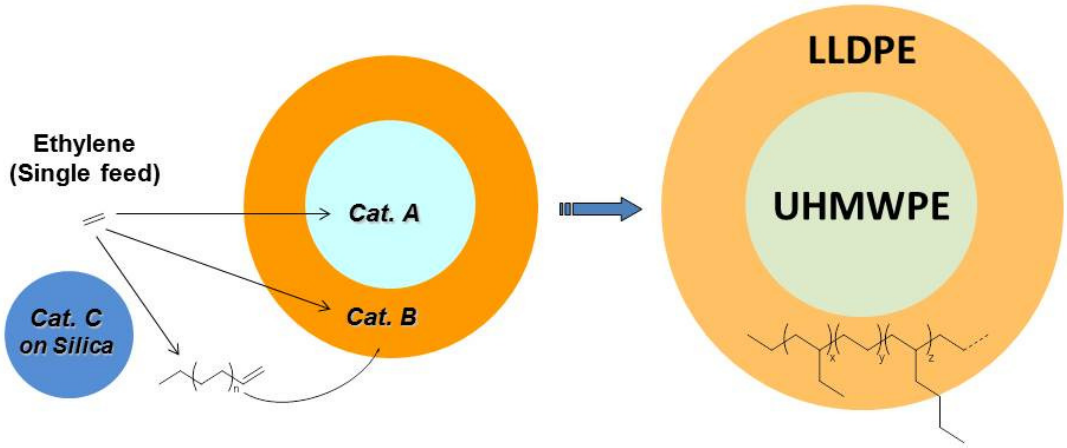

Figure 6-4. Schematic drawing of the procedure for UHMWPE core-LLDPE shell particles

For the UHMWPE-LLDPE core-shell particles, it can be performed by a cooperative action of three different metallocene catalysts. As shown in *Figure 6-4*, catalyst **A** supported in the core is for UHMWPE synthesis. For LLDPE synthesis on the shell using only ethylene, two more catalysts are employed. Catalyst **B** supported on the shell copolymerizes ethylene with α-olefins that are generated *in situ* by catalyst **C** supported on silica, separately.

6.3 Results and discussion

The concept of core-shell polyolefin particles, consisting of spatially resolved two different polymers (atatic and isotatic polypropylene) in core and shell, respectively, has already been proven with selectively loaded metallocene catalysts by a step-wise approach.[28] Based on this previous study, to enhance the processability of ultra high molecular weight polyethylene (UHMWPE), synthesis of UHMWPE particles with a layer of linear low density polyethylene (LLDPE) has been demonstrated. In order to synthesize UHMWPE-LLDPE core-shell particles via one-pot ethylene polymerization, three different metallocene catalysts are required as follow: catalyst **A** is responsible for the production of UHMWPE. For the production of LLDPE via tandem catalysis, catalyst **B** copolymerizes ethylene with α-olefins (mainly, 1-butene and 1-hexene) that are generated *in situ* by catalyst **C**.

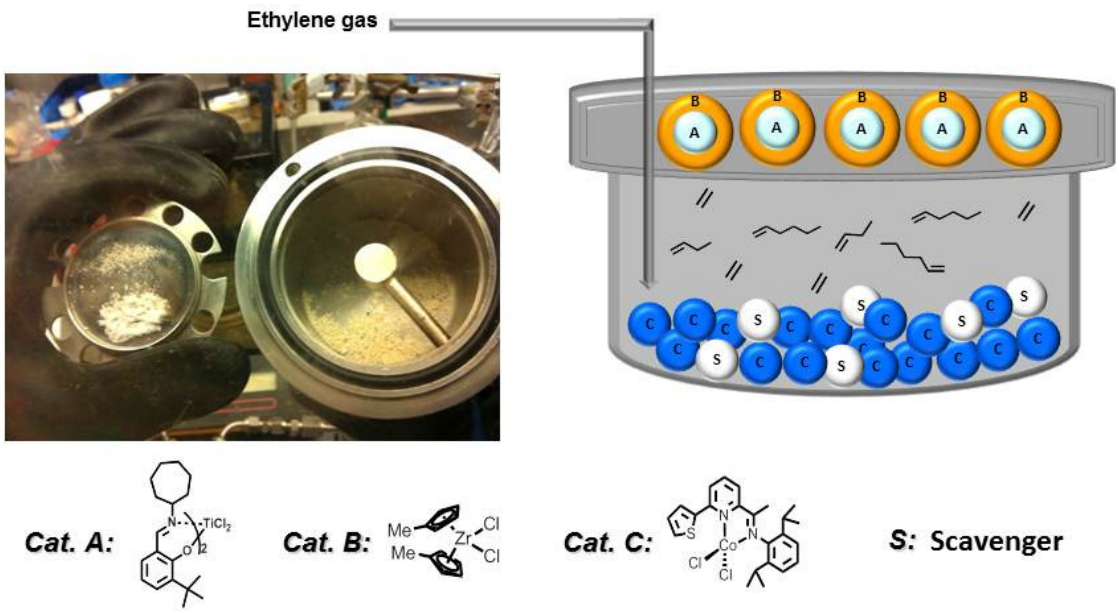

Figure 6-5. Tandem copolymerization system towards UHMWPE-LLDPE core-shell particles in a gas phase reactor

In order to demonstrate the synthesis of UHMWPE-LLDPE core-shell particles, a good selection of metallocene catalysts will be essential based on the requirements. For the synthesis of UHMWPE, Naundorf in our group have previously performed by employing one of the group IV transition metal complex bearing two phenoxy-imine ligands (FI catalysts), bis[*N*-(3-*t*-butylsalicylidene)cycloheptylaminato]titanium(IV) dichloride, which generally displays a high activity towards ethylene polymerization.[40] Therefore the titanium complex is chosen as model catalyst for **A**. For LLDPE synthesis via tandem catalysis using ethylene as a single feed, a cooperative action of two catalysts is required. Indeed, the

synthesis of LLDPE was successfully performed via a combination of bis(methylcyclopentadienyl)zirconium(IV) dichloride $[(MeCp)_2ZrCl_2]$ with iminopyridyl cobalt(II) complex $[CoCl_2N_2^{2Th}]$ in **Chapter 5**. Therefore, this combination has been selected for catalysts **B** and **C**, respectively. A complex of **A**/MAO is supported on silica particles (core), and subsequently, a solution of polystyrene nanoparticles and catalyst **B**/MAO were applied to build a layer around the core particles. As shown in *Figure 6-5*, the core-shell particles with selectively loaded catalysts **A** and **B** on core and shell, respectively, were placed on the silver coated plate in a gas phase reactor. Separately, silica particle-immobilized catalyst **C** was prepared and placed in the bottom of the reactor with DMAO as a scavenger.

6.3.1 Individual polymerizations

Prior to employing the catalysts (**A**, **B** and **C**) all together in a single particle, determination of the individual activity towards the synthesis of UHMWPE (with catalyst **A**) and LLDPE (with catalysts **B** and **C**) in our facility will be required. These individual studies will provide brief information of two distinct catalytic systems in terms of average weight molecular weights (M_w), melting points (T_m) and activities. The individual polymerizations for UHMWPE (runs 1 − 2) and LLDPE (runs 3 − 5) were performed and the results are summarized in *Table 6-1*.

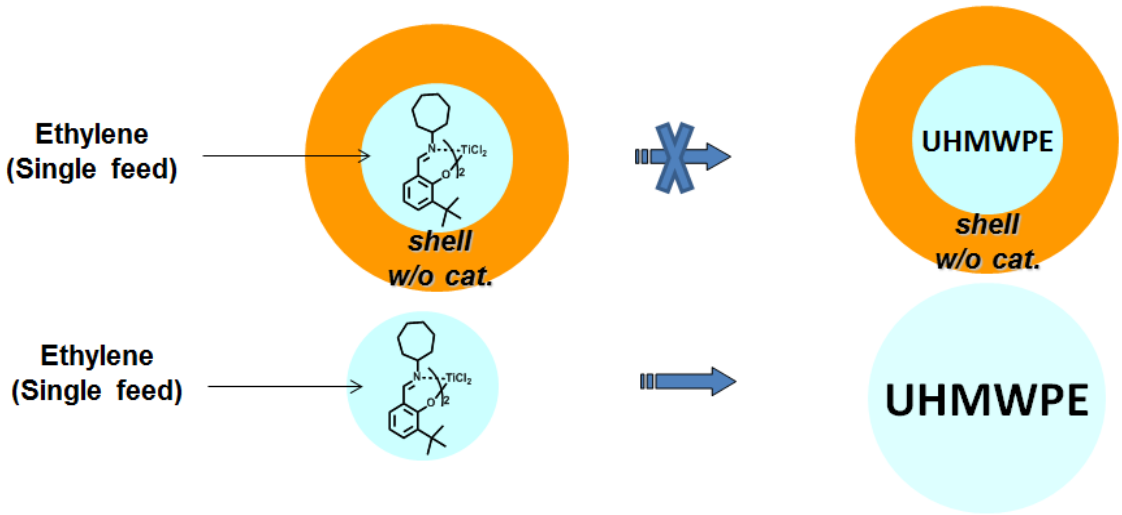

Figure 6-6. Individual synthesis for UHMWPE

For UHMWPE synthesis (*Figure 6-6*), catalyst **A** supported on silica particles (core), covered with a layer of polystyrene (PS) nanoparticles (shell), were prepared and initially

tested in a gas phase reactor under 3.0 bar of ethylene pressure. However, no activity was observed. This could be explained by the restricted diffusion of ethylene, caused by the highly packed shell layer. Therefore, a silica-supported catalyst **A** in the absence of shell layer was prepared and ethylene polymerized.

As a result, the weight average molecular weight (M_w) of the obtained polymers shows approximately 1.7 and 1.3 × 10^3 kg·mol^{-1} with polydispersities of 2.8 and 2.9 at 40 °C and 50 °C of ethylene polymerization temperature, respectively (runs 1 – 2, *Table 6-1*). The M_w of the obtained polymers is uncharacteristic of a UHMWPE.[41, 42] However, the melting points (T_m) of the polymers are in the range of 143 − 145 °C, which is typical of UHMWPE. For this conceptual study, catalyst **A**, bis[*N*-(3-*t*-butylsalicylidene)cycloheptylaminato]titanium(IV) dichloride, was selected as a model catalyst. The standard temperature for ethylene polymerization was selected as 40 °C, as obtained polymer showed higher M_w which is more convenient to distinguish with LLDPE which has generally one order of magnitude lower M_w.

Table 6-1. Results of individual polymerizations for UHMWPE and LLDPE[a)]

run	A [Ti]	B [Zr]	C [Co]	M_w[b)]	M_w/M_n[b)]	T_m[c)]	A[d)]	total branch[e)]	C_2 br	C_4 br
	μmol	μmol	μmol	kg·mol^{-1}		°C		‰	%	%
1	2.64	-	-	1300	2.9	145	1450	-	-	-
2	2.64	-	-	1680	2.8	143	830	-	-	-
3	-	0.67	-	794	7.4	141	246	-	-	-
4	-	0.67	0.47	450	5.6	115	360	10	>99	<1
5	-	0.67	0.93	328	4.8	111	180	13	>99	<1

a) Initial polymerization temperature: 40 °C, ethylene pressure: 3 bar;
b) analyzed by GPC (PS standard);
c) determined by DSC;
d) activity expressed as kg of polymer (mol of Ti·h·bar)$^{-1}$ for runs 1 – 2 and kg of polymer (mol of Zr·h·bar)$^{-1}$ for runs 3 – 5;
e) number of branches per 1000 carbon atoms calculated from ^{13}C NMR at 130 °C.

For individual LLDPE synthesis via concurrent tandem catalysis (CTC), core particles were prepared without catalysts and subsequently covered with the PS nanoparticles along with catalyst **B** (*Figure 6-7*). To perform the synthesis via CTC, silica-supported catalyst **C**, which *in-situ* generates short chain α-olefins from ethylene, was separately prepared and placed in the bottom of the reactor.

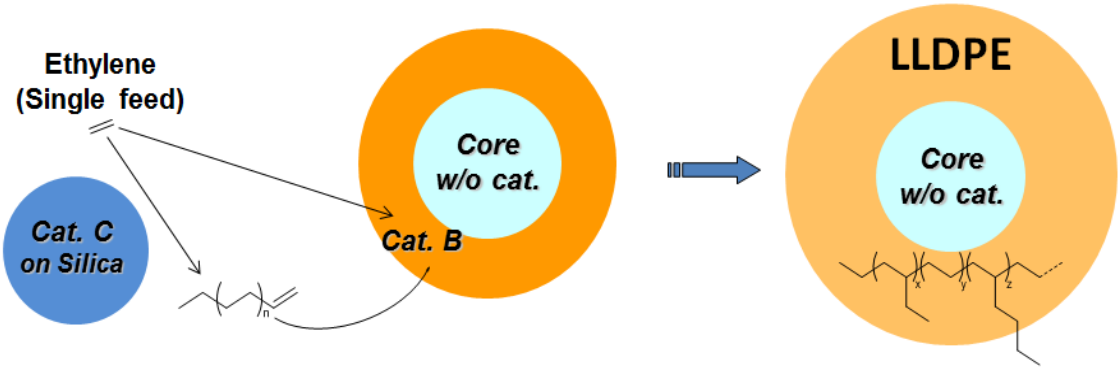

Figure 6-7. Individual synthesis for LLDPE

By varying the amount of catalyst **C** from 0 to 0.93 μmol (runs 3 − 5, *Table 6-1*), a decrease in T_m is detected from 141 to 111 °C. With 0.47 μmol of catalyst **C** (run 4, *Table 6-1*), the activity of the tandem catalytic system is slightly increased, when compared to the homopolymerization catalyzed by only **B** (run 3, *Table 6-1*). The increase in the catalytic activity for copolymerization below a certain concentration of comonomers can be attributed to a decrease of polymer crystallinity, which may lower the diffusion rates of the ethylene to the active sites.[43] By further increasing the amount of catalyst **C** to 0.93 μmol (run 5, *Table 6-1*), the activity decreases to 180 kg of polyolefin·(mol of Zr·h·bar)$^{-1}$. This can be explained by the increased presence of comonomers, which are generated in a higher concentration by catalyst **C**, hamper the diffusion of ethylene to active site of catalyst **B**.

To elucidate the existence of branches, ^{13}C NMR spectra of the obtained polymers were used to determine the total number of branches, which range from 10 to 13 per 1000 carbon atoms with almost exclusive ethyl branches. These features indicate that LLDPE is produced by a combination of catalysts **B** and **C** under mild condition (3 bar of ethylene and 40 °C).

6.3.2 Combined polymerization for synthesis of UHMWPE-LLDPE core-shell particles

Core-shell particle-immobilized catalysts **A** and **B** on core and shell, respectively, were prepared for one-pot synthesis of UHMWPE particles having a LLDPE layer, since the catalytic activity of two distinct systems (catalyst **A** for UHMWPE synthesis; the combination of catalyst **B** and **C** for LLDPE synthesis) was proven. By varying the amount of oligomerization catalyst **C** from 0 to 0.93 μmol, ethylene polymerization was performed with the core-shell particles and the results are summarized in *Table 6-2*.

Table 6-2. Results of ethylene polymerized core-shell particles[a)]

run	A0 [Ti]	B [Zr]	C [Co]	M_w[b)]	M_w/M_n[b)]	T_m[c)]	A[d)]	total branch[e)]	C_2 br	C_4 br
	μmol	μmol	μmol	kg·mol^{-1}		°C		‰	%	%
1	2.64	0.67	-	908	10	141	830	-	-	-
2	2.64	0.67	0.47	1307	12.1	143	1464	3	>99	<1
3	2.64	0.67	0.93	990	13.2	137	650	5	>99	<1

a) Initial polymerization temperature: 40 °C, ethylene pressure: 3 bar;
b) analyzed by GPC (PS standard);
c) determined by DSC;
d) activity expressed as kg of polymer (mol of Ti·h·bar)$^{-1}$ for runs 1 – 2 and kg of polymer (mol of Zr·h·bar)$^{-1}$ for runs 3 – 5;
e) number of branches per 1000 carbon atoms calculated from ^{13}C NMR at 130 °C.

By increasing the amount of catalyst **C** from 0 to 0.47 μmol (run 1 *vs.* run 2, *Table 6-2*), an increase in activity from around 0.8 to 1.5 × 10^3 kg of polyolefin·(mol of Zr and Ti·h·bar)$^{-1}$ and M_w from approximately 9.1 to 13.9 × 10^2 kg·mol^{-1} is observed. These features indicate that the comonomers, generated *in-situ* by catalyst **C** and subsequently incorporated into the polymer backbone, decrease crystallinity of the polymer formed on the shell and allow for easy diffusion of ethylene to the active sites of catalyst **A** and **B**. A slight increase in T_m from 141 to 143 °C further supports the argument that catalyst **A** immobilized in the core consumes more ethylene to produce UHMWPE, which has higher T_m than HDPE.

By further increasing the amount of catalyst **C** from 0.47 to 0.93 μmol (run 3, *Table 6-2*), M_w and activity are decreased to 1.0×10^3 kg of polyolefin·(mol of Zr and Ti·h·bar)$^{-1}$ and 6.5×10^2 kg·mol^{-1}, respectively. In contrast to the case of 0.47 μmol of catalyst **C** (run 3, *Table 6-2*), lower M_w and activity can be explained by a negative "comonomer effect", caused by too concentrated α-olefins.[43] It might also be associated with a high activity of catalyst **C** so that less ethylene remained in the reactor, as shown in run 5, *Table 6-1*. A slight decrease in T_m from 143 to 137 °C (run 2 *vs.* 3, *Table 6-2*) gives a brief account for limited diffusion of ethylene7 to catalyst **A**.

Surprisingly, monomodally distributed DSC endotherms are detected in the obtained polymers from the core-shell particles (runs 1 – 2, *Table 6-2*). Depending on the contents and the types of LLDPE, however, both mono- and bimodal DSC endotherms of the UHMWPE/LLDPE blend can be obtained (*Figure 6-8*). Bimodally distributed DSC endotherms were found when above 60 % content of the UHMWPE in the blend exists.[19] By increasing the contents of UHMWPE, an increase in T_m was observed since it has a significantly higher T_m.

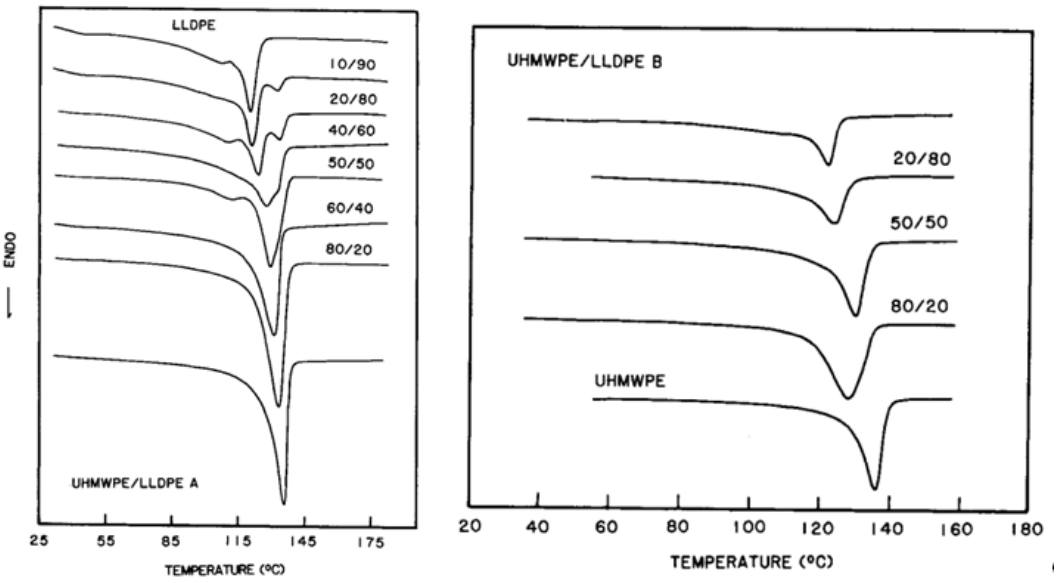

Figure 6-8. The DSC endotherms for various blends of UHMWPE/LLDPEs

To check the comonomers incorporated into the polymer backbone, the obtained polyolefins are measured by ^{13}C NMR at 130 °C. With variation of catalyst **C** from 0 to 0.93 μmol (runs 1 – 3, *Table 6-2*), the number of total branches ranged from 0 to 5 per 1000 carbon atoms is calculated. These values are lower than the data obtained from individual cases (runs 4 – 5, *Table 6-1*) as LLDPE coexists with UHMWPE. In the presence of catalyst **C**, almost exclusive ethylene branches (> 99 %) are detected. However, these features only prove a blend of UHMWPE and LLDPE.

6.3.3 Visualization of ethylene polymerized core-shell particles

In order to elucidate the LLDPE layer around the UHMWPE particles, visualization of the polymer particles was conducted by a combination of cryo-sectioning and various microscopic techniques. Firstly, scanning electron microscopy (SEM) was performed for better understanding of the fragmentation behavior of the ethylene polymerized core-shell particles. As shown in *Figure 6-10a*, most of the ethylene polymerized particles are found as "replica" of their corresponding supports with various size and broad size distribution (*Figure 6-9 vs. Figure 6-10*). By comparison with the non-ethylene polymerized particles, a significant increase in particle size was observed as previously reported.[44-46]

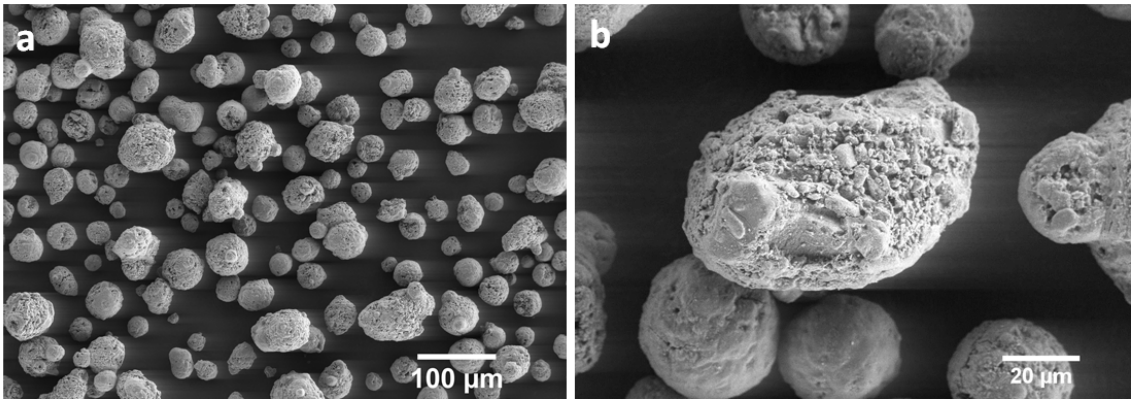

Figure 6-9. SEM micrographs of silica particles

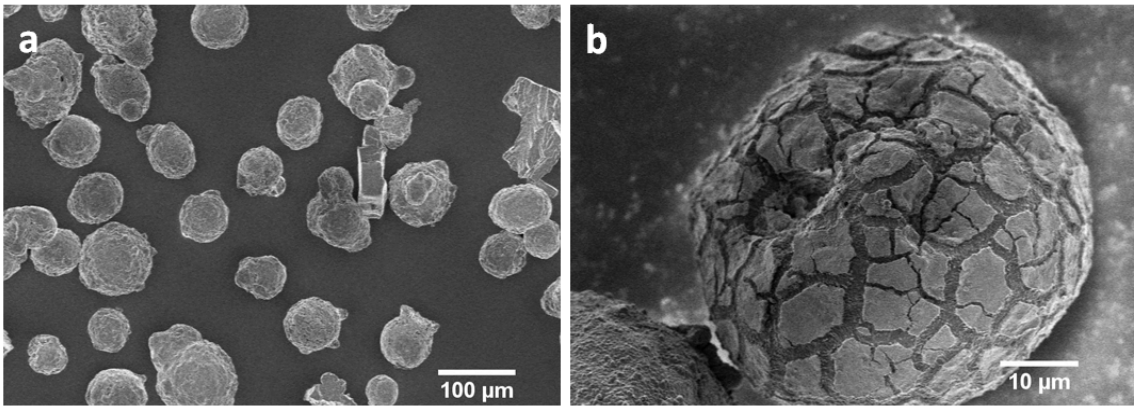

Figure 6-10. (a) SEM micrograph of ethylene polymerized core-shell particles, and (b) with a higher resolution

When taking a closer look at the ethylene polymerized particles, fragmented surface of the ethylene polymerized core-shell particles is observed (*Figure 6-10b*). It indicates that ethylene polymerization took a place on the surface of the core-shell particles and

contributed to the increased particle size. As previously stated, a solid proof of the core-shell morphology could not be established by SEM only.

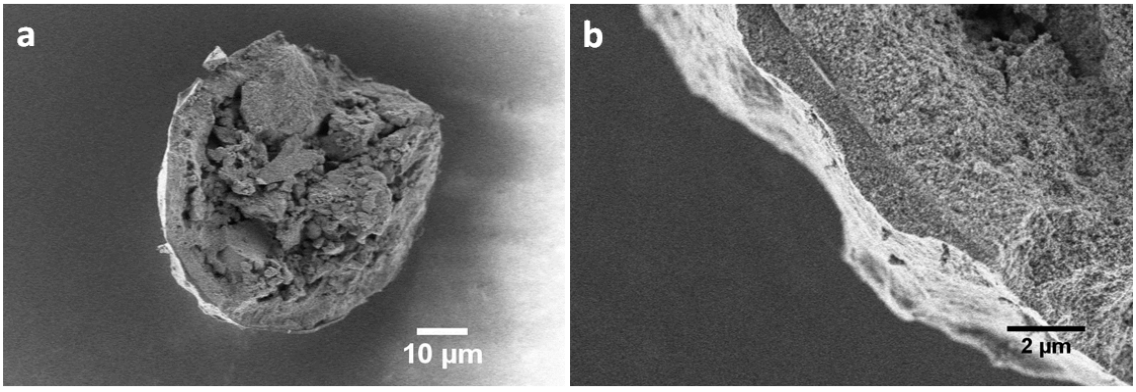

Figure 6-11. SEM micrographs of the LN_2-fractured core-shell particles after ethylene polymerization in a gas phase reactor

Fracturing of the ethylene polymerized core-shell particles was conducted after cooling the particles with liquid nitrogen, as previously demonstrated (**Chapter 4**). A fractured particle is found with unfragmented silica granules in the core (*Figure 6-11a*). Furthermore, in the middle of the particles, artifacts of the silica particles originated from agglomerated granules of silica particles are observed. By taking a closer look (*Figure 6-11b*), a slightly different topology is observed around the core particle with irregular thickness.

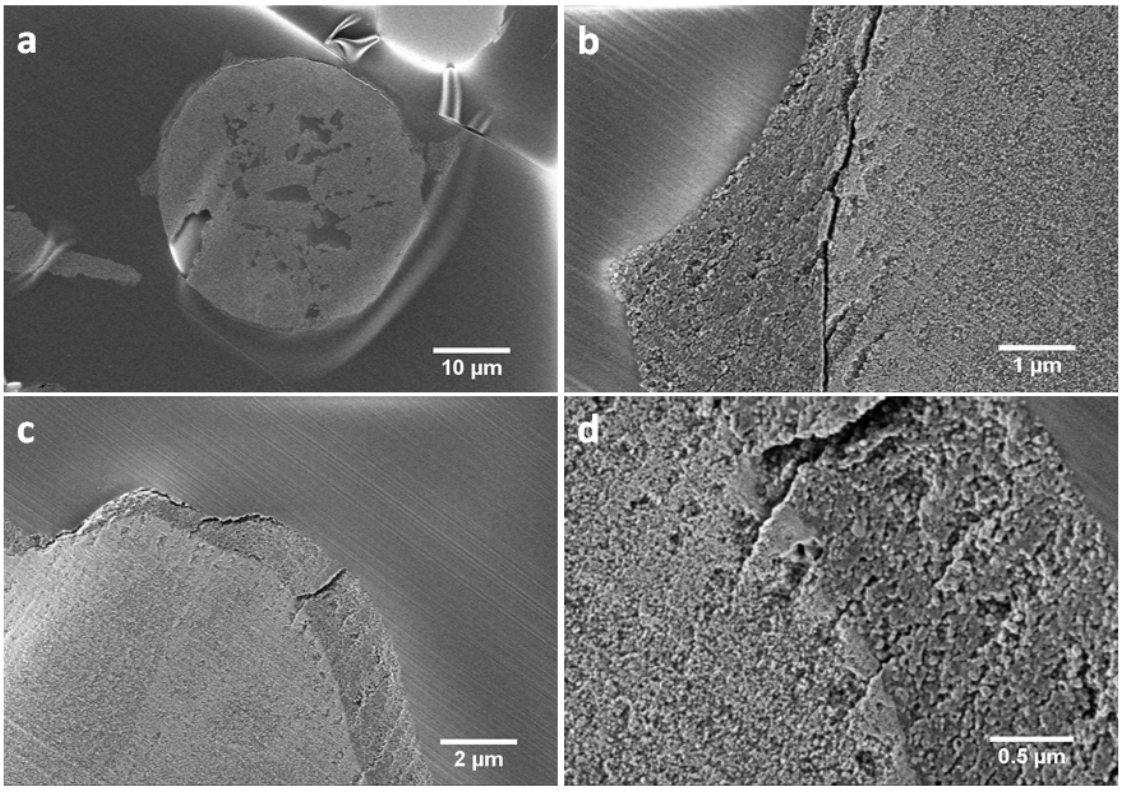

Figure 6-12. (a-d) SEM micrographs of the cross-sectioned core-shell particles after ethylene polymerization in a gas phase reactor

As further investigation of an inner morphology of the particles were limited by employing this approach, cryo-sectioning the ethylene polymerized particles was therefore combined with another optical methods to provide the best insight of the particles. SEM images of the cryo-sectioned particles, obtained after ethylene polymerization, show a slightly distinguishable boundary between core and shell (*Figure 6-12*).

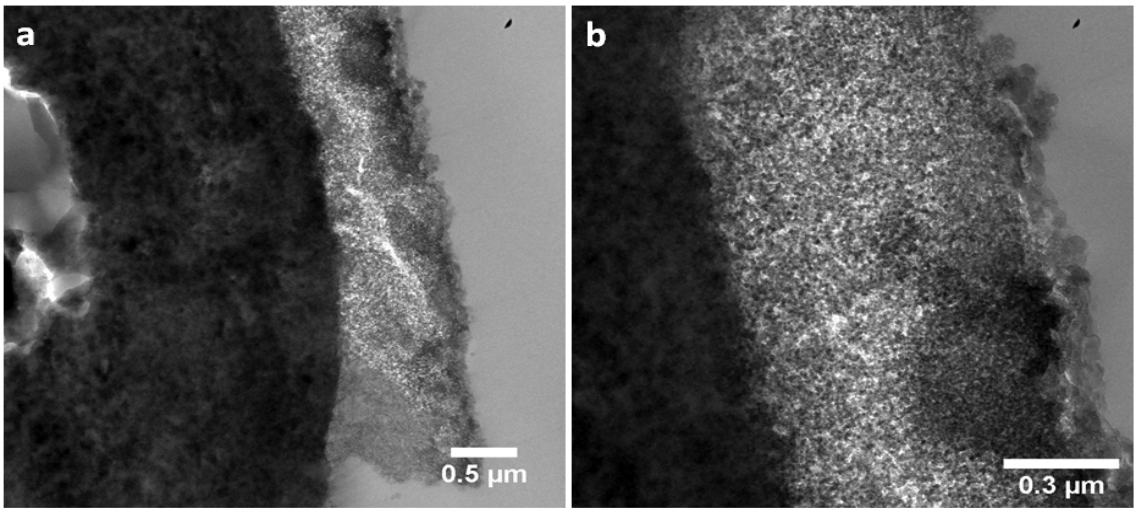

Figure 6-13. TEM micrographs of cryo-sectioned core-shell particles after ethylene polymerization

Transmission electron microscopy (TEM) images in the bright field imaging mode clearly display two distinct morphologies with different brightness (*Figure 6-13*). The difference in brightness comes from the sample thickness and the atomic content. For instance, thicker regions of the samples or regions with a higher atomic number will appear daker. Since the core region comprised silica which has a highest atomic number in the sample, this region scatters more electrons and therefore appears darker. This helps elucidate the locations of the supports having an inorganic core with an organic shell.

In order to further investigate the formation of the core-shell particles with spatially resolved two polyolefins, scanning transmission electron microscopy (STEM) was conducted with cryo-sectioned particles (*Figure 6-14*). Elemental mapping over the particle can be applied in order to check the distribution of silica and aluminum, since STEM is suitable for mapping by energy dispersive X-ray (EDX) spectroscopy. Silicon should be exclusively detected in the core, owing to the core material of the particles is mainly comprised of silica. Aluminum should be detected over the entire particles, as methylaluminoxane (MAO), contains aluminum, applied in the entire procedure to prepare

a support in a core-shell structure. Therefore, comparing the distribution of aluminum and silicon will indicate that there is a boundary between core and shell.

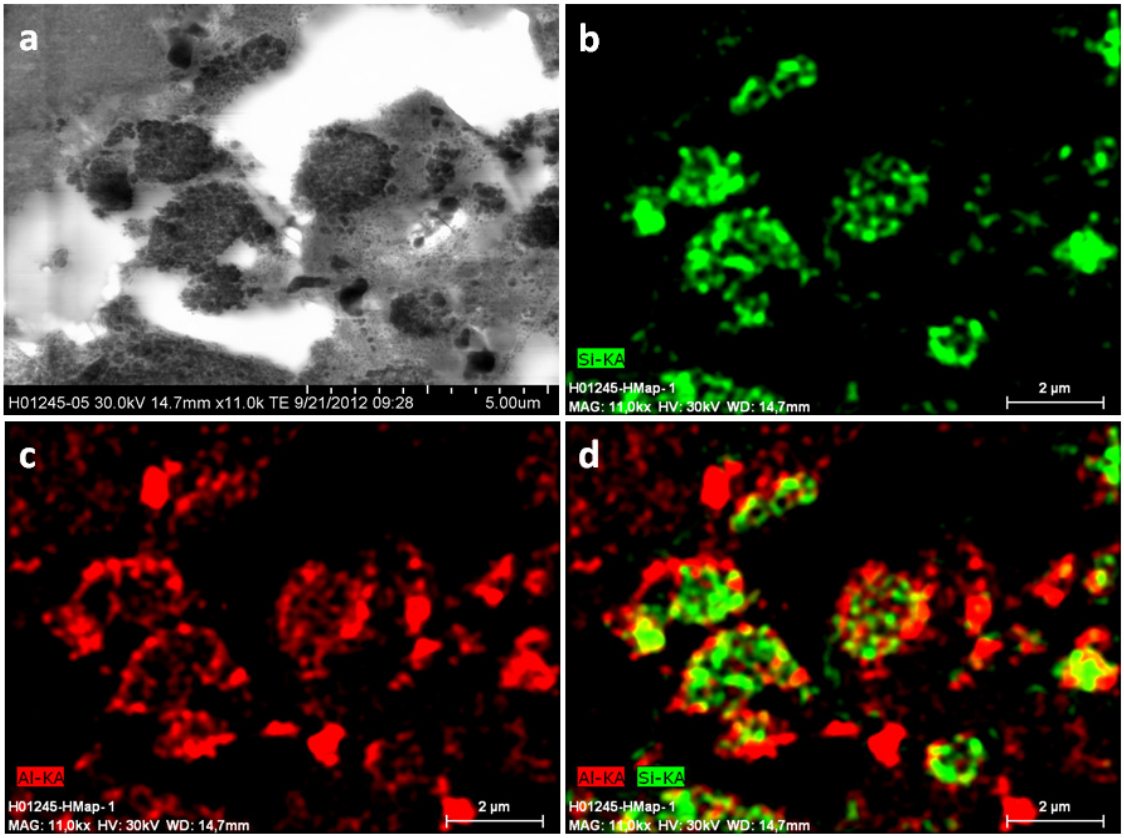

Figure 6-14. (a) STEM micrograph of ethylene polymerized core-shell particle after cryo-sectioning, distribution map of (b) aluminum and (c) silicon over the particle, and (d) over-laid image of (b) and (c)

As shown in *Figure 6-14*, elemental mapping over the particles follow. Aluminum (*Figure 6-14b*) is detected over the particle that exactly matches with its corresponding STEM image. Silicon (*Figure 6-14c*) is found inside the particle with a smaller area. An over-laid image (*Figure 6-14d*) of aluminum and silicon shows distinguishable boundaries between core and shell. Even though the thickness of the shell around the particle was irregular, the existence of silicon was limited in the core of the particle.

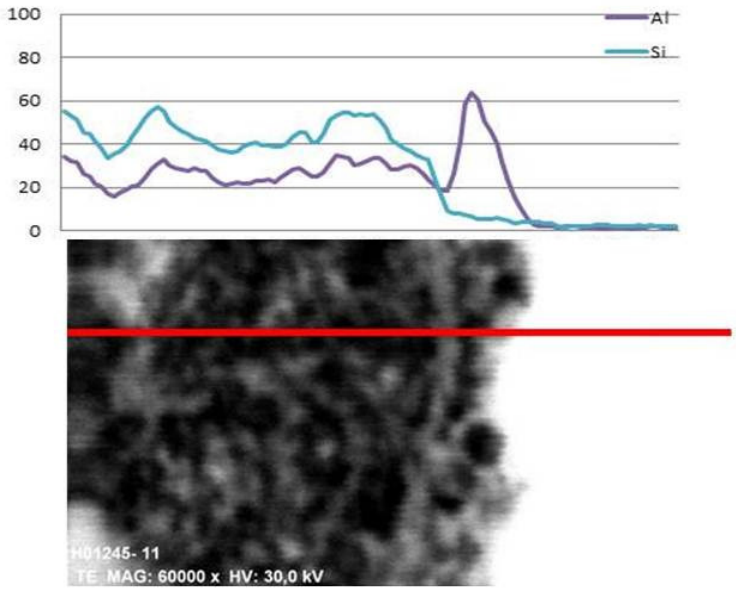

Figure 6-15. (top) The graph of elements distribution over the red line of the polymerized core-shell particle and (bottom) its corresponding SEM micrograph taken under transmission mode.

While building up the layer using PS nanoparticles around the silica particles (core), more amount of MAO was used than the procedure for the core, as MAO works not only as an activator but also as an adhesive for PS nanoparticles. Thus aluminum should be detected around the shell with higher intensity. Hyper-mapping through a line of the STEM image is demonstrated (*Figure 6-15bottom*). Aluminum is detected over the entire particle whereas silicon is exclusively detected in the core (*Figure 6-15top*). Moreover, a higher intensity of aluminum is detected in the outer particle with a thickness of approximately 200 nm as there was no signal of silicon. The higher intensity of aluminum and no existence of silica and in the outer particle are also one of the indications that there is a significant boundary of core and shell.

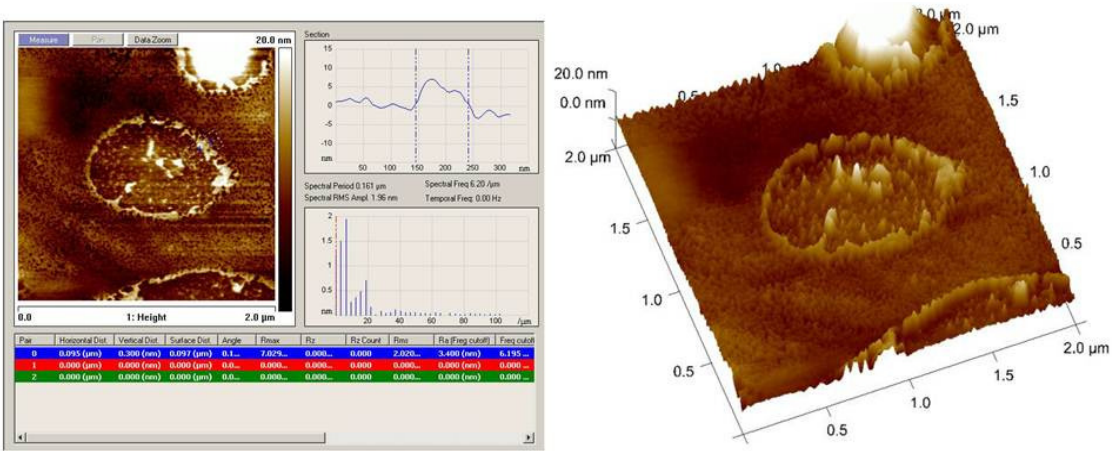

Figure 6-16. AFM image from tapping mode of the core-shell particles

Furthermore, the core-shell particles embedded in the epoxy resin were investigated with atomic force microscopy (AFM) in a tapping mode. Since UHMWPE has a higher hardness than LLDPE, AFM tapping mode was considered as an option to elucidate the spatially resolved polyolefins. The AFM image of the ethylene polymerized core-shell particles shows that there is a rim around the particles with approximately 100 nm thicknesses (*Figure 6-16*). The thickness of the shell is smaller than that of the results shown on the previous pages. Due to the position of the cryo-sectioning and a broad size distribution of ethylene polymerized core-shell particles, however, the diameter of the particles can be varied. The AFM images also contribute again that the morphology of the polymerized particles is "core-shell" structured particles.

In order to further visualize the ethylene polymerized core-shell particles, laser scanning confocal fluorescence microscopy (LSCFM) has been applied.[47, 48] In contrast to destructive methods such as cryo-sectioning, it can be simply employed by a dye staining of an object or direct linkage with a dye to an object chemically. For this study, polystyrene (PS) nanoparticles chemically linked with a styryl-boron-dipyrromethene (BODIPY) dye were synthesized according to a procedure in **Chapter 4**.

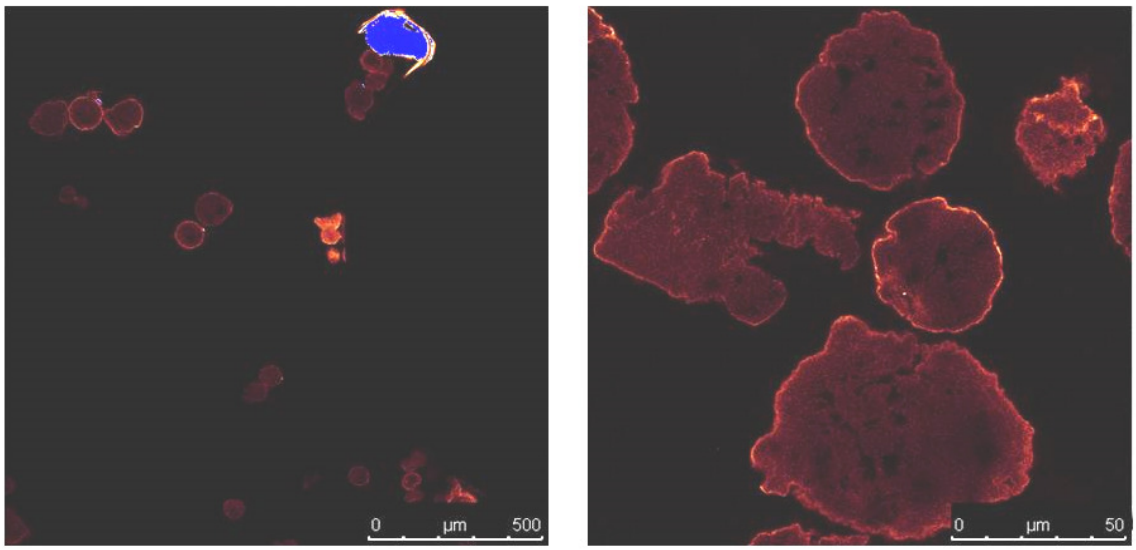

Figure 6-17. LSCFM images from the polymerized core-shell particles, stained with BODIPY dye exclusively on the shell

The core-shell particles having two catalysts were prepared with the BODIPY-tagged PS nanoparticles. The exclusively shell-stained core-shell particles were polymerized with ethylene under the same conditions, which were used for non-stained core-shell particles. As shown in *Figure 6-17*, the LSCFM images reveal a fluorescent hollow circle formed by a

shell of the PS nanoparticles with a thickness of a few micrometers. Even after the ethylene polymerization, these fluorescent circles remained on the outer surface of the silica. Additionally, LSCFM images exhibit two distinct morphologies corresponded to an inorganic core with an organic shell.

6.4 Conclusion

To synthesize UHMWPE particles coated with a layer of LLDPE via a one-pot procedure, the combination of two techniques (concurrent tandem catalysis for LLDPE synthesis and a selective loading technique of metallocenes on supports in a core-shell particle) is demonstrated. This procedure uses only ethylene as single feed. After ethylene polymerization, SEM micrographs show that a core-shell replica with an increased diameter is produced. However, a solid proof of the core-shell morphology is not established by SEM only. In order to elucidate spatially resolved LLDPE/UHMWPE in single particles, visualizing the inner morphology of the ethylene polymerized core-shell particles is conducted with cryo-sectioning and optical techniques (SEM, TEM, STEM, AFM and LSCFM). SEM and TEM micrographs of cryo-sectioned particles display a slightly distinguishable boundary between core and shell. Furthermore, STEM combination with EDX and hyper-mapping show the exclusively-distribution of silica in the core of the particles. AFM images also contribute again that the morphology of the polymerized particles is "core-shell" structured particles. For fragmentation studies via LSCFM, core-shell particles are prepared using fluorescence dye (BODIPY)-chemically linked PS nanoparticles. After ethylene polymerization, selectively BODIPY-linked core-shell particles reveal a fluorescence hollow circle with a few μm. These all features demonstrate the synthesis of spatially resolved LLDPE/UHMWPE particles by using core-shell structured supports with selectively loaded catalysts. Since UHMWPE particles are spatially coated with LLDPE, this method would be an alternative method to improve the processability of UHMWPE.

6.5 Experimental part

6.5.1 General procedure and materials

The imino(pyridine) cobalt complex, $CoCl_2N_2^{2Th}$, was synthesized [redacted] according to a published procedure[49] and used as received. The FI catalyst, bis[*N*-(3-*t*-butylsalicylidene)cycloheptylaminato]titanium(IV) dichloride was synthesized according to published procedures[42] and used.

6.5.2 Preparation of core-shell particles

6.5.2.1 Preparation of core particles

According to the procedure described in **Section 5.5.3**, immobilization of the bis[*N*-(3-*t*-butylsalicylidene)cycloheptylaminato]titanium(IV) dichloride on silica particles were performed. The silica particle-immobilized bis[*N*-(3-*t*-butylsalicylidene)cycloheptylaminato]titanium(IV) dichloride was ready to use in individual polymerization or further incorporation of an organic shell.

6.5.2.2 Synthesis of latex particles for shell

According to the procedure described in **Section 4.6.3**, the polystyrene (PS) nanoparticles for building up the shell around the silica (core) particles were synthesized.

6.5.2.3 Preparation of core-shell particle

Core-shell particles, supported with bis[*N*-(3-*tert*-butylsalicylidene)cycloheptylaminato]titanium(IV) dichloride and bis(methylcyclopentadienly)zirconium(IV) dichloride (MCP) in the core and shell, respectively, were prepared based on the procedure in the literature.[28] To redisperse the prepared silica particles (650 mg) containing bis[*N*-(3-*tert*-butylsalicylidene)cycloheptylaminato]titanium(IV) dichloride, dry toluene (20 mL) were added. To the dispersed solution, a suspension of the polystyrene (PS) nanoparticles (130 mg) was constantly added over 2 h. During the addition of the suspension, after 10

min, a MCP/MAO solution was added simultaneously over 1.5 h. The supernatant solution was removed and the product particles were dried under vacuum. The maximum loaded amount of bis[*N*-(3-*tert*-butylsalicylidene)cycloheptylaminato]titanium(IV) dichloride and MCP was calculated to be 52.8 μmol titanium and 13.4 μmol zirconium/g of core-shell particle, respectively.

6.5.3 Immobilization procedure for $CoCl_2N^{2Th}$ on silica particles

According to the procedure described in **Section 5.5.3**, immobilization of the cobalt complex on silica particles were performed. The maximum loaded amount of $CoCl_2N_2^{2Th}$ on the silica particles was calculated to be 33.8 μmol cobalt/g of silica particle.

6.5.4 Polymerization procedure in a gas phase reactor

All polymerizations were performed according to the procedure described in **Section 3.5.6**. The silica particle-immobilized $CoCl_2N_2^{2Th}$/MAO was placed in the bottom of the reactor along with DMAO solid as a scavenger to purify ethylene once again. The core-shell particles, prepared in **Section 6.5.2.3**, were mounted on the silver-coated plate in the gas phase reactor.

6.5.5 Characterization of materials

All polymers were characterized with DSC, GPC, NMR, SEM and LSCFM according to the procedure described in **Section 3.5.7**. For scanning transmission electron microscopy (STEM), the cryo-sectioned samples with an approximate thickness of 200 nm were investigated in field emission SEM (Hitachi SU 8000 Type I). Energy dispersive X-ray spectroscopy (EDX) and hyper-mapping of silicon, and aluminum were performed with Brucker solid state detector (SSD, XFlash detector 5010) in SEM. For atomic force microscopy (AFM), the embedded particles in epoxy resin after cryo-sectioning was applied and investigated using cantilever (Olympus) under tapping mode.

6.6 References

[1] G. Cazacu, M. C. Pascu, L. Profire, A. I. Kowarski, M. Mihaes, C. Vasile, *Industrial Crops and Products* **2004**, *20*, 261.

[2] J. Song, C. M. Thurber, S. Kobayashi, A. M. Baker, C. W. Macosko, H. C. Silvis, *Polymer* **2012**, *53*, 3636.

[3] P. Vadhar, T. Kyu, *Polymer Engineering & Science* **1987**, *27*, 202.

[4] A. Plochocki, *"Polyolefin Blends," in "Polymer Blends," D. R.Paul and S.Newman, eds, Academic Press* **1978**, p. 319.

[5] L. M. R. O. Olabisi, and M. T. Shaw, *"Polymer-Polymer Miscibility," Academic Press, New York* **1979**.

[6] *Encyclopedia of Polymer Science and Engineering; John Wiley & Sons: New York* **1985**, *Vol. 6*, p 495.

[7] S. M. Kurtz, O. K. Muratoglu, M. Evans, A. A. Edidin, *Biomaterials* **1999**, *20*, 1659.

[8] A. H. B. Stephen Li, *The Journal of Bone & Joint Surgery* **1994**, *76*, 1080.

[9] J. J. Wu, C. P. Buckley, J. J. O'Connor, *Biomaterials* **2002**, *23*, 3773.

[10] R. A. G. Steve M. Kurtz, John Martell, *The UHMWPE Handbook. Ultra High Molecular Weight Polyethylene in Total Joint Replacement; Elsevier Academic Press: New York* **2004**.

[11] N. C. Parasnis, K. Ramani, *Journal of Materials Science: Materials in Medicine* **1998**, *9*, 165.

[12] P. G. L. M. Fang, X. W. Cao, *eXPRESS Polymer Letters* **2011**, *5*, 674.

[13] S. Ronca, G. Forte, A. Ailianou, J. A. Kornfield, S. Rastogi, *ACS Macro Letters* **2012**, *1*, 1116.

[14] H. Jenkins, A. Keller, *Journal of Macromolecular Science, Part B* **1975**, *11*, 301.

[15] S. K. Bhateja, E. H. Andrews, *Polymer Engineering & Science* **1983**, *23*, 888.

[16] T. Kyu, P. Vadhar, *Journal of Applied Polymer Science* **1986**, *32*, 5575.

[17] Y. Chen, H. Zou, M. Liang, P. Liu, *Journal of Applied Polymer Science* **2013**, *129*, 945.

[18] M. Okamoto, A. Kojima, T. Kotaka, *Polymer* **1998**, *39*, 2149.

[19] S.-G. Lee, T.-J. Kang, *Polymer Bulletin* **1998**, *40*, 95.

[20] T. Tinçer, M. Coşkun, *Polymer Engineering & Science* **1993**, *33*, 1243.

[21] R. A. Shanks, J. Li, L. Yu, *Polymer* **2000**, *41*, 2133.

[22] H. Retsos, I. Margiolaki, A. Messaritaki, S. H. Anastasiadis, *Macromolecules* **2001**, *34*, 5295.

[23] T. S. Halbach, Y. Thomann, R. Mülhaupt, *Journal of Polymer Science Part A: Polymer Chemistry* **2008**, *46*, 2755.

[24] M. Xie, H. Li, *Journal of Applied Polymer Science* **2008**, *108*, 3148.

[25] J. F. Ross, W. A. Bowles, *Industrial & Engineering Chemistry Product Research and Development* **1985**, *24*, 149.

[26] *http://www.novolentechnology.com/swf/NOVOLEN_NEU_16.swf*.

[27] *http://www.tasneemarketing.com/Capacity_and_Technology_ACP_Technology*.

[28] T. Diesing, G. Rojas, M. Klapper, G. Fink, K. Mullen, *Angew Chem Int Ed Engl* **2009**, *48*, 6472.

[29] S. Matsui, T. Fujita, *Catalysis Today* **2001**, *66*, 63.

[30] R. W. Barnhart, G. C. Bazan, T. Mourey, *Journal of the American Chemical Society* **1998**, *120*, 1082.

[31] D. L. Beach, Y. V. Kissin, *Journal of Polymer Science: Polymer Chemistry Edition* **1984**, *22*, 3027.

[32] J.-C. Wasilke, S. J. Obrey, R. T. Baker, G. C. Bazan, *Chemical Reviews* **2005**, *105*, 1001.

[33] C. Bianchini, G. Giambastiani, A. Meli, I. Rios, A. Toti, E. Passaglia, M. Frediani, *Topics in Catalysis* **2008**, *48*, 107.

[34] A. Toti, G. Giambastiani, C. Bianchini, A. Meli, S. Bredeau, P. Dubois, D. Bonduel, M. Claes, *Chemistry of Materials* **2008**, *20*, 3092.

[35] F.-W. Yan, H. Xu, C.-Y. Guo, M.-G. Zhang, X.-H. Zhang, H.-J. Yang, G.-Q. Yuan, *Journal of Applied Polymer Science* **2009**, *112*, 2298.

[36] Z. Zhang, C. Guo, N. Cui, Y. Ke, Y. Hu, *Journal of Applied Polymer Science* **2004**, *94*, 1690.

[37] J. Zhang, B.-G. Li, H. Fan, S. Zhu, *Journal of Polymer Science Part A: Polymer Chemistry* **2007**, *45*, 3562.

[38] M. Yang, W. Yan, X. Hao, B. Liu, L. Wen, P. Liu, *Macromolecules* **2009**, *42*, 905.

[39] E. D. Schwerdtfeger, C. J. Price, J. Chai, S. A. Miller, *Macromolecules* **2010**, *43*, 4838.

[40] C. Naundorf, D. Ferrari, G. Rojas, G. Fink, M. Klapper, K. Mullen, *Macromol React Eng* **2009**, *3*, 456.

[41] Y. T. T. Fujita, M. Mitani, S. Matsui, J. Saito, M. Nitabaru, K. Sugi, H. Makio, T. Tsutsui, *EP 0 874 005, 1998*.

[42] H. Makio, N. Kashiwa, T. Fujita, *Advanced Synthesis & Catalysis* **2002**, *344*, 477.

[43] J. H. Z. dos Santos, T. Uozumi, T. Teranishi, T. Sano, K. Soga, *Polymer* **2001**, *42*, 4517.

[44] M. Klapper, S. Nenov, T. Diesing, K. Müllen, *Macromolecular Symposia* **2007**, *260*, 90.

[45] S. Nenov, C. G. Clark, M. Klapper, K. Müllen, *Macromolecular Chemistry and Physics* **2007**, *208*, 1362.

[46] C. Naundorf, D. Ferrari, G. Rojas, G. Fink, M. Klapper, K. Müllen, *Macromol React Eng* **2009**, *3*, 456.

[47] Y. J. Jang, K. Bieber, C. Naundorf, N. Nenov, M. Kapper, K. Mullen, D. Ferrari, S. Knoke, G. Fink, *E-Polymers* **2005**.

[48] Y. J. Jang, C. Naundorf, M. Klapper, K. Mullen, *Macromolecular Chemistry and Physics* **2005**, *206*, 2027.

[49] C. Bianchini, G. Giambastiani, G. Mantovani, A. Meli, D. Mimeau, *Journal of Organometallic Chemistry* **2004**, *689*, 1356.

CHAPTER 7

Hollow Silica Particles

Abstract: Hollow silica particles (HSPs) are used for a support in metallocene-catalyzed polyolefin synthesis demonstrating the synthesis of polyethylene particles with well-controlled wall-nut morphology. The HSPs with a diameter of around 1.2 μm and a thickness of approximately 100 nm are prepared by the Stöber method using scarifying templates of poly(styrene-*co*-acrylic acid). By controlling the pore size of HSPs which is affected by the content of acrylic acid, metallocene catalysts are selectively loaded only inside HSPs. After the ethylene polymerization, the presence of fragmented HSPs around the polyethylene particles indicates the selective loading of the metallocene inside the HSPs. The obtained polyethylene shows a typical value of high density polyethylene, although the productivity of this system is quite low compared to the silica case. By means of cryo-sectioning, ethylene polymerized particles are investigated to visualize the morphology at the early stage of ethylene polymerization. It is interesting that HSPs can be used as metallocene supports affording well-controlled polyethylene particles. Since fragmented HSPs are exposed outside of the obtained polyethylene particles. This selective loading of metallocene catalysts can be applied to produce high purity polyethylene by conveniently removal of HSPs using conventional de-ashing procedure.

7 Hollow Silica Particles

7.1 Introduction

Since the Ziegler-Natta (Z/N) process has been supported on the $MgCl_2$, it allows for enhanced productivity and better morphology control of the obtained polymer. However, the heterogenization of the Z/N process encountered a problem such as removal of unreacted supports, which acts as impurities in the final product. By further developments of the Z/N processes with the help of internal and external donors, productivity has nowadays been ultimately improved by two orders of magnitude (See also **Section 1.4.2**).[1, 2] However, the supports ($MgCl_2$) still remain in the final product. In film applications, which are the biggest markets for polyolefins, the remained supports scatter the light, and thus decreased clarity of the processed films.

As highly purified polyolefins are required to achieve an increased clarity, radical processes, working under high pressure (> 1000 bar) without a support, are still utilized although it has the oldest history and high cost (**Section 1.3.1**).[3] Due to economic and security reasons, gas-phase and combined process are nowadays utilizing dominantly in industrial polyolefin productions by the development of supporting systems and production processes.[4] In these cases, the supports and the active catalyst should be uniformly distributed over the products and following the fragmentation in order to obtain a colorless and clear product.[5] Since the supports are broken down to sub-nanometer fragments, light scattering can be reduced. Heterogenization of a catalyst is mandatory for industrial mass productions due to the following main reasons: i) prevention of reactor fouling; ii) better processability of the product; and iii) ease of handling during the procedure.

7.2 Objective

Less supporting materials logically result in less amount of support in the final products. For these reasons, supports with empty core, high porosity, and suitable mechanical strength are considered as a good candidate for supporting metallocenes. Indeed, Wen et. al. demonstrated porous hollow silica particles (HSPs) for supports in metallocene-catalyzed ethylene polymerization.[6] As illustrated in *Figure 7-1*, ethylene polymerization has been performed everywhere and thus encapsulation of HSPs by polyethylene has been achieved. This polymerization behavior was explained by that porous HSPs have immobilization sites for metallocene catalysts not only on the external surface, but also on the pore channels and internal surface of the supports.[6]

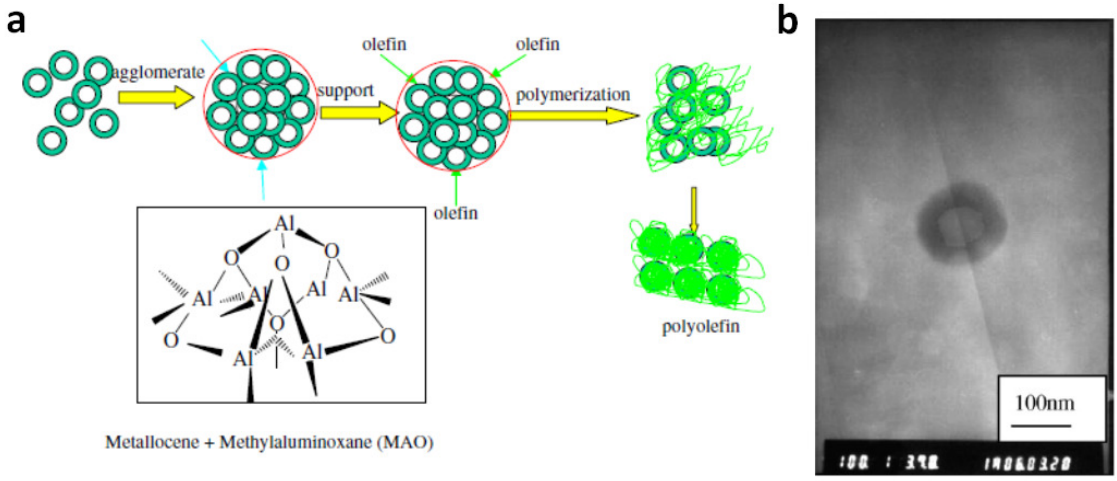

Figure 7-1. (a) Scheme of support agglomeration and (b) TEM micrograph of the polyolefin particle

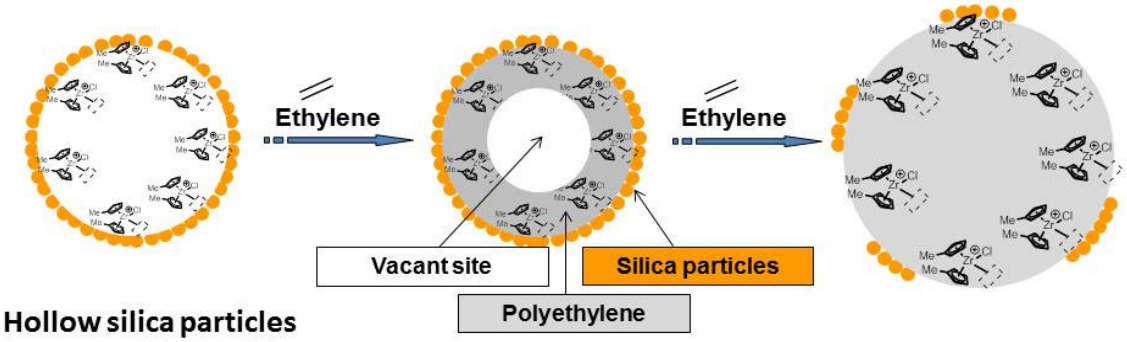

Figure 7-2. Schematic drawing of immobilized catalyst inside HSP and fragmentation of HSP during ethylene polymerization

In contrast to that, in this Chapter, exclusive usage of internal surface of HSPs as immobilization sites will be addressed to provide a better morphology control of the final

product and also minimize the content of supports (*Figure 7-2*). For selectively controlling the immobilization sites of the HSPs, the synthesis of porous HSPs was performed via a modified Stöber method using templates which comprise of poly(styrene-*co*-acrylic acid) microspheres. In this chapter, their applicability as porous inorganic supporting materials has been demonstrated in a heterogeneous metallocene/MAO catalytic system.

7.3 Results and discussion

7.3.1 Synthesis of hollow silica particles

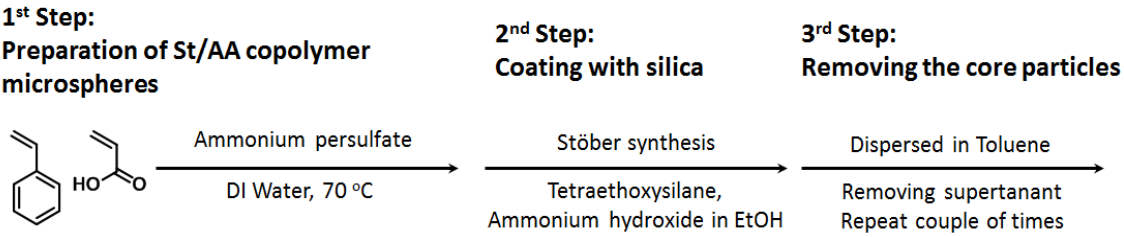

Figure 7-3. Synthetic procedure of hollow silica particles

To reduce the content of supports in polyolefin product, silica particles possessing empty core were considered. *Figure 7-3* features the general synthetic procedure for hollow silica particles (HSPs). To introduce empty cores, template particles, which can be conveniently removed, were first prepared by copolymerization of styrene, acrylic acid (controlling functional group) and divinyl benzene (crosslinker) with ammonium persulfate as an initiator in emulsion polymerization.[7] This led to styrene-*co*-acrylic acid particles with approximately 1.0 μm diameter, for use as templates for HSPs. As the number of silica particles can be controlled by the content of acrylic acid on the template particles, the synthesis of silica particles was performed around the templates via a modified Stöber method with hydrolysis of tetraethoxysilane (TEOS) and ammonium hydroxide in ethanol.

After removal of the templates by dispersing in toluene, the average diameter of the obtained particles was determined by SEM to be approximately 1.2 μm (*Figure 7-4a*). On the surface of the obtained particles, fully-covered small grains (< 50 nm diameter) are observed (*Figure 7-4b*). To verify the formation of hollow silica particles, it was determined by TEM (*Figure 7-4c*) which reveals the empty space in the core. To elucidate the formation of the empty core, the HSPs were cryo-sectioned with a thickness of around 60 nm. The cryo-TEM micrograph clearly reveals the formation of hollow silica particles with an internal diameter of *ca.* 1 μm and a wall thickness of around 100 nm (*Figure 7-4d*).

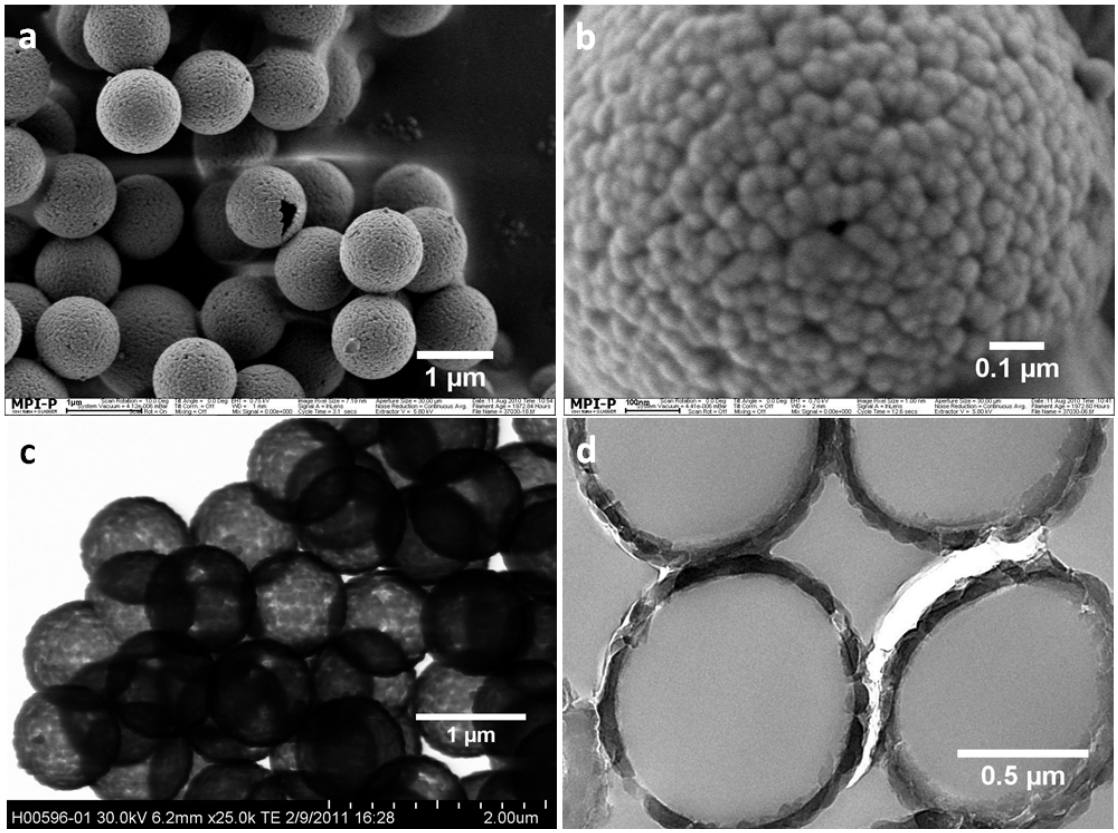

Figure 7-4. (a-b) SEM micrographs of HSPs, (c) TEM micrographs of HSPs and (d) TEM micrograph of cryo-sectioned HSPs

7.3.2 Ethylene polymerization

To perform the ethylene polymerization, a selective loading of a catalytic complex (metallocene/MAO) exclusively at internal surface of the HSPs was conducted. Due to the cage-like structure of MAO, no pretreatment with methylaluminoxane (MAO) as a scavenger was applied since MAO might block the pores of the HSPs. Thus prior to be used as the catalyst support, removing residual moisture in the HSPs was crucial. The HSPs were dried at elevated temperature for 48 h under reduced pressure in order to minimize the content of the adsorbed water, and used as supports for a metallocene immobilization. A metallocene complex [$(MeCp)_2ZrCl_2$] was chosen since it is a relatively small complex among the metallocenes and has been proven as a robust catalytic system in previous studies (**Chapters 3 – 6**). Upon pre-activation of the $(MeCp)_2ZrCl_2$ with an extremely low ratio of MAO ([Al]/[Zr]= 170), it was added to the HSPs dispersed in toluene. After a mild shaking for 3 h, the HSPs were washed with toluene several times to remove the un-immobilized catalytic species and MAO. After drying under reduced pressure, the HSPs treated with $(MeCp)_2ZrCl_2$/MAO were investigated for ethylene polymerization. The

results of ethylene polymerization with the $(MeCp)_2ZrCl_2$/MAO-supported HSPs in a gas-phase reactor are summarized in *Table 7-1*.

Table 7-1. Results of ethylene polymerization with MAO/MCP-supported HSPs[a)]

entry	amount of HSPs	polymerization time	productivity	T_m[b)]	M_w[c)]	M_w/M_n[c)]
	mg	min	g of PE·(g HSP hr)$^{-1}$	°C	kg·mol^{-1}	
1	5	60	21.6	134.5	720	6.8
2	5	60	24.5	135.6	648	7.9
3	5	2	n/a	-	-	-

a) Polymerization under 3 bar of ethylene at 40 °C in a gas phase reactor;
b) determined by DSC;
c) analyzed by GPC (PS-standard).

To elucidate the $(MeCp)_2ZrCl_2$/MAO-immobilized on the HSPs are capable of producing polyethylene, obtained polymers were characterized. By checking the weight balance of the supports and the obtained polymer (entries 1 – 2, *Table 7-1*), productivities were calculated and show a narrow range from around 22 to 25 × gPE·(gHSP·h)$^{-1}$. As compared to conventional silica particles, these values of productivity are around three orders of magnitude lower due to the fewer coordinating sites for the catalytic species.[8, 9] A typical value of melting points (T_m) for a high density polyethylene (HDPE) was determined to be ~ 135 °C. This is associated with the fact that the HSPs have no negative influence on the polymerization behavior of the catalytic system. Indeed, similar values of T_m have been observed in the previous studies (**Chapters 3 – 6**). Average weight molecular weights (M_n) of the obtained polymers display in the range of approximately 7.2 and 6.5 × 10^2 kg·mol^{-1} with polydispersities of 6.8 and 7.9 (entries 1 – 2, *Table 7-1*). It is in good agreement with that catalytic system [$(MeCp)_2ZrCl_2$/MAO] were successfully supported on the HSPs.

7.3.3 Morphology studies

To verify the place for ethylene polymerization on HSPs, morphology studies of the ethylene polymerized HSPs were conducted with SEM. As shown in *Figure 7-5*, extremely uniform polyethylene products are observed with an average diameter of 4 μm and a

narrow size distribution. In most of the cases, small fragments of HPSs are found at the exterior of the polyethylene particles. This observation is a solid evidence that catalytic system, $(MeCp)_2ZrCl_2$/MAO, is almost exclusively immobilized at the interior of the HSPs. In comparison to conventional silica or $MgCl_2$ supports, the use of HSPs might be another excellent solution to get polyolefin products with well-defined particle morphology. Some of the HSPs (yellow circle in *Figure 7-5b*) are found with their original morphology which indicates that no catalytic system was supported. The original morphology (yellow circle in *Figure 7-5b*) can be associated with that catalytic system can be easily washed away due to the broken surfaces on the HSPs.

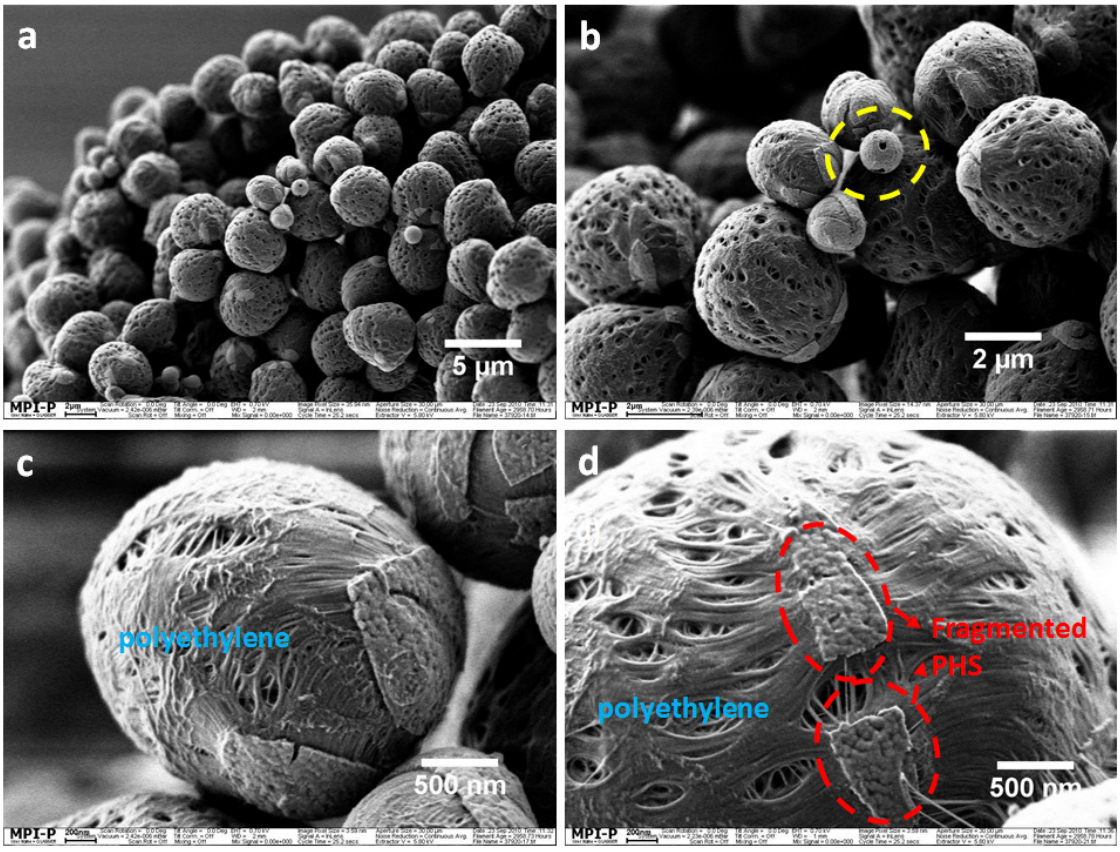

Figure 7-5. SEM micrographs of polyethylene particles after gas phase polymerization using hollow silica particles

After revealing the selective immobilization of the catalytic system exclusively inside the HSPs, further investigation of the $(MeCp)_2ZrCl_2$/MAO-supported HSPs at the early stage of ethylene polymerization would be essential. Therefore, the HSPs were ethylene polymerized for 1 and 2 min. To study the inner morphology of the ethylene polymerized HSPs, they are cryo-sectioned and are measured by SEM (*Figure 7-6*). If ethylene polymerization starts at the internal surface of the HSPs and further proceeds to the center

of the HSPs, vacant sites of the HSPs might be detected at the early stage of ethylene polymerizations (*Figure 7-2*). The TEM micrograph of the cryo-sectioned HSPs obtained after 2 min of ethylene polymerization exhibits that some of HSPs have vacant sites with a smaller than 200 nm. It also indicates that the catalytic species [$(MeCp)_2ZrCl_2$/MAO] are supported only inside the HSPs and furthermore ethylene polymerization was initially proceeded at the internal surface of HSP. Due to the short reaction time, however, the productivity was not calculated (entry 3, *Table 7-1*).

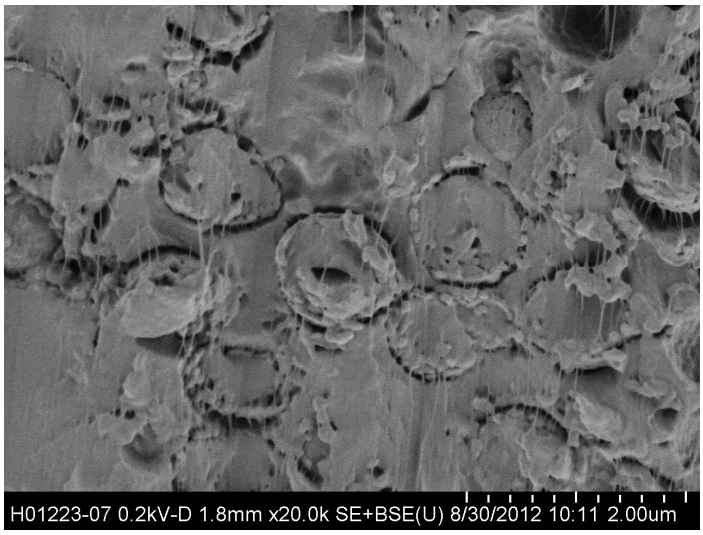

Figure 7-6. SEM micrograph of cryo-sectioned HSPs after 2 min ethylene polymerization

7.3.4 Synthesis of core-shell particle with the hollow silica particles

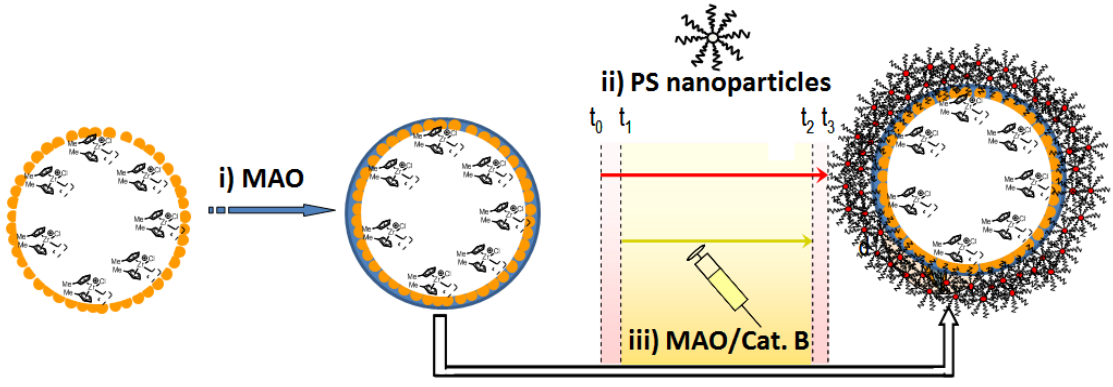

Figure 7-7. Schematic drawing of the strategy for core-shell particles with HSPs

Since the $(MeCp)_2ZrCl_2$/MAO is selectively loaded inside the HSPs, organic-inorganic hybrid support system for core-shell particles can be applied with the HSPs as core materials with PS nanoparticles (*Figure 7-7*). As demonstrated in **Chapter 6**, core-shell particles have been prepared with silica particles (core) and polystyrene nanoparticles (shell).

Prior to building the shell around the MCP/MAO-supported HSPs, one could consider that they still have open pores which can be used for immobilizing other catalysts. In order to block the open-pores of the HSPs, MAO solution was added. The MAO-treated HSPs are observed with a different surface topology (*Figure 7-4 vs. Figure 7-8*). Some defects are found on the surface of HSPs. Their features prove that the HSPs are covered with MAO, which has an oligomer structure and can act as an adhesive.

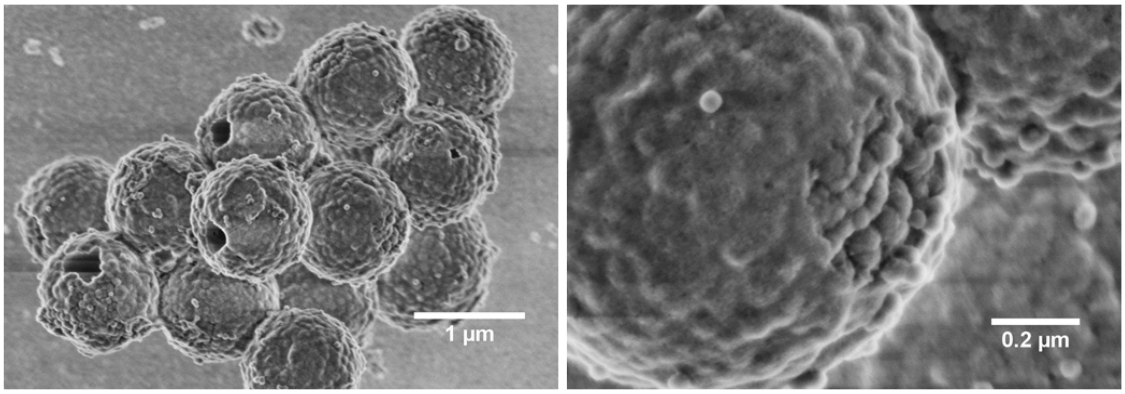

Figure 7-8. SEM micrographs of HSPs covered with polystyrene nanoparticles

To build core-shell support particles using the MAO-treated HSPs as core materials, polystyrene particles are applied along with another metallocene catalyst. The *rac*-(dimethylsilyl-bis(2-methylbenzindenyl)zirconium(IV) dichloride (MBI) is chosen since it has been previously tested.[10] As shown in *Figure 7-7*, the MBI/MAO was added along with polystyrene (PS) nanoparticles to the MAO-treated HSP dispersed in toluene. After this procedure, the particles were dried under reduced pressure and characterized with SEM (*Figure 7-9*).

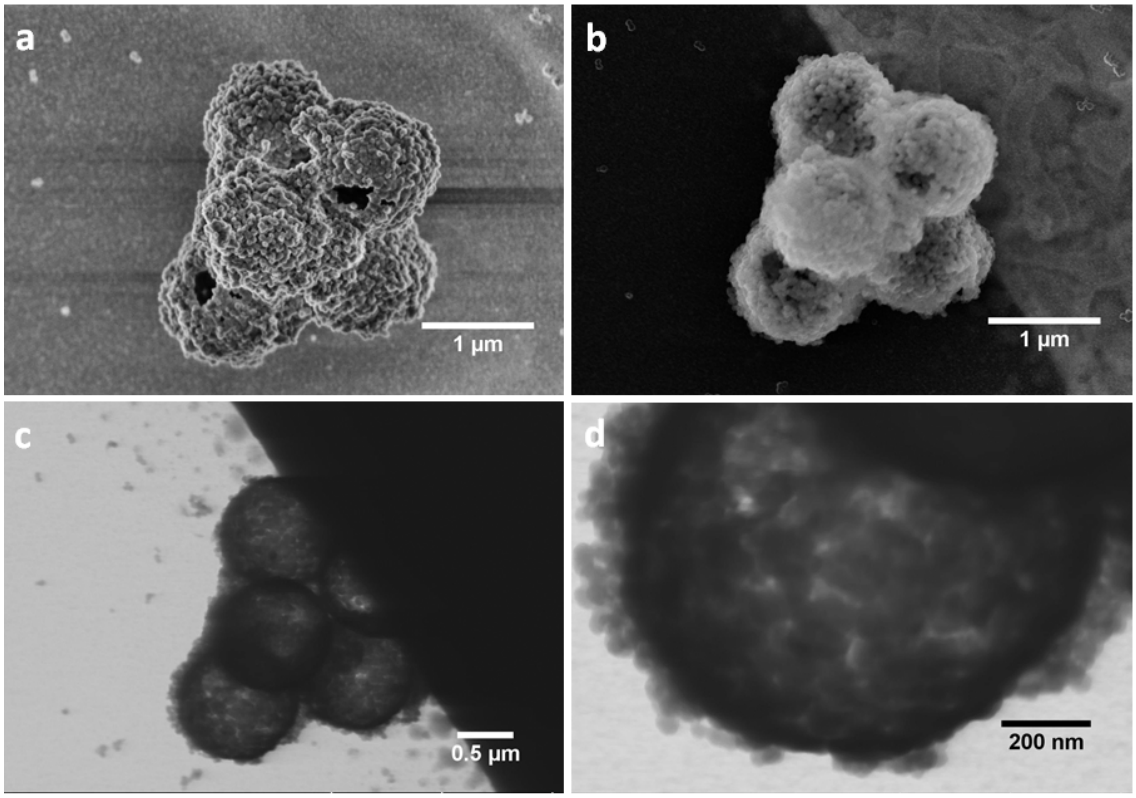

Figure 7-9. (a) SEM micrographs of HSPs (b) in dark field, (c) in bright field, and (d) with higher resolution

SEM micrographs of *Figure 7-9* exhibit agglomerated PHSs with rough surfaces unlike the smooth surface of HSPs (*Figure 7-4c*). Furthermore, small particles with approximate diameter of 60 nm are observed around the HSPs (*Figure 7-9c,d*). This can be explained by the polystyrene nanoparticles surrounding the HSPs in the presence of MAO as the same behavior has been observed with silica particles in **Chapter 6**. This feature is associated with the formation of agglomerated polystyrene nanoparticles around the HSPs along with MAO and MBI. The non-covalent interaction between poly(ethylene oxide) groups from polystyrene nanoparticles and MAO/metallocene complex leads to the formation of core-shell particles with HSPs (core) and polystyrene nanoparticles (shell). The core-shell particles, which are comprised of [$(MeCp)_2ZrCl_2$/MAO] in the HSP (core) and MBI/MAO on the agglomerated PS nanoparticles (shell), were polymerized under 3 bar of ethylene in a gas-phase reactor.

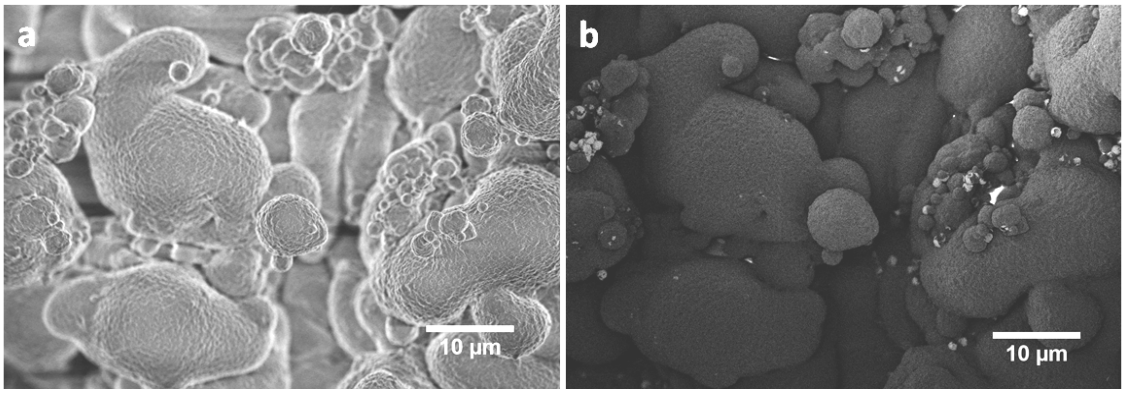

Figure 7-10. SEM micrographs of ethylene polymerized HSPs covered with PS nanoparticles (a) in dark field and (b) in bright field

To visualize the formation of spatially resolved core-shell particles, ethylene polymerized particles are first measured by scanning electron microscopy (SEM). The SEM micrographs in *Figure 7-10* reveal that broad size distributions of products are formed in the range of around 2 to 20 µm, and that agglomerates are found. In order to conveniently elucidate the formation of core-shell particles after ethylene polymerization, the presence of the fragmented HSPs is investigated by SEM in bright field which can detect the portion of higher atomic elements. In most of the cases, fragments of HSPs are detected around the particles with an approximate diameter of 2 µm (*Figure 7-10b*). It is assumed that some of HPSs were not covered with PS nanoparticles and thus the MBI/MAO could be supported around the HSPs.

7.4 Conclusion

The synthesis of silica particles having an empty core is demonstrated via the Stöber method on a scarifying template. By removal of the templates, the hollow silica particles (HPSs) having an average diameter of 1.2 μm and a wall thickness of 100 nm are synthesized and are used as supports in metallocene-catalyzed olefin polymerization. Unlike the conventional silica supports for metallocene, HSPs can fundamentally suppress the amount of supports as impurities hampering the clarity of polyolefin products. After ethylene polymerization for 1 h under 3 bar at 40 °C, small fragments of the HSPs were found exclusively at the surface of the polyethylene particles with a mean diameter of around 4 μm. This indicates that a catalytic species consisting of metallocene/MAO was selectively immobilized inside the HSPs, and the HSPs were broken by the pressure of the produced polyethylene.

Furthermore, spatially resolved core-shell particles based on the HSPs are formed via a step-wise process using the layer of polystyrene nanoparticles along with second catalytic species. The HSPs are applied to clearly elucidate the boundary of core-shell particles after ethylene polymerization. Under the same polymerization conditions (for 1 h at 3 bar and 40 °C), polyethylene is obtained with a broad size distribution ranging from few μm to 20 μm. Due to the agglomeration of HSPs with MAO, further studies are not conducted.

However, it is important that metallocene/MAO is selectively supported inside the HSPs affording polyolefin particles with a uniform and well-controlled morphology. Since the supports (fragmented HSPs) are exposed, an additional removal procedure of the fragmented supports such as via a steam cracker would be more convenient than the cases of conventional silica supports. Thus, highly purified polyolefins can be produced via selective loading of metallcene at the interior of the HSPs. Furthermore, since this is a heterogeneous catalytic system, polymerization can be performed under mild conditions when compared to radical polymerization process.

7.5 Experimental part

7.5.1 Preparation and characterization of hollow silica particles

Hollow silica particles (HSPs) were prepared [redacted] according to the literature[7] and donated for the study. For morphological observations with scanning electron microscopy (SEM), the HSPs were placed on a graphite tape and measured at low-voltage using a LEO 1530 Gemini, Zeiss. For inner-morphology observations, the HSPs were embedded in an epoxy resin and sectioned with various thicknesses using Leica ultracut UCT under liquid nitrogen stream. For cryo-transmission electron micrographs (TEM), the *ca.* 60 nm thick samples were placed on a 300 mesh carbon-coated copper grid and measured with a Zeiss EM912 operating at 80 kV.

7.5.2 Selective immobilization of MCP in the hollow silica particles

Prior to immobilization procedure with a metallocene, the hollow silica particles (HSPs) were dried under reduced pressure for 48 h. Under inert atmospheres, the HSPs (100 mg) were placed in 25 mL of round-bottom Schlenk flask with 5.0 mL of the dried toluene. In order to extract the residual water in the HSPs, the flask was mounted on a shaker at 100 rpm. After 3 h of shaking, the toluene was removed and 5.0 mL of fresh toluene was added and shaken again at 100 rpm. This procedure was repeated 3 times to minimize the content of water in the HSPs. After removal of toluene from the flask, a mixture of 4.0 mL toluene and 1.0 mL of a 1.0 M MAO solution (prepared from DMAO) was added in flask and shaken for an additional 3 h to ensure the complete removal of the residual water in the HSPs by the scavenger effect of MAO. After removal of unreacted MAO solution, the HSPs were washed with fresh toluene (3 × 5 mL) and were waited for the addition of a catalytic solution. For the preparation of a catalytic solution, bis(methylcyclopentadienyl)zirconium(IV) dichloride (MCP) (10 mg, 0.03 mmol) was dissolved in toluene (5 mL) and stirred for 5 min to preactivate by the addition of 1 mL of MAO solution. The MAO-preactivated MCP solution was added to the flask containing the HSPs at room temperature, and the flask was shaken at 100 rpm overnight. The resulting HSPs were washed with fresh toluene (3 × 5 mL) and dried under reduced pressure. The maximum loaded amount of MCP in the HSPs was calculated to be 25 μmol Zr/g HSP. The aluminum to zirconium ratio was estimated to be 170:1.

7.5.3 Ethylene polymerization of the MCP-supported HSPs in a gas phase reactor

All polymerizations were performed according to the procedure described in **Section 3.5.6**. The MCP/MAO-supported HSPs were placed on a silver coated plate in a gas phase reactor.

7.5.4 Immobilization of MBI on the MCP-supported HSP

In order to synthesize the core-shell particles, the MCP-supported HSPs were used as a core particle and subsequently applied based on the procedure in a literature.[10] For the formation of shell, *rac*-(dimethylsilyl-bis(2-methylbenzindenyl)zirconium(IV) dichloride (MBI) was applied as a catalyst.

7.5.5 Ethylene polymerization of core-shell particles in a gas phase reactor

For ethylene polymerization with the core-shell particles prepared in **Section 7.2.4**, same procedure was applied as described in **Section 7.5.3**.

7.5.6 Characterization of polyethylene

All polymers were characterized with DSC, GPC, NMR, SEM and cryo-TEM according to the procedure described in **Section 3.5.7**.

7.6 References

[1] Y. V. Kissin, "*Isospecific Polymerization of Olefins with Heterogeneous Ziegler-Natta Catalysts*", Springer-Verlag, New York, 1985.

[2] M. E.P., "*Polypropylene Handbook*", Jr. Hanser Publishers, München, 1996.

[3] *http://www.klmtechgroup.com/PDF/Articles/Fluidized-Bed-Reactor.pdf*.

[4] J. R. Severn, J. C. Chadwick, R. Duchateau, N. Friederichs, *Chemical Reviews* **2005**, *105*, 4073.

[5] F. Langhauser, J. Kerth, M. Kersting, P. Kölle, D. Lilge, P. Müller, *Die Angewandte Makromolekulare Chemie* **1994**, *223*, 155.

[6] J.-F. Chen, J.-R. Song, L.-X. Wen, H.-K. Zou, L. Shao, *Journal of Non-Crystalline Solids* **2007**, *353*, 1030.

[7] M. D'Acunzi, L. Mammen, M. Singh, X. Deng, M. Roth, G. K. Auernhammer, H.-J. Butt, D. Vollmer, *Faraday Discussions* **2010**, *146*, 35.

[8] B. L. Moroz, N. V. Semikolenova, A. V. Nosov, V. A. Zakharov, S. Nagy, N. J. O'Reilly, *Journal of Molecular Catalysis A: Chemical* **1998**, *130*, 121.

[9] V. F. Tisse, F. Prades, R. Briquel, C. Boisson, T. F. L. McKenna, *Macromolecular Chemistry and Physics* **2010**, *211*, 91.

[10] T. Diesing, G. Rojas, M. Klapper, G. Fink, K. Mullen, *Angew Chem Int Ed Engl* **2009**, *48*, 6472.

CHAPTER 8

Dendritic Borates

Abstract: It is believed that controlling the nucleophilicity of cocatalysts, *e.g.* borates, results in catalytic activity of metallocene towards olefin polymerization. Herein, the synthesis of yet larger, bulkier and weakly coordinating derivatives of $[B(C_6F_5)_4]^-$ is established, and the ability to modulate the catalytic activity towards metallocene-catalyzed ethylene polymerization as cocatalysts is demonstrated. The borates are synthesized by substituting the *para*-position of $[B(C_6F_5)_4]^-$ with polyphenylene dendrons via Diels-Alder cycloaddition of tetraphenylcyclopentadienones to ethynyl functionalized tetrakis(tetrafluorophenyl)borate. The first generation polyphenylene-dendronized borate already represents a larger borate species than any borate reported. By increasing the generation via divergent dendritic growth, the diameter of the dendritic borates is conveniently controlled along with coordinating tendencies towards countercation. Since borates can generally be used as cocatalsyts for metallocene complexes, the controllable coordinating tendencies of the dendritic borates are investigated with *rac*-$C_2H_4(Ind)_2ZrMe_2$ for metallocene catalyzed polyolefin synthesis. The olefin polymerization activity reaches a maximum (1.9×10^4 kgPE·(mol Zr h bar)$^{-1}$) when the 2nd generation of dendritic borate is applied as cocatalyst whereas a lower activity (1.5×10^4 kgPE·(mol Zr h bar)$^{-1}$) is observed with $[B(C_6F_5)_4]^-$. By applying 3rd generation of the dendritic borate, the largest borate is achieved and the coordinating tendency is further weakened. However, the olefin polymerization activity drastically drops to 0.7×10^4 kgPE·(mol Zr h bar)$^{-1}$.

8 Dendritic Borates

8.1 Introduction

The properties of metallocene and post-metallocene systems are a high catalytic activity, narrow range of molecular masses of the obtained product, the ability of catalyzing copolymerization of ethylene with higher α-olefins and the possibility of controlling the catalytic properties. Owing to these outstanding properties, conventional industrial polyolefin productions for Ziegler-Natta and Phillips systems have been replacing with metallocene and post-metallocene systems. In order to produce polyolefins with metallocene and post-metallocene systems, they must be pre-activated by addition of cocatalysts. Better understanding in cocatalysts in required as they are also profoundly important in polyolefin synthesis. Thus, besides the polymerization mechanism with metallocenes, a brief overview of cocatalysts is given with their role, types and examples of modification studies.

8.1.1 Polymerization mechanism

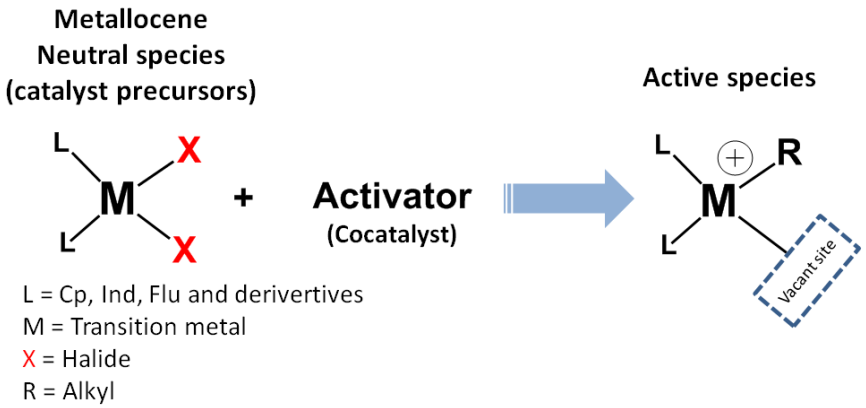

Figure 8-1. General procedure for activation of metallocene or post-metallocene catalysts

In order to initiate olefin polymerizations with metallocene complexes, addition of an activator is mandatory. The role of the activators is substituting two halides of metallocene complex by alkyl groups, and subsequently abstracting one of the alkyl groups to generate mono-alkylated species having a vacant site (*Figure 8-1*). In case of dialkylated metallocene complexes, only abstraction of one alkyl group is required in the absence of substitution of the halides. Since metallocene complexes are generally named catalysts, the activators are commonly referred to "cocatalysts".

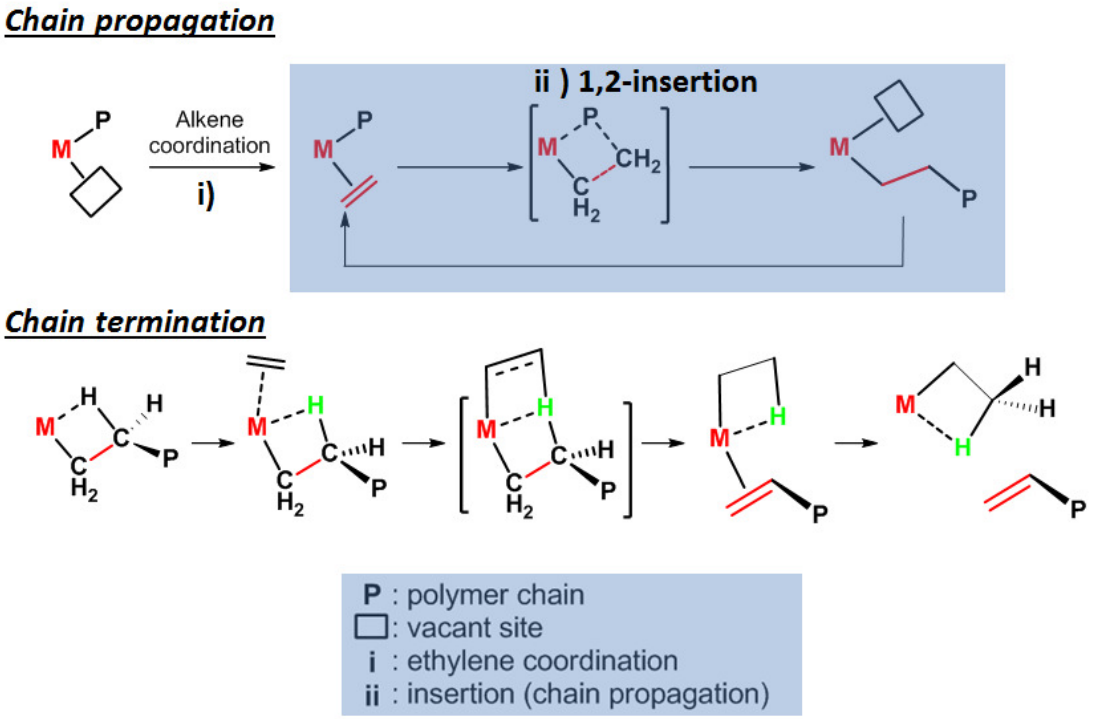

Figure 8-2. Polyolefin chain growth and termination

Upon the activation of metallocene catalysts by cocatalysts (*initiation*), the activated species possess an electron-deficient character and a vacant site. As illustrated in *Figure 8-2*, electron-rich molecules such as olefins (alkene) can coordinate to the vacant site. By mainly 1,2-insertion of olefins (or occasionally 2,1-insertion with propylene), the length of the polymer chain is extended (*chain propagation*).[1-3] The olefin polymerization is usually terminated by β-hydrogen transfer mechanism which occurs by hydrogen transfer from the growing polymer chain to an incoming olefin (*chain termination*).[4] This mechanism is known as "Cossee-Arlman mechanism" and most credibly believed so far. Depending on the chain propagation and termination steps, molecular weights and distribution can be determined as well as catalytic activity towards olefin polymerization.

8.1.2 Effect in catalytic activity of metallocenes

In order to control the catalytic activity of metallocenes towards olefin polymerization, there are two distinct pathways.[5] First, the electrophilicity of the metal center in the metallocene complex can be altered by simply tailoring the ligand structures. For instance, by introducing more electron-withdrawing groups to the metallocene complex, the electron density of the metal center can be decreased while the electrophilicity is increased. It was speculated that an increase in the electrophilicity of the metal should enhance the catalytic

activity.[5] In most cases, however, such an increase resulted in a decreased catalytic activity which may be linked to a stronger binding of the counterion. Despite that, intensive efforts have been made by this strategy and led to important developments in organometallic chemistry.[6-10]

Another approach is possible by modification of the cocatalyst structures. Similar to tuning the ligand structures of metallocenes, the nucleophilicity of cocatalysts can also be controlled. In particular, chemical modification of borate compounds to delocalize the negative charge more effectively has been reported.[11-18] Such a modification influences the interaction between activated metallocene (cation) and borates (anion). It has revealed that the nucleophilic counteranions (borates) have an effect on the catalytic activity of metallocene towards olefin polymerization.[5] Thus examples of modified borates are given in following section after introducing various types of cocatalyst.

8.1.3 Types of cocatalyst

8.1.3.1 Aluminum-based cocatalysts

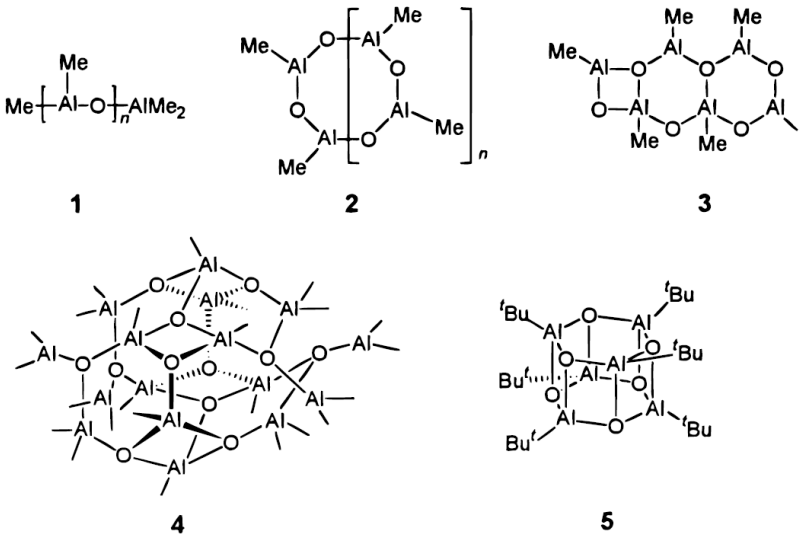

Figure 8-3. Proposed structures for methylaluminoxane (MAO)

Methylaluminoxane (MAO) has increased the activity of metallocene catalysts by six orders of magnitude relative to alkylaluminums. Although MAO leads to a high activity, understanding the mechanism of the reaction between MAO and metallocene complexes is not clearly studied due to the undefined structure of MAO (*Figure 8-3*).[5] Besides that, a major concern of the polyolefin industries is the high production cost of MAO, which arises from the high cost of TMA and also from the requirement of MAO production

equipment.[5] Furthermore, the ratio of MAO/metallocene catalyst (hundreds to thousand fold) is required to activate metallocene complexes. However, the catalytic system of metallocene complexes with MAO is generally robust and reproducible as excess amount of MAO acts as scavenger.

8.1.3.2 Boron-based cocatalysts

To find other effective cocatalysts besides MAO, boron-containing compounds have gained the attention since they have a chemically defined structure.[5] It has been observed that organoboranes like $B(C_6F_5)_3$, or organoborates such as $[HNR_2Ph][B(C_6F_5)_4]$ and $[Ph_3C][B(C_6F_5)_4]$ can generate highly active metallocene species for olefin polymerization when combined with dialkylated metallocenes.[15] In contrast to MAO, these boron compounds are chemically defined and thus have become possible to define the structure of activated complexes. Furthermore, only stoichiometric amounts of these boron compounds to dialkylated metallocene are required to generate active specie of metallocene,[5] since abstraction of one alkyl group from the metallocene is the role of the boron compounds. Although $[R][B(C_6F_5)_4]$-based activators have proven to be highly effective for olefin polymerization, they suffer from poor solubility in hydrocarbons and especially poor thermal stability and crystallizability of the cationic complexes derived therefrom, which results in very short catalytic lifetimes. These features limit the industrial application in polyolefin synthesis.

8.1.4 Weakly coordinating anions

In order to reduce the nucleophilicity of cocatalysts, the coordination ability of anions must be decreased. Indeed, there are complex anions such as BF_4^-, ClO_4^-, PF_6^- and BPh_4^- which are referred to as "weakly coordinating anions" (WCAs). This term is recommended by Strauss instead of "non-coordinating anions" after studies that these anions are clearly coordinating to cationic species.[19] To further weaken the coordinating ability of WCAs, chemical modifications have been performed.[14, 17-19] For producing better WCAs, the general requirements are described as followed: 1) singly charged character, 2) no basic sites, 3) chemically stable moieties, and 4) inert, hydrophobic surface, and a bulky structure.[20] Along these guidelines, the improvement in the design of more WCAs will be addressed in this chapter.

8.2 Objective

Among the boron-based compounds, borates can be classified as WCAs. Many important applications of WCAs are derived from their electrophile stabilizing properties. One of the most investigated applications is the utilization of WCAs as cocatalysts in the metallocene-catalyzed polyolefin synthesis.[11, 21-25]. To activate metallocene complexes, WCAs ideally serve as exact stoichiometric substitutes whereas methylaluminoxane (MAO) is typically employed in universal excess (up to 1000-fold). Due to the large sizes and weakly coordinating properties, tetrakis(pentafluorophenyl)borate, $[B(C_6F_5)_4]^-$, and its derivatives have frequently been used as cocatalysts for metallocene complexes.[26, 27]

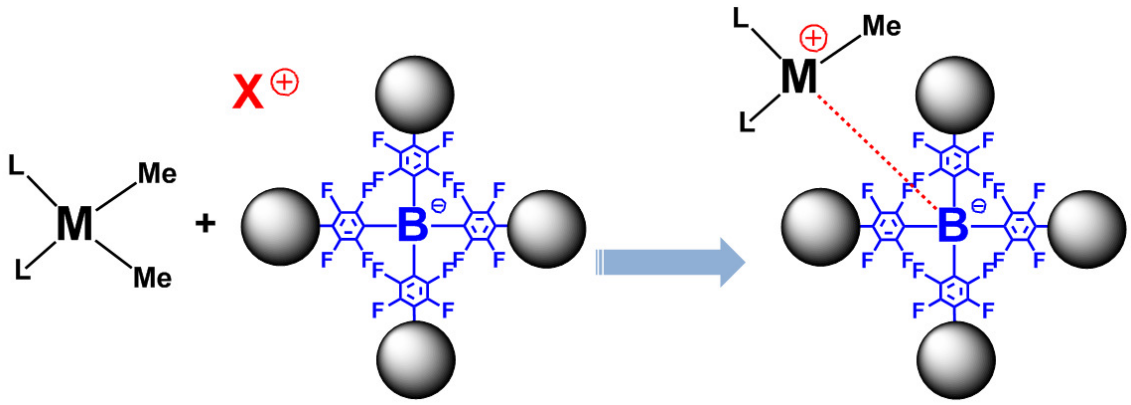

Figure 8-4. General approach for adjusting the diameter of borates

In order to effectively reduce the coordinating ability of the $[B(C_6F_5)_4]^-$, larger and bulkier ligands have been introduced to increase their overall size. It is thought that the distribution of the anion charge (borate) over a larger area is weakening the coordination strength.[28] The electron-withdrawing ability of fluorine atoms serves to delocalize the negative charge.[28] By using the approach shown in *Figure 8-4*, some examples have been reported.[11, 13, 15, 18, 23] In particular, Marks and co-workers synthesized triphenylcarbenium (TPC) borates having *tert*-butyldimethylsilyl (TBS) and triisobutylsilyl (TIPS) groups on the *para*-position of commercial borate (*Figure 8-5*).[11, 23] As a result of performing ethylene polymerization with $(1,2\text{-}Me_2Cp)_2ZrMe_2$, catalytic activities followed by the approximate order of $[TPC][B(C_6F_4TBS)_4] \approx [TPC][B(C_6F_4TIPS)_4] > [TPC][B(C_6F_5)_4]$ were reported. By using these bulky borates, furthermore, a slightly increase in average molecular weight (M_n) of polyethylene was detected. Although the polymerization tests were performed for less than 1 min, they explained that the increase in catalytic activity towards ethylene polymerization is due to the bulkier size of borates which might reduce the nucleophilicity by shielding effect.

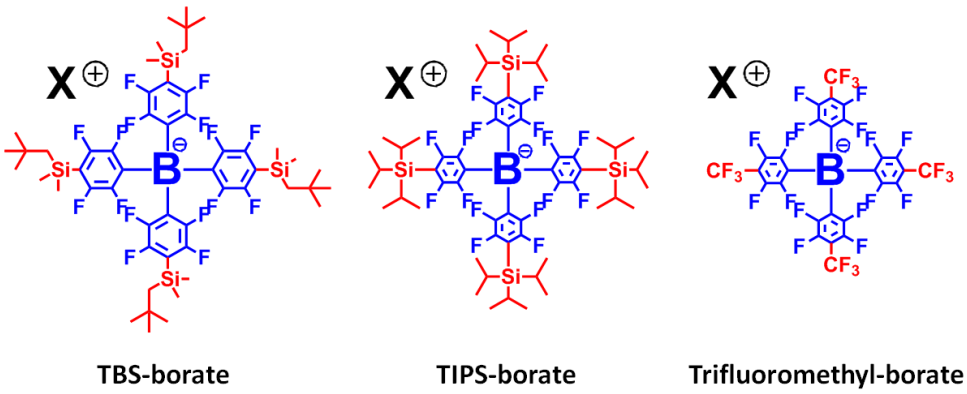

Figure 8-5. Examples of *para*-position substituted borates

Herrmann and coworkers synthesized trifluoromethyl-substituted borates, $[B(C_6F_4\text{-}CF_3)_4]^-$, with two different countercations, triphenylcarbenium (TPC) and *N,N´*-dimethyl anilinium (DMA) (*Figure 8-5*).[15] They tested these borates as cocatalysts for *rac*-$C_2H_4(Ind)_2ZrMe_2$ in ethylene polymerization under various temperatures. Despite the larger size of the borates having trifluoromethyl groups, the catalytic activity was lower compared to that of conventional cocatalysts such as MAO and $[DMA][B(C_6F_5)_4]$. However, enhanced thermal stability of the ion pair, *rac*-$C_2H_4(Ind)_2ZrMe^+/B(C_6F_4\text{-}CF_3)_4^-$, was exhibited due to the perfluorinated nature of the ligand framework. In a comparison of countercations, TPC-borates featured slightly higher activities than DMA-borates in all tested temperatures. They explained that a weaker donation from aniline may stabilize the Lewis acidic cationic metallocene and thus lower the activity.

For efficient WCAs, herein, the introduction of polyphenylene dendrimer to the *para*-position of $[B(C_6F_5)_4]^-$ is addressed. In contrast to virtually all other types of dendrons, polyphenylene dendrimers readily fulfill the following requirements for the structural design of efficient WCAs: 1) entirely built from chemically stable moieties; 2) considerably hydrophobic; 3) absence of basic oxygen or nitrogen sites; and 4) stiff, rigid and non-collapsible structure. Furthermore, the whole size of anions (borate) can conveniently be controlled by the divergent growth of dendrimer generation. These dendritic borates will be tested with regard to their individual impact on cocatalytic performance in metallocene-catalyzed polyolefin synthesis.

8.3 Results and discussion

8.3.1 Preparation of dendritic borates

The synthesis of tetrabutylammonium (TBA) dendritic borates was established by David Türp.[29] As featured in *Figure 8-6*, he reported that the *para*-position of $[B(C_6F_5)_4]^-$ was substituted by polyphenylene dendrons via Diels-Alder cycloaddition of tetraphenylcyclopentadienone to ethynyl-functionalized tetrakis(tetrafluorophenyl)borate.[29] By functionalized tetraphenylcyclopentadienone building blocks, the synthesis of dendritic borates with higher generations was also demonstrated. As a consequence, the modification of borates allows for an increase in size of anions and thus reduces the coordinating tendencies, and further supplies their rigid structure with a non-collapsible shell. In case of second and third generations of dendritic borates, shell density was controlled by degree of branching to maximize the effect of steric screening.

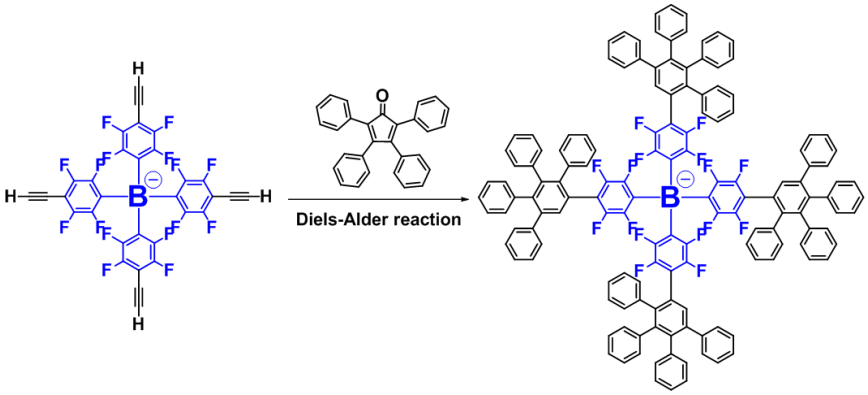

Figure 8-6. Synthetic procedure for dendritic borate

However, the usages of the dendritic borates were unsuitable in metallocene-catalyzed polyolefin synthesis since the TBA is incapable of activating dialkylated metallocene species. To overcome the issue, commonly applied borates consist of counter cations such as *N*,*N*´-dimethylanilinium (DMA) and triphenylcarbenium (TPC) which can activate the dialkylated metallocene. Therefore, a cation exchange of TBA to DMA and TPC is desired. However, their direct counter cation exchange was not achieved by a simple addition of corresponding halide salts of DMA and TPC to TBA borates. Thus, TBA borates were first converted to the corresponding Li salts by ion-exchange column chromatography.[30] By applying the optimized ion-exchange technique, a complete conversion to TPC and DMA dendritic borates was achieved due to the higher lattice energy of Li salts. Large and

weakly coordinating anions having a counter cation of TPC and DMA were successfully synthesized. These borates were characterized by various NMR (^{1}H, ^{7}Li, ^{11}B, ^{13}C and ^{19}F), field desorption mass spectrometry (FD-MS) and matrix-assisted laser desorption/ionization-time of flight (MALDI-ToF) MS. The preparation and characterization of these dendritic borates used in this study was performed by Ralf Moritz at MPIP.

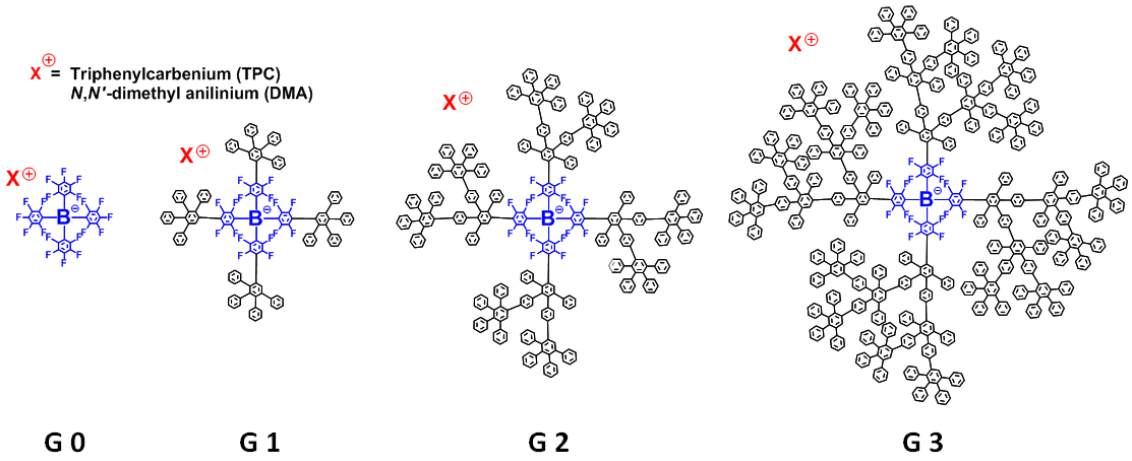

Figure 8-7. Chemical structures of various dendritic borates

The chemical structure of these borates is given in *Figure 8-7*. To give better understanding, a commercial borate is referred to G0. Depending on the generations of dendritic borates, they are termed to G1, G2 and G3, respectively. Since these borates have two different counter cations, borates with a corresponding counter cation of *N*,*N*´-dimethylanilinium (DMA) and triphenylcarbenium (TPC) are named to [DMA][Gx] and [TPC][Gx], respectively.

8.3.2 Olefin polymerization with dendritic borates

To determine the catalytic activity of the dendritic borates as cocatalysts, ethylene polymerizations using a dimethyl *ansa*-zirconocene, *rac*-$C_2H_4(Ind)_2ZrMe_2$, as a model catalyst were performed. It is already proven that *rac*-$C_2H_4(Ind)_2ZrMe_2$ works sufficiently with borates, since the same type of catalyst has been tested in the group of W. Herrmann.[15] The determination of ethylene polymerization productivities of *rac*-$C_2H_4(Ind)_2ZrMe_2$ with various dendritic borates as a function of anion size will give more insight in understanding the quantification of anion effects and the determination of the contribution of various anions to the reaction barrier.

Prior to experiments with dendritc borates, finding a standard reaction condition in our facility is conducted with a commercial borate, [TPC][$B(C_6F_5)_4$]. Since there are too many parameters which can effect to the polymerization, some of the parameters, such as polymerization time (3 min), ethylene pressure (3 bar), stirring speed (1500 rpm), amount/type of scavenger and diluent were fixed, and their effect in activity was not investigated in this study. The influence of the reation temperature and a ratio of [TPC][$B(C_6F_5)_4$]/[*rac*-$C_2H_4(Ind)_2ZrMe_2$] ([B]/[Zr]) on activity of the ethylene polymerization was investigated. The polymerizations were carried out in a 250 mL slurry reactor with a 100 mL of toluene in the presence of 200 μmol of triisobutylaluminum (TiBA) as a scavenger. The results of ethylene polymerization experiments are summarized in *Table 8-1*.

Table 8-1. Results of ethylene polymerization using *rac*-$C_2H_4(Ind)_2ZrMe_2$ and [TPC][$B(C_6F_5)_4$] under various reaction conditions[a)]

entry	cation	anion	reaction temp	[B]/[Zr]	activity
			°C		10^3 kgPE·(mol Zr h bar)$^{-1}$
1	TPC	G0	20	1	2.8
2	TPC	G0	40	1	8.6
3	TPC	G0	60	1	12.3
4	TPC	G0	60	1.1	12.8
5	TPC	G0	60	1.2	15.1
6	TPC	G0	60	1.5	13.4

a) Ethylene polymerizations were carried out under 3.0 bar of ethylene using [TPC][$B(C_6F_5)_4$] and *rac*-$C_2H_4(Ind)_2ZrMe_2$ in 100 mL of toluene in the presence of 200 μmol triisobutylaluminum (TiBA) as scavenger, with a stirring rate of 1500 rpm;
b) determined by DSC;
c) analyzed by GPC (PS-standard).

By varying the polymerization temperature with a fixed ratio of [B]/[Zr]=1 (entries 1 – 3, *Table 8-1*), the effect on the activity was studied. Activity reaches a maximum at 60 °C with 12.3×10^3 kgPE·(mol Zr h bar)$^{-1}$ under this condition (entry 3, *Table 8-1*). By selecting the standard reaction temperature as 60 °C, the effect of the ratio of [B]/[Zr] was investigated (entries 3 – 6, *Table 8-1*). Ideally, the maximum activity should be observed with a value of

[B]/[Zr] ≈ 1, while there is no poison that can eliminate the activated metallocene species. In this study, the optimum value of [B]/[Zr] is observed at a value slightly higher than 1 (entry 5, *Table 8-1*). This can be attributed to the fact that the reaction contains small amounts of impurities, such as moisture and oxygen, which were scavenged by a slight excess of the borate. By applying a higher value of [B]/[Zr] to the system (entry 6, *Table 8-1*), the activity did not continue to increase substantially. Note that this optimum value can be drastically changed by modifying one of parameters such as drying procedure of a reactor and diluent, status of a glove box, a type of catalysts and etc. To identify this number exactly, however, more work would be necessary in the future.

By using the fixed parameters of temperature (60 °C) and ratio of [B]/[Zr] (1.2/1), the influence of rigidly dendronized anions with various sizes (with diameters up to *ca.* 5 nm) on catalytic activity in ethylene polymerization was investigated. The results of ethylene polymerization experiments are summarized in *Table 8-2*.

Table 8-2. Results of ethylene polymerization using *rac*-$C_2H_4(Ind)_2ZrMe_2$ and various generations of borate[a)]

entry	cation	anion	reaction time	activity	T_m[b)]	M_w[c)]	M_w/M_n[c)]
			min	10^3 kgPE·(mol Zr h bar)$^{-1}$	°C	kg·mol^{-1}	
1[d)]	TPC	G0	3	15.1	135.2	173	6.8
2	TPC	G1	3	18.1	134.1	156	5.5
3	TPC	G2	3	19.2	135.6	154	5.2
4	TPC	G3	3	7.6	136.5	131	4.7
5	DMA	G0	3	15.9	134.9	132	6.3
6	DMA	G1	3	7.7	135.7	125	4.7
7	DMA	G2	3	6.1	135.4	124	4.6

a) Ethylene polymerizations are carried out under 3.0 bar monomer pressure at 60 °C using *rac*-$C_2H_4(Ind)_2ZrMe_2$ in 100 mL of toluene in the presence of 200 μmol triisobutylaluminum (TiBA) as scavenger, with a [B]:[Zr] ratio of 1.2:1 and a stirring rate of 1500 rpm;
b) determined by DSC;
c) analyzed by GPC (PS-standard);
d) extracted from entry 5 in *Table 8-1*.

By introducing the polyphenylene dendrons, enhanced solubility of the dendritic borate salts and the corresponding active species has been observed in non-polar solvents such as toluene and hexane, which are common diluents for olefin polymerization. Such an increased solubility in toluene by attaching polypheneyle dendrons was also observed with TBA dendritic borates.[28] As shown in *Table 8-2*, the catalytic activity reaches a maximum with [TPC][G2] which displays around 15 × 10^3 kgPE·(mol Zr h bar)$^{-1}$, followed by the approximate order of [TPC][G1] > [TPC][G0] ≈ [DMA][G0] > [TPC][G3]. By increasing the size of the borate, the coordinating strength of cation and anion is weakened and thus affects the polymerization activity. The order of the activity is also attributed to a decrease in nucleophilicity of the borates by the divergent growth of polyphenylene dendrons. It is initially believed that nucleophilicity can be far decreased by applying the largest borate (G3) (entry 4, *Table 8-2*). However, a drastic decrease in catalytic activity is observed instead, as compared to the one of [TPC][G2]. Upon further consideration, this is not surprising. The larger borate allows for nearly free cationic metallocene [*rac*-$C_2H_4(Ind)_2ZrMe^+$] which readily forms an inactive dimeric specie due to its thermodynamic instability. The formation of these dimeric metallocene species results in a decrease in the actual number of active species for olefin polymerization, which explains the lower catalytic activity of this system. This suggests that there is an optimum coordinating strength of cation and anion, and also a limiting size to the borate which can be successfully used as cocatalysts. In this study, further increase in dendritic borates was not investigated.

By differentiating counteractions (TPC and DMA), their influence on the polymerization properties is also studied (entries 1 − 4 *vs.* 5 − 7, *Table 8-2*). TPC-borates mostly exhibit slightly higher activities than with the corresponding DMA-derivatives for the *rac*-$C_2H_4(Ind)_2ZrMe_2$. In case of G2 borates, [DMA][G2] shows a drastical reduction in activity as compared to [TPC][G2] (entry 3 *vs.* 7, *Table 8-2*). This is attributed to the presence of a weak donation from the aniline, which may stabilize the Lewis acidic cationic metallocene [*rac*-$C_2H_4(Ind)_2ZrMe^+$], and therefore may lower the catalytic activity.

To determine which type of polyethylene is produced, melting points (T_m) were determined by DSC and display a typical value for high density polyethylene (~ 135 °C). The weight-averaged molecular weights (M_w) of the polyethylene were also investigated by GPC. By increasing the size of the borates, a slightly decrease in M_w is shown together with narrower molecular weight distributions (MWD). The M_w in the range of 124 to 173 kg·mol^{-1} are typical values for metallocene catalysts. The MWDs between approximately 4 and 6 are unusually broad which indicates the formation of a multi-site catalyst. However,

polyethylene with these MWDs is relatively easy to process compared to the one with an approximate MWD of 2.

8.4 Conclusion

In this study, new types of borate were prepared by divergent approach using dendirmer chemistry and investigated as cocatalysts for *rac*-$C_2H_4(Ind)_2ZrMe_2$ in homogeneous polyolefin synthesis. It is believed that coordination strength between cocatalysts and metallocene catalysts can be weakened by distributing the anion charge (borate) to a larger area. Based on this strategy, the coordinating ability of a commercial borate $[B(C_6F_5)_4]^-$ (G0) was synthetically reduced by substituting the *para*-position with polyphenylene dendrons, and it resulted in the preparation of 1st generation of dendritic borate (G1). By the modification of polyphenylene dendrons, further bulkier and larger borates (2nd (G2) and 3rd (G3) generation) were synthesized. Since these dendritic borates have tetrabutyl ammonium (TBA) as a counter cation, to be applied as a cocatalysts for metallocenes, the cation were exchanged to triphenylcarbenium (TPC) and *N*,*N*´-dimethylanilinium (DMA) which are common cations for the commercial borates.

In case of TPC as countercation, the catalytic activity of *rac*-$C_2H_4(Ind)_2ZrMe_2$ reached a maximum with G2, followed by the approximate order of G1 > G0. By further increase in the size of borate (G3), however, the activity was drastically decreased. It can be explained by that the formation of dimeric metallocene species results in a decrease in the actual number of active species for olefin polymerization. In case of DMA-borates, they mostly displayed lower activities than that of the corresponding TPC-derivatives. This is attributed to the presence of a weak donation from the aniline, which may stabilize the Lewis acidic cationic metallocene [*rac*-$C_2H_4(Ind)_2ZrMe^+$], and therefore may lower the catalytic activity.

This study suggests that there is an optimum coordinating strength of cation (activated metallocene) and anion (borate), and also a limiting size to the borate which can be successfully used as cocatalysts.

8.5 Experimental part

8.5.1 General procedures and materials

Dimethyl metallocene catalyst, *rac*-$C_2H_4(Ind)_2ZrMe_2$, was prepared by the reaction of *rac*-$C_2H_4(Ind)_2ZrCl_2$ (Strem) with $MgMe_2$ in toluene, followed by the purification of the product via recrystallization. Dendritic borates were prepared [redacted]. For comparison experiments with dendritc borates, the commercial borates, triphenylcarbenium (TPC) and *N*,*N*´-dimethylanilinium (DMA) tetrakis(pentafluorophenyl)borates were purchased from Acro and used as received. The scavenger, tirisobutylaluminum (TIBA), was purchased from Aldrich as a 10 wt% solution in toluene. Ethylene (Linde AG, grade 5.0) was purified by passing through purification columns of BASF R3-15 deoxygenation catalyst (BASF AG, Ludwigshafen), activated 4 Å molecular sieves, 5 Å molecular sieves (750 mL, Supelco) and Supelpure®-O oxygen/moisture trap (750 mL, Supelco) in that order. The purified ethylene was used for polymerization experiments in a slurry reactor.

8.5.2 Preparation of dendritic borates

The synthesis of tetrabutylammonium dendritic borates was established [redacted].[29] In order to utilize the dendritic borates as cocatalysts in metallocene-catalyzed polyolefin synthesis, the exchange of tetrabutylammonium to other counter-cations, *e.g.* triphenlycarbenium (TPC) and *N*,*N*´-dimethylanilinium (DMA), was performed and characterized [redacted]. A general experiment procedure for these dendritic borates is described in following section.

8.5.2.1 Lithium borates

Since a direct exchange from tetrabutylammonium borates to TPC or DMA is limited, lithium borate salts were first prepared using a similar method reported in the literature.[30] A column packed with Amberlite IR-120 (H^+ form) was prepared. To convert Amberlite IR 120 to Li^+ form, the column containing Amberlite IR-120 (H^+ form) was loaded with a solution of lithium hydroxide monohydrate. Subsequently, the column was washed generously with water until constant neutral pH. The column was equilibrated progressively

with eluent (THF/H_2O 8:2). The process was carried out using gravity as the driving force at room temperature. The column, packed with Amberlite IR 120 (Li^+ form), was ready for the counter-cation exchange. The tetrabutylammonium borate salts were passed through the column for preparation of lithium borates. After removal of the combined eluents, the obtained residue was taken up in a minimum amount of THF, precipitated in hexane, filtered and dried to yield the lithium borate salts as white to yellow solids. Prior to preparation of DMA and TPC borate salts, these lithium salts were characterized with ^{7}Li, ^{1}H NMR and mass spectroscopy.

8.5.2.2 *N*,*N*´-Dimethylanilinium borates

N,*N*´-Dimethylanilinium hydrochloride and lithium borates were placed in a round Schenk flask and dried overnight under reduced pressure. To the flask, toluene was added under inert conditions and the mixture was stirred for 5 h at room temperature. The solid LiCl, formed during the reaction, was filtered off. After removal of the solvent in vacuo, the crude product was dissolved in dichloromethane (DCM), precipitated in hexane, filtered and dried to afford *N*,*N*´-dimethylanilinium borates as a colorless powder. These DMA salts were characterized with ^{1}H NMR and mass spectroscopy. These dried borates were stored in a glove box under an inert condition.

8.5.2.3 Triphenylcarbenium borates

Same procedure described in **Section 8.4.2.2.** was followed except for triphenylcarbenium (TPC) chloride instead of *N*,*N*´-dimethylanilinium hydrochloride. Triphenylcarbenium borates were achieved as a slightly yellow powder. These DMA salts were characterized with ^{1}H NMR and mass spectroscopy.

8.5.3 Characterization of the dendritic borates

Using NMR and mass spectroscopy, the dendritic borates were characterized [redacted]. ^{1}H, ^{7}Li and ^{13}C spectra were referenced using the remaining solvents signals as an internal standard. For ^{11}B and ^{19}F spectra, $BF_3{\cdot}OEt_2$ (0 ppm) and fluorobenzene (-103 ppm) were used for internal standards, respectively. Field desorption (FD) mass spectrometry (MS) was performed on a VG Instruments ZAB 2-SE-FPD using 8 kV

accelerating voltage. Matrix-assisted laser desorption/ionization-time of flight (MALDI-ToF) MS was performed on a Bruker Reflex spectrometer. Samples for MALDI-ToF MS were prepared by mixing the analyte with dithranol as matrix in THF in a ratio of 1/250. Negatively charged ions were detected using the appropriate polarity of the field.

8.5.4 Ethylene polymerization experiments in a slurry reactor

For reproducible polymerization, maintenance of slurry reactor and glove box has been made under extreme care to minimize the residual water and oxygen, which are the poison for active metallocene species. Prior to ethylene polymerization, a 0.3 L of Büchi glass reactor, equipped with a double-wall jacket for controlling temperature, was dried overnight under reduced pressure at 85 °C. The temperature was controlled by an external thermostat (Hueber, Unistat 360) and detected by a thermocouple detector (Pt100). The dried reactor was flushed with argon (1 bar) and was evacuated again with vacuum. After repeating the vent-fill procedure 3 times, the reactor was thermostated to the desired reaction temperature. In a glove box, a 100 mL of dry toluene containing 1.0 mL of triisobutylaluminum solution (25 wt% in toluene) was prepared in 250 mL of Schlenk flask. After stabilizing the temperature, the toluene was transferred to the reactor via a cannula under inert condition. Subsequently, the argon atmosphere in the slurry reactor was substituted with a desired pressure of ethylene and constantly kept during the polymerization. The desired amount of *rac*-$C_2H_4(Ind)_2ZrMe_2$ dissolved in toluene was added to a solution of the borates with a stoichiometric ratio of [B]/[Zr]. After stirring for 5 min at room temperature, the catalytic solutions of the borate/*rac*-$C_2H_4(Ind)_2ZrMe_2$ was transferred into the injection system via a syringe under argon stream. Upon injecting the catalytic solution into the reactor via high pressure of argon (9 bar), ethylene polymerization was initiated and the information for polymerization, such as internal temperature, actual monomer consumption and total consumption of the monomer, was online registered by A/D-Wandler (Keithley UPCI-3101). The amount of ethylene consumed during the polymerization reaction was measured by a mass flow controller (5850 TRC 126 ZBD 41, Brooks Instrument). After the polymerization, the ethylene gas was released and the polymerization was terminated by adding 10 mL of methanol. The resulting polymer suspension was poured into 250 mL of methanol/HCl (3/1, *v*/*v*) to precipitate the polymer and was stirred for 16 h. After filtration, the obtained polymer was dried at 60 °C under reduced pressure.

8.5.5 Polymer characterization

All polymers were characterized with DSC, GPC and NMR according to the procedure described in **Section 3.5.7**. To calculate the activity of the ethylene polymerization, the obtained polymer was dried under vacuum for 2 days, and weight of the dried polymer was checked by gravimetric. From the weight of the obtained polymer, the catalytic activity was derived.

8.6 References

[1] E. J. Arlman, P. Cossee, *Journal of Catalysis* **1964**, *3*, 99.

[2] P. Cossee, *Journal of Catalysis* **1964**, *3*, 80.

[3] E. J. Arlman, *Journal of Catalysis* **1964**, *3*, 89.

[4] P. Margl, L. Deng, T. Ziegler, *Journal of the American Chemical Society* **1998**, *121*, 154.

[5] J.-N. Pédeutour, K. Radhakrishnan, H. Cramail, A. Deffieux, *Macromolecular Rapid Communications* **2001**, *22*, 1095.

[6] R. F. Jordan, *Adv. Organomet. Chem.* **1991**, *32*, 325.

[7] H. H. Brintzinger, D. Fischer, R. Mülhaupt, B. Rieger, R. M. Waymouth, *Angewandte Chemie International Edition in English* **1995**, *34*, 1143.

[8] V. C. Gibson, S. K. Spitzmesser, *Chemical Reviews* **2002**, *103*, 283.

[9] P. B. Konstantin, *Russian Chemical Reviews* **2007**, *76*, 253.

[10] D. J. Darensbourg, S. J. Wilson, *Green Chemistry* **2012**, *14*, 2665.

[11] L. Jia, X. Yang, A. Ishihara, T. J. Marks, *Organometallics* **1995**, *14*, 3135.

[12] E. Y.-X. Chen, T. J. Marks, *Chemical Reviews* **2000**, *100*, 1391.

[13] K. Fujiki, J. Ichikawa, H. Kobayashi, A. Sonoda, T. Sonoda, *Journal of Fluorine Chemistry* **2000**, *102*, 293.

[14] J. Zhou, S. J. Lancaster, D. A. Walker, S. Beck, M. Thornton-Pett, M. Bochmann, *Journal of the American Chemical Society* **2000**, *123*, 223.

[15] F. A. R. Kaul, G. T. Puchta, H. Schneider, M. Grosche, D. Mihalios, W. A. Herrmann, *Journal of Organometallic Chemistry* **2001**, *621*, 177.

[16] M. Mager, S. Becke, H. Windisch, U. Denninger, *Angewandte Chemie International Edition* **2001**, *40*, 1898.

[17] G. Rodriguez, P. Brant, *Organometallics* **2001**, *20*, 2417.

[18] J. van den Broeke, B.-J. Deelman, G. van Koten, *Tetrahedron Letters* **2001**, *42*, 8085.

[19] I. Krossing, I. Raabe, *Angewandte Chemie International Edition* **2004**, *43*, 2066.

[20] D. Türp, *Doctorate dissertation at Johannes Gutenberg-Universität in Mainz* **2013**.

[21] S. W. Ewart, M. J. Sarsfield, E. F. Williams, M. C. Baird, *Journal of Organometallic Chemistry* **1999**, *579*, 106.

[22] Y. Li, M. Cokoja, F. E. Kühn, *Coordination Chemistry Reviews* **2011**, *255*, 1541.

[23] L. Jia, X. Yang, C. L. Stern, T. J. Marks, *Organometallics* **1997**, *16*, 842.

[24] M.-C. Chen, J. A. S. Roberts, A. M. Seyam, L. Li, C. Zuccaccia, N. G. Stahl, T. J. Marks, *Organometallics* **2006**, *25*, 2833.

[25] J. A. S. Roberts, M.-C. Chen, A. M. Seyam, L. Li, C. Zuccaccia, N. G. Stahl, T. J. Marks, *Journal of the American Chemical Society* **2007**, *129*, 12713.

[26] Y. Sarazin, D. L. Hughes, N. Kaltsoyannis, J. A. Wright, M. Bochmann, *Journal of the American Chemical Society* **2007**, *129*, 881.

[27] K. Seppelt, *Angewandte Chemie International Edition in English* **1993**, *32*, 1025.

[28] K. Mpoukouvalas, D. Tŭrp, M. Wagner, K. Mullen, H.-J. r. Butt, G. Floudas, *The Journal of Physical Chemistry B* **2011**, *115*, 5801.

[29] D. Türp, M. Wagner, V. Enkelmann, K. Müllen, *Angewandte Chemie International Edition* **2011**, *50*, 4962.

[30] E. Alcalde, I. Dinarès, A. Ibáñez, N. Mesquida, *Molecules* **2012**, *17*, 4007.

CHAPTER 9

Summary and Outlook

9 Summary and Outlook

9.1 Summary

The main aim of the work presented in this dissertation was the morphology control in metallocene-catalyzed polyolefin synthesis. This was studied by selective immobilization techniques on a variety of supports such as porous polyurethane particles (**Chapter 3**), electrospun fibers (**Chapter 4 and 5**), inorganic-organic hybrid core-shell particles (**Chapter 6**) and hollow silica particles (**Chapter 7**). Another aspect of this dissertation was modulating a catalytic activity by controlling a size of boron-based cocatalysts (**Chapter 8**).

The aim of **Chapter 3** was the synthesis of an ideal support for the immobilization of metallocene catalysts. To date, the preparation of supports for metallocenes has needed a two-step procedure. The demands required the one-pot synthesis of well-defined, spherical, porous and micrometer-sized polyurethane (PU) particles. For this objective, the synthesis of porous PU microspheres was demonstrated in a simple one-pot reaction by the help of a nonaquoues emulsion polymerization. Furthermore, porosity of PU particles was conveniently adjusted by the amount of the employed water in the emulsion polymerization. The influence of the PU microspheres with a controlled porosity on the catalytic activity and the characteristics of the produced polyolefin such as molecular weight, molecular weight distirubution and morphology were investigated. A nearly linear correlation between porosity and catalytic activity were observed. However, the porous PU particle-supported metallocene system displayed relatively lower activity as compared to the conventional silica support. Since a homogeneous distribution of metallocene catalysts on the supports and homogeneous fragmentation of the supported catalyst within the polyolefin products are important, they were also studied with laser scanning confocal fluorescence microscopy (LSCFM) by staining with Rhodamine B. They were fragmentable, and the catalyst was evenly loaded within the whole particle due to the open pore structure. Although not all necessary properties to consider the microporous PU particles as the ideal support were fulfilled, the porous PU particles are advantageous in terms of tunable porosity, open pore, and isotropic shape as well as one-step procedure of support particle preparation.

In **Chapter 4** and **5**, the production of polyolefin fibers and mats in a one-pot procedure synthesis was demonstrated. Olefin polymerizations on a fibrous template as supports for

metallocenes were performed, since heterogeneous metallocenes generally replicate the original shape of the supports. Therefore, polyethylene oxide (PEO)-functionalized polystyrene (PS) nanoparticles were transformed into fibers by colloid electrospinning. As PEO groups are capable of interacting with pre-activated metallocene species (cationic character) strongly, the non-covalent interaction of PEO groups and activated catalsyts afforded well-defined polyethylene fibers. The diameter of the fiber products was conveniently controlled by the polymerization time. By means of SEM and cryo-TEM, the inner morphology of the produced fibers was investigated. They display a core-sheath structure consisting of PS nanoparticles and PVA in the core and PE in the sheath. As PEO-fuctionalized PS nanoaprticles are chemically linked with a styryl boron-dipyrromethene (BODIPY) dye, the PE fibers obtained were investigated with LSCFM and showed a fluorescent continuous inner core with a diameter of the electorspun fibers. The results from LSCFM also support that core (PS and PVA)-sheath (PE) structured fibers are achieved. A study of producing high density polyethylene (HDPE)-coated fibers was conducted by immobilizing $(MeCp)_2ZrCl_2$ in **Chapter 4**. Subsequently, to show the typical applications of anisotropic supports, the synthesis of linear low density polyethylene (LLDPE) in a gas phase reactor using relatively novel technique "concurrent tandem catalysis" was performed. Thus, in **Chpater 5**, the gas-phase tandem catalysis system using ethylene as a single monomer feed was domonstrated with a cooperative action of two catalysts. For ethylene oligomerization, a cobalt complex $CoCl_2N_2^{2Th}$ was immobilized on silica particles. For ethylene copoplymerization with the oligomers (*in-situ* generated by $CoCl_2N_2^{2Th}$), $(MeCp)_2ZrCl_2$ was immobilized on the electrospun fibers. The influence of the ratio of $[CoCl_2N_2^{2Th}]/[(MeCp)_2ZrCl_2]$ on the tandem activity in LLDPE synthesis was studied as well as the effect on the number of branches and melting points. The gas-phase tandem catalysis promoted the formation of LLDPE-coated fibers containing from 8 to 15 branches per 1000 carbon atoms with the almost exclusive existence of ethyl branches (higher than 99 %). Furthermore, the $CoCl_2N_2^{2Th}$-supported on silica particles were recovered and used without a significant loss in catalytic activity.

The aim of **Chapter 6** was to study an alternative method to enhance the processablitity of ultra high molecular weight polyethylene (UHMWPE). Individual systems for UHMWPE and LLDPE synthesis were first tested to qualitatively and quantitatively determine the roles of the catalysts. Since the LLDPE synthesis via tandem catalysis system, which was employed by two catalysts $[CoCl_2N_2^{2Th}$ and $(MeCp)_2ZrCl_2]$ using ethylene as a single monomer feed, was successfully performed in **Chapter 5**, the same catalytic system was

adopted in this chapter. Thereafter, the synthesis of UHMWPE-LLDPE core-shell particles via a combination of tandem catalysis and selective catalyst loading of metallocene catalysts was performed. SEM micrographs showed that a core-shell replica with an increased diameter was produced. However, a solid proof of the core-shell morphology was not established by SEM only. In order to elucidate spatially resolved LLDPE/UHMWPE in single particles, visualizing the inner morphology of the ethylene polymerized core-shell particles was conducted with cryo-sectioning and optical techniques (SEM, TEM, STEM, AFM and LSCFM). SEM and TEM micrographs of cryo-sectioned particles displayed a slightly distinguishable boundary between core and shell. Furthermore, STEM combination with EDX and hyper-mapping showed the exclusively-distribution of silica in the core of the particles. AFM images were also attributed to the fact that the morphology of the polymerized particles was "core-shell" structured particles. For fragmentation studies via LSCFM, core-shell particles are prepared using fluorescence dye (BODIPY)-chemically linked PS nanoparticles. After ethylene polymerization, selectively BODIPY-linked core-shell particles revealed a fluorescence hollow circle with a few μm. These features demonstrated the synthesis of spatially resolved LLDPE/UHMWPE particles by using core-shell structured supports with selectively loaded catalysts. Since UHMWPE particles are spatially coated with LLDPE, this method would be an alternative method to improve the processability of UHMWPE.

Chapter 7 discussed the production of polyolefins with lower amounts of supports which hamper the clarity of polyolefin products. To fundamentally reduce the amount of supports, hollow silica particles (HSPs) as supports were applied in metallocene-catalyzed olefin polymerization. After ethylene polymerization for 1 h under 3 bar at 40 °C, small fragments of the HSPs were found exclusively at the surface of the polyethylene particles with a well-defined and an uniform morphology. This morpholgy strongly indicates that catalytic species were selectively immobilized inside the HSPs, and the HSPs were broken by the pressure of the produced polyethylene. Since the supports (fragmented HSPs) are exposed, an additional removal procedure of the fragmented supports such as via a steam cracker would be more convenient than the cases of conventional silica supports. Thus, highly purified polyolefins can be produced. Since this is a heterogeneous catalytic system, polymerization can be performed under mild conditions when compared to radical polymerization process. Furthermore, ease of handling the product can be achieved.

In previous chapters, this dissertation was dealing with heterogeneous polyolefin synthesis in various supports. In contrast to that, **Chapter 8** was focused on modulating the catalytic activity of metallocene catalysts by controlling the size of borates as cocatalysts in homogeneous polymerization of olefins. The reduction in nuclephilicity of borates was performed by chemical modification of the commercial borate [$B(C_6F_5)_5$] with dendrimer chemistry. Previously, the synthesis of dendritic borates with a counter cation of tetrabutyl ammonium (TBA) was established by David Türp at MPIP. To be applied as a cocatalysts for dialkylate metallocenes, the cation-exchange to triphenlycarbenium (TPC) and *N*,*N*´-dimethylanilinium (DMA) was performed [redacted]. The influence of various size of the dendritc borates on the catalytic activity of *rac*-$C_2H_4(Ind)_2ZrMe_2$ in homogeneous polyethylene synthesis was investigated. In case of TPC as a counter cation, by increasing the generations, a slightly enhanced activity was observed and reached a maxium with 2nd generation at 60 °C and 3 bar of ethylene pressure. By further increase in the size of borate (3rd generation of the dendritic borate), however, a drastic decrease in activity was exhibited. The decrease was attributed to the fact that there is an optimum distance between cocatalysts and metallocene catalysts. DMA-borates mostly exhibit lower activities than with the corresponding TPC-derivatives for the *rac*-$C_2H_4(Ind)_2ZrMe_2$. This is specluated to the presence of a weak donation from the aniline, which may stabilize the Lewis acidic cationic metallocene [*rac*-$C_2H_4(Ind)_2ZrMe^+$], and therefore may lower the catalytic activity.

9.2 Outlook

9.2.1 Polymeric binder

A polymeric binder, such as poly(vinylidene fluoride) and poly(3,4-ethylendioxythiophene)-poly(styrenesulfonate), is used in the anode and cathode of lithium-ion liquid or polymer cells which play a critical role in the cell performance. In order to carry out a polymeric binder into industrial field, these materials must be high electrochemical, thermal, and chemical stability and furthermore, excellent adherence and coherence.

Poly(vinylidene fluoride) (PVDF), one of the most used binders in commercial batteries, is a semi-crystalline and well known polymer for thermal, chemical, oxidation resistance and exceptional hydrolytic stability. The crystalline phase of the polymer provides thermal stability while the amorphous phase accommodates the desired membrane flexibility. All these properties make PVDF as an attractive material for microfiltration, ultrafiltration, and membrane distillation. However, PVDF requires the use of *N*-methyl-2-pyrrolidone (NMP) in the processing. Despite the widespread use of NMP, it has some disadvantages such as high cost, environmental issue associated with NMP recovery and the severe processing control of the relative humidity (to be less than 2%). Although the PVDF has strong binding strength, the low flexibility of PVDF can easily deteriorate cycle life characteristics of the battery due to breaking of the bond between active materials when the active material and a carbon material and consequently expansion/contraction process occurs during charging and discharging.[1, 2] Furthermore, fluorine in PVDF binder is one of the degradation products that generate stable LiF in the battery. Depending on the liquid electrolyte, the formation reaction of LiF and other harmful products with double bond is accelerated.[3] Consequently, this research must be focused on identifying suitable alternative non-fluorinated binders having a certain elasticity and higher thermal stability.

There has been much research on cyclic olefin copolymers using transition metal catalysts. Cyclic monomers are polymerized either by ring opening metathesis polymerization (ROMP) or by direct olefin polymerizations with different catalysts such as metallocenes. In the second case, the properties can be adjusted by the copolymerization with ethylene, as shown in *Figure 9-1*. However, polymers synthesized by ROMP have significantly poor thermal stability due to unsaturated main chain. Therefore, there have been attempts to

stabilize the main chain of the polymer by hydrogenation. Although a polymer prepared by this method improves oxidative stability, however, the thermal stability is reduced.

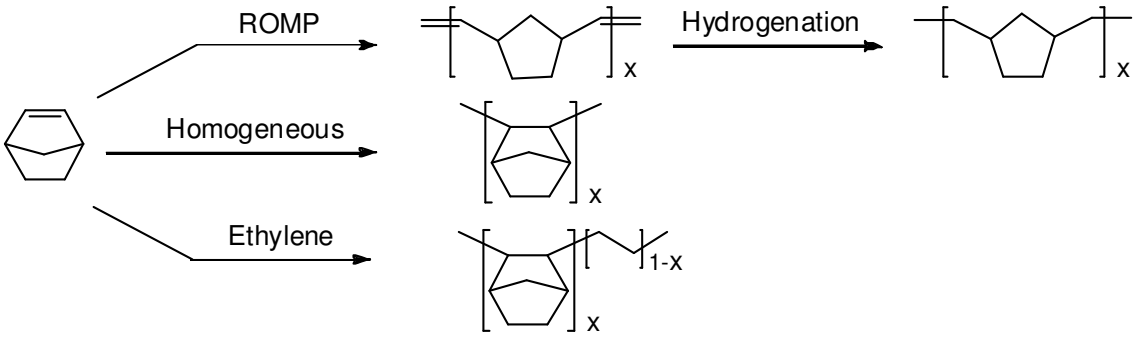

Figure 9-1. General synthetic routes of poly(norbornene) via ROMP with Grubbs catalyst, homo- and copolymerization with ethylene with metallocene catalyst

More promising is the synthesis of norbornene polymers by direct olefin polymerization with metallocenes. In the year of 1990, a homogeneous polymerization of norbornene using a zirconium-based metallocene catalyst was reported by Kaminsky and coworkers.[4] However, the polymer prepared by this method was highly crystalline and had poor solubility in organic solvents, and thermal decomposition occurred without a T_g (glass transition temperature). Due to these factors, pure polynorbornene itself is difficult to process. Thus, further studies on this method could not be conducted. In order to overcome the problem of polynorbornene as mentioned above, cyclic monomers such as norbornene are copolymerized with ethylene to decrease brittle properties, named cyclic olefin copolymer (COC). By introducing ethylene or other alpha olefins, it becomes an amorphous polymer which combines flexibility of olefins with strength and rigidity of norbornene. The T_g of ethylene-norbornene copolymers (up to 180 °C), for instance, can be altered linearly with increasing the norbornene (NB) comonomer content.[3, 4] Some properties including T_g, viscosity, and stiffness will be varied due to monomer content. Crystallinity in our opinion is not necessarily required for the requested high mechanical stability. A high T_g should be sufficient to stabilize the system and furthermore to offer a good processability.

Additionally the introduction of polar functional groups can be proposed to enhance the binder properties. Due to the large difference in polarity between the polyolefin separator and the highly polar organic electrolyte, it leads to poor wettability in the non-aqueous electrolyte (1.0 M $LiPF_6$–EC/DMC).[5] Thus by introducing polymer binder containing

polar functional groups, the inorganic particle-coated separator exhibits good thermal stability and wettability in non-aqueous liquid electrolytes.

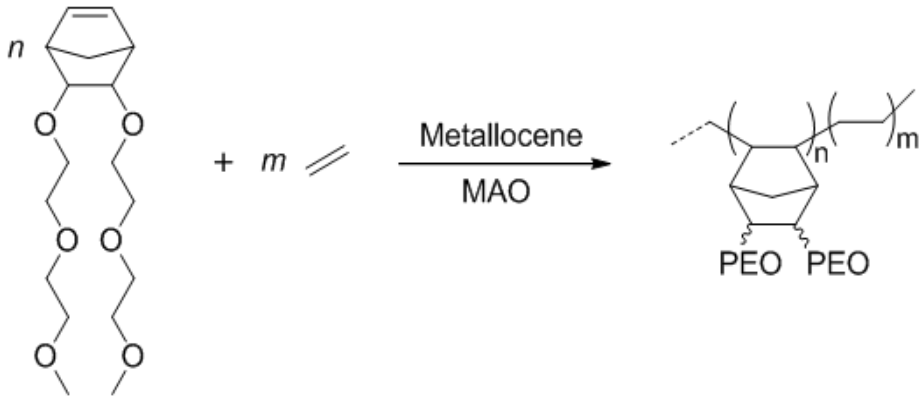

Figure 9-2. A synthetic route of poly(ethylene oxide)-functionalized PNB-*co*-PE polymers via a transition metallocene catalyst

In addition to introduction of polar functionality, for an application as a binder to LIBSs there is no real driving force to make an interaction between COC and alumina particles. Therefore, functionalized NB[6, 7] can be considered to improve the interaction. Gnanou and coworkers performed the copolymerization of mono-functionalized NB containing polyethylene oxide (PEO) with 1,5-cyclooctadiene via ROMP.[8] By functionalization of NB with PEO unit, the adhesion of the polymer backbone can substantially be improved, but pay the cost of increasing the dielectric constant due to the polarity of the functional group.[7] In order to decrease the rigidity of the system, and might decrease dielectric constant, ethylene units can be added to the backbone. In *Figure 9-2*, synthetic route to copolymerize PEO-functionalized NB with ethylene via metallocene is proposed. By increasing the incorporation ratio of ethylene units, some properties like T_g, viscosity and stiffness can be controlled.

By the help of the PEO unit(s), the copolymers can strongly interact with alumina as shown in *Figure 9-3*. Depending on properties of polymer, some factors such as length of PEO, incorporation ratio of functionalized NB, molecular weight, and etc can be optimized. In addition to optimization, functionalized-NB and ethylene can be copolymerized in a variety of compositions to determine the optimum composition in terms of adhesion, thermal stability, mechanical, and electrical properties.

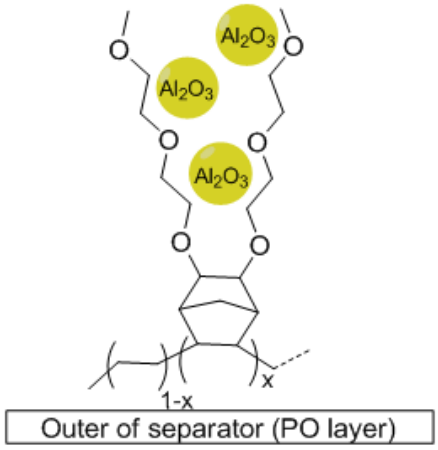

Figure 9-3. A suggested formation of the PNB-*co*-PE polymer with alumina particles

Another approach to a binder is the use of a polymeric material containing covalently bound heteroatoms. It has been of interest for membranes in fuel cells applications.[9] Specifically, phosphorus-containing polymers have become prominent in recent research. For instance, polyethylene structures containing precisely placed phosphonic acids via acyclic diene metathesis (ADMET) were synthesized.[10] The main advantage of synthesis of polyolefin containing functional group via ADMET is the place of each functional group can be tailored with same distance. In *Figure 9-4*, functionalized polyolefin having phosphonic acid and pyridine synthesize via ADMET can be proposed as an alternative method.

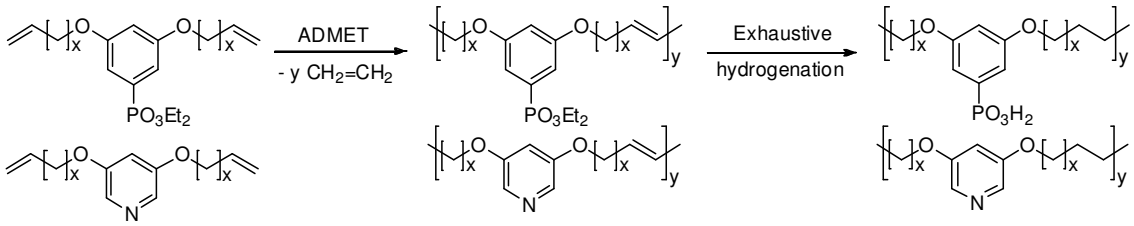

Figure 9-4. Synthetic schemes of functionalized polyolefin having groups of phosphonic acid or pyridine via ADMET

By means of isothermal titration calorimetry (ITC), Khalid et al. in our group have demonstrated by investigating the interaction of inorganic particle such as silica with the hydrophilic polymers consisting of poly(ethylene oxide) methacrylate, poly(ethylene glycol) methacrylate phosphate and etc.[11] In a similar manner, interaction between alumina particle and the proposed polymers as shown in *Figure 9-3* can be investigated. Furthermore, by using anisotropic supports (shown in **Chapter 4**), the copolymers of PEG-NB-*co*-ethylene can be directly synthesized in a form of fibers or fiber matrix (*Figure 9-5*).

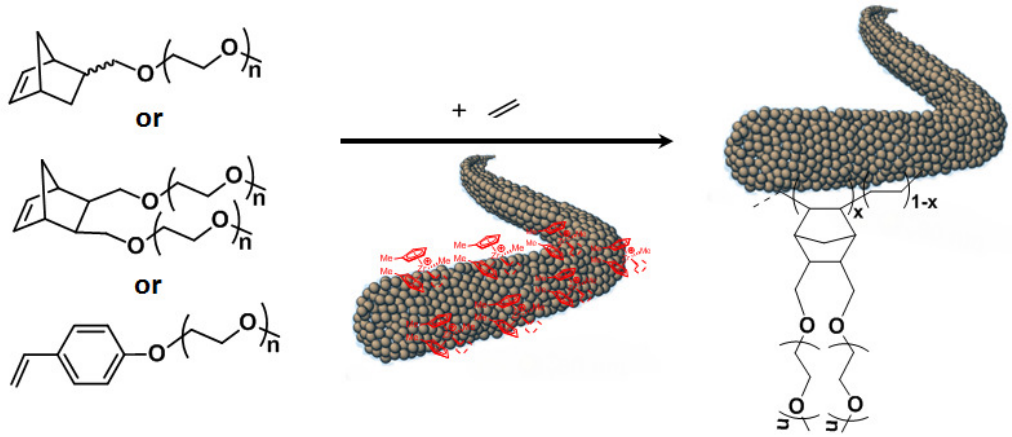

Figure 9-5. Synthesis of fibers with PEG-functionalized copolymers

9.2.2 Immobilized dendritic borates/metallocene system

In **Chapter 8**, activation of *rac*-$C_2H_4(Ind)_2ZrMe_2$ with dendritic borates was demonstrated and their activity towards homogeneous ethylene polymerization was investigated. As previously stated in **Chapter 1**, homogeneous polymerization with metallocene catalysts has several drawbacks such as poor reaction control, reactor fouling, and lack of morphology control whereas high catalytic activities and no impurities in the final products. Therefore, immobilizing the dendritic borates/metallocene system can be considered.

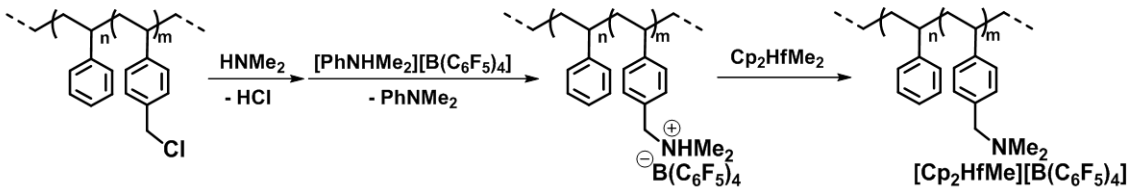

Figure 9-6. Supporting metallocene/borate system on PS resin

Roscoe et at. reported immobilization method of $Cp_2HfMe_2/B(C_6F_5)_4$ system on dimethylamine-functionalized polystyrene resins (*Figure 9-6*).[12, 13] Soga et at. also reported alternative method of immobilizing metallocene/$B(C_6F_5)_4$ system on 4-vinylpyridine-copolymerized PS resin (*Figure 9-7*).[14]

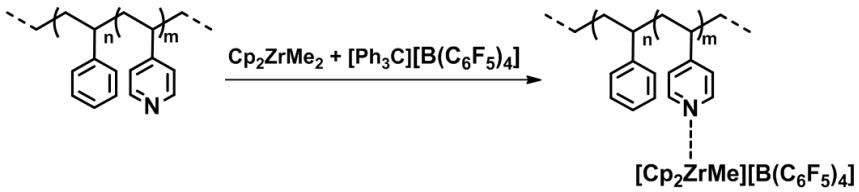

Figure 9-7. Supporting metallocene/borate system on PS resin containing pyridine units

As synthesis of PS nanoparticles has been performed in this dissertation, PS particles can be modified by adding pyridyl or dimethylamine during copolymerization. The dendritc bortaes (**Chapter 8**) can also be immobilized on the modified PS particles for heterogeneous olefin polymerization.

9.3 References

[1] A. Guerfi, M. Kaneko, M. Petitclerc, M. Mori, K. Zaghib, *Journal of Power Sources* **2007**, *163*, 1047.

[2] S. F. Lux, S.-S. Jeong, G.-T. Kim, S. Passerini, M. Winter, A. Balducci, *ECS Transactions* **2010**, *25*, 21.

[3] H. Maleki, G. Deng, I. Kerzhner-Haller, A. Anani, J. N. Howard, *Journal of The Electrochemical Society* **2000**, *147*, 4470.

[4] W. Kaminsky, A. Bark, I. Däke, "31. Polymerization of Cyclic Olefins with Homogeneous Catalysts", in *Studies in Surface Science and Catalysis*, K. Tominaga and S. Kazuo, Eds., Elsevier, 1990, p. 425.

[5] J.-A. Choi, S. H. Kim, D.-W. Kim, *Journal of Power Sources* **2010**, *195*, 6192.

[6] V. Heroguez, S. Breunig, Y. Gnanou, M. Fontanille, *Macromolecules* **1996**, *29*, 4459.

[7] N. R. Grove, P. A. Kohl, S. A. Bidstrup Allen, S. Jayaraman, R. Shick, *Journal of Polymer Science Part B: Polymer Physics* **1999**, *37*, 3003.

[8] A. Chemtob, V. Héroguez, Y. Gnanou, *Journal of Polymer Science Part A: Polymer Chemistry* **2004**, *42*, 2705.

[9] U. B. Seemann, J. E. Dengler, B. Rieger, *Angewandte Chemie International Edition* **2010**, *49*, 3489.

[10] K. L. Opper, D. Markova, M. Klapper, K. Müllen, K. B. Wagener, *Macromolecules* **2010**, *43*, 3690.

[11] K. Chiad, S. H. Stelzig, R. Gropeanu, T. Weil, M. Klapper, K. Müllen, *Macromolecules* **2009**, *42*, 7545.

[12] S. B. Roscoe, J. M. J. Fréchet, J. F. Walzer, A. J. Dias, *Science* **1998**, *280*, 270.

[13] S. B. Roscoe, C. Gong, J. M. J. Fréchet, J. F. Walzer, *Journal of Polymer Science Part A: Polymer Chemistry* **2000**, *38*, 2979.

[14] K. Musikabhumma, T. Uozumi, T. Sano, K. Soga, *Macromolecular Rapid Communications* **2000**, *21*, 675.

CHAPTER 10

General Experimental Part

10 General Experimental Part

10.1 General information

All experiments were performed under air-free and oxygen-free condition using Schlenk techniques with argon or in a glove-box filled with nitrogen. The glove box (mBarun, LabMaster i30) was purchased and maintained below 1 ppm level of oxygen and moisture, which were detected by active O_2 (mBarun, MB-OX-SE1) and active moisture (mBarun, MB-MO-SE1) probe, respectively. Catalyst of the glove box was regularly regenerated with a formiergas 10 (Linde), which is comprised of 90 % N_2 and 10 % H_2.[1] Argon (Westfalen, grade 4.6) and nitrogen (Air Liquide, grade 5.0) were purified through Hydrosorb- (Air Liquide, small cartridge H_2O free) and Oxysorb- (Air Liquide, small cartridge O_2 free) columns. Toluene (Acros) was used after further distillation over Na/K with benzophenone as a color indicator. Chemicals were dried over CaH_2, NaH or activated molecular sieve and used after distillation under inert condition. Silica particles (Evonik, Sipernat® 50) were kindly donated and used for immobilization of catalysts after drying for 48 h at 300 °C and 1.0×10^{-3} mbar. A oligomerization catalyst, imino(pyridine) cobalt complex ($CoCl_2N_2^{2Th}$), was synthesized [redacted] according to a published procedure[2] and used for studies in **Chapters 5 – 6**. Bis(methylcyclopentadienyl)zirconium(IV) dichloride, $(MeCp)_2ZrCl_2$ (97 %, Aldrich), was used without further purification in **Chapters 3 – 7**. Bis[*N*-(3-*t*-butylsalicylidene)cycloheptylaminato]titanium(IV) dichloride was synthesized according to a published procedure[3] and used for studies in **Chapter 6**. For polymerization using borates in **Chapter 8**, a dimethyl metallocene catalyst, *rac*-$C_2H_4(Ind)_2ZrMe_2$, was prepared by the reaction of *rac*-$C_2H_4(Ind)_2ZrCl_2$ (97 %, Strem) with $MgMe_2$ in toluene, followed by the purification of the product via recrystallization. A 10 wt% of methylaluminoxane (MAO) solution in toluene (Aldrich) was used. Dry MAO (DMAO - Me_3Al-free MAO) was prepared according to literature procedures.[4] First, MAO solution was evaporated and dried at 60 °C under reduced pressure overnight to remove the residual toluene and trimethylaluminium (TMA). The resulting solid was stored in a brown bottle under inert conditions and redissolved in toluene before usage. Polyurethane particles (**Chapter 3**) were synthesized [redacted]. Electrospinning of polystyrene nanoparticles (**Chapters 4 – 5**) was performed [redacted]. Hollow silica particles were synthesized [redacted] for research in **Chapter 7**. Dendritic borates were synthesized [redacted] and used for research in **Chapter 8**.

10.2 Purification procedure for gases and liquids

All gases and liquids applied for metallocene immobilization and a polymerization are "polymer grade". Due to the high sensitivity of catalytic system to impurities such as oxygen and moisture, dramatic influences on the reaction rates of the polymerizations can be observed. Therefore, building up a robust purification procedure for gases and liquids is mandatory. Details of purification methods for each gases and applied liquids are described in following section.

10.2.1 Purification of olefin gases

Commercially available ethylene or propylene monomer contains impurities which are originated from cracking procedure.[5] The problem is that the impurities act as poisons for activated metallocene complexes in olefin polymerization. In particular, ethylene contains by-products such as acetylene, CO and CO_2.[6] Although these by-products are in minute levels, they significantly reduce the polymerization rate. In order to ensure the ethylene feed is poison-free or has at least few ppb units of poisons, the supply has to be purified using a series of columns before polymerizations. Typically, purification columns have a palladium for removal of acetylene, a copper oxide (CO), a copper (O_2) and activated molecular sieves (moisture). Depending on the purification performance with columns, catalytic activity can be differed. As a result, it is often observed that olefin polymerization under quasi-condition is hard to be reproduced in a different lab.

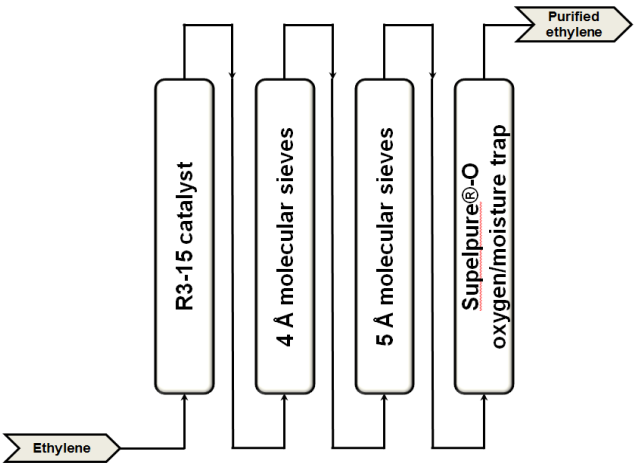

*Figure 10-1.*Schematic drawing of purification columns for ethylene

For the studies of the dissertation, high purity of ethylene (Linde AG, grad 5.0) was purchased and used after further purification. The ethylene gas was purified by passing

through purification columns of BASF R3-15 deoxygenation catalyst (BASF AG, Ludwigshafen), activated 4 Å molecular sieves, 5 Å molecular sieves (Supelco) and Supelpure®-O oxygen/moisture trap (Supelco) in that order (*Figure 10-1*). These columns are comprised of components listed as below:

- The first column of R3-15 catalyst is comprised of CuO and ZnO. The column is applied for the absorptive removal of O_2, CO and H_2. It.
- The column of 4 Å molecular sieves was assembled in Max-Planck-Institute für Kohlenforschung (MPIK) and used for removal of materials which are not bigger than 4 Å such as NH_3, SO_2, CO_2, H_2S, C_2H_4, C_2H_6, and C_3H_6. This column can also absorb water.
- 5 Å molecular sieves (Supelco) physically remove H_2O and other heavy hydrocarbon contents.
- Supelpure®-O oxygen/moisture trap (Supelco) contains oxygen-removing catalysts coated on molecular sieves. The trap can reduce oxygen to less than 2 ppb when the level in the incoming gas does not exceed 10 ppm and also can remove water vapor.

10.2.2 Purification of inert gases

Argon (Westfalen, 4.6) and nitrogen (Air Liquide, 5.0) were purified through Hydrosorb- (Air Liquide, small cartridge H_2O free) and Oxysorb (Air Liquide, small cartridge O_2 free) columns. The purified gases were used for flushing reactors, filling a glove box and distillation of solvents.

10.2.3 Toluene purification

The purification of toluene (Acros) was performed via distillation over sodium/potassium in the presence of benzophenone as an indicator under argon stream. The distilled toluene was delivered to a glove box and stored in a bottle filled with activated molecular sieves (4 Å). The molecular sieves were activated by heating at 150 °C under reduced pressure at least 2 days. The toluene was used after storing for at least 24 h. For running a slurry reactor with a low amount of catalysts, the toluene was further scavenged with a 1.0 wt% of triisobutylaluminum solution (a 1.0 M in toluene) before applying to the slurry reactor.

10.3 Implementation of metallocene immobilization

Immobilization procedure of metallocenes was preceded in a glove box filled with purified argon, as these catalysts are extremely sensitive to moisture and oxygen. Prior to immobilization, all support materials were dried under reduced pressure and delivered into the glove box. In particular, silica particles (Evonik, S-50) were dried for 48 h at 300 °C and 1.0×10^{-3} mbar. Generally, the supports were several times washed with dried toluene to extract residual water. Depending on the supports, pretreatment with methylaluminoxane (MAO) or triisobutylaluminum (TiBA) was performed to drastically suppress the content of moisture. After drying under reduced pressure, the supports were dispersed in toluene and waited for the addition of a catalyst. For preparation of a catalytic solution, a metallocene complex was dissolved, and cocatalyst (MAO or borate) was added and stirred for a desired time. The activated catalytic solution was added to the dispersed supports in toluene, and the mixture was shaken overnight. After removal of solution, the supports were dried and waited for olefin polymerization.

10.4 Gas-phase polymerization

10.4.1 Experimental set-up of the gas-phase reactor

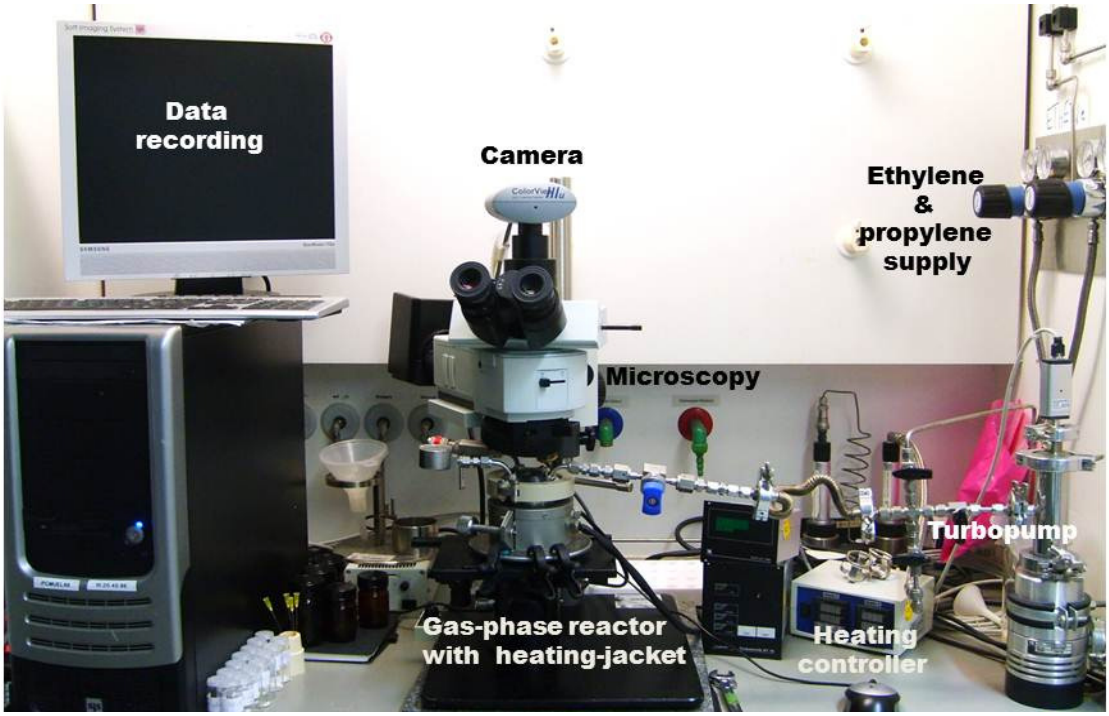

Figure 10-2. Experimental set-up of gas-phase reactor

Experimental set-up of an autoclave (gas-phase reactor) equipped with a video-microscopy is shown in *Figure 10-2*. The detail of the gas-phase reactor is also shown in *Figure 10-3* and described as follow: The interior volume of the reactor is approximately 50 mL. In the middle of the reactor, there is a plate on which catalyst-immobilized support materials can be placed for observation. The plate is coated with silver which has a particularly good conductivity for better heat transfer to the support materials (samples). In the bottom of the reactor, scavenger can be placed to additionally purify ethylene or propylene gas. The reactor is closed by a steel cover with a snap closure and further sealed by an O-ring. The samples are observed through a window which is embedded in the center of the steel cover. The reactor is heated electronically by a heating jacket, connected to an external heat controller. To monitor internal temperature of the reactor, a thermocouple (Pt100 sensor) is introduced.

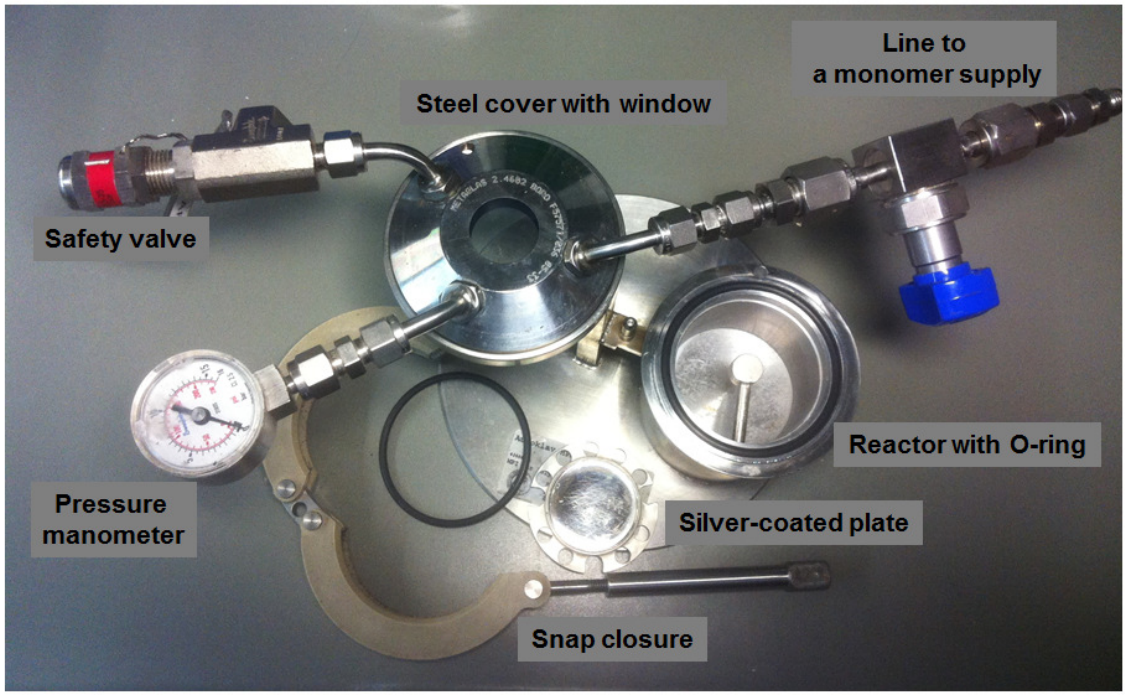

Figure 10-3. Details of the gas phase reactor (autoclave)

The reactor is designed for a maximum pressure of 10 bar and has a safety valve, open at a pressure above 9 bar, to protect excess pressure. The internal pressure of the reactor is monitored by a pressure manometer. To supply a monomer gas and argon, or apply a vacuum to the reactor, one more inlet is installed with a valve. The monomer gas is initially supplied to the bottom of the reactor chamber through the inlet so that gas contacts with scavenger, which placed below the sample plate in the reactor chamber. The design of the inlet to the bottom of the reactor also prevent the blowing the samples placed on the plate.

The inlet with a blue colored valve is connected with a vacuum line, which can produce a vacuum of 5×10^{-4} mbar. This is created by a combination of an oil-free vacuum pump with a turbo molecular trap.

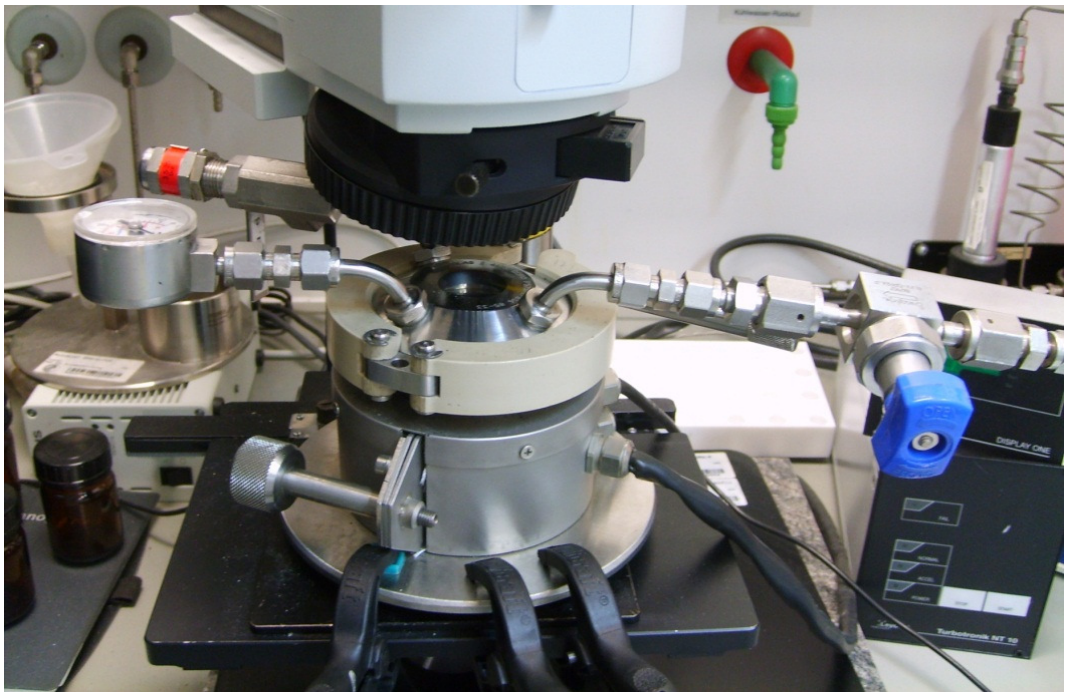

Figure 10-4. Gas phase reactor after installation and during olefin polymerization

For sample observation, a microscope (Olympus BX41M) with two optical lenses (LMPlanFI lenses with 5× and 10× magnification) is applied (*Figure 10-4*). During the polymerization, the images of samples are photographed for a desired time interval via the digital camera Colorview. The light source of the microscope is a halogen light W. To prevent movement of the reactor, it is fixed to an object table by clips.

10.4.2 Implementation of the gas-phase reactor

For preparation of the polymerization with the reactor, removal of moisture and oxygen in the reactor is crucial. Thus, the reactor was evacuated overnight under the vacuum to a final pressure of 5×10^{-4} mbar, while heated to 80 °C. After heating the reactor under vacuum, the reactor was vent-filled with argon several times to minimize the impurities and delivered into a glove box. As illustrated in *Figure 10-5*, in the bottom part of the reactor chamber, dried MAO (DMAO) was used as a scavenger to further purify the introduced monomer gas. A small portion of silica particles (immobilized with pre-activated catalyst) as an internal standard were also applied with DMAO to validate the polymerization

condition. On the silver coated plate, investigated object (catalyst supported sample) was placed.

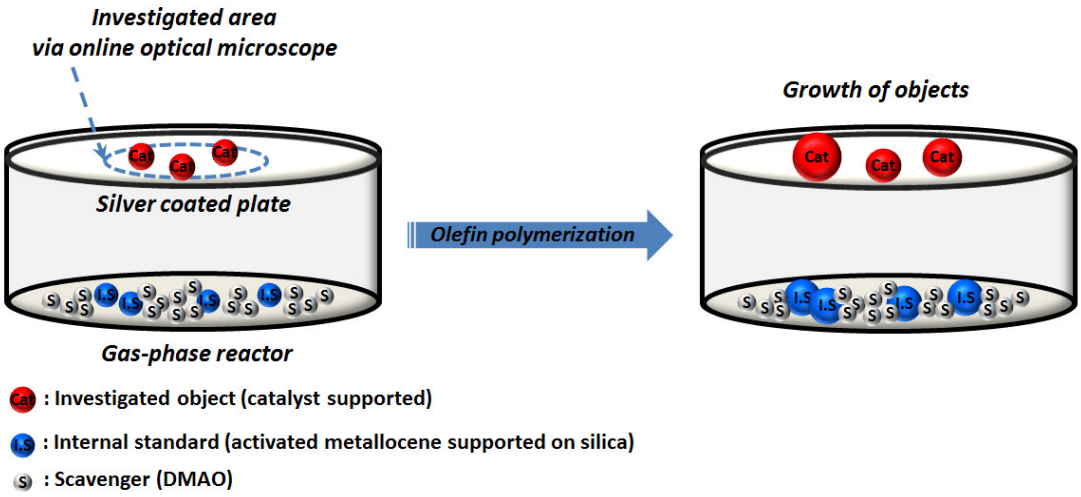

Figure 10-5. Schematic drawing of implementing a gas phase reactor

After removal from the glove box, the reactor was connected with the gas line. Since the line was exposed to the air, the line was evacuated under vacuum and heated for 45 – 60 min. For video-microscopic observation, a suitable site was searched on the catalyst plate using cross-table and focused at the desired magnification. After the start of imaging in defined intervals (commonly 10 s), the polymerization was started by injecting the desired monomer gas pressures. To terminate the polymerization, the pressure was released and stopped the imaging.

10.4.3 Analysis of particle growth

From the images obtained from the reactor during the polymerization, a kinetic data can be evaluated by calculating the growth of individual particles. Even though the particles have a two dimensional image taken by the camera, it is assumed that they are spherical particles and have an isotropic grow. The particle diameter could be represented as a volume of the particle. After selecting only isolated individual particles, the automated image processing was carried out using Window-based PS AnalySIS software (Softimage system) as shown in *Figure 10-6*. The curves of the particle growth as a function of the polymerization time could be determined by the processing.

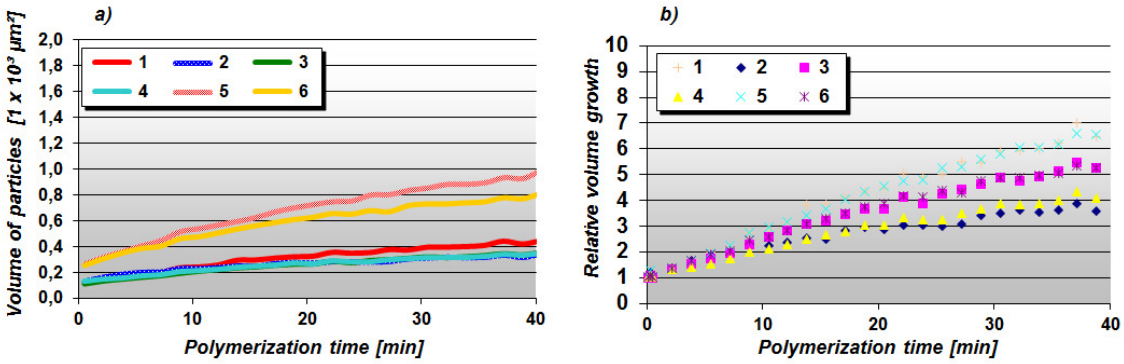

Figure 10-6. Graphs of (a) volume of selected particles and (b) relative volume growth as a function of polymerization time

10.5 Slurry polymerization under low pressure

10.5.1 Experimental set-up of the slurry polymerization

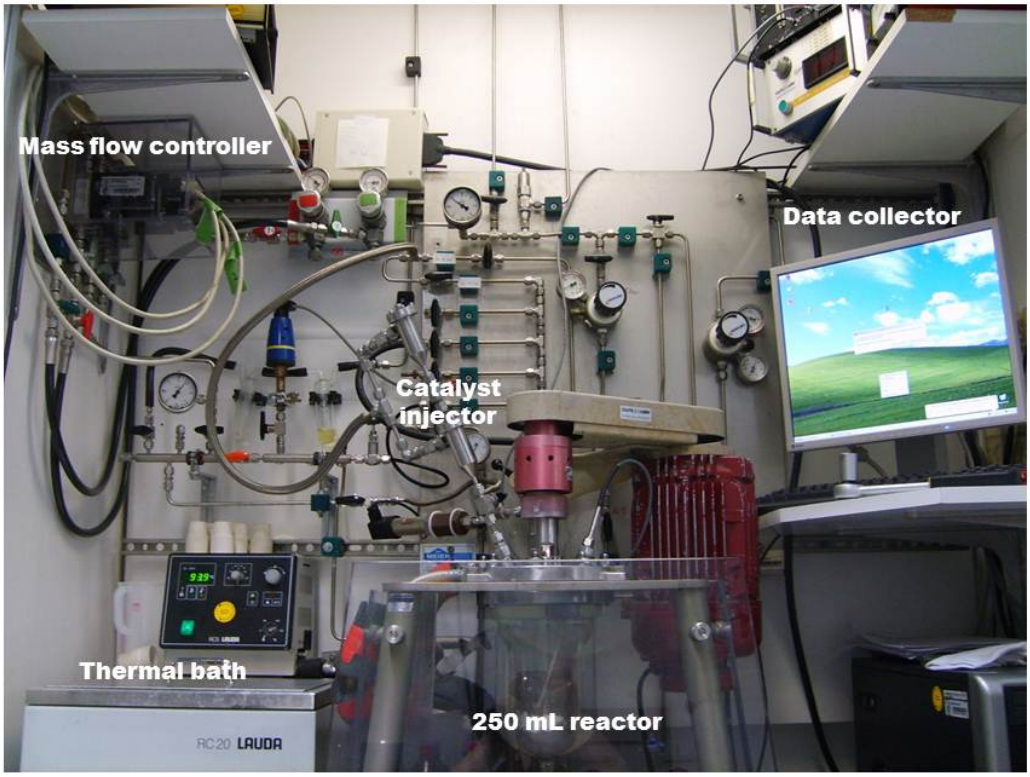

Figure 10-7. Set-up of slurry polymerization reactor

The slurry polymerizations were carried out in a 1000 mL volume of a dual-wall glass autoclave (Büchi AG) as shown in *Figure 10-7*. The total volume of the reactor can be varied by changing an internal vessel with a volume of 250, 500 and 750 mL. The monomer consumption was measured by a flow-meter (5850 TRC 126 ZBD 41, Brooks

Instrument), supplied with three different channels measuring the monomer flow with a speed of 0 − 100, 0 − 1000 or 0 − 5000 mL/min. Depending on the catalytic activity, one of the channel was chosen. Reactor temperature was controlled by an external thermostat (Unistat 360, Hueber) and detected by Pt100, installed through the autoclave. The information for polymerization test such as temperature, actual monomer consumption and total consumption of the monomer were online registered by A/D-Wandler (Keithley UPCI-3101).

The catalytic solution was transferred by an injector under a high pressure of argon to the reactor. The injector apparatus consists of two interconnected chambers stainless steel, each having a connection via the argon flushing of the opened chambers (0.5 bar) or for injecting argon of the catalyst (1 − 9 bar) can be fed, and having a drain valve. The lower of the two compartments was used to hold the catalytic solution, while the top was charged with solvents to the lower chamber must be rinsed. The flow diagram of the equipment for slurry polymerization is featured in *Figure 10-8*.

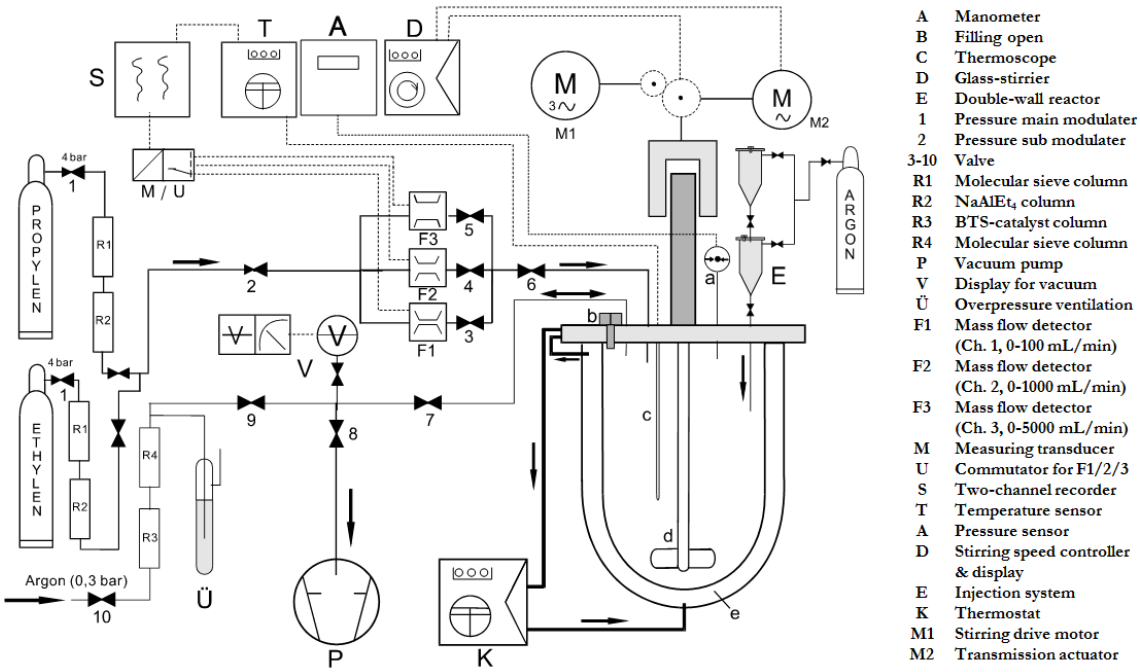

Figure 10-8. Flow diagram of the equipment for slurry polymerization

10.5.2 Implementation of the slurry polymerization

In the preparation of the reaction, the slurry reactor was dried under vacuum for at least 4 h at 85 °C. Since a final pressure of the reactor reached to approximately 1×10^{-1} mbar,

the reactor was flushed with argon and evacuated with vacuum. After the repetition of the vent-fill procedure several times, the reactor was charged with 0.5 bar of argon. Subsequently, a desired reaction temperature and monomer pressure were set, and waited for a reaction. A desired amount of diluent for polymerization is prepared in a glove box. After removal from the glove box, the diluent was transferred to the reactor under argon stream via a cannula. Upon the addition of the diluent, the argon stream in the reactor was evaluated and replaced with monomer gas. This vent-fill procedure was repeated several times to remove residual argon in the reactor. After reaching the desired reaction temperature, controlled by an external thermostat, the ethylene was released once again due to the expanding phenomena from an increase of internal temperature. The reactor filled with the diluent was ready for injecting a catalytic solution to perform slurry polymerization.

For delivering the catalytic solution (or suspension) to the reactor, preparation was performed in the glove box under inert conditions. A desired amount of a catalyst was dissolved in 2.0 mL of solvent, preferred same as the diluent. The catalytic solution was activated by an addition of a desired amount of MAO solution (a 1.0 M in toluene) and stirred for 5 min, and transferred to 3.0 mL volume of syringe equipped with 15 cm length of a metal needle. One additional syringe containing with 2.5 mL toluene was prepared for rinsing the catalytic solution, while injecting to the reactor.

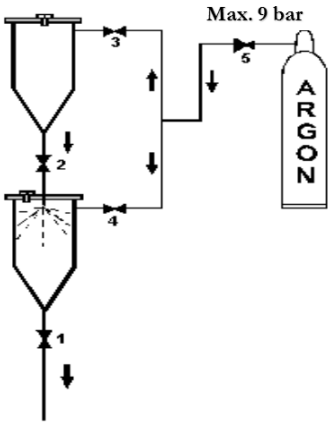

Figure 10-9. Injection system with dual chambers
(1-2) Two-way valves chambers; (3-4) intake valves with coupling for the argon supply; and (5) controlling a pressure of the supplied argon

After removal of the two syringes from the glove box, they were transferred under argon pressure to the dual injection chambers (*Figure 10-9*), installed on the top of the reactor. The two syringes filled with catalytic solution and rinsing solution were transferred to lower and upper chamber, respectively. The chambers were pressured with argon, which must be

higher than the pressure inside the reactor. The polymerization recording program (MPIK, Mülheim, Germany) was opened and filled with specific information of the polymerization. Before executing the polymerization, the polymerization conditions, such as temperature, constant monomer pressure, stirring speed and channel for recording, were checked and the polymerization was started by pressing the "start-record" button on the program. Thereafter, the catalytic solution in the lower chamber was injected to the reactor and subsequently, the lower chamber was rinsed by opening the upper chamber. After the desired polymerization time, the data recording was stopped, drained and the excess pressure in the reactor, the reaction quenched by the addition of methanol. The polymer obtained was filtered off and 300 mL of methanol, fitted with 5 mL conc. hydrochloric acid, stirred for 12 h, filtered off again and stirred for an additional 12 h in 300 mL of methanol. After filtering off, the resulting polymer was dried at 80 °C for 24 h in a vacuum oven.

10.6 Instruments for characterization

- Atomic force microscopy (AFM): Brucker, Dimension 3100 CL with a cantilever for non-contact mode (Olympus, OMCL-AC160TS).
- Burnauer, Emmett and Teller (BET): Micromeritcs Tristar II 3020 analyzer (USA) with nitrogen adsorption and desorption isotherms at 77 K.
- Differential scanning calorimeter (DSC): Mettler digital scanning calorimeter 300 with a heating rate of 10 K/min in the temperature range of 20 − 200 °C.
- Dynamic light scattering (DLS): Malvern-Zetasizer 3000 HAS with a fixed scattering angle of 90° and on an ALV/LSE-5004-correlator using a He/Ne-laser operating at 632.8 nm
- Energy dispersive X-ray spectroscopy (EDX) and Hyper-mapping: Brucker solid state detector (SSD, XFlash detector 5010) in SEM (Hitachi, SU 8000 Type I).
- Fourier transform infrared (FTIR): Nicolet 730 spectrometer using thermo electron endurance attenuated total reflection (ATR) single-reflection ATR crystal.
- Gel permeation chromatography (GPC): For polyethylenes, Waters GPC2000 high-temperature module in 1,2,4-trichlorbenzene with 135 °C *vs.* polystyrene standard; For UHMWPE, Waters 150-C GPC with TSK-Gel columns (two TSKgelGMH$_{HR}$-H(S)HT and TSKgelGMH$_6$-HTL) in 1,2,4-trichlorbenzene with 145 °C *vs.* polystyrene standard; For polyurethane, MZ-Gel SDplus 10E6, 10E4 and 500 columns in tetrahydrofuran (THF) as the eluent *vs.* PMMA standards.

- Laser scanning confocal fluorescence microscopy (LSCFM): Zeiss Axiovert 200M equipped with a LSM 510 ConfoCor 2.
- Nuclear magnetic resonance (NMR): 300 MHz (Bruker AMX 300), 500 MHz (Bruker DRX 500)
- Scanning electron microscopy (SEM): Hitachi (SU 8000 Type I), Gemini 912 (LEO 1530, Zeiss) at low-voltage in the range of 200 and 700 V.
- Stimulated emission depletion microscopy (STED): Leica TCS SP5X equipped with an HQ560/50Mfilter (Chroma Inc.). The objects were excited with the power for the λ=514 or 488 nm argon laser and depleted with 592 nm.
- Scanning transmission electron microscopy (STEM): field emission SEM (Hitachi SU 8000 Type I).
- Transmission electron micrographs (TEM): Zeiss EM912 operating at 80 kV.

10.7 Analytic methods for inner-morphology

10.7.1 Cryo-sectioning

For inner-morphology studies of an object, a destructive method as cryo-sectioning is an option. Prior to the cryo-sectioning procedure, an object must be embedded. The embedding procedure of the object was performed using EpoFix Kit (Struers) containing a hardener (12.5 g, main component: triethylenetetramine) and resin (1.5 g, main component: bisphenol A). The mixture of epoxy resin was aged at ambient temperature for 1 h to remove air bubbles as the bubbles are resulting artifact in the cryo-sectioned samples. The epoxy resin was transferred to an empty mold by half and cured overnight at the room temperature. The object was placed on the mold by half filled with epoxy and second half the mold was filled with fresh prepared epoxy resin. Note that the object must be located in the middle of the mold for better measurements. After curing the epoxy resin overnight, the object was trimmed with Leica EM TRIM equipped with a diamond knife. The trimmed object was placed in Leica ultracut UCT under liquid nitrogen (LN_2) flow. In order to obtain better cryo-sectioned samples, the object must be cooled below its glass transition temperature (T_g). After 1 h of the cooling, the object was trimmed again with Trim 20 (Diatome, diamond trim blade 20) and sectioned (Diatome, ultra-cryo-diamond knife 35) with various thicknesses in the range of 50 to 200 nm. For cryo-transmission electron microscopy (TEM) measurement, the samples with ~ 60 nm thickness were

placed on a 300 mesh carbon-coated copper grid. For scanning transmission electron microscopy (STEM), ~ 200 nm thick samples were placed on a silicon wafer (10 × 10 mm). For atomic force microscopy (AFM), the embedded particles in epoxy resin after cryo-sectioning was applied.

10.7.2 Laser scanning confocal fluorescence microscopy (LSCFM)

Laser scanning confocal fluorescence microscopy (LSCFM) was performed using a Zeiss Axiovert 200M equipped with a LSM 510 ConfoCor 2. In contrast to TEM requiring additional procedures such as cryo-sectioning, LSCFM is a non-destructive method and can be simply employed by either staining an object with a dye or using a chemically modified dye to an object.[9, 10] LSCFM is a relatively new technique which has been applied to study the fragmentation behavior of supports in polyolefins. This is demonstrated by optical sectioning showing the distribution of the different support fragments in the polyolefin product particles (*Figure 10-10*).

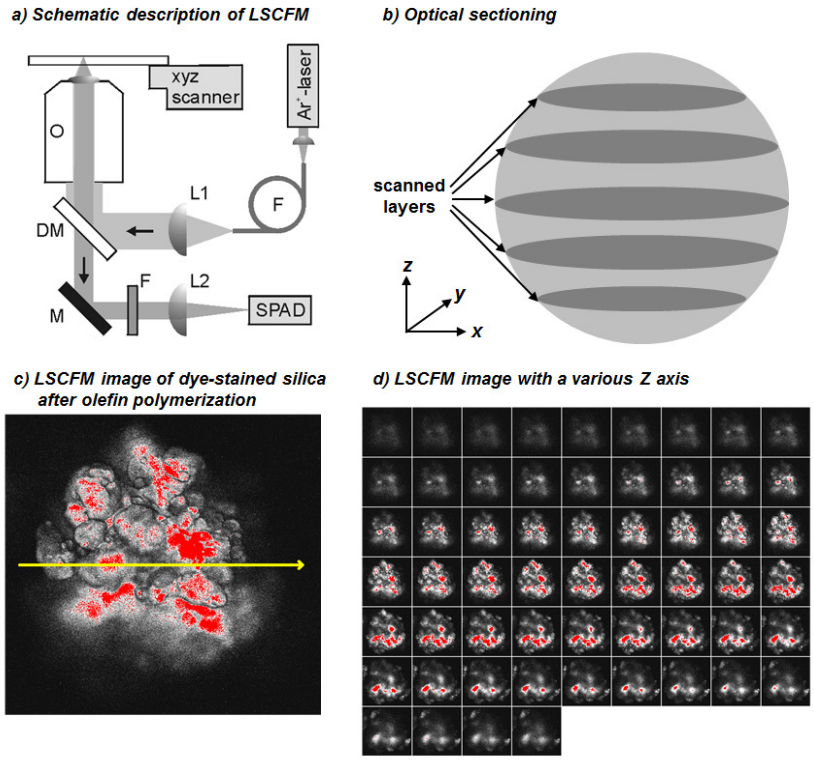

Figure 10-10. (a) Schematic description of LCSFM and (b) optical sectioning, (c) LSCFM image of support distribution of a fragmented PE particle and (d) with a various Z axis

10.7.3 Stimulated emission depletion microscopy (STED)

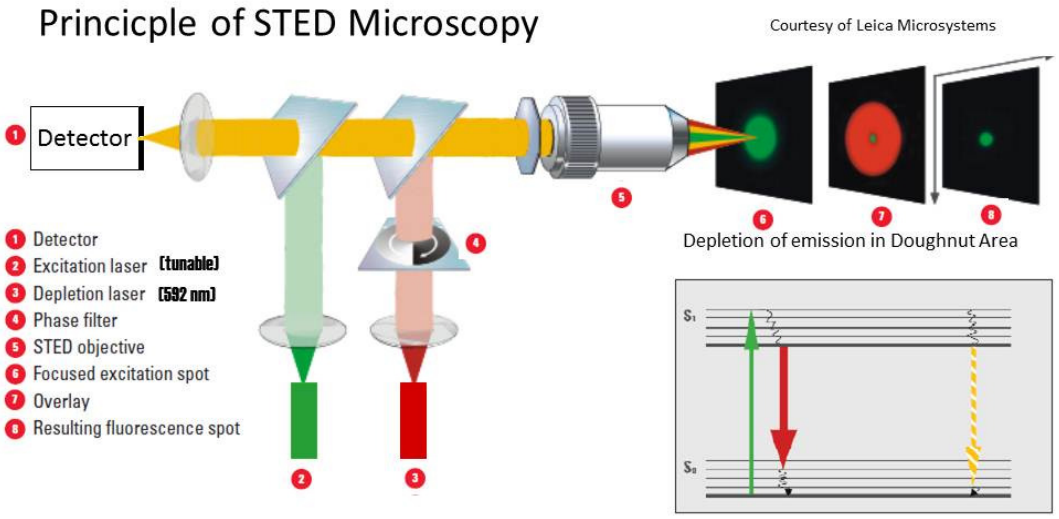

Figure 10-11. STED microscopy

Stimulated emission depletion (STED) microscopy was applied to visualize polystyrene nanoparticles which have a smaller size than the limitation of LSCFM. STED microscopy is a decent technique which was invented by Stephan Hell.[11] It is quite similar to LSCFM except for employing one more additional laser which has a different wavelength. By combination of two different lasers, resolution of detected objects can be enhanced and thus STED is capable of detecting a single object with below few ten nanometers. For the studies in the dissertation, STED microscopy was performed using Leica TCS SP5X equipped with an HQ560/50Mfilter (Chroma Inc.). As show in *Figure 10-11*, a fluorescence dye in an object was excited with the laser of a tunable power (λ = 458 or 514 nm). A CW laser with λ = 592 nm was used for the depletion of the fluorescence signal for the excited dye. Due to the depleted fluorescence signal, the resolution of the image can be resulted in few tenth nanometers.[12]

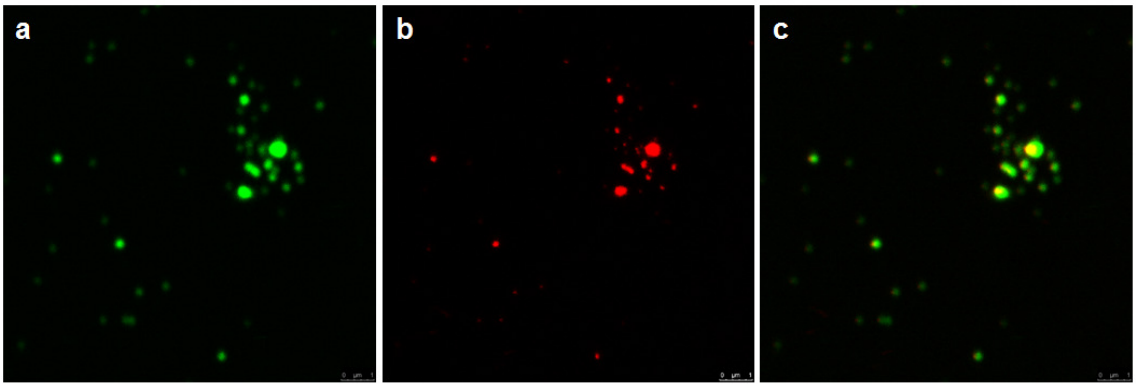

Figure 10-12. (a) LSCFM and (b) STED micrographs of agglomerates of BODIPY-tagged polystyrene nanoparticles, and (c) over-laid image of (a) and (b)

In **Chapter 4**, synthesis of polystyrene (PS) nanoparticles was demonstrated in a miniemulsion using styrene, divinylbenzene and a styryl boron-dipyrromethene (BODIPY) dye. Since the PS nanoparticles have an average diameter of ~ 60 nm and chemically tagged with a fluorescence dye (BODIPY), they can be applied to STED microscopy. The PS nanoparticles were characterized with LSCFM and STED at the same position for comparison. As shown in *Figure 10-12*, STED image (b) shows higher resolution as compared to that of LSCFM image (c). Although STED was not well studied in this dissertation, this technique can be applied in the future for fragmentation stuies in heterogeneous polyolefin synthesis.

10.8 References

[1] *http://www.linde-gas.com/en/products_and_supply/shielding_gases/formier_10.html*.

[2] C. Bianchini, G. Giambastiani, G. Mantovani, A. Meli, D. Mimeau, *Journal of Organometallic Chemistry* **2004**, *689*, 1356.

[3] H. Makio, N. Kashiwa, T. Fujita, *Advanced Synthesis & Catalysis* **2002**, *344*, 477.

[4] T. Hasan, A. Ioku, K. Nishii, T. Shiono, T. Ikeda, *Macromolecules* **2001**, *34*, 3142.

[5] L. Kniel, O. Winter, K. Stork, "*Ethylene, keystone to the petrochemical industry*", New York, 1980.

[6] inv. M. B. Steve Blankenship, Mingyong Sun, Michael A. Urbancic; *EP 2318482 A2*

[7] W. Kaminsky, C. Strübel, H. Lechert, D. Genske, S. I. Woo, *Macromolecular Rapid Communications* **2000**, *21*, 909.

[8] D.-H. Lee, K.-B. Yoon, W.-S. Huh, *Macromolecular Symposia* **1995**, *97*, 185.

[9] Y. J. Jang, K. Bieber, C. Naundorf, N. Nenov, M. Kapper, K. Mullen, D. Ferrari, S. Knoke, G. Fink, *E-Polymers* **2005**.

[10] Y. J. Jang, C. Naundorf, M. Klapper, K. Mullen, *Macromolecular Chemistry and Physics* **2005**, *206*, 2027.

[11] V. Westphal, S. O. Rizzoli, M. A. Lauterbach, D. Kamin, R. Jahn, S. W. Hell, *Science* **2008**, *320*, 246.

[12] *http://en.wikipedia.org/wiki/STED_microscopy*.

CHAPTER 11

Supporting Information

11 Supporting Information

11.1 Acknowledgements

I am very pleased to defend my dissertation in a memorable year for polyolefin chemists. The year of 2013 is the 60th anniversary of first patent in polyethylene and the 50th anniversary of Ziegler-Natta's Nobel Prize for their great discovery.

[redacted]

[redacted]

[redacted]

[redacted]

[redacted]

[redacted]

[redacted]

[redacted]

JOE, DaeJune

August, 2013

Mainz, Germany

11.2 Curriculum Vitae

[redacted]

Publications

1. Markus Klapper, Daejune Joe, Sven Nietzel, Klaus Müllen, (Invited review paper to Chemistry of Materials Anniversary Issue - January 2014)
   "Smart catalyst - support systems for olefin polymerization" s*ubmitted to Chemistry of Materials*, **2013** (ACS)

2. Daejune Joe, Sven Nietzel, Robert Dorresteijn, Yi Gerkamnn, Gerhard Fink, Markus Klapper, Klaus Müllen, "*In-situ* generation of polyolefin composites on polyurethane particles by metallocenes" s*ubmitted to Journal of Polymer Science Part A: Polymer Chemistry*, **2013** (Wiley)

3. Daejune Joe, Florian E. Golling, Kathrin Friedemann, Daniel Crespy, Markus Klapper, Klaus Müllen, "Anisotropic supports in metallocene-catalyzed polymerizations: templates to obtain polyolefin fibers", s*ubmitted to Macromolecular Rapid Communications*, **2013** (Wiley)

4. Daejune Joe, Ralf Moritz, Martin Baumgarten, Markus Klapper, Klaus Müllen, "*MAO-free cocatalysts for modulating catalytic activity of metallocene*" *in preparation of the manuscript*

5. Daejune Joe, Doris Vollmer, Markus Klapper, Klaus Müllen, "*hollow silica particles for supports in metallocene-catalyzed polyolefin synthesis*" *in preparation of the manuscript for Polymer Bulletin* (Springer)

6. Daejune Joe, Giuliano Giambastiania, Kathrin Friedemann, Daniel Crespy, Markus Klapper, Klaus Müllen, "Cocurrent tandem polymerization of LLDPE on electrospun fibers based on polystyrene nanoparticles" *in preparation of the manuscript for Polymer Chemistry*, **2013** (RSC)

7. Rajesh Munirathinam, Daejune Joe, Jurriaan Huskens, Willem Verboom, "Regioselectivity control of the ring opening of epoxides with sodium azide in a microreactor", *J. Flow Chem*, **2012**, *2(4)*, 129–134 (DOI: 10.1556/JFC-D-12-00013)

8. Markus Klapper, Michael S. Hoffmann, Daejune Joe, Till Diesing, Giovanni Rojas, Corinna Naundorf, Gerhard Fink, Klaus Müllen
   "Modern methods for morphology control in polyolefin synthesis" Polymer Preprints *(American Chemical Society, Division of Polymer Chemistry)* **2011**, 52(1)

9. Dae June Joe, Chun Ji Wu, Taekki Bok, Eun Jung Lee, Choong Hoon Lee, Won-Sik Han, Sang Ook Kang, Bun Yeoul Lee
   "Ortho-Phenylene-Bridged Cp/Sulfonamido Titanium Complexes for Ethylene/1-Octene Copolymerization" Dalton Trans. **2006**, 4056-4062 (2006.09.07), IF 3.003

10. Na, S. J.; Joe, D. J.; Sujith, S.; Han,W.-S.; Kang, S. O.; Lee, B. Y.

"Bimetallic nickel complexes of macrocyclic tetraiminodiphenols and their ethylene polymerization" J. Organomet. Chem. **2006**, *691*, 611-620 (2006.02.01), IF 2.025

11. Dae June Joe, Chun Ji Wu, Sujith S, Won-Sik Han, Sang Ook Kang, Bun Yeoul Lee "Ortho-phenylene-bridged cyclopentadienyl/amido titanium complexes for ethylene/1-hexene copolymerizations" Organometallics **2006**, *25*, 2133-2134 (2006.04.24), IF 3.473

12. Sujith, S.; Joe, D. J.; Na, S. J.; Park, Y.-W.; Choi, C. H.; Lee, B. Y. "Ethylene/(polar norbornene) copolymerizations by bimetallic salicylaldimine nickel catalysts" Macromolecules **2005**, *38*, 10027-10033 (2005.12.29), IF 3.898

13. Joe, D. J.; Lee, B. Y.; Shin, D. M.
"Synthesis and structure of 1.2.3-substituted cyclopentadienyl titanium(IV) Complexes" Bull. Kor. Chem. Soc. **2005**, *25***,** 233-237, IF 0.890

14. Joung, U. G.; Kim, T. H.; Joe, D. J.; Lee, B. Y.; Shin, D. M., Chung,Y. K.
"Pyridineenolato and pyridineenamido complexes of zirconium, titanium, and aluminum" Polyhedron **2004**, *23*, 1587-1594, IF 1.568

Patents

1. Lee, Choong Hoon; Lee, Eun Jung; Jung, Seungwhan; Ha, Jong Joo; Seo, Beomdoo; Lee, Bun Yeoul; Joung, Ui Gab; Joe, Dae June
"Preparation of transition metal complex containing non-coordinated amine group for olefin polymerization catalyst" Applicant: LG Chem, Ltd.
WO 2007007991A1 (20070118), US 7531608B2 (20090512), DE 112006001795T5 (20060707), JP 2009500402T (20060707), CN 101218262 (20080108)

2. Lee, Choong Hoon; Lee, Eun Jung; Jung, Seungwhan; Ha, Jong Joo; Seo, Beomdoo; Lee, Bun Yeoul; Joung, Ui Gab; Joe, Dae June
"Olefin polymerization with transition metal complex containing a phenylene bridge as a catalyst" Applicant: LG Chem, Ltd.
WO 2007007992A1 (20060707), US 2007010637A1 (20060710), DE 112006001798T5 (20060707), JP 2009500403T (20060707), CN 101223195A

(20080108)

Internatinal conference presentations

1. Daejune Joe, Kathrin Friedemann, Daniel Crespy, Markus Klapper and Klaus Müllen
   "A platform for polyolefin fibers", Chemelot International Polyolefins Symposium (CIPS) 2012, Maastricht, The Netherlands, October 7-10, **2012**

2. Markus Klapper, Daejune Joe, Florian E. Golling, Sven Nietzel and Klaus Müllen
   IUPAC World Polymer Congress, Blacksburg, Virginia, USA, June 24-29, **2012**

3. Daejune Joe, Florian E. Golling, Fink Gerhard, Markus Klapper and Klaus Müllen
   "Morphology control in polyolefin synthesis via self-assembled hybrid supports" 8th Ziegler-Natta Colloquium, Kanazawa, Japan, March 27-30, **2012**

4. Daejune Joe, Doris Vollmer, Markus Klapper and Klaus Müllen
   "Asymmetric and hollow particles for development of novel supports in polyolefin synthesis" 8th Ziegler-Natta Colloquium, Kanazawa, Japan, March 27-30, **2012**

5. Daejune Joe, Anke Kaltbeitzel, Markus Klapper and Klaus Müllen
   "STED microscopy: an easy tool to study the fragmentation of supports and distribution in the polyolefin product particle." 8th Ziegler-Natta Colloquium, Kanazawa, Japan, March 27-30, **2012**

6. Markus Klapper, Michael S. Hoffmann, Daejune Joe, Till Diesing, Giovanni Rojas, Corinna Naundorf, Gerhard Fink and Klaus Müllen
   "Modern methods for morphology control in polyolefin synthesis" Abstracts of Papers, 227rd ACS National Meeting, Anaheim, CA, United States, March 27-31, **2011**, POLY-61

7. D.J. Joe, T. Diesing, G. Rojas, M. Klapper, G. Fink and K. Müllen
   "Spatially resolved satalysis for controlling the morphology of polymer particles" 7th LSP/JAIST International colloquium on heterogeneous Ziegler-Natta catalysts, Sorrento, Italy (**2010**, June, 24-25) Oral presentation

8. D.J. Joe, T. Diesing, M. Klapper and K. Müllen
   "Unusual methods for morphology control in polyolefin synthesis" Poster number 39, 3rd Blue Sky Conference on catalytic olefin polymerization, Sorrento, Italy (**2010**, June, 20-23)

9. D.J. Joe, R.J.M. Egberink, J. Huskens, W. Verboom and D.N. Reinhoudt
   "Organic synthesis in microfluidic chips: Ring-opening reactions of epoxides and acid-catalyzed acetalization of p-anisaldehyde" Poster number 49A, CW-NWO meeting 2009, Scientific meeting on the area of Organic Chemistry, Lunteren, The Netherlands (**2009**, 10, 19-21)

10. Dae June Joe, Chun Ji Wu and Bun Yeoul Lee
    "Construction of ortho-phenylene-bridged Cp/amido titanium complexes and their ethylene/α-olefin copolymerizations" IUPAC International symposium on advanced polymers for emerging technologies, p21, Korean polymer society, Busan, (**2006**.10.10-13) Invited

11. Chun Ji Wu, Dae June Joe, Sujith S and Bun Yeoul Lee
    "Construction of ortho-phenylene-bridged Cp/amido titanium complexes by Suzuki-coupling reaction and their ethylene/1-octene copolymerization" PC 2006 (International symposium on polymer chemistry), p285 State Key laboratory of polymer physics and chemistry, Dalian, China, (**2006**.06.07-11)

12. Dae June Joe and Bun Yeoul Lee
    "Construction of ortho-phenylene-bridged Cp/amido titanium complexes by Suzuki coupling reaction and their ethylene/1-octene copolymerization" Asian polyolefin workshop 2005, Catalyst Society of Japan, Japan (**2005**.12)

13. Sujith S, Dae June Joe, Sung Jae Na, Young-Whan Park and Bun Yeoul Lee
    "Higher activity and higher polar monomer incorporation by bimetallic salicylaldimine nickel catalysts", Abstracts of papers, OMCOS-13, Geneva, Switzerland, 17-21, July, **2005**, P-240

14. Young Chul Won, Eun Sook Cho, Ui Gab Joung, Dae June Joe and Bun Yeoul Lee

"2-Lithio-3-methoxy-1,3-dimethylcyclopentene: synthetic equivalent of 2-lithio-1,3-dimethylcyclopentadiene and synthon for 6-alkyl-1,4-dimethylfulvenes" Abstracts of papers, 227rd ACS National Meeting, Anaheim, CA, United States, March, 28–April 1, **2004**

Scholarships and achievements

1. Best performance during Master period, Molecular Science & Technology, Ajou University, Feb, 2007
2. Brain Korea 21 Scholarship, Korea Research Foundation, 2004 − 2005

References